THE DEFORMATION CHARACTERISTICS OF A 12% CHROMIUM STEEL

BY

ANDREW BRINK

A thesis submitted to the Faculty of Engineering, University of Cape Town in fulfilment of the degree of Master of Science in Applied Science.

Department of Metallurgy and Materials Science,
University of Cape Town.

August 1983

ACKNOWLEDGEMENTS

I would like to thank those who have been involved in this project, but acknowledgement to all would be difficult.

Firstly, my supervisor, Professor Anthony Ball for his help and advice; Helgard Böhm for her patience and assistance in the laboratory; Nick Dreze for his machining expertise and help in the workshop; Bernard Greeves for his photographic skill;
Dr David Crawford and Dane Gerneke for their help with the electron microscope; Elinor Diamond for her capable assistance in the preparation of this document and lastly colleagues within the Department for their comradeship and support.

I would like to acknowledge, too, the financial support of Middelburg Steel and Alloys (Pty) Ltd.

work hardening stages, however, could be delineated, each with individual parameters. These stages, designated from I to III, are representative of specific work hardening modes. It is shown that the work hardening in the dual-phase temperature regime attenuates to a very low value and this fact can be attributed to dynamic recrystallisation of the straining ferrite and to the deformation induced nucleation of strain-free austenite. It was also found that the high temperature tensile strengths and deformation energies of these alloys demonstrate minima at around 900°C which could be of economic importance in terms of hot-working operations. Evidence for grain boundary sliding and elongations of up to 140% suggest the existence of superplasticity at elevated temperature, but only at very slow strain rates. The presence of large cuboid titanium carbo-nitrides have been found to detrimentally influence the mechanical properties of these alloys through void nucleation, coalescence and growth.

CONTENTS

SYMBOLS AND ABBREVIATIONS

SYMBOLS

A	=	composition dependent constant
b	=	material constant
b	=	burgers vector
C	=	strength coefficient (Modified Swift)
C_2	=	temperature dependent constant
D	=	initial diameter
E	=	Young's modulus
ΔH	=	activation enthalpy
K	=	strength coefficient (Hollomon)
k	=	temperature dependent constant
K'	=	strength coefficient (Ludwik)
l	=	initial specimen gauge length
m	=	strain rate sensitivity
n	=	Hollomon strain hardening coefficient
n"	=	Modified Swift strain hardening coefficient
n'	=	Ludwik strain hardening coefficient
P	=	load applied
Q	=	activation energy of diffusion
r	=	radius
s	=	seconds
t	=	heating time
T	=	temperature
V	=	volume
$\bar{v}$	=	average dislocation velocity
W	=	work done

Greek symbols

$\dot{\gamma}$ = shear strain rate

ϵ = strain

ϵ_e = engineering strain

ϵ_o = material constant

ϵ_{neck} = strain to the start of necking

ϵ_{frac} = strain to fracture

$\dot{\epsilon}$ = strain rate

Ψ = structure function

κ = Boltzman constant

ρ_m = density of mobile dislocations

σ = true stress

σ_e = engineering stress

σ_o = material constant

τ = shear stress

LIST OF EQUATIONS

1: $$\sigma = K\epsilon^{n}$$

2: $$\sigma = \sigma_0 + K\dot{\epsilon}^{n'}$$

3: $$\ln(d\sigma/d\epsilon) = \ln(k'n') + (n'-1)\ln\epsilon$$

4: $$\epsilon = \epsilon_0 + C\sigma^{n''}$$

5: $$\ln(d\sigma/d\epsilon) = (1 - n'')\ln\sigma - \ln(Cn'')$$

6: $$\sigma_{\epsilon,T} = C_2\dot{\epsilon}^{m}$$

7: $$\sigma_{\epsilon,T} = k\dot{\epsilon}^{m}\sigma^{n}$$

8: $$m = \partial(\ln\sigma)/\partial(\ln\dot{\epsilon})$$

9: $$\epsilon_{neck} = n/(1 - 2m)$$

10: $$\epsilon_{frac} = bm^2[Do/lo]$$

11: $$\epsilon_{frac} = \exp[2m/(1 - m)] - 1$$

12: $$m = \frac{\ln(\sigma_2/\sigma_1)}{\ln(\dot{\epsilon}_2/\dot{\epsilon}_1)}$$

13: $$\dot{\gamma} = \psi \exp[-H(\tau)/\kappa T]$$

14; $$r = A\, t^{1/3}$$

15: $$\sigma = \sigma_e(1 + \epsilon_e)$$

16: $$\epsilon = \ln(1 + \epsilon_e)$$

17: $$W = V\int_0^{\epsilon} \sigma\, d\epsilon$$

CHAPTER ONE

GENERAL INTRODUCTION

Chromium is an essential alloying element in the stainless steel industry, where addition of a minimum of eleven percent of this material to iron can impart to the resulting alloy a degree of resistance to corrosive chemical attack. It was against a background of vast South African reserves of chromite ore and of an ever expanding market for corrosion resistant materials world-wide that Middleburg Steel & Aloys (PTY) Ltd. embarked on a programme to develop a high strength, low alloy, chromium steel which could be a cost effective replacement for coated mild steel. Due to the expense of chromium as an alloying element, however, it was planned that the cost benefit over low carbon steel would be achieved through the possible lowering of maintainance costs resultant from improved corrosion resistance. In addition to this, the consequence of an increased strength to weight ratio over mild steel could realize an economical materials saving through the use of reduced component cross sections.

The steel which has been developed is designated 3CR12 (which is an acronym for Chromium Containing Corrosion Resisting 12% Chromium). It is a titanium stabilized, weldable and corrosion resistant steel with a composition close to that of the ferritic AISI type 409. However, after annealing between two intercritical temperatures, an intrinsic fine grained, dual-phase microstructure categorises 3CR12 as a duplex steel.

The term "duplex" or "dual-phase" refers to a class of low alloy steels which was originally developed to satisfy an increasing need, primarily in the transportation industry, for new high strength materials which permit weight reduction without sacrificing formability or dramatically increasing costs. Their microstructure consists of a ferrite matrix with a finely

dispersed second phase of martensite. The martensite acts as a load carrying constituent in the soft ferrite matrix; the matrix supplies the system with the essential ductility.

When annealed within the dual-phase temperature range, 3CR12 exhibits the good formability, ductility and toughness combinations associated with these types of steel. This, together with a high work hardening tendency, good scaling resistance up to 700°C, useful mechanical properties up to 550°C and the added advantage of being corrosion resistant, has made 3CR12 an attractive steel for use as a high strength, light weight structural material for fabricational applications in industry. Extensive use for 3CR12 has been found in corrosive and high wear type mining environments and recently the South African Railways have specified the use of 3CR12 in their construction programme for electrification masts.

1.1 THE PROBLEM

Southern Cross Steel, a division of Middleburg Steel and Alloys and South Africa's sole manufacturer of stainless steel, are producing sheets of 3CR12 in their Middleburg plant by a continuous hot-rolling process. Heated to temperatures close to 1200°C, the steel is fed through a Tippins Single Stand Steckel Mill at rates of up to two hundred metres per minute (photo 1.1). A typical reduction in one pass is of the order of twenty-five percent, which corresponds to a strain rate of approximately twenty per second in the direction of rolling.

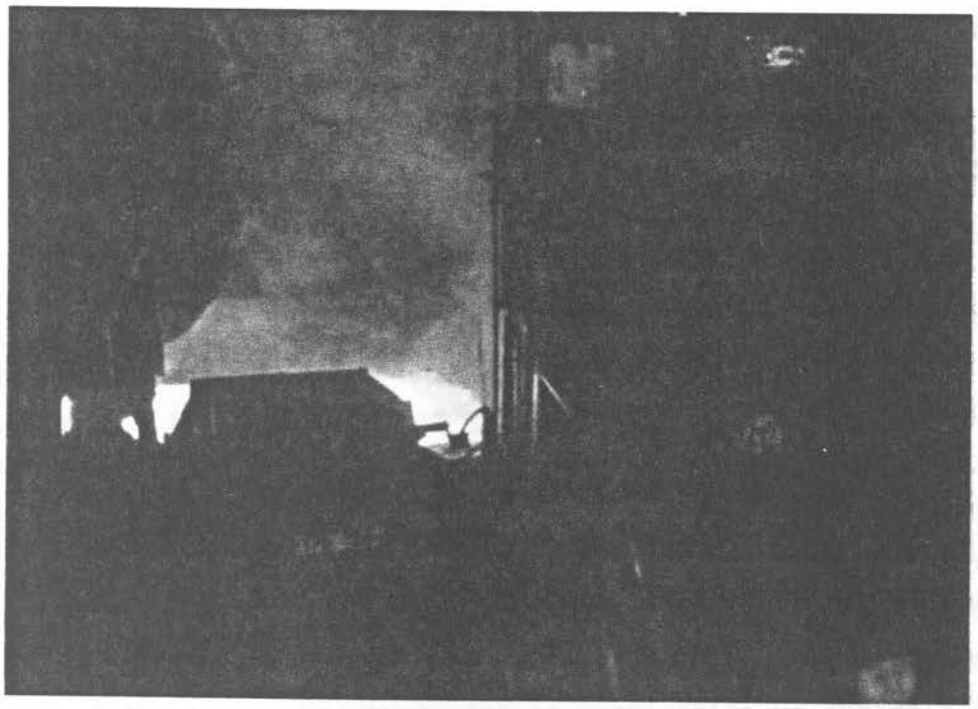

Photo 1.1 3CR12 being fed through the Steckel Mill at Southern Cross Steel.

Even at high temperatures where the steel is relatively maleable, this remarkably high deformation rate requires an enormous energy input. Information relevant to 3CR12's plastic forming behaviour at forging temperatures and at these high straining velocities is thus being sought which can predict the most economical rolling conditions for its production. In order to achieve this, an attempt has been made to gain an insight into its high temperature mechanical properties, strain rate sensitivity and deformation mechanisms.

1.2 OBJECTIVES

The objectives of this dissertation are outlined briefly to give direction to the discussion which is to follow.

Primarily, work was to be done in order to gain detailed information on the mechanical behaviour of 3CR12 alloys. Variables to be studied were to include temperature (25 - 1200°C), variation in nickel concentration (0.6 and 1.2%) and strain rate (between 10^{-1} and 10^{-4} s^{-1}) to quantify their effect on properties such as the yield and tensile strengths, strain to fracture and the energies associated with deformation. Particular interest was to be displayed in the actual deformation modes of the steel, together with an examination of the role that inclusion particles play in the initiation of fracture.

In order to carry out the above, a tensile testing system had first to be designed and constructed which could adequately cope with the experimental parameters mentioned.

CHAPTER TWO

A SURVEY OF THE RELATED LITERATURE

2.1 3CR12

2.1.1 Metallurgical Lineage

Refering to the binary iron-chromium equilibrium diagram (Fig. 2.1), it can be seen that chromium acting as a ferritising agent, restricts the occurrence of the γ-loop to the extent that above 13% Cr, the binary alloys are ferritic over the whole temperature range.

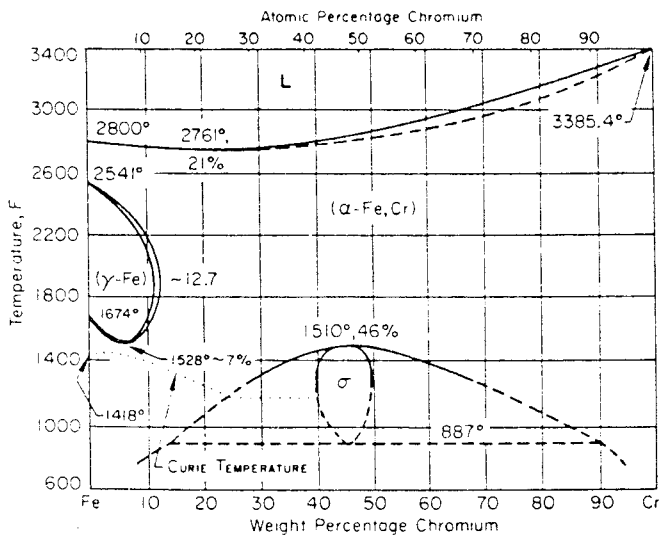

Fig. 2.1 The Fe-Cr equilibrium diagram

It will be noted, however, that between 12% and 13% Cr there is a narrow region where both α and γ phases co-exist and on quenching from this region, a dual-phase microstructure consisting of martensite and ferrite can be obtained. The γ-loop is extended to higher chromium levels by the addition of austenitising agents such as carbon and nickel, which also have the effect of

widening the dual-phase field. However, by a careful balance of alloying elements, it has been possible to retain a microduplex structure in 3CR12 at the limiting 12% chromium level so vital for corrosion resistance. Table 2.1 gives the chemical composition limits for 3CR12 which are very close to those for AISI type 409.

C	N	Ni	Mn	Si	P	S	Cr	Ti
0.03 max	0.03 max	1.6 max	1.5 max	1.0 max	0.03 max	0.03 max	11-12	4(C+N) min

TABLE 2.1: CHEMICAL COMPOSITION PERCENTAGE LIMITS FOR 3CR12.

2.1.2. Resumé of 3CR12 development

3CR12, being a relatively new steel, has enjoyed the attentions of numerous metallurgical laboratories who, under contract to Middelburg Steel and Alloys, have been conducting research over the past number of years into its structure, properties and behavioural characteristics. A prototype field testing programme has also been instituted (Southern Cross Laboratories, 1981) to determine the suitability of 3CR12 in a wide range of applications and to obtain corrosion performance data under various conditions. Ideal testing sites for the testing of a corrosion resisting steel were found in the South African gold and coal mining industries where, by nature of their operation, vast amounts of material are consumed annually by corrosion and wear. It should be noted at this stage that although the basic composition of 3CR12 has remained the same, prototype compositions have varied, mainly in chromium, titanium and nickel concentrations during the steel's development, thus producing some range in observed properties of 3CR12 in general. Two

composition types have emerged: one containing 0,67% nickel and refered to as 3CR12 and another with 1,2% nickel, notated 3CR12Ni. The term "3CR12 alloy" will therefor be used when no particular reference to nickel content is intended.

Ball and Hoffman (1981), using optical and electron microscopy, established the microstructures and recrystalisation characteristics of 3CR12 alloys after heat treatments between 600°C and 900°C and found that nickel content, titanium addition and heat treatment were important parameters affecting the transition temperatures. Considerable effort is presently being spent in quantifying the effect that additions of titanium, in particular, and final rolling temperature have on the annealing response and microstructure of 3CR12 and 3CR12Ni.

In her work on the phase equilibria and microstructure of 3CR12 alloys, Protopapas (1983) mapped equilibrium phase diagrams as a function of nickel content and annealing temperature. Her work indicated dual-phase regimes comprising austenite (martensite on cooling) and ferrite (Fig. 2.2) and demonstrated the influence of thermal history and alloying element additions on the resultant microstructure and consequent mechanical properties.

Schaffer (1983) determined the time temperature transformation diagrams for the transformation between austenite and ferrite in 3CR12 and investigated the factors controlling these transformations. The 3CR12 alloy used in his study did not become fully austenitic above the Ae_3, but lay in the nose of the gamma loop of the Fe-Ni phase diagram. Figure 2.3 shows the rate of isothermal transformation from ferrite to austenite. It can be seen that at 860°C at least 10^3 seconds (~5 hours) is required before an equilibrium volume fraction of austenite is

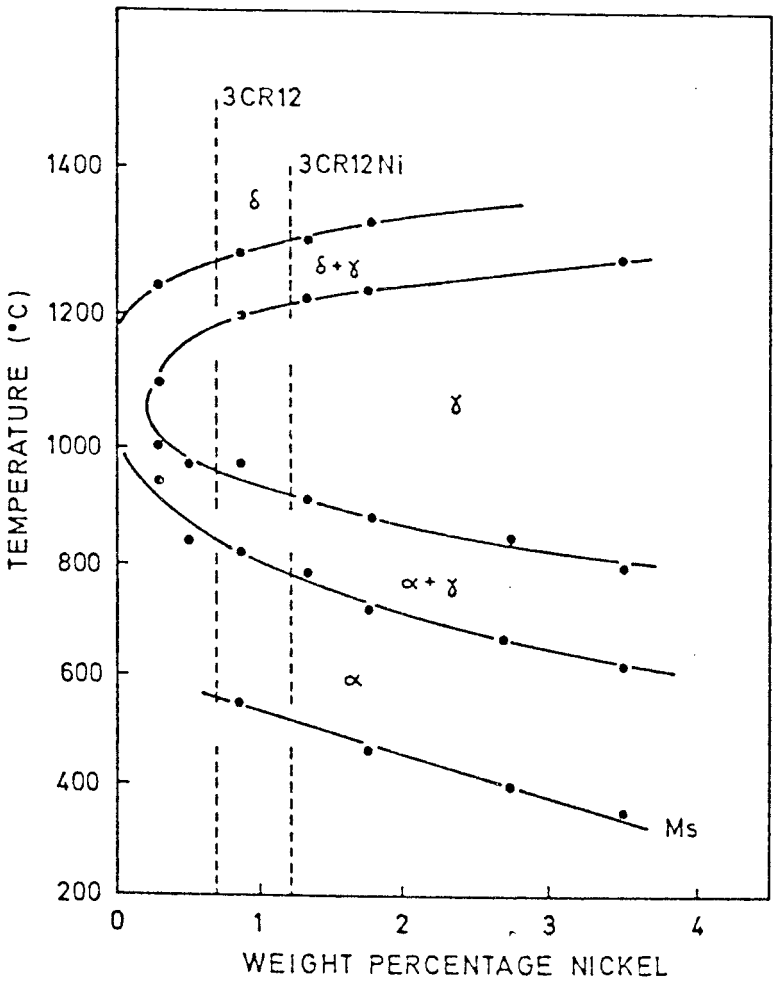

Fig. 2.2 The iron-nickel phase diagram for 3CR12 alloys containing 12% chromium (Protopappas, 1983).

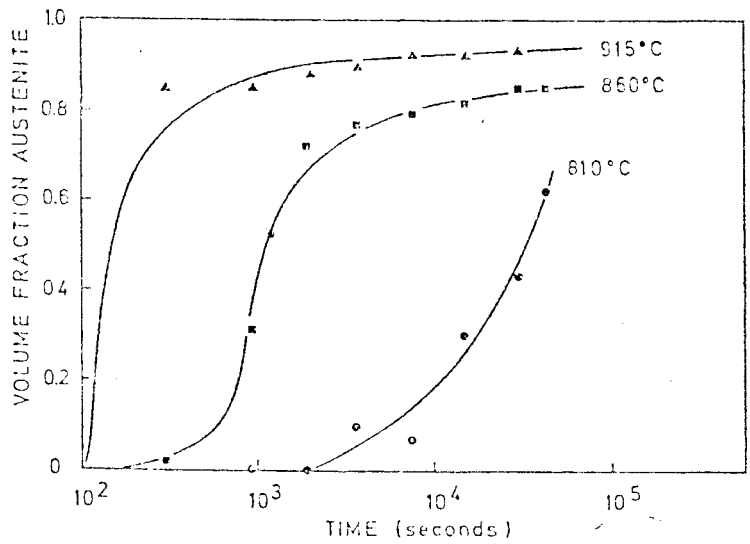

Fig. 2.3 Volume fraction austenite vs time for isothermal soaking temperatures for 3CR12 containing 0.67% nickel (Schaffer, 1983).

reached.

Work into the weldability of 3CR12 showed that the material is weldable up to 12mm gauge using AWS 300 series filler electrodes and normal welding procedures. (Southern Cross Laboratories, 1981). Modified Straus corrosion tests carried out on weldments showed no sign of intergranular attack, although the martensite in the heat affected zone was more prone to corrosion. The Department of Materials Science and Metallurgical Engineering, University of Pretoria (1981) investigated the susceptibility of 3CR12 to stress corrosion cracking (SCC) under low stress conditions. In a 3.5% NaCl and 0.5% acetic acid solution saturated with H_2S, 3CR12 tended to fail in an intergranular fashion. Sondenberg (1980), showed that SCC occurred in $MgCl_2$ solutions at temperatures above 100°C and that stress accelerated pitting could occur under active conditions in 3.5% NaCl.

Noël (1981), doing in-situ wear tests under low stress and mildly corrosive conditions in mining environments, found that 3CR12 had a relative wear resistance three times that of mild steel. Taking into account the relative wear/cost ratio of the steel, he proposed that 3CR12, due to its dual-phase nature and inherent corrosion resistant properties, was a viable material for usage in shaker conveyors in the South African mining industry.

In their work on the mechanical properties of the dual-phase 3CR12 and 3CR12Ni alloys, which included high temperature tensile tests in the range 25°C to 900°C, Ball and Hoffman (1981) concluded that the stable, fine grained structure obtained by annealing at temperatures between 675°C and 750°C is responsible for the attractive strength, toughness and forming properties which they had measured. They considered, too, that the presence

of the duplex structure during any warm forming process would impart a very uniform state of plastic deformation to the steel. Evidence was found for superplasticity in the 3CR12Ni composition at 880°C, the existence of which has also been hinted at by the CSIR after their elevated temperature tensile tests (Southern Cross Laboratories, 1981). An interesting aspect relevant to warm forming was recognised at 300°C, where the minimum in elongation for both alloys existed. Stress strain curves for the tests at this temperature showed regular instabilities, suggesting dynamic strain ageing during deformation. It was also found that the yield and ultimate tensile strengths dropped off rapidly in the temperature range from 300°C to 700°C.

Numerous impurity particles of various sizes and degress of coherency have been reported by both Ball and Hoffman (1981), and Schaffer (1983), occurring within grains and along grain boundaries. These precipitates are rich in titanium and phosphorous and some, in addition, contain nickel. Analysis by Ball and Hoffman indicated that cuboid titanium carbo-nitride particles are frequently associated with aggregates of sulphides and that these are often arranged in stringers. The latter point is discussed further in section 2.4.

2.2 THE PLASTIC RESPONSE OF MATERIALS WITH SPECIAL EMPHASIS ON DUAL-PHASE STEELS

The need to lower automobile vehicle weights and thereby improve fuel economy has become greater over the past decade and has resulted in much interest being generated in steels which can allow significant weight reductions without the sacrifice of strength. High strength low alloy (HSLA) steels can offer increased strength to weight ratios over normal plain carbon steels, but their limiting factor is their inherently low formability. To overcome this disadvantage, steels having a

ferrite matrix and containing a less deformable martensite phase have been developed which combine the conflicting requirements of both high strength and improved formability.

Concurrent development of these dual-phase steels occurred in Japan and the United States with publications and research having increased exponentially since their inception in the mid 1970's. Various developments have made it clear, however, that a dual-phase microstructure by itself does not automatically guarantee good formability, but that the objective of good formability combined with high strength can be accomplished by proper control of steel composition and process variables. The key to the improved ductility/formability of dual-phase steels lies in their inherent resistance to localised deformation i.e. necking (Demeri,1981). This ability to resist necking, which is reflected by attainment of larger uniform elongations in the tensile test, is primarily due to their capacity to work harden at very high rates.

Matsuoka and Yamamori (1975) were amongst the first investigators to show that intercritical annealing to produce a ferrite martensite microstructure can result in a high work hardening rate, decreased yield strength and continuous yielding characteristics, when compared to conventional HSLA steels. The following dual-phase steel mechanical property requirements have been proposed (Rashid, 1977):

* No yield point (a smooth continuous stress strain curve).
* A 0.2% offset yield strength of 345 ± 39.5MPa.
* At 2 to 4% strain, a flow stress of 520 to 550 MPa.
* An ultimate tensile strength of 620-655 MPa.
* A total elongation of $>$27%.

To explain the deformation behaviour of dual-phase steels, the composition of the steel, the mechanical properties of the constituent phases and the distribution of the hard phase must be considered. Several deformation models have been proposed, but little success has been enjoyed in fully understanding their structure property relationships. Tomota and Kuroki (1976) have developed equations describing the mechanical behaviour of dual-phase structures, taking into account the internal stresses produced by inhomogeneous strain distribution. Mileiko (1979), using continuum mechanics has assumed strain is equal in both phases and that stresses are partitioned by the rule of mixtures. The mechanical properties of the composite is thus intermediate between those of the two constituents. Applying Ashby's work hardening theory to dual-phase steels (Ashby, 1966), which predicts that the work hardening rate is dependent on the ratio f/d where f is the volume fraction second phase and d is the mean second phase island diameter, Balliger and Gladman (1981) found that during tensile deformation, martensite islands do not deform at all until strains well in excess of the maximum uniform strain have been reached.

Authors such as Tomota and Kuroki (1976), Davies (1978) and Rigsby, Abraham, Davenport, Franklin and Pickens (1979) have found that the tensile strength of these materials increases as the volume fraction of martensite increases, although the ductility decreases at the same time. Improved fracture behaviour is obtained when the martensite islands are unconnected, when the martensite ferrite interface is free from precipitates to act as stress raises and when the hard phase is relatively tough (Koo and Thomas, 1977). In his review paper on the deformation aspects of speciality steels, Smallman (1983) reports that the optimum volume fraction of martensite is about 20% for sheet forming operations. In agreement with Davies (1978) , Marder (1982) states that the effect of martensite on the UTS and elongation to fracture can be represented by linear equations for martensite volume fractions up to 0,65.

Rizk and Bourell (1982) investigated the contribution that dislocation density has on the strength of dual-phase steels. During the martensite transformation, with its associated volume expansion, an abundance of new free dislocations is formed in the ferrite matrix. The movement of these dislocations and their interactions with each other affect the yield strength of the composite and enhance the mechanical strength of these steels by a factor that is a function of the martensite volume fraction. Szewczyk and Gurland (1982) found that ductile fracture in dual-phase steels begins with void formation at martensite/ferrite interfaces. Large inclusions and martensite banding were also found to affect the fracture process.

2.2.1 Work hardening and the analysis of work hardening behaviour.

While the low observed initial flow stresses of metal crystals can be shown to be due to slip by movement of dislocations, it is equally true that the subsequent work hardening arises when dislocations are hindered in their movement through the crystals, so that a higher stress must be imposed to continue the deformation. Many obstacles to dislocation movement exist, the most important being other dislocations, grain and sub-grain boundaries, solute atoms, particles and regions of second phase.

The work hardening behaviour in steels is commonly analysed with the aid of idealised mathematical stress-strain equations. The most common is the Hollomon equation:

$$\sigma = K\epsilon^{n} \qquad (1)$$

where σ is true stress, ϵ is the true plastic strain, K the strength coefficient and n an empirical constant known as the work hardening parameter. Analyses of various steels, however, have shown that a unique work hardening parameter, n, does

often not describe the deformation behaviour at all levels of strain. Investigators such as Cribb and Rigsby (1979) and Ramos, Matlock and Kraus (1979) have analysed dual-phase steels with widely ranging tensile strengths, at room temperature and in terms of a three stage work hardening behaviour. Earlier than this, Bergström and Aronsson (1970) found that alpha-iron demonstrates a "double-n" behaviour up to 600°C at various strain rates.

Stage behaviour and its rationale have been most fully developed for the face centred cubic metals such as copper and nickel, as cited by Cribb and Rigsby (1979), where four different deformation behaviours in the polycrystalline materials can be distinguished. In the initial accommodation stage (up to~0.001 strain), multiple slip starts in the largest grains and spreads to neighbouring grains. This stage ends and stage I begins when all grains are deforming by multiple slip. Stage I thus differs fundamentally from easy glide in face centred cubic single crystals and is terminated at ~0.01 strain. Stage II and stage III in polycrystalline materials are both analogous to the corresponding single crystal stages; in stage II slip occurs locally on a single system with hardening interaction from secondary systems. For face centred cubic single crystals at elevated temperatures, the slope of stage II work hardening is relatively independant of temperature (Honeycombe, 1968) although in polycrstals the effect of grain growth and change in the elastic modulus with increased temperature can affect the work hardening in this stage. Stage III is characterised by dynamic recovery. Essentially then stage III progressively negates the hardening which takes place during stage II. With increase in test temperature the recovery mechanism becomes more significant and the transition from stage II to stage III becomes indistinguishable.

Monteiro and Reed-Hill (1971) claim that the work hardeninging analyses for steels within limits defined by work hardening transition strains, can be better expressed by the Ludwik equation:

$$\sigma = \sigma_{\circ} + K'\epsilon^{n'} \qquad (2)$$

where the parameters K' and n' can be obtained by a Jaoul-Crussard type analysis. In this type of analysis the derivative of (2) is taken to give:

$$\ln (d\sigma/d\epsilon) = \ln (K'n') + (n'-1) \ln\epsilon \qquad (3)$$

and a plot of $\ln d\sigma/d\epsilon$ vs $\ln\epsilon$ yields the value of n' and K' independent of the existence of $\sigma_{\circ}$. Ramos et al (1979) showed that this analysis can delineate several distinct stages of strain hardening in the deformation of dual-phase steels and a similar analysis based on the Modified Swift equation:

$$\epsilon = \epsilon_{\circ} + C\sigma^{n''} \qquad (4)$$

which is differentiated to obtain:

$$\ln(d\sigma/d\epsilon) = (1-n'') \ln\sigma - \ln(Cn'') \qquad (5)$$

has been used by Cribb and Rigsby (1979) who, by utilising a log $d\sigma/d\epsilon$ vs $\log\sigma$ plot, determined the parameters C and n" for various stages of strain in these materials.

Characteristics of the various regions of a Jaoul- Crussard plot are related schematically to the shapes of the corresponding stress strain curves in Figs. 2.4 and 2.5 (Matlock, Kraus, Ramos and Huppi, 1979). In Figure 2.4 a parabolic true stress-strain curve is shown. This corresponds to a straight line on a Jaoul-Crussard plot and is characterised by the constant n in equation (1) and n' in equation (2). The deformation behaviour shown in Fig. 2.4 is usually assumed to represent a material

which ideally deforms in a uniform manner. In figure 2.5, the stress strain-curve has been drawn to exhibit regions in which the curvature changes. For example, between points A and B the stress-strain curve is linear i.e. a constant strain hardening is assumed. The corresponding Jaoul-Crussard plot also exhibits distinct regions, labelled I, II, and III, in which the region between points A and B represents constant strain hardening. In practice, however, the changes in curvature of stress-strain curves are more continuous than shown in figure 2.5 and stage II deformation is usually characterised by a negative slope instead of a horizontal line.

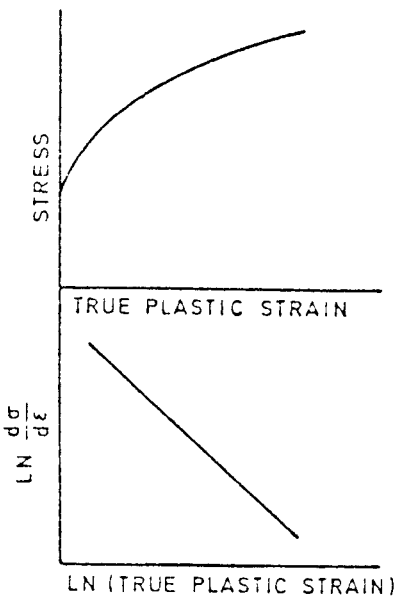

Fig. 2.4

A schematic comparison of a parabolic stress-strain curve with the corresponding linear Jaoul-Crussard plot.

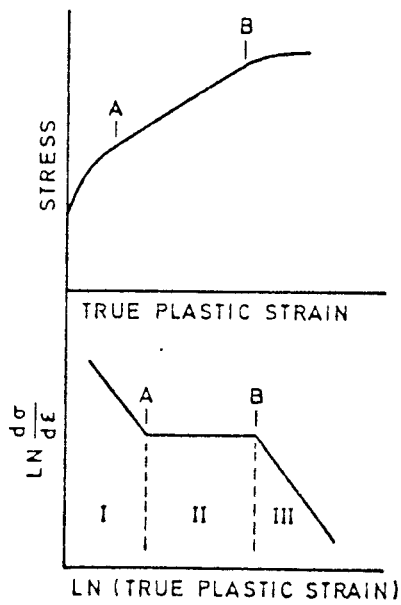

Fig. 2.5

A schematic comparison of a stress-strain curve in which the strain hardening behaviour varies with strain with the corresponding Jaoul-Crussard plot exhibiting, by variation slope, distinct stages in strain hardening.

A similar stage by stage deformation sequence to that outlined for face centred cubic polycrystalline material have been proposed for dual-phase steels at room temperature by Cribb and Rigsby (1979). Their assumptions are outlined below and are based on experimental data acquired through the use of a Jaoul-Crussard type analysis of both equations (2) and (4).

Stage I: This stage results from the homogenous deformation of the ferrite matrix produced by mobile dislocations surrouding the uniformly distributed martensite particles.

Stage II: In this stage the rate of decrease in work hardening is attenuated. This stage is associated with constrained deformation of the ferrite caused by the presence of rigid martensite. With increased amounts of martensite the distinction between stage I and II becomes less apparent.

Stage III: This stage begins with the formation of dislocation cell structures after which further deformation is probably governed by cross-slip and dynamic recovery processes in the ferrite and yielding of the martensite.

The effects of strain rate and temperature on the work hardening of an 18% Cr 8% Ni austenitic stainless steel have recently been investigated by Monteiro, Le May and de Almeida (1981), who, by using the Jaoul-Cryssard analysis of the Ludwik equation found that the stress-strain curves of this steel consistently displayed stage II and III work hardening behaviour over the temperture range from 100°C to 800°C and that this behaviour is influenced markedly by dynamic strain ageing at lower temperatures and by dynamic recovery processes above 600°C.

2.2.2 Superplasticity

The term superplasticity has been used to describe extraordinary elongations obtained during tensile deformation of polycrystalline materials. In general, superplastic materials exhibit low resistance to plastic flow in specific temperature and strain rate regions, their strengths being highly strain rate sensitive.

Interest in superplasticity has been centred mainly on non-ferrous alloys and little work has been carried out on ferrous materials. Ball and Hutchison (1969) found that grain boundary sliding is the predominant mode of deformation during extensive superplastic flow of the aluminium zinc eutectoid alloy. They state that for superplasticity to be displayed in a material, it is necessary that the grain size is stable and smaller than the dislocation cell structure that would normally form under conditions (temperature and stress) of deformation. One ferrous alloy which exhibits superplastic flow is a highly alloyed duplex stainless steel containing 26% Cr-6.5% Ni and this has been reported to give tensile elongations exceeding 600% at 900°C (Smith, Norgate & Ridley, 1976). The prerequisites for fine structure superplasticity have been extensively reviewed by Sherby, Caligiuri, Kayali and White (1981). With regard to dual-phase steels, however, authors such as Ball and Hoffman (1981) and Honeycombe (1981) agree that in these materials, where by suitable thermo-mechanical treatment it is possible to obtain very fine microduplex structures, typically ~5 microns, superplasticity can be exhibited.

Superplastic metals and alloys generally exhibit a strain rate sensitivity exponent of the order $m = 0.5$ which can correspond to elongations in excess of 400%.

2.2.3 Strain rate sensitivity

Strain rate sensitivity has for some time been recognised as an important ingredient in the development of superplasticity in metals. Various attempts have been made to relate the flow stress for a given strain and temperature to strain rate. This material characteristic is usually defined by a strain rate sensitivity exponent, m, such that:

$$\sigma_{\epsilon,T} = C_2\dot{\epsilon}^m \qquad (6)$$

where $\sigma_{\epsilon,T}$ is the flow stress at some strain and temperature, $\dot{\epsilon}$ is the strain rate and C_2 is a temperature dependent constant. (McGregor Tegart, 1966). Rai and Grant (1975), however, proposed the modified phenomenological equation as a substitute for (6) where:

$$\sigma_{\epsilon,T} = k\dot{\epsilon}^m\epsilon^n \qquad (7)$$

and n is the work hardening parameter in equation (1) and k is a temperature dependent constant. Hamilton and Ghosh (1980) cite the definition of m as essentially being:

$$m = \partial(\ln\sigma)/\partial(\ln\dot{\epsilon}) \qquad (8)$$

This would follow from (7) if the material under consideration was perfectly viscous (i.e. n = o).

The physical reason for the importance of m has been described by investigators such as Hart (1967), and Ghosh (1977) who have shown that the strain rate sensitivity relates to the capability of a material to resist necking. Most steels show an increase in flow stress as the strain rate is increased and this increase has an important influence on the formation of a neck. Necking occurs when strain hardening becomes low and the increase in flow stress, due to strain hardening, becomes less than the increase in stress due to the decrease in cross sectional area with

further strain. As a neck begins to form, the local strain rate inside the neck increases, but a high strain rate sensitivity will cause sufficient increase in flow stress to delay the formation of the neck, thus resisting plastic instability i.e. as m increases, so does the resistance to necking and higher elongations are a consequence.

Various methods using applied mechanics and a macroscopic approach have been applied to predict the elongation to fracture of materials that fail by necking. Four of these are outlined below:

(a) Rossard (1966) has shown that the strain at the start of necking is given by:

$$\epsilon_{neck} = n/(1-2m) \qquad (9)$$

His theory would predict infinite plasticity at m = 0.5 provided n has a finite positivie value.

(b) Morrison (1968) indicated that the dimensions of the tensile specimen will dictate the total elongation observed and showed that:

$$\epsilon_{frac} = bm^2[D_o/l_o] \qquad (10)$$

where ϵ_{frac} is the strain to fracture, b is a material constant and D_o and l_o are the initial diameter and length of the sample respectively.

(c) Burke and Nix (1975), using a finite element approach, showed that:

$$\epsilon_{frac} = \exp[2m/(1-m]-1 \qquad (11)$$

2.2.3.1 Determination of m values

While the mechanical influence of strain rate sensitivity is understood, the experimental measurement of the parameter is controversial. Values for m are usually determined by a differential cross-head speed technique (Hedworth & Stowell, 1971). This entails, in principle, deforming a specimen at one strain rate $\dot{\epsilon}_1$ and noting the stress (σ_1), then changing the strain rate to $\dot{\epsilon}_2$ and measuring the second flow stress (σ_2). Utilizing this method in conjunction with equation (8), m can be calculated as follows:

$$m = \frac{\log (\sigma_2/\sigma_1)}{\log (\dot{\epsilon}_2/\dot{\epsilon}_1)} \qquad (12)$$

McGregor Tegart (1966) suggests another method whereby if expression (6) is obeyed then a plot of log true stress and log true strain rate will give a straight line of slope m.

The techniques for determining m of superplastic alloys by the strain rate change method were reviewed by Hedworth and Stowell (1971a) and were found to be inconsistant and unsatisfactory. A major difficulty arises because, as superplastic materials are not viscous, the flow stress is a function of both strain and strain rate; such procedures then result in values of m which are strain dependent and not accurately definable. Rai and Grant (1975) point out another problem encountered with accurate measurements of m at high temperatures. Due to the effect of grain growth, the flow stress is influenced as a direct result of increased grain size which is accentuated at elevated temperatures and which affects the observed m value. Change in grain size can thus be introduced as another variable in the strain rate relationship at high temperatures.

2.3 HIGH TEMPERATURE DEFORMATION

2.3.1 Recovery, recrystallisation and deformation models

Recovery and recrystallisation have traditionally been considered as mechanisms of restoration through which cold worked metal returns partially or completely to its condition prior to working. These mechanisms usually operate when a metal is annealed at a high homologous temperature for a period of time. Annealing is usually carried out in the absence of an applied stress or strain in which case the recovery or recrystallisation that occurs is termed static. However, recovery and recrystallisation can also take place under dynamic straining conditions. When metals are deformed under both hot-working and creep conditions, strain hardening is counter-balanced by the concurrent softening processes of dynamic recovery and recrystallisation. See for example the review by R. Lagneborg (1972). During dynamic recovery, mechanisms such as cross slip, climb and node unpinning permit the dislocations to unravel from hardened networks and annihilate each other. During dynamic recrystallisation, new grains nucleate and grow; they deform as they grow, however, with the result that recrystallisation takes place again and again. During dynamic recrystallisation, dynamic recovery occurs in both old and new grains.

When metals are deformed to high strains at high temperatures and constant strain rate, the structure observed on rapid quenching after deformation depends on the particular metal studied. A well deformed substructure consisting of dislocation tangles is found in aluminium and ferritic alloys which is similar to that observed after creep and is indicative of recovery as the operative softening process. In contrast, in copper, nickel and austenitic alloys, the original grains are replaced with nearly equi-axed recrystallised grains by dynamic recrystallisation which is the operative softening process in these cases (Luton & Sellars, 1969).

During transient high temperature tensile testing there are four experimental variables, any three of which can be considered independent. These are the applied or developed stress, the temperature, the strain rate and the initial structure. The term structure refers to three different aspects of the microstructure: the mean sub-grain size, their misorientation and the average dislocation density within the sub-grains. Under steady-state conditions, these three aspects of the microstructure are frequently functions of the steady-state stress, so that there are only two independent experimental variables i.e. temperature and strain rate.

Various models have been proposed to describe the behaviour of these variables under hot-working conditions. The most general relationship for the shear strain rate under transient and steady state high temperature deformation is of the following type (Jonas, 1969):

$$\dot{\gamma} = \psi \exp[-\Delta H(\tau)/\kappa T] \qquad (13)$$

where ψ is a function of the structure, the activation enthalpy ΔH is a function of the applied shear stress, κ is the Boltzman constant and T has its usual significance. Luton and Jonas (1970) have proposed a strain rate equation, extended to high temperatures, and based on the Orowan relation where $\dot{\gamma} = \rho_m b \bar{v}$. The symbol ρ_m represents the density of mobile dislocations, b the Burgers vector and $\bar{v}$ the average dislocation velocity. The value $\bar{v}$ is considered to be temperature and stress dependent, the form of which is obtained from rate theory.

2.3.2 The flow curve at high temperatures

In their review paper, Immarigeon and Jones (1974) outlined the stress-strain relationships for recrystalised metals deformed at

high analogous temperatures. When increasing the load at constant nominal strain rate, an interval can be noted during which the plastic strain in the sample increases from zero to the approximate strain rate of the test. During this interval the state of stress in the material rises rapidly, although not as steeply as it does at conventional temperatures. Typical loading slopes during initial loading range from ~E/50 at high temperatures and low strain rates to ~E/5 at relatively low temperatures and high strain rates where E is the Young's modulus of the material at room temperature.

Yield drops are not, in general, observed in high temperature tensile tests and the "yield" stress is defined instead in terms of a plastic strain offset. In the plastic region of the stress strain curve, the work hardening rate gradually decreases with increased strain. It should be noted that in the case where the flow rate is limited by dynamic recovery processes alone, the work hardening rate should not become negative, but in practice, however, the flow curve usually drops off as a result of dynamic recrystallisation. In the case of the flow curve under conditions of dynamic recovery, all the softening processes involve single dislocations which are anihilated in individual events. During dynamic recrystallisation dislocations are annihilated in large numbers through the migration of high angle boundaries. By this means, the lattice in which these dislocations reside is destroyed and replaced by a new and substantially perfect one in a single integral operation. As mentioned above, the occurrence of dynamic recrystallisation modifies the apearance of the flow curve produced at constant strain rate. At high strain rates in the hot-working range, the flow stress rises to a maximum at the peak strain, then work softens to a steady state value intermediate between the yield stress and peak stress. A comparison of the two types of curves can be seen in figure 2.6.

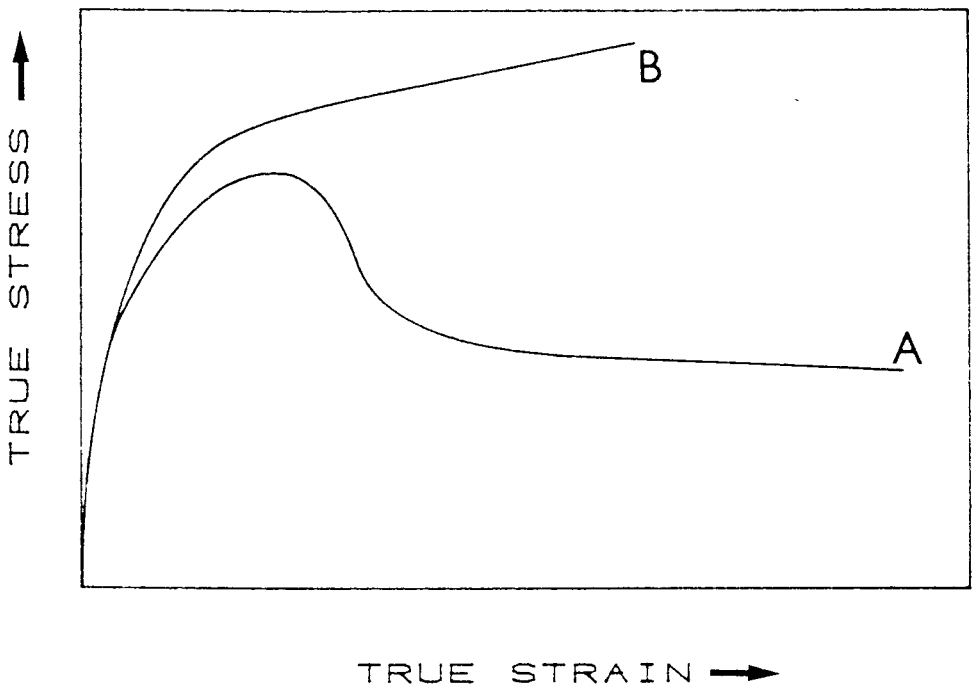

Fig. 2.6 (A) Typical stress-strain shape for dynamic recrystallisation: strain hardening to a peak stress followed by work softening to a steady state level. (B) Under dynamic recovery the work hardening rate remains positive.

2.3.3 The temperature dependence of the elastic response of metals

Although the elastic modulus is a material constant, being essentially a measure of the interatomic bond strengths, it is a parameter which varies with temperature. As the temperature of a metal increases, so does its elastic response, with a corresponding decrease in the elastic modulus.

To give an idea of this variation, Routbourt, Reid, Fischer and Dever (1971) are quoted who, using ultrasonic techniques, measured the elastic moduli of a iron-silicon alloy in the temperature range from 77K to 1300K. The relationship of the shear modulus c' is shown in figure 2.7.

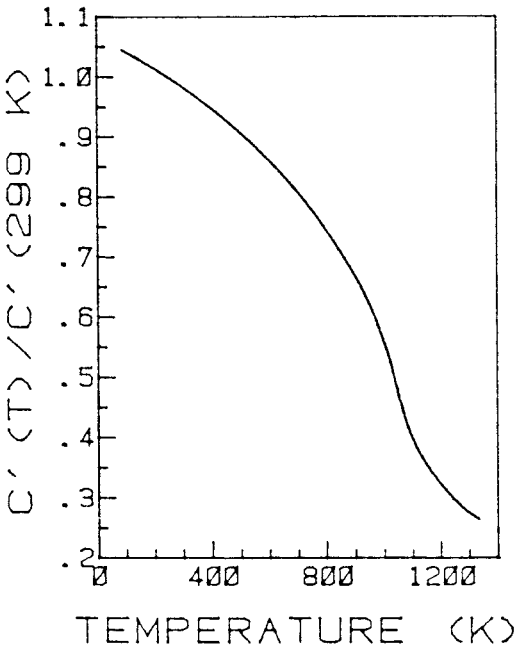

Fig. 2.7 The temperature dependence of the elastic modulus c' for Fe + 5.86 Si. (Routbourt et al,1971)

2.4 THE ROLE OF TITANIUM IN STEEL

As has been previously mentioned (Table 2.1), 3CR12 alloys contain titanium, which is specifically added as a stabilizing element in an attempt to reduce the risk of intercrystalline corrosion and thus improve the weldability. This element has a greater affinity for carbon than for chromium, binding the carbon as titanium carbide and thereby suppressing the formation of chromium carbides. This inhibits the sensitisation of the steel. The amount of titanium generally considered necessary for

effective stabilization is four times the carbon content, but this, however, represents an over-simpliciation. As titanium nitride and titanium carbide are structurally identical, with the carbon or nitrogen occuppying octahedral positions in the lattice, the constituent is often called titanium carbo-nitride. Microstructurally, pure TiN is observed as a very well defined bright yellow cubic particle and with the addition of carbon, a maize colour develops. (Peckner and Benstein, 1979.)

Titanium is used for the precipitation hardening of some HSLA steels under controlled conditions, but the precipitation of large titanium carbo-nitrides can lead to poor tensile properties through void nucleation and growth. These particles can also adversely affect surface finish and if arranged in stringers can induce lammelar tearing, decreasing formability. For these reasons titanium precipitation has been a subject of concern in this project. It is therefore pertinant to discuss briefly the physical properties of titanium carbides and nitrides and then to consider their precipitation behaviour, with specific reference to the banding phenomenon mentioned in section 2.1.2.

2.4.1 Properties of titanium carbo-nitrides

The phase TiC has a face centred cubic structure which is stable over the range $TiC_{0.28}$ to $TiC_{0.8}$ and thus exhibits a wide range of stochiometry. The maximum melting point of the compound TiC is 3067°C. It is stable to hydrogenation up to 2400°C, but nitriding will occur in an atmosphere of nitrogen at 1000°C-1300°C.

Titanium nitride is the only compound in the titanium nitride system. The hexagonal phase of alpha-titanium dissolves nitrogen up to the composition $TiN_{0.23}$ and the cubic titanium nitride phase exists over a wide range of compositions starting from $TiN_{0.42}$. Its melting point is 2950°C.

The free energy data for the two compounds is given in Table 2.2 and can be compared to that of chromium carbide.

REACTION	$-\Delta H^\circ_{298}$	ΔS°_{298}	TEMPERATURE RANGE °C
$2Ti(s) + N_2(g) = 2\ TiN(s)$	80 400	7.4	25-1700
$Ti(s) + C(s) = TiC(s)$	43 900	5.8	25-1700
$23/6\ Cr(s) + C = C_{23}C_6(s)$	98 300	151.8	25-1400

TABLE 2.2: STANDARD FREE ENERGY DATA.
(McGammon, 1971).

2.4.2 The precipitation of the carbides and nitrides of titanium.

Generally, titanium nitride particles precipitate in steels in cubic or rectangular prism shapes of varying sizes. Matsuda and Okumura (1978), in their work on the dissolution, coalesence and precipitation, found that the growth of TiN particles due to coalescence followed the empirical equation:

$$r = At^{1/3} \qquad (14)$$

where r : the radius of the TiN particle
t : heating time
A : a constant which varies with the composition of the steel

Equation (14) indicates that the volume (r^3) of a particle increases in proportion to the heating time. Growth is presumed to take place by an Oswald ripening type process with an activation energy of diffusion of Q = 100kcal/mol.

The melting points of both TiC and TiN are extremely high and these compounds are stable at elevated temperatures as discussed under section 2.4.1. However, Matsuda and Okumura found that partial dissolution of titanium carbo-nitride particles takes place at ~1250°C into the austenite phase and that subsequent heating in the temperature range between ~650°C and ~1150°C can cause re-precipitation. Fast heating rates (as found in welding) tended to cause the TiN particles to partition into rows or bands within the austenite and the larger the mean particle size, the more frequent was the banding phenomenon. It was noted, too, that TiN particles in the rows were larger than those distributed randomly in the matrix. Also, a precipitation free zone tended to exist on either side of the row. Matsuda and Okumura explain this phenomenon qualitatively, assuming microscopic non uniformities in the concentrations of solute titanium and nitrogen which effect their time temperature precipitation relationship.

Banding of TiC precipitates on a much smaller scale has been noted by investigators such as Honeycombe (1976), Freeman and Honeycombe (1977) and Follstaedt (1980) where titanium has been used to produce high strength steels. The procedure used has been to dissolve the maximum soluble titanium and carbon in the austenite phase, rapidly quench and then isothermally transform the alloy to ferrite at temperatures of 600°C - 800°C. This produces a banded structure (interphase precipitation) of fine TiC precipitates which are believed to form at the austenite ferrite interface as it propagates through the steel. Particle sizes vary according to the transformation temperatures due to precipitate ripening and vary from 5nm below 750°C to a reasonably coarse 110nm at higher temperatures.

2.5 THE ROLE OF PARTICLE INCLUSIONS WITH RESPECT TO VOID FORMATION DURING DEFORMATION

Inclusions play an important role in the tensile fracture process

of steels where, in certain instances, the crack nucleation mechanism and not the crack growth is the most important variable. Microcracks are often found at inclusion matrix interfaces (Baker & Charles, 1972) and (Rozovsky, Hahn, and Avitzur, 1973) and dimple failues provide the most convincing evidence for the importance of second phase particles in fracture mechanisms (Klevebring, Bogren & Mahrs, 1975).

Using pure iron containing silicon inclusion particles, Klevebring et al have investigated the critical inclusion size for nucleation of microcracks at inclusions during such forming operations as rolling and forging. Under these conditions cracks are expected to propagate during loading and thus limit the material's mechanical properties. They found that the effect of temperature upon the critical inclusion size to cause microvoid formation is small within the ferrite and austenite regions, but that the critical size in austenite is some 30 percent greater than in ferrite. They reported this critical inclusion size to range from 2.5 to 3.5 microns for the temperature region from 600°C to 1200°C. Smith et al (1976) have noted that during the high temperature deformation of a duplex stainless steel, cavities tended to form at both the titanium carbo-nitride particles, at austenite/ferrite boundaries and also at titanium carbo-nitride/matrix interfaces. Density measurements showed that the total volume of cavities increased with increasing strain, decreasing strain rate, increasing temperature and increasing grain size. They maintained that premature tensile failure was thus due to the nucleation, growth and coalescence of these cavities. The formation of cavities during superplastic deformation of steels has also been reported by Humphries and Ridley (1974).

The growth and coalescence of voids leading to the final ductile failure of steels has been dealt with in detail from a plasticity viewpoint by Rice and Tracy (1969) and McClintock (1971), who elucidated the importance of negative pressures in the flow field

in hastening the plastic hole expansion process. On the experimental side there have been conflicting observations reporting the nucleation of cavities from inclusions anywhere from immediately upon yielding to after the development of very large plastic strains. Cavities have been reported to nucleate both on interfaces by tearing the inclusion away from the surrounding ductile matrix or by the cracking of non deformable inclusions (Argon & Safoglu, 1975). Cox and Low (1975) found that titanium carbo-nitrides in 4340 steel often shatter upon plastic straining of the surrounding matrix and that larger particles tend to shatter at lower strains. This is substantiated by Argon et al who examined TiC inclusions at the bottom of dimples and showed them to fragment by cleavage.

CHAPTER THREE

SYSTEM DESIGN AND SET-UP

The tensile test is a source of quantitative information concerning the relationship between extension and the applied stress when a material is deformed and it is a widely used method for determining the mechanical properties of steels. As has been mentioned, the stress-strain relationships under tensile loading are markedly affected by temperature and strain rate, and a primary aim for this project was to set up and commission a testing rig which could suitably enable the investigation of these two parameters with respect to the mechanical properties of 3CR12 alloys.

3.1 THE FURNACE

In order that tests could be carried out in the temperature range from 25°C to 1200°C, the design and construction of a small electric furnace was necessitated, which could heat a tensile specimen when in position on the testing rig.

A platinum, 10% Rhodium alloy was selected as the most suitable material for the high temperature element. In order to remain within the specified current loading range for Pt/Rh wire, and because the operating voltage is proportional to element length, (restricted in this case), 110V was found to be the optimum voltage for an estimated required output of 600 watts. The element was thus designed to the specifications listed in Table 3.1.

Max operating temperature:		1200°C
Power	:	600 watts
Operating voltage	:	110 volts
Current at 1200°C	:	5.5 amps
Resistance at 1200°C	:	20 ohms
Current density	:	0,00021 amps per "
Pt/Rh wire gauge	:	27
Element length	:	5.8 m

TABLE 3.1 FURNACE ELEMENT SPECIFICATIONS

As the furnace was to operate under vacuum, it was necessary to maintain the overall porosity of the unit to a practical minimum, thus reducing a problem of degassing which occurs during pump-down. The degassing problem was ultimately overcome by using a complete stainless steel casing and a dense pyrophylite insulating inner core, around which the element was wound. The design detail is shown in Fig. 3.1.

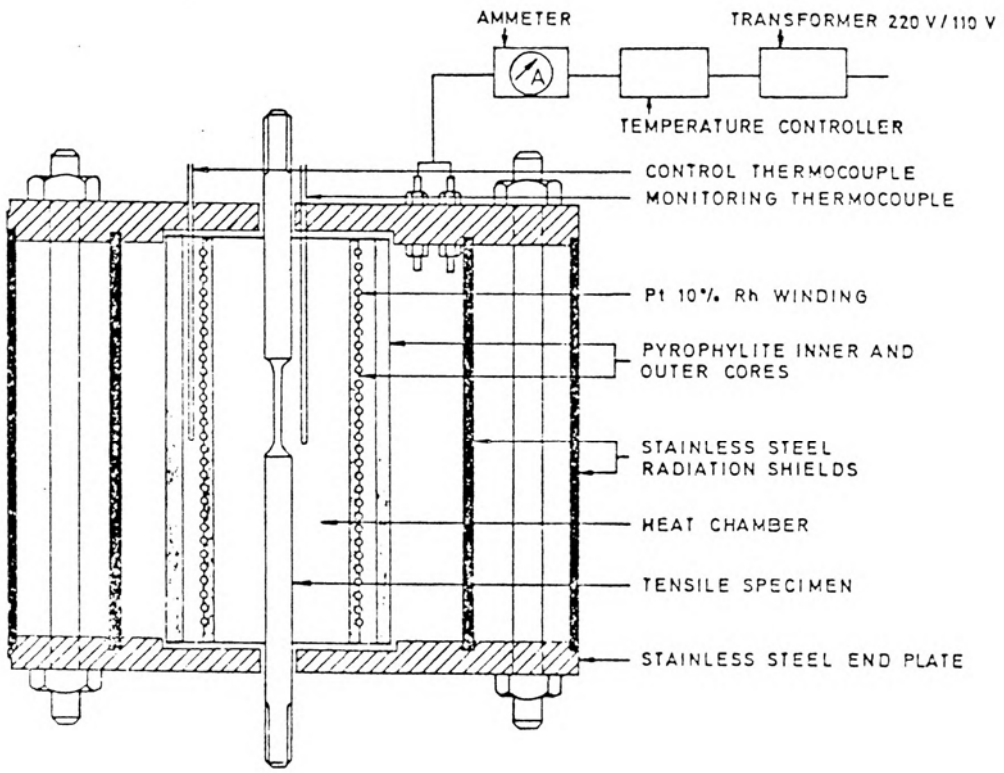

Fig. 3.1 Design detail for the furnace

The furnace was controlled by a thyristor-governed temperature controller with a variable power output. This facility allowed for control of current, reducing the damaging surge which is associated with the reduced resistivity of the platinum/rhodium element at low temperatures and on start-up.

A chromel-alumel thermocouple acting as the thermal controller was situated as close as possible to the element windings, thus minimising temperature fluctuation (a maximum of 5°C at 1200°C). A second thermocouple was located in near proximity to the specimen, enabling measurement of the ambient temperature experienced by the specimen. Photo 3.1 shows the furnace in place on the testing rig.

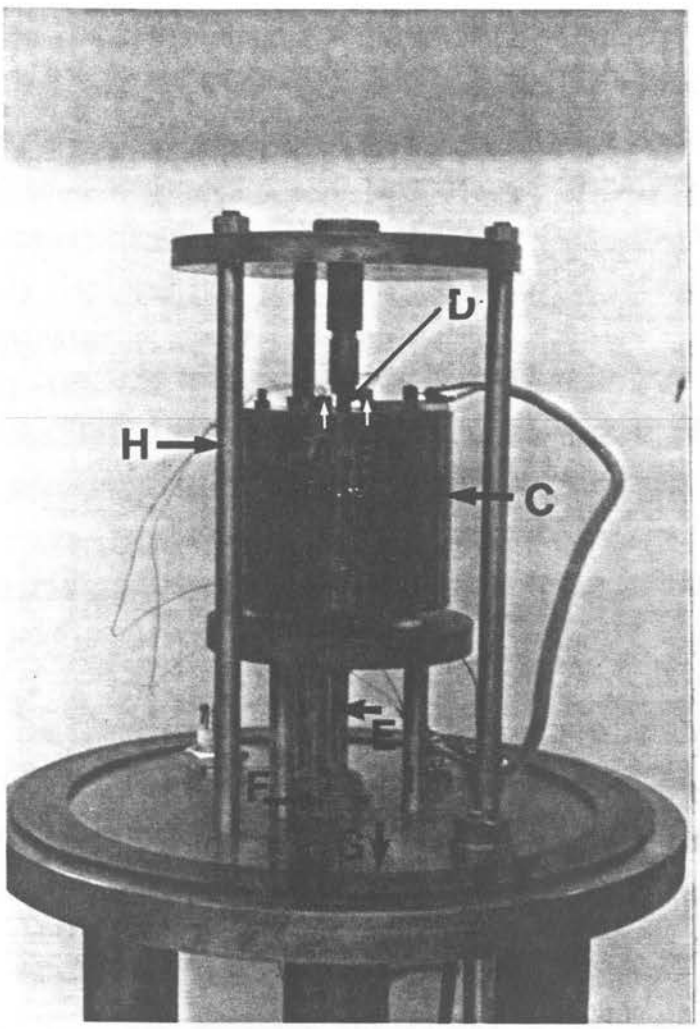

Photo 3.1 The furnace in position on the testing rig. The following can be noted:

A & B : Thermocouples
C : Furnace body
D : Tensile specimen screwed into position and encompassed by the furnace
E : Actuator rod
F : Actuator rod vacuum seel
G : Vacuum seel for vacuum chamber
H : Test rig load frame

3.2 THE LOAD FRAME AND TESTING RIG

An ESH servo-hydraulic testing machine was used. This machine lends itself well to the type of tests which were carried out as factors such as cross-head speed, load and displacement can be monitored to a high degree of precision. Also, dynamic changes in cross-head speed during a tensile test can be easily and effectively implemented by using the machines sophisticated ramp input generator. However, by nature of its servo-hydraulic operation, the ESH is not a very stiff machine and stiffness calibrations had to be carried out in order to compensate for load-chain compliance effects.

A testing rig which could house a tensile specimen under vacuum was designed and constructed to fit onto the ESH load frame (photo 3.3). Testing under vacuum had two distinct advantages: Firstly, the vacuum achieved (less than 10^{-4} torr) minimised the oxidation of the specimens at the high test temperatures encountered and, as scale on the gauge length surface influences stress-strain characteristics, more accurate measurements could be made. Secondly, the fracture surface of the specimen, after cooling from elevated temperatures under vacuum, was left contamination free, enabling subsequent microscopic examination.

The vacuum chamber itself consisted of three parts, as it had to be easily removed and readily reassembled for each test. The circular wall of this chamber was divided into a transparent section for experimental observation and a round mild steel section, this giving the chamber extra height. The top consisted of an aluminium disc, through which the connecting pipe to a vacuum diffusion pump passed. The top also accommodated a purge valve, vacuum gauge and needle valve, providing the facility for the introduction of controlled atmospheres into the testing system. The chamber, as a whole, seated onto the base of the testing rig, which, in turn, housed a vacuum seal through which

the actuator rod could pass.

3.3 DATA CAPTURE AND PROCESSING

In the initial stages of the project, the need for an advanced data capture and computer processing system became evident and outlined below are the motivations behind the development of such a facility, together with some problems encounted before its final implementation.

During a tensile test, load-extension data was outputted from the ESH servo-hydraulic tester in terms of a voltage on a 10V scale and a hard copy of this could be recorded by a chart recorder. This raw data, however, had then to be processed in order to attain an accurate stress-strain curve for the test. Individual extension points selected at exerimentally significant intervals along the curve were corrected for load chain compliance effects experienced at their particular load. Thus corrected, the data could then be arithmetically converted to stress-strain values and replotted. To manually carry out the replotting procedure from a voltage/voltage chart recorder curve was an arduous task subject to errors. Especially at high strain rates, where the duration of a test was of the order of 0.5 sec, chart recorder traces became compressed due to chart speed limitations. Direct manual measurements taken from curves were subject to inaccuracies, because of resolution difficulties. These resolution problems became especially real when a small curve was obtained due to poorly selected full scale settings, a fault which was easily made when a test range constituted widely varying loads and elongations.

A facility was thus augmented for automatically digitising load-extension co-ordinates recorded on chart paper to minimise copying errors and enable fast and efficient computerised analysis. This system, although an improvement on the manual

one, was however, very clumsy as it involved the physical translation of analogue data (chart trace) to digital data via a computerised digitising tabloid with its limited resolution. Also, it did not allow accurate erudification of the raw data curve, as the curve had still to be traced by hand using a digitising cursor. A second system was then developed to capture data directly from the servo-hydraulic tester, eliminating the need to use a chart recorder altogether. On-line data could then be acquired directly by using a data logger for slow strain rate tests and by a transient recorder which enabled high speed data acquisition. Subsequent manipulation and plotting was carried out by a mini computer. Fig. 3.2 outlines diagramatically the final testing system employed.

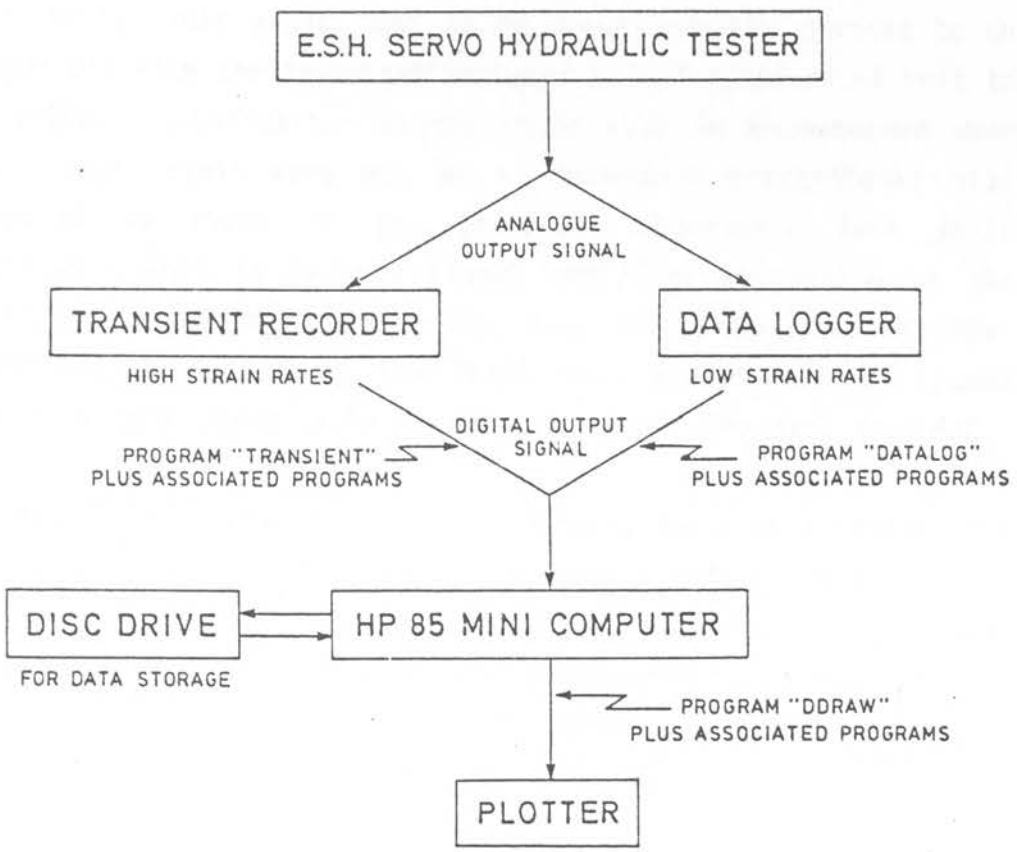

Fig. 3.2 Diagrammatic representation of the testing system.

3.3.1 Transient recorder

A DL902 Transient Recorder was used. This is a digital instrument designed to capture single shot events and to present them for continuous display on a cathode ray oscilloscope. A plug-in card position is incorporated which allowed the unit to be interfaced with a mini computer. The instrument features two independent signal inputs each of which can digitise and store waveforms at a maximum sample rate of 1MHz per channel, each signal being recorded simultaneously in a 2048 bit sample memory. Thus, a tensile test lasting say 0.25s could be recorded as 2048 load extension points, each at a time interval of 2.4×10^{-4} of a second.

Using the transient recorder in the system, however, was not without its drawbacks. Output from the ESH, operating on a -10 volt to +10 volt scale, had to be electronically divided to be compatible with the transient recorder's full scale of -5 volt to +5 volts. Quantisation errors could also be encountered when test input levels were not of a reasonable proportional size compared to those of the transient recorder's full scale settings. This is because signal amplitude resolution in the DL902 is limited to 1 part in 256, i.e. if the maximum test input level was only half of the DL902 full scale setting, signal amplitude resolution would be reduced to only one part in 256/2.

The transient recorder was used to conduct tests at a strain rate of 10^{-1} per second, which was the fastest practical rate at which the ESH could operate. At faster cross-head speeds, the signal output tended to become contaminated excessively with electrical noise. Photo 3.2 shows the DL902 with the result of a high strain rate test displayed on the oscilloscope above it. Both a load and an extension curve can be seen as a function of time. The two channels are then combined by a mini computer and manipulated to give a resultant stress-strain curve.

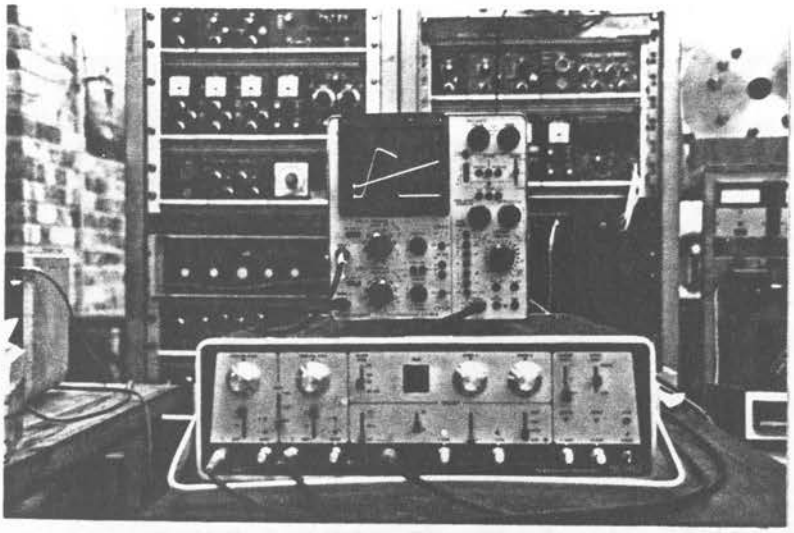

Photo 3.2 The DL902 transient recorder and oscilloscope displaying the result of a high strain rate test.

3.3.2 Data Logger

A Hewlett Packard 3497A Data Acquisition Unit was used for tests carried out at slow strain rates ranging from $10^{-2}s^{-1}$ to $10^{-4}s^{-1}$. As the output from the ESH is essentially an analogue signal, the data logger was used primarily as an analogue to digital converter, changing the output signal to an acceptable digital form for compatibility with the HP85 computer.

3.3.3 HP85 and peripherals

An HP85 mini computer together with a disc drive and plotter were used to process and plot the results of the tensile tests.
Photo 3.3 shows the testing system set up. Note that the data logger (G) in this instance was being used instead of the transient recorder.

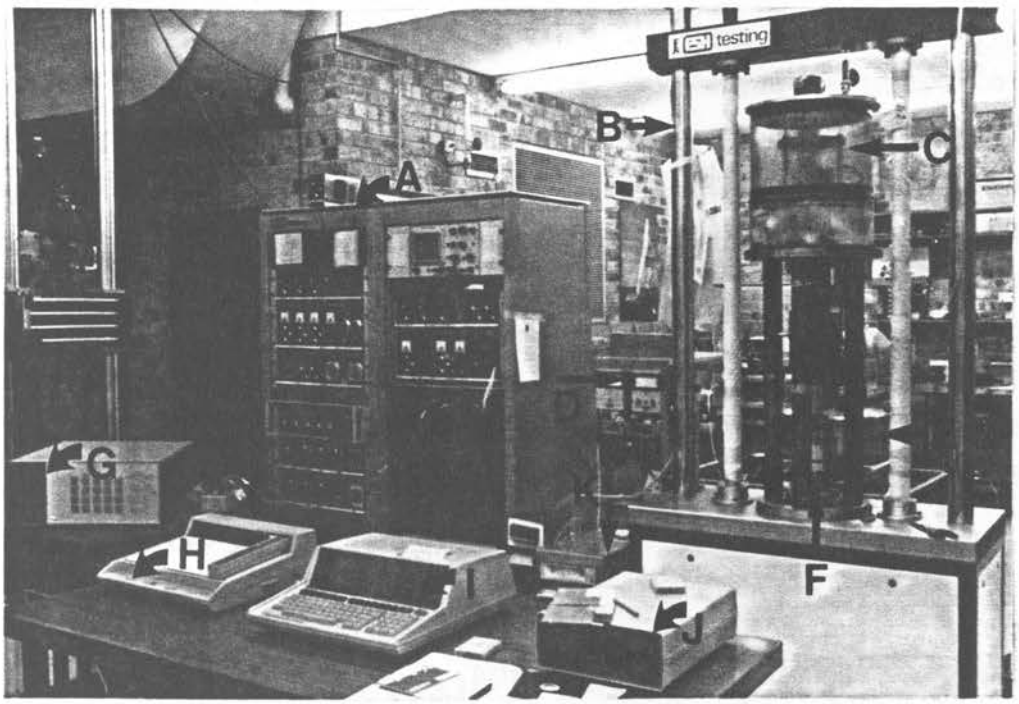

Photo 3.3 The testing system

A: ESH control unit
B: Load frame
C: Testing rig and furnace contained within the vacuum chamber
D: Vacuum pump controls
E: Rotary and diffusion vacuum pumps
F: Actuator
G: Data logger
H: Plotter
I: HP85 mini computer
J: Disc drive
K: Temperature controller

3.3.4 Computer software

Considerable effort was spent in writing the BASIC software to enable the successful interfacing of the ESH to the computer

system mentioned above, and to carry out subsequent processing and analysis of results. The useful ability of the HP85 to chain together or concatenate different programs while retaining selected data stored in common, allowed the program system to be divided up into manageable segments, each with its own specific task. This had the double advantage of both retaining a certain amount of logical order within the computer software system, together with allowing a system to be created, which under normal circumstances would have been far too large to fit into program memory as one integral program. Summarised descriptions of the software, together with the actual code written for the acquisition, processing and analysis of the output from the ESH are presented in Appendix I.

Fig. 3.4 illustrates a typical stress-strain output plot for a high temperature tensile test in which load-elongation data has been converted to true stress-true strain values, using the conventional formulae:

$$\sigma = \sigma_e \ (1 + \epsilon_e) \qquad (15)$$

$$\epsilon = \ln \ (1 + \epsilon_e) \qquad (16)$$

Here σ is true stress, ϵ is true strain, σ_e is engineering stress and ϵ_e is engineering strain. The program also provided the facility to plot load-elongation or engineering stress-strain values.

The programmed analysis allowed for the measurement of the following values:

(i) UTS and corresponding strain
(ii) 0.2% proof stress and its corresponding strain
(iii) maximim strain to failure.

Area analysis done by a numerical integration process allowed areas under the curve to be measured. Three separate areas were considered: these were from zero stress, zero strain to (a) the yield point (b) the UTS strain and (c) the strain to failure.

Although discussed later, it may be pointed out that the true stress-true strain plot can only be considered accurate to the strain at which necking is initiated. Beyond this strain equations (15) and (16) become invalid.

No corrections were made for thermal expansion of the tensile specimen at elevated temperatures as the difference in the true stress and strain attributable to this was felt to be insignificant. To validate this assumption the calculated true stress and strain values corresponding to the ultimate tensile strength (UTS) obtained for 3CR12 at 1000°C (equations 15&16), were compared with the values obtained by incorporating an assumed thermal expansion co-efficient correction factor of 14 x 10^{-6} per °C (as for type AISI 409 stainless steel). The difference in the two stress and strain values amounted to 2% at the UTS and the engineering strain to fracture differed by only 1.2%.

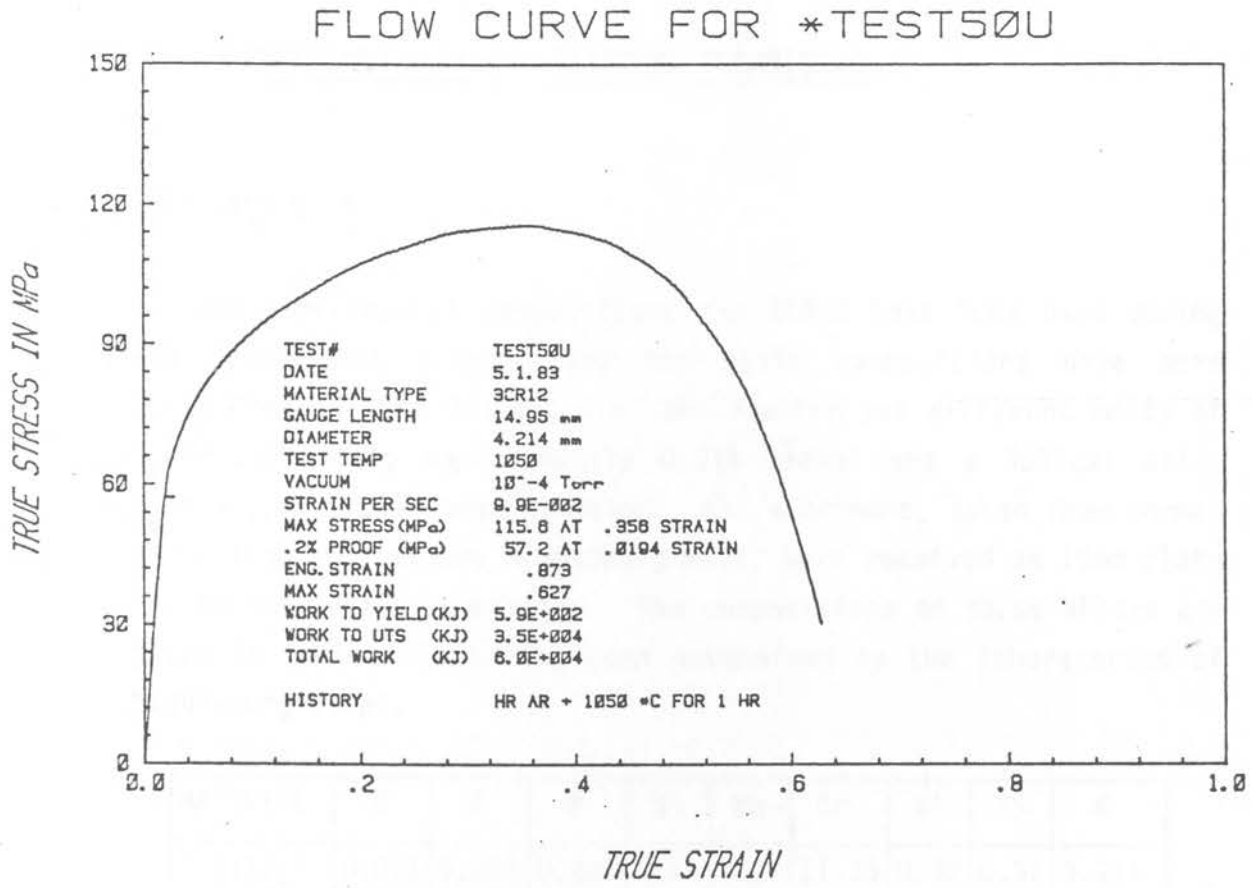

Fig. 3.3 A typical computer output result from a high temperature tensile test.

CHAPTER FOUR

EXPERIMENTAL AND ANALYTICAL TECHNIQUES

4.1 MATERIALS USED

Various experimental compositions for 3CR12 have been used during its development program and two basic compositions have been considered in this project i.e. two similar yet different melts of 3CR12 containing approximately 0.63% nickel and a 3CR12Ni alloy with a 1,2% Nickel concentration. All specimens, taken from normal production runs at the Middleburg mill, were received as 10mm plate in the hot-rolled condition. The compositions of these alloys are given in Table 4.1, having been determined by the laboratories of Middleburg Steel.

MATERIAL	C	S	P	Si	Mn	Cr	Ni	Ti	N
$3CR12_{(1)}$	0.021	0.019	0.023	0.51	1.21	11.36	0.62	0.31	0.014
$3CR12_{(2)}$	0.024	0.015	0.020	0.53	1.91	11.19	0.67	0.31	0.011
3CR12Ni	0.027	0.011	0.022	0.47	0.90	11.71	1.21	0.23	0.019

TABLE 4.1 : COMPOSITION OF TEST ALLOYS (WT%).

During the initial stages of the project alloy $3CR12_{(1)}$ was used in the as-received condition which was first subjected to a one hour anneal at 1000°C to remove the residual hot-rolled microstructure. However, following a request by the sponsors of this work, all later experimentation was conducted on $3CR12_{(2)}$ and 3CR12Ni. Both of these alloys were examined in the hot-rolled condition (HRAR: hot-rolled, as-received).

It can be noted that the composition of $3CR12_{(1)}$ and $3CR12_{(2)}$ are very simmilar. To avoid confusion $3CR12_{(1\&2)}$ will normally be referred to simply as 3CR12 and the subscripts will only be retained in certain instances to link experimental work with a particular material.

4.2 METALLOGRAPHY

Microstructural examination of the test alloys after various heat treatments was carried out using conventional metallographical techniques. In an attempt to optimise the etching procedure for 3CR12 alloys, a 10% aqueous oxalic acid solution heated to 60°C was found to perform well as an electrochemical etchant at an 11 volt potential difference. Etching times were kept constant at 35 seconds for 3CR12Ni and 25 seconds for 3CR12. Oblique lighting was used on a Reichert "MeF2" optical microscope to enhance the surface relief of the steel. A diamond pyramid micro-hardness tester was used to determine the micro-hardness of different phases in order to differentiate between martensite and ferrite.

4.2.1 Specimen annealing furnace

All heat treatments were conducted in a vacuum furnace which allowed fine and accurate control of temperature.

4.2.2 Volume fraction analysis

The volume fraction of the martensite and ferrite was determined for $3CR12_{(2)}$ which had undergone various annealing treatments. This was performed by a point counting method described by Hilliard and Cahn (1961) and Hilliard (1968). An 11 x 11 graticule was applied 30 times to each specimen to give a 10% accuracy at the 95% confidence level.

4.3 BULK HARDNESS MEASUREMENTS

The bulk hardness of the 3CR12 alloys after various heat treatments was measured using a Vickers pyramid indentor at 30kgf. All values quoted are the averages from 5 individual indentations.

4.4 TENSILE TESTS

Using the testing rig described in Chapter 3, constant velocity tensile tests were carried out on as-received 3CR12 and 3CR12Ni in the temperature range from room temperature to 1150°C at nominal strain rates of between 10^{-4} and 10^{-1} per second. The cross-head velocity was calculated to provide the desired strain rate at the beginning of a test, but especially at high temperatures where elongations were large, the instantaneous strain rate tended to decrease with increasing strain. Prior to the implementation of the computerised system (Section 3.3) annealed $3CR12_{(1)}$ was tested at a strain rate of 10^{-3} per second. The curves for these particular tests were manually manipulated to give the true stress-true strain relationships after correction for load chain compliance effects.

The primary object in this section of work was to obtain a profile of the tensile characteristics in the temperature range mentioned above. Test temperature intervals ranged from approximately 100°C at lower temperatures to around 20°C at higher temperatures. All specimens were soaked at their test temperature for one hour to allow complete temperature equilibriation. In view of the consistancy of the results obtained and the time/cost factor involved to make and break the specimens, usually only one test was conducted at any specific temperature. However, the general nature of the high temperature testing was concomitant with repetition, especially when using the transient recorder (Section 3.3.1) where factors such as premature triggering and the choice of correct sampling time lowered the success rate of the tests. When there was doubt as to the validity of a result, confirmatory tests were carried out.

4.4.1 Tensile specimens

Lengths of $10mm^2$ square section were cut from as-received hot-rolled plate at 90° to the rolling direction and then machined to the required tensile specimen geometry. A problem was encountered with the choice of specimen dimensions for testing over the entire temperature range, as tensile strengths varied from around 40 to 1000 MPa. With the particular load cell employed, which had a maximum capacity of 5kN and a superimposed noise level of 1% of this, it was necessary to operate at the higher end of its scale to retain good resolution; at lower loads the noise level tended to mask true experimental results. The use of one specimen dimension could therefore favour only a single section of the test temperature spectrum, compromising the resolution in other areas of the range.

To overcome this difficulty, it was decided to employ one standard dimension for low and intermediate temperatures and a more substantial size for higher temperature tests. Owing to the high tensile strength of the 3CR12Ni alloy, received only after fairly extensive work had been completed on 3CR12, a third and still smaller dimension had to be introduced for room and low temperature experiments on this alloy. As the grain size of 3CR12 alloys is typically small (~10 microns in the dual-phase condition), size effects due to different specimen geometries were not assumed to be significant.

All three specimen sizes were homologous in size, machined such that the gauge length l_o= 3,545 x diameter. The specimens themselves had threaded ends to screw-locate directly onto screw type fittings on the tensile rig. Figure 4.1 gives their basic design and dimensions. Note the proportionately long grip length which alienates the screw grips from the hot zone of the furnace. The relatively small specimen diameters allowed good heat distribution within the specimen.

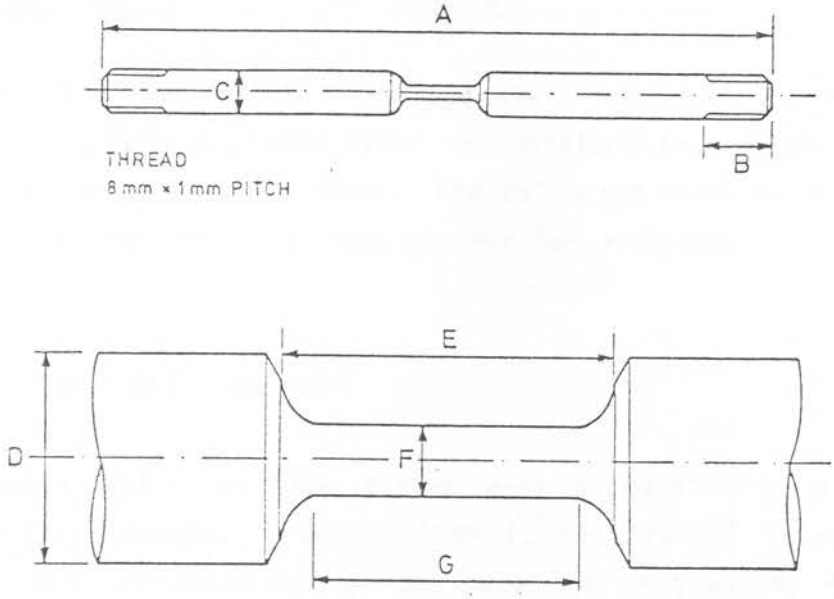

DIMENSION (mm)	CROSS SECTIONAL AREA mm^2			TOLERANCE (mm)
	3.1	6.0	14.0	
A	120	120	120	±1
B	9	9	9	---
D	8	8	8	+0.1 -0.1
E	9.09	11.78	16.96	+0.05 -0.00
F	2.00	2.76	4.22	+0.02 -0.02
G	7.09	9.78	14.96	+0.05 -0.01

Fig. 4.1: Tensile specimen dimensions

4.5 COMPUTER ANALYSIS OF TENSILE RESULTS

Chapter 3 in conjunction with Appendix I describes essentially how a true stress-true strain curve was obtained from tests at various temperatures and strain rates. The following section is devoted to explaining how this test data was further analysed.

4.5.1 Deformation energies

The areas under the flow curves were calculated by a numerical integration process (program DDRAW 1, section 1.7 in appendix I) which give an indication of the work per unit volume required to deform the specimens to particular strains. This can be explained by considering an incremental extension dl when a load P is applied. The incremental work done, dW is:

$$dW = P \times dl$$

$$= \sigma \times A \times dl = \sigma \times V \times dl/l_o$$

$$\text{therefore} \quad W = V \int_o^{\epsilon} \sigma \, d\epsilon \qquad (17)$$

The area thus gives the minimum work per unit volume for a change of shape by homogenous deformation. (McGregor Tegart, 1966.)

4.5.2 Work hardening characteristics

The computer program "WORKHARDEN" was developed to investigate the strain hardening behaviour of 3CR12 and 3CR12Ni alloys. Three empirical equations were used in the investigation:

(i) The Hollomon equation: $\sigma = K\epsilon^n$

(ii) The Ludwick equation: $\sigma = \sigma_o + K'\epsilon^{n'}$ which is differentiated to obtain:

$$\ln(d\sigma/d\epsilon) = \ln(n'k') + (n-1)\ln\epsilon$$

THE DEFORMATION CHARACTERISTICS OF A 12% CHROMIUM STEEL

BY

ANDREW BRINK

A thesis submitted to the Faculty of Engineering, University of Cape Town in fulfilment of the degree of Master of Science in Applied Science.

Department of Metallurgy and Materials Science,
University of Cape Town.

August 1983

(iii) The modified swift equation: $\epsilon = \epsilon_o + C\sigma^{n''}$ which is differentiated to obtain:

$$\ln (d\sigma/d\epsilon) = (1-n'')\ln\sigma - \ln(Cn'')$$

In the Holloman analysis, the constants K and n were determined from a plot of $\log\sigma$ versus $\log\epsilon$. A Jaoul-Crussard analysis, based on the Ludwik equation was used to determine the parameters n' and K', which were evaluated from a $\ln d\sigma/d\epsilon$ versus $\ln\epsilon$ plot. Similarly, an analysis based on the modified Swift equation utilizing a $\ln d\sigma/d\epsilon$ versus $\ln\sigma$ plot gave the n" parameter.

The nature of the testing environment prevented the dynamic measurement of the decrease in cross-sectional area during a tensile test and the original cross-sectional area had thus to be used for stress calculation purposes. Because of this, the calculated true stress and strain values became inaccurate after the initiation of necking due to the associated non-uniform reduction in cross-sectional dimension. Data analysis was therefore limited to the region of the curve from the yield point to the instability strain only.

4.5.2.1 Program "WORKHARDEN" logic

The modus operandi of the program written specifically to handle the above outlined analyses is given in Fig. 4.1.

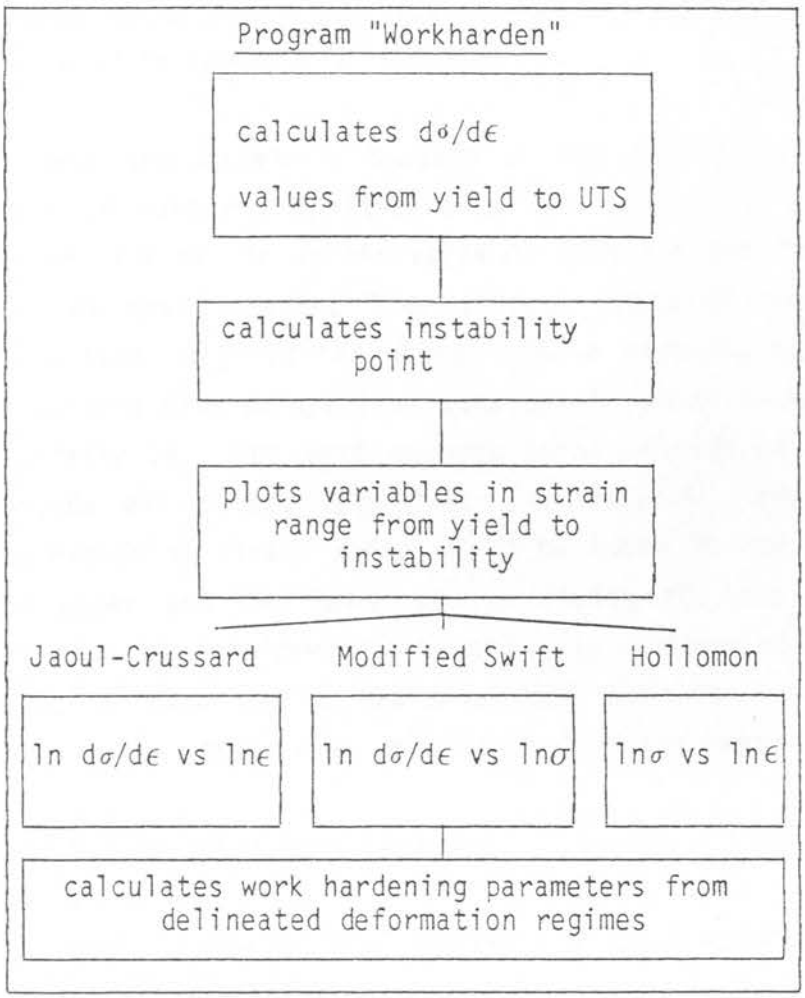

Fig. 4.2 Program skeleton for strain hardening investigation.

(i) Calculation of $d\sigma/d\epsilon$

The value $d\sigma/d\epsilon$ is essentially the slope of the tangent to the stress strain curve which varies in the strain range from yield to the UTS. Typically this region of the curve would consist of approximately 100 - 150 data points averaged as discussed in Appendix I, 1.5 (c).

To best approximate a tangent at any particular strain, a group of data points (typically 4-7) would be selected on either side of the strain value in question and the equation for the best straight line through these points would be calculated to yield the slope. Curve segments were defined to contain data points from data point number #x to #x + say typically 14. The next segment to be considered would then include all points from #x+1 to #x+1+14 etc. and the corresponding strain value would be taken as the average of the upper and the lower strain limits for the particular group being considered. In this way a continually varying group of data points would provide the rate of change of stress with strain over the required strain range.

(ii) Instability point computation

The point of instability, defined by the Considère criterion (Jonas, Holt & Coleman,1976) where $d\sigma/d\epsilon$ was taken as the intersection point of the true stress true strain curve with the curve of $d\sigma/d\epsilon$ versus strain. See Fig. 4.3.

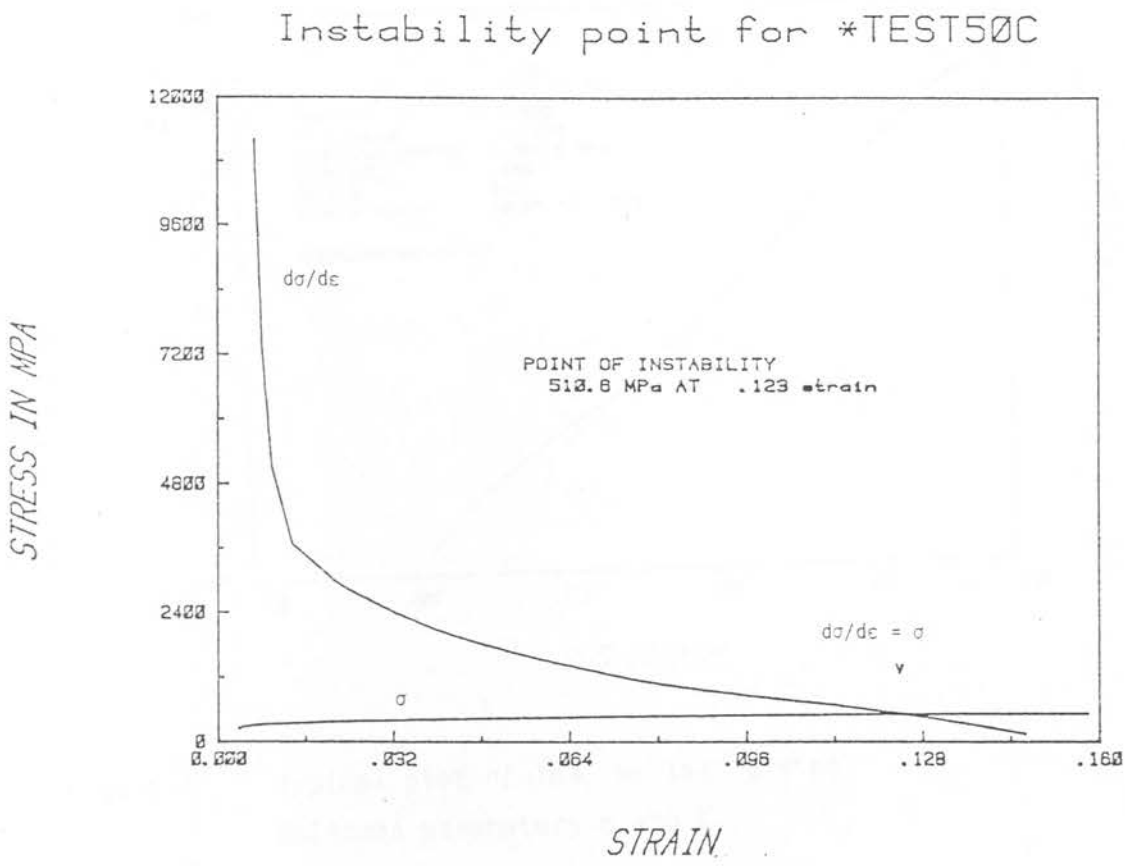

Fig. 4.3 Construction showing the evaluation of the instability point for a tensile test.

Figures 4.4, 4.5 and 4.6 are typical output results depicting delineated work hardening regimes resultant from the Hollomon analysis and from the Jaoul-Crussard type analyses of the Ludwik and modified Swift equations.

Note that the three delineated regions in figures 4.5 and 4.6 were taken over the same strain ranges. Only data from yield to the instability point (denoted by ^) is considered.

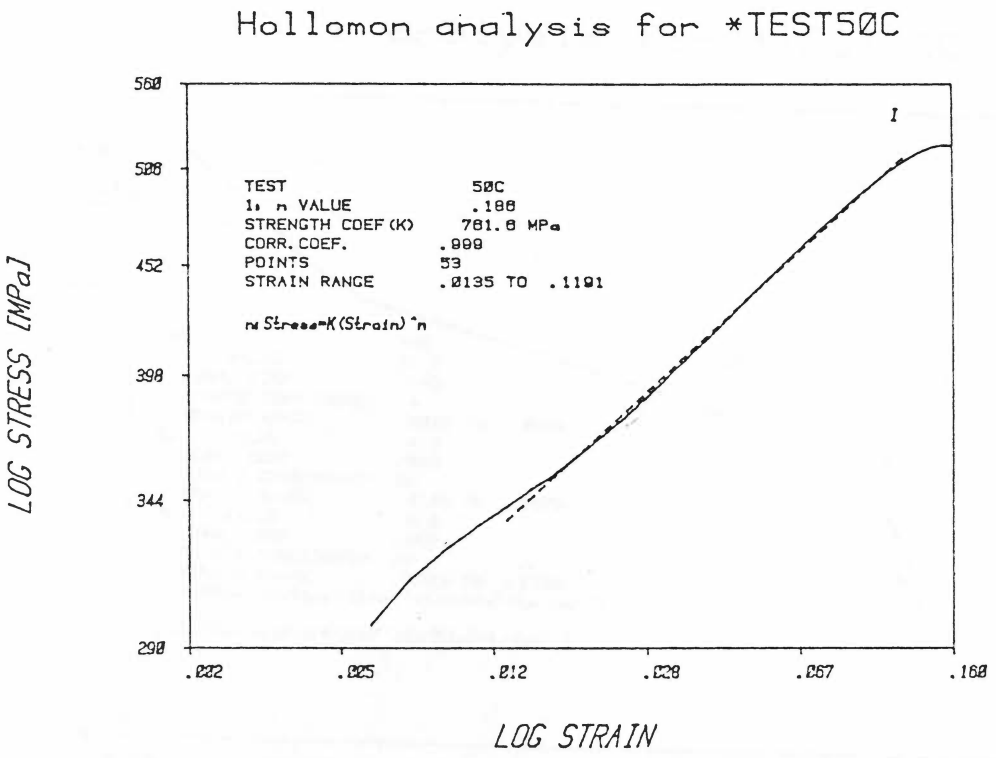

Fig. 4.4 Typical plot of $\ln\sigma$ vs $\ln\epsilon$ giving Holloman parameters n and K.

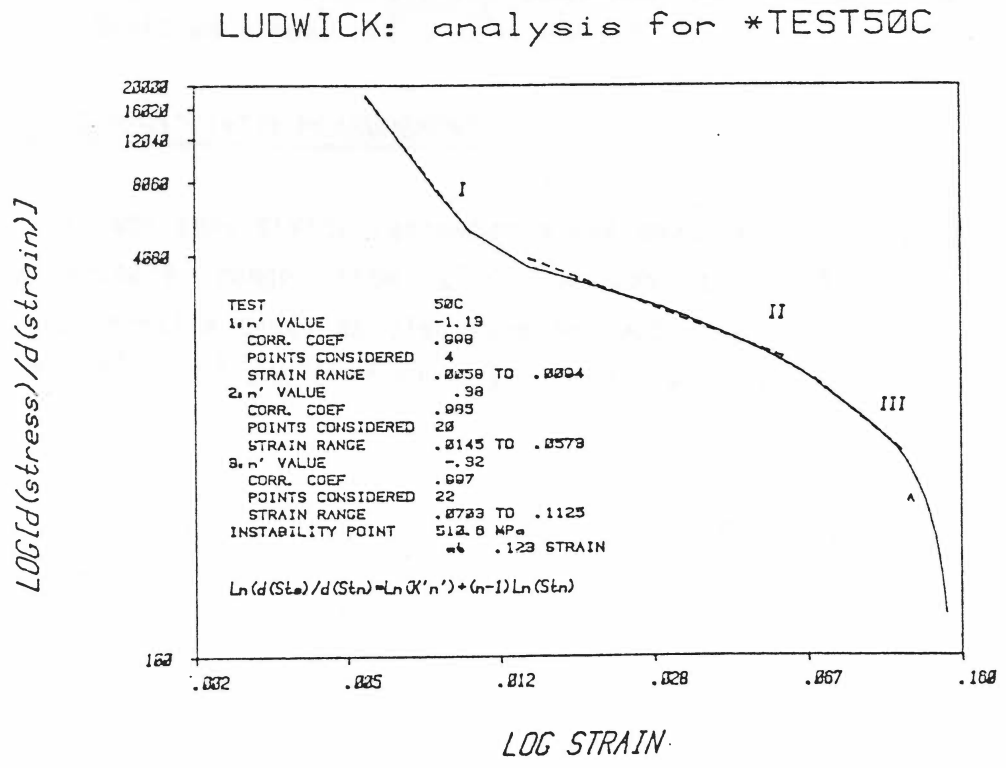

Fig. 4.5 Typical plot of the Jaoul-Crussard type analysis for the Ludwik equation yielding the n' parameter

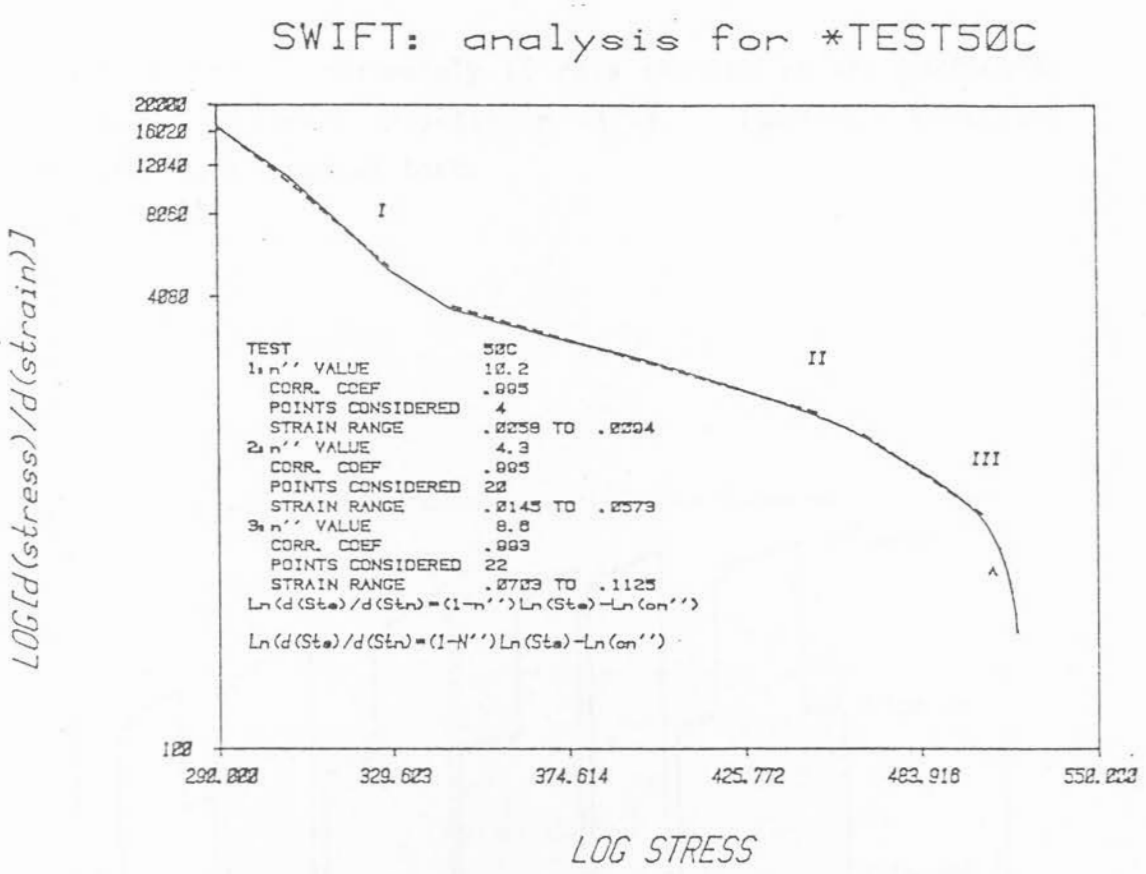

Fig. 4.6 Typical plot giving the n" parameter for the modified Swift equation.

4.6 STRAIN RATE SENSITIVITY MEASUREMENT

The strain rate sensitivity parameter m was measured for 3CR12 in the temperature range from 25°C through to 1150°C using rate-change tensile tests as discussed in section 2.2.3.1. Strain rates of 10^{-2}, 10^{-3} and 10^{-4} were used and m was calculated from the formula:

$$m = \frac{\ln (\sigma_2/\sigma_1)}{\ln (\dot{\epsilon}_2/\dot{\epsilon}_1)}$$

An average from approximately 15 rate changes at any particular temperature yielded a resultant m value. Figure 4.7 shows the flow curve of a typical test.

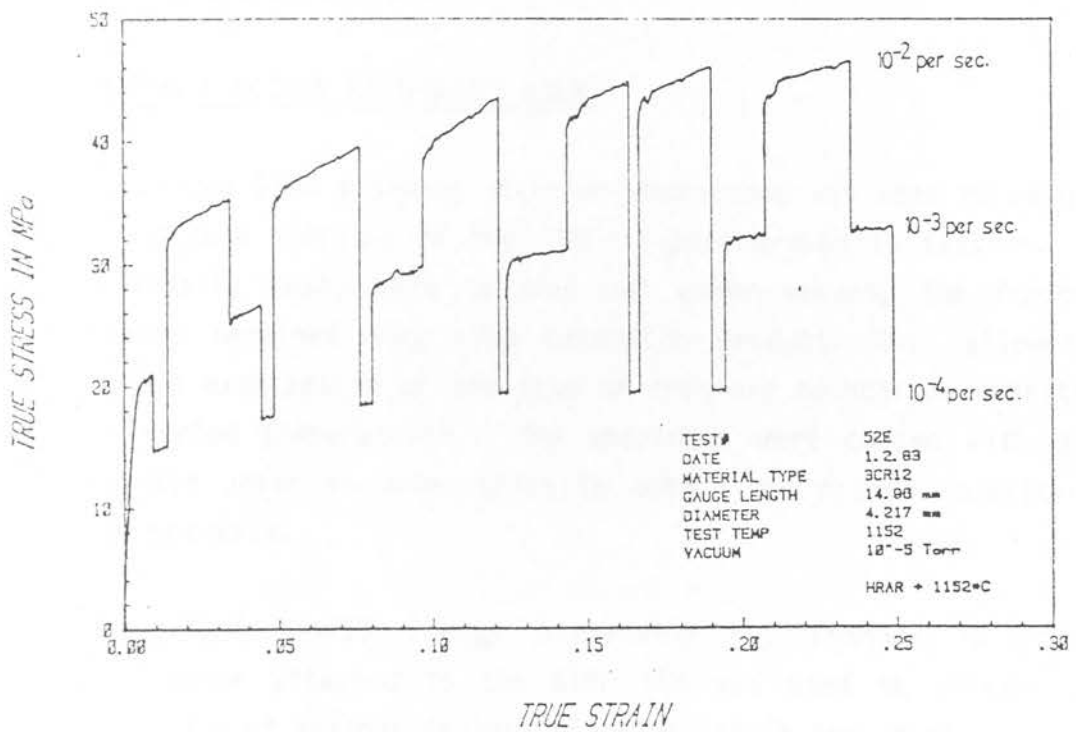

Fig. 4.7 Typical rate-change flow curve of 3CR12 (test temperature of 1152°C).

4.7 YOUNG'S MODULUS MEASUREMENTS

Presupposing an elastic modulus (E) of approximately 200 GPa at room temperature and a tensile specimen size similar to those used in the testing rig with its 5KN maximum capacity, an extension of less than 1,5 microns would have had to be resolved in order to obtain a 5% accuracy in the value of E. This required resolution is at the lower limits of the linear variable differential

transformers (LVDT's) fitted to the ESH servohydraulic tester. Results obtained were at best of the order of 150 ± 50 GPa.

Thus, despite considerable efforts to achieve representative E values for the 3CR12 alloys tested in the testing rig by correcting for load-chain compliance effects, accurate values were only obtained from strain gauging specially machined specimens at room temperature and using a Huggenburger strain gauge amplifier for strain determination.

4.8 SCANNING ELECTRON MICROSCOPY (SEM)

A Cambridge S180 scanning electron microscope was used to examine the fracture surfaces of the 3CR12 alloys broken in tension. As all tensile tests were carried out under vacuum, the fracture surfaces remained free from oxidation product. This allowed a detailed examination of the type of fracture mechanisms operating at elevated temperatures. The specimens were coated with gold palladium prior to examination to obtain the highest quality of image possible.

A Kevex Micro-X700 Energy Dispersive Multichannel Analytical Spectrometer attached to the S180 SEM was used to analyse the composition of various inclusions found within the steel.

CHAPTER FIVE

RESULTS

5.1 THE MICROSTRUCTURAL RESPONSE OF 3CR12 ALLOYS TO HEAT TREATMENT

As the effects of temperature on the tensile deformation of 3CR12 alloys were to be explored, it was first necessary to gain a general understanding of the materials' microstructural response to heat treatments similar to those at which tensile testing was to take place.

The 3CR12 alloys used in the investigation varied in both composition and prior heat treatment. For clarity a summary of the material, its starting condition and then associated experimental work is outlined below.

	Material	Starting Condition	Experimental
(i)	$3CR12_{(1)}$ and 3CR12Ni	Annealed at 1000°C (furnace cool)	Microstructural response and variation in hardness after a one hour soak at temperatures between 25°C and 1050°C followed by an oil quench.
(ii)	$3CR12_{(1)}$	Annealed at 1000°C (furnace cool)	Effect of annealing temperature (one hour soak at intervals within the temperature range from 25°C to 1000°C followed by furnace cool) on the room temperature mechanical properties.

Material	Starting Condition	Experimental
(iii)		
$3CR12_{(2)}$	As-received (hot-rolled)	Microstructural response and variation in hardness after a one hour soak at temperatures between 730°C and 1150°C, followed by an oil quench.
(iv)		
$3CR12_{(2)}$	as for (iii).	The effect of volume percent martensite on bulk hardness.

Photos 5.1 to 5.3 show the as-received microstructures of $3CR12_{(1)}$, $3CR12_{(2)}$ and 3CR12Ni, all in the hot-rolled condition. $3CR12_{(1)}$ and $3CR12_{(2)}$, although having approximately the same composition, vary in their as-received microstructure and hardness due to their varying thermal history (different melt origions). The microstructure, however, can be described as dual-phase with islands of low carbon lath martensite surrounded by a matrix of ferrite. 3CR12Ni has a higher volume fraction of martensite in the as-received condition, with islands of delta ferrite having been elongated during the rolling process into long stringers.

$3CR12_{(1)}$ and 3CR12Ni, after a prior anneal at 1000°C (photos 5.4 and 5.5), were soaked at various temperatures for a further hour at the test temperature in the range from 25°C to 1050°C followed by an oil quench. Table 5.1 and Figs. 5.1 & 5.2 show the resultant effect on hardness and microstructural condition. The quenched-in microstructure of the $3CR12_{(1)}$ alloy remains duplex throughout

the temperature range, except for a brief region around 700°C where the microstructure becomes essentially ferritic. 3CR12Ni, however, tends to be martensitic throughout the test range, exhibiting a dual-phase microstructure only from above ~750°C to ~950°C. A microstructure of semi-decomposed or tempered martensite exists at ~750°C, but the delta ferrite stringers remain visible throughout the range. Both alloys experience a sharp drop off in hardness attaining a minimum at around 750°C due to the existence of soft ferrite at this temperature .

3CR12 ALLOYS IN THE AS-RECEIVED HOT-ROLLED CONDITION

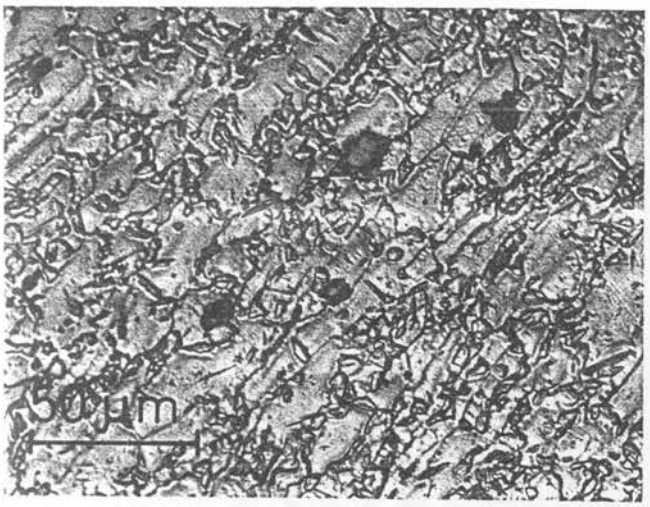

Photo 5.1

$3CR12_{(1)}$
HV_{30}: 190

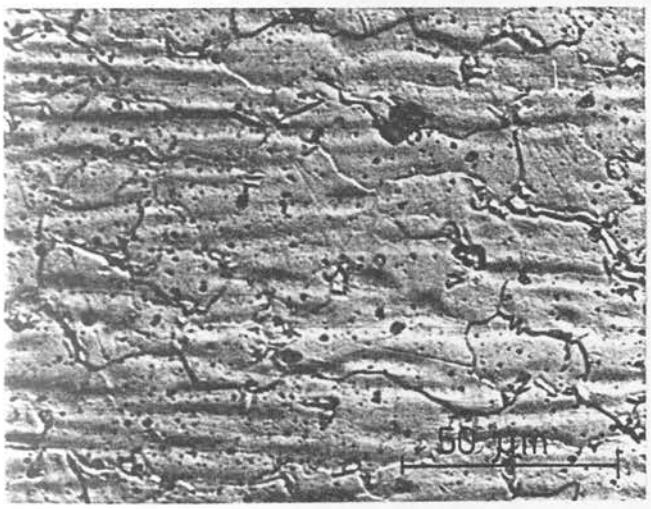

Photo 5.2

$3CR12_{(2)}$
HV_{30}: 230

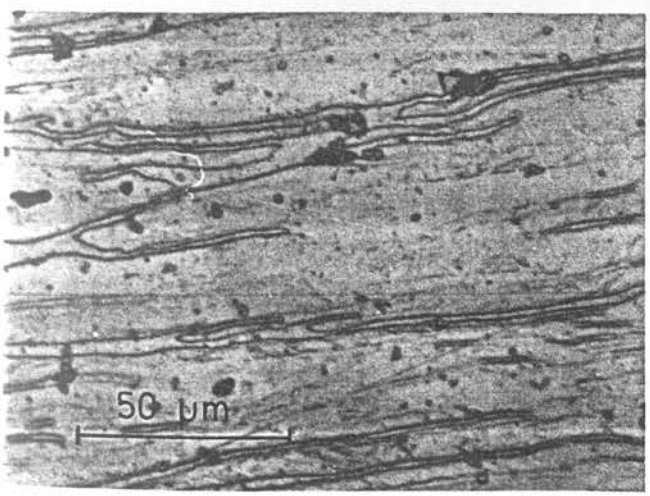

Photo 5.3

3CR12Ni
HV_{30}: 333

1 HOUR ANNEAL AT 1000°C

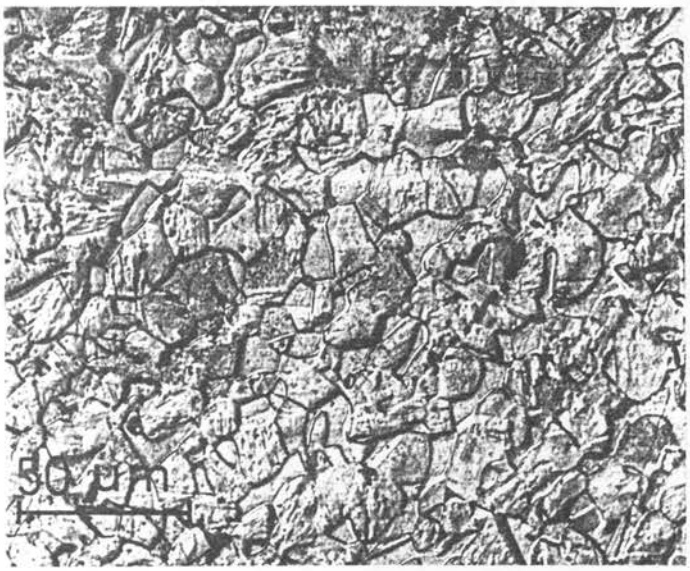

Photo 5.4

3CR12(1)
HV_{30}: 262

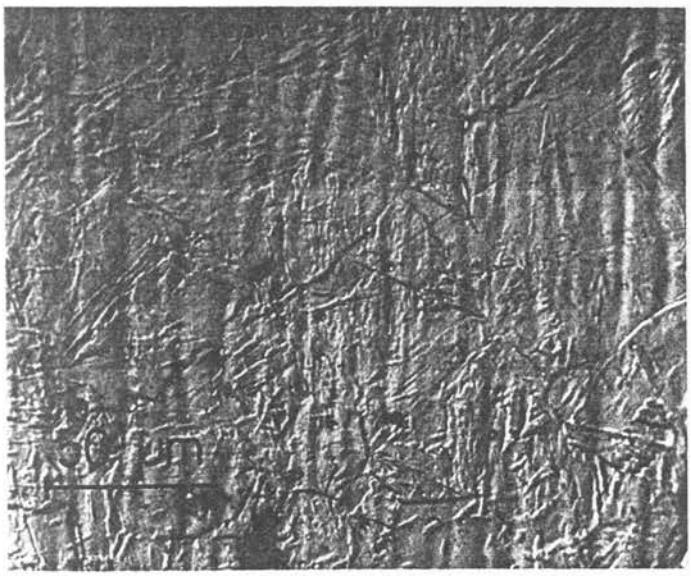

Photo 5.5

3CR12Ni
HV_{30}: 302

Note the difference in grain size between 3CR12 and 3CR12Ni in this condition.

TEMPERATURE °C	HARDNESS HV_{30} $3CR12_{(1)}$	3CR12Ni
25	217	295
150	220	298
250	221	297
350	223	308
450	227	299
600	221	283
650	183	243
700	169	216
750	150	211
800	163	249
850	206	262
900	231	291
950	248	302
1000	265	308
1050	263	302

TABLE 5.1: THE EFFECT OF QUENCH TEMPERATURE ON HARDNESS FOR $3CR12_{(1)}$ AND 3CR12NI - HELD FOR ONE HOUR AT INDICATED TEMPERATURE THEN QUENCHED IN OIL. ALL SPECIMENS HAD A PRIOR ANNEAL AT 1000°C FOR ONE HOUR.

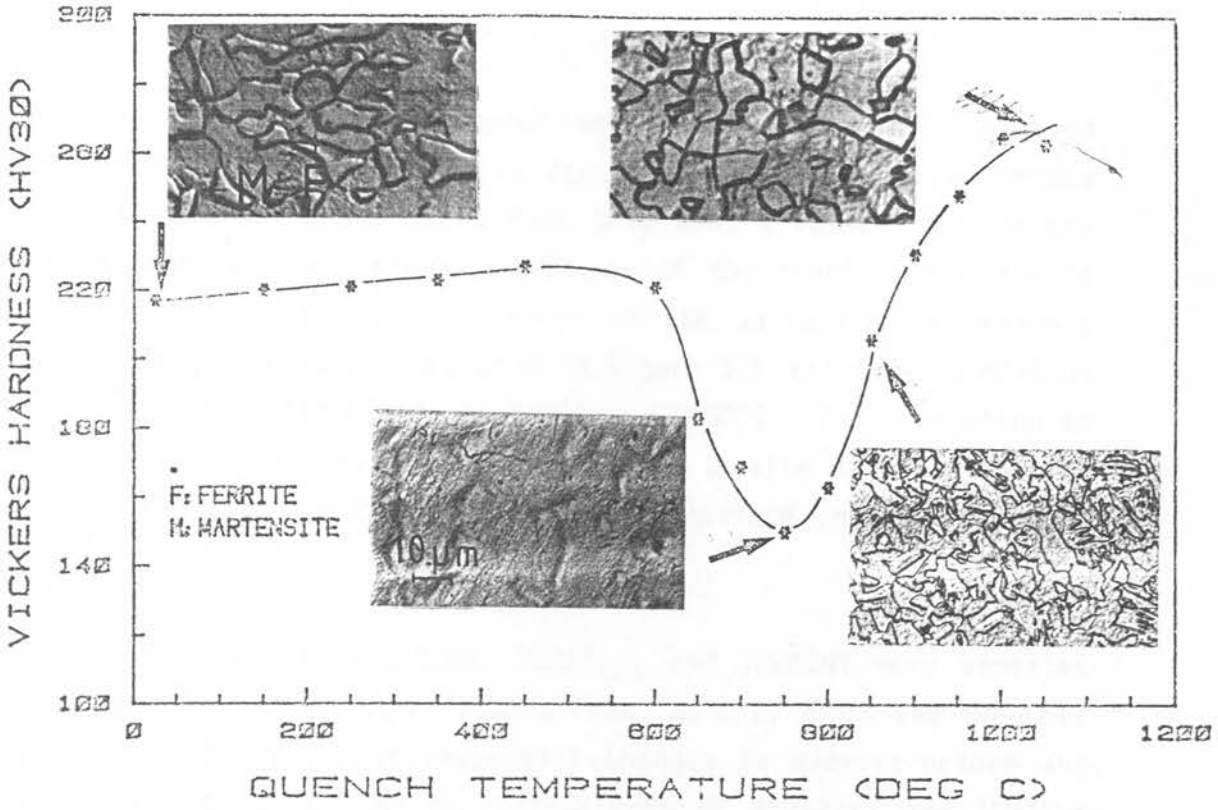

FIGURE 5.1: EFFECT OF SOAKING TEMPERATURE (1 HR) ON HARDNESS & MICROSTRUCTURE FOR 3CR12 (1)

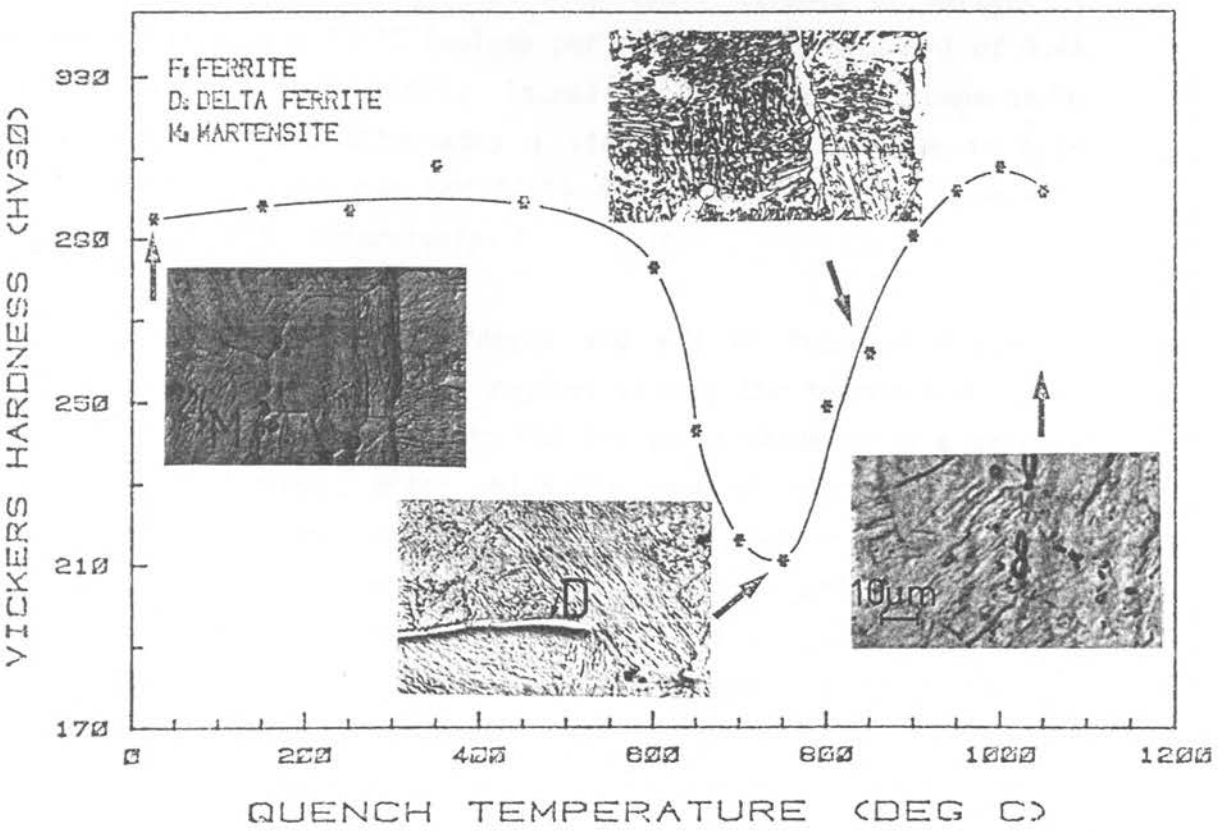

FIGURE 5.2: EFFECT OF SOAKING TEMPERATURE (1HR) ON HARDNESS & MICROSTRUCTURE FOR 3CR12NI

The alloy $3CR12_{(1)}$, with a prior anneal of 1000°C, was subjected to various soaking temperatures for 1 hour followed by a furnace cool. Figure 5.3 shows the effect this heat treatment has on the room temperature mechanical properties of the steel. The tensile strength follows a similar pattern to the variation in hardness with soaking temperature depicted in Figure 5.1 and shows a minimum at around 800°C with maxima at~400°C and~1050°C. The elongation to fracture traces an inverse pattern to the tensile strength showing minima at around 400°C and 1050°C and a maximum in the region of 800°C.

In the as-received condition, $3CR12_{(2)}$ and 3CR12Ni were annealed for 1 hour at various temperatures from 730°C to 950°C and then oil quenched to study the consequential changes in microstructure and to compare these to the microstructures of $3CR12_{(1)}$ and 3CR12Ni in the 1000°C prior annealed condition. Table 5.2 and Figure 5.4 refer: as with $3CR12_{(1)}$, from ~730°C to ~778°C, $3CR12_{(2)}$ is essentially ferritic (HV_{30}:141) with small islands of martensite appearing at around 800°C (volume per cent martensite (VPM) of 8.4% with a hardness of HV_{30}:147). Increasing the annealing temperature from 800°C to 843°C attenuates a steep rate of increase in both hardness (HV_{30}: 228) and VPM (79%) and at 950°C these values are HV_{30}: 270 and 91% respectively.

The relationship between hardness and VPM in figure 5.4 can be delineated into two distinct regimes within the temperature range of 800°C to 950°C. From 0% to 78% VPM there tends to be a gradual increase in hardness, after which the rate of increase, although remaining linear, is somewhat enhanced. A similar trend for the increase in micro-hardness of the martensite islands is displayed in Figure 5.4 (Table 5.3). In Figure 5.5 it can be seen that there is a significant increase in both volume percent martensite and hardness after quenching $3CR12_{(1)}$ from temperatures above 800°C.

It can be seen in photos 5.6 to 5.9 that, apart from increasing the volume percent martensite, an increasing quench temperature has a large grain refining influence on the ferrite matrix from ~800°C to ~843°C.

The hardness response of as-received 3CR12Ni to annealing temperature in the testing range from 730°C to 950°C (Table 5.2) follows a comparable trend to $3CR12_{(1)}$ and differs little from its behaviour observed under similar conditions, but with a prior anneal at 1000°C (Table 5.1). One difference between the two alloys which can be noted is that 3CR12Ni tends to enter the dual-phase region at a lower temperature compared to the $3CR12_{(2)}$ alloy (photos 5.10 and 5.11). At 730°C evidence for nucleated austenite (martensite at room temperature) can be seen in 3CR12Ni, whereas in 3CR12, a temperature of 778°C is still not sufficient to nucleate austenite (photo 5.6).

At temperatures above ~1100°C significant grain growth occurs in the 3CR12 alloys. Although 3CR12 retains the dual-phase microstructure right through from ~800°C to this temperature, 3CR12Ni passes through a wholely austenitic range before re-entering the dual-phase region at around 1150°C. Photo 5.12 shows the dual-phase microstructure with enhanced grain size obtained when $3CR12_{(2)}$ is soaked at 1150°C for 1 hour. The micro-hardness (15 pond) for the martensite and ferrite on quenching is 171 and 98 respectively.

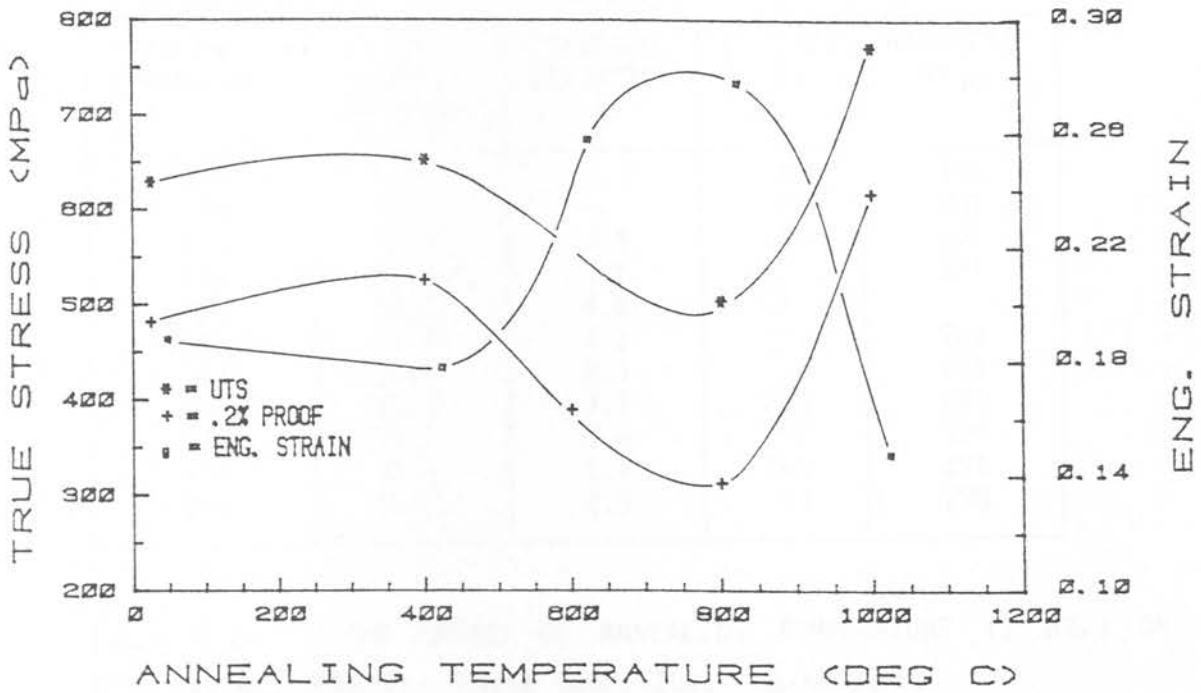

(STRAIN RATE 10^{-3} PER SECOND)			
ANNEALING TEMPERATURE	UTS (MPa)	0.2% PROOF STRESS (MPa)	ENGINEERING STRAIN TO FRACTURE
25°C	628.9	481.4	0.19
400°C	652.0	525.0	0.18
600°C	652.6	389.2	0.26
800°C	504.0	313.0	0.28
1000°C	771.2	616.8	0.15

Fig. 5.3: The effect of annealing temperature on the mechanical properties of 3CR12(1). All specimens received a prior anneal at 1000°C before being annealed at the indicated temperatures for 1 hour.

MATERIAL	3CR12 (2)			3CR12NI
ANNEALING TEMPERATURE (°C)	VOLUME PERCENT MARTENSITE	STANDARD DEVIATION %	HARDNESS HV_{30}	HARDNESS HV_{30}
730	0	-	141	158
778	0	-	141	231
800	8.4	3.9	147	256
824	44.0	5.1	177	281
830	55.0	4.8	185	-
843	76.4	4.2	211	281
862	82.9	2.3	228	281
882	83.4	3.7	238	289
902	86.7	3.8	252	294
924	90.4	2.4	260	294
950	91.0	2.5	270	298

TABLE 5.2: THE EFFECT OF ANNEALING TEMPERATURE (1 HR.) ON 3CR12(2) AND 3CR12NI. PRIOR CONDITION: AS-RECEIVED.

ANNEALING TEMPERATURE (°C)	VOLUME PERCENT MARTENSITE	MARTENSITE MICROHARDNESS VPN (8 POND)
824	44.0	133
843	76.4	137
882	83.4	150
950	91.0	192

TABLE 5.3: THE EFFECT OF ANNEALING TEMPERATURES (1 HR.) ON THE MARTENSITE MICRO-HARDNESS OF 3CR12(2). PRIOR CONDITION: AS-RECEIVED.

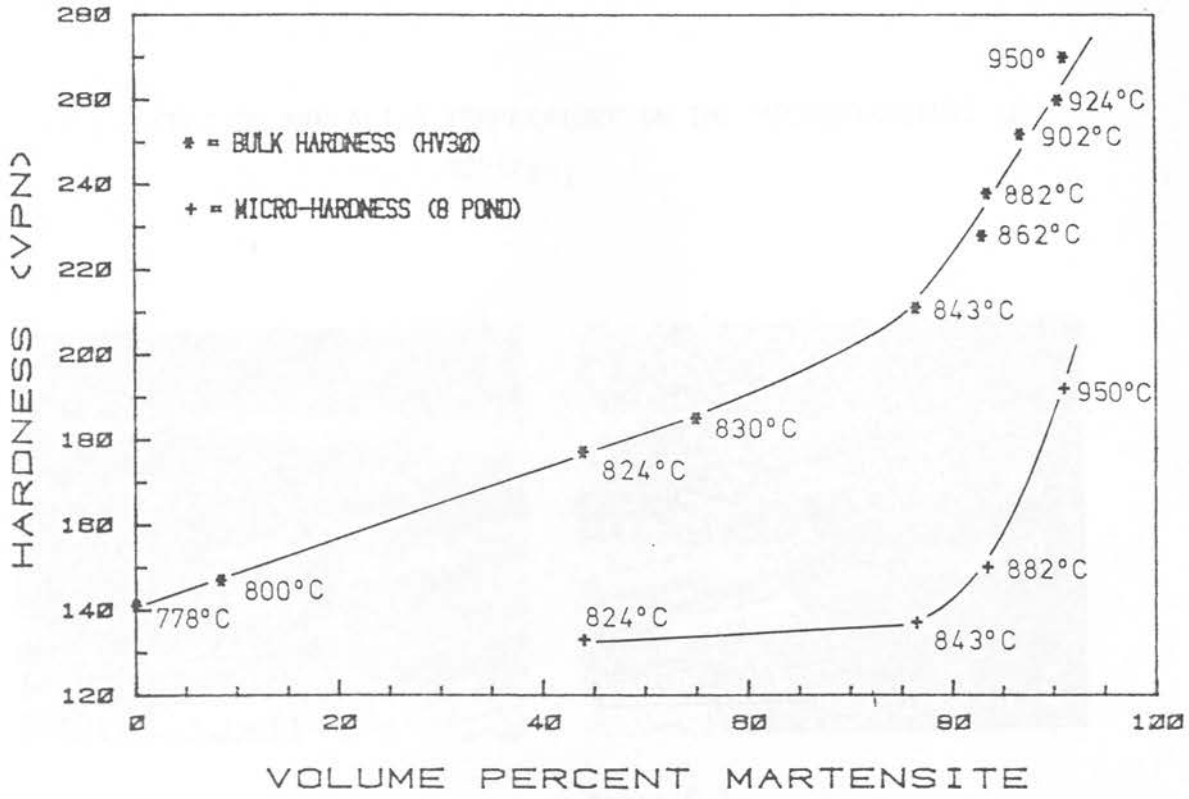

FIGURE 5.4: EFFECT OF VPM ON THE BULK HARDNESS AND MARTENSITE MICRO-HARDNESS

(3CR12 : AS-RECEIVED PLUS 1 HR ANNEAL)

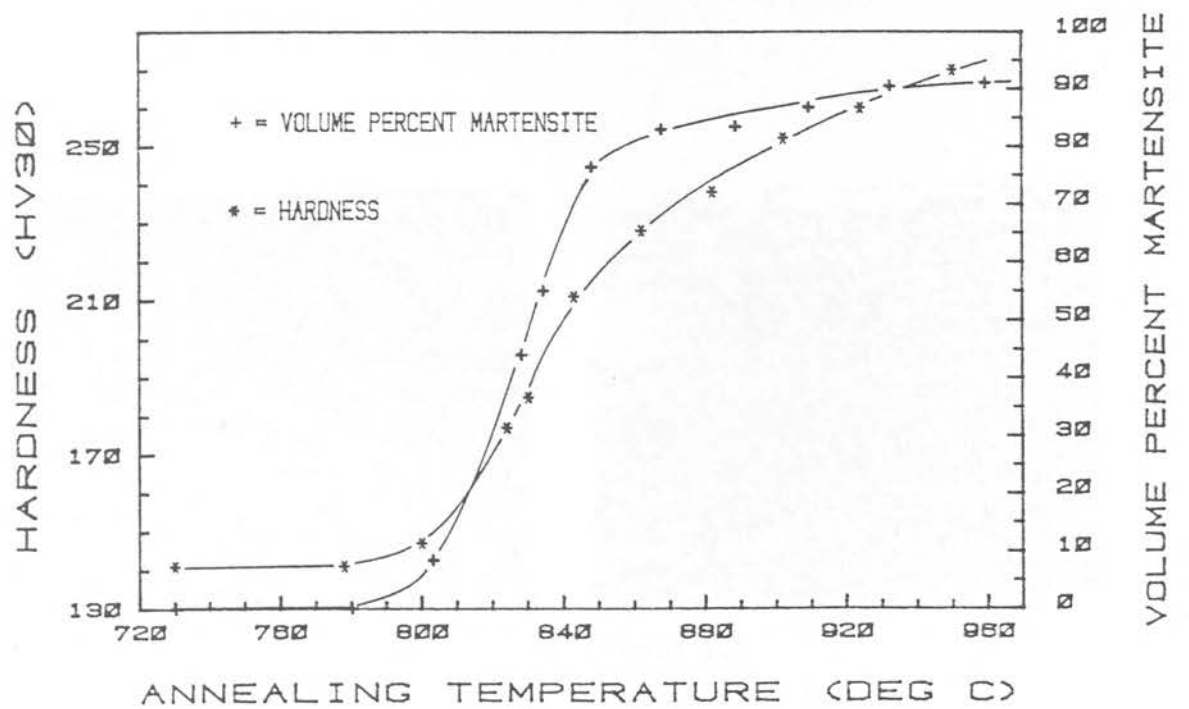

FIGURE 5.5: THE EFFECT OF ANNEALING TEMPERATURE WITHIN THE DUAL-PHASE REGION ON HARDNESS & VPM FOR 3CR12

THE EFFECT OF ANNEALING TEMPERATURE ON THE MICROSTRUCTURE OF 3CR12(2)

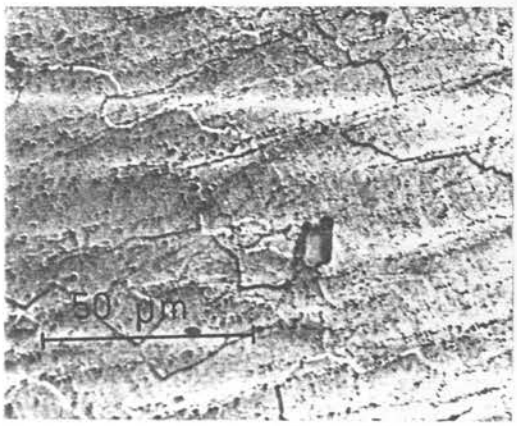

Photo 5.6
Quench from 778°C
HV_{30}: 141
VPM: 0%

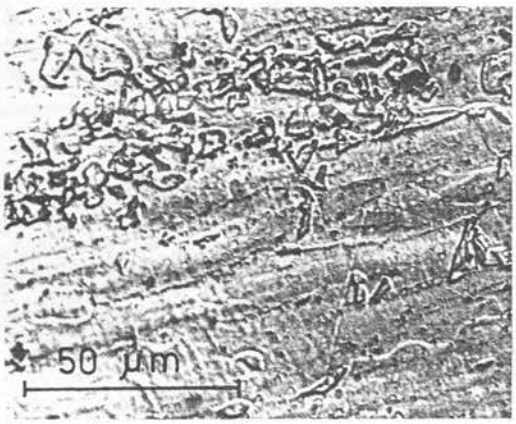

Photo 5.7
Quench from 800°C
HV_{30}: 147
VPM: 8%

Photo 5.8
Quench from 843°C
HV_{30}: 211
VPM: 78%

Photo 5.9
Quench from 952°C
HV_{30}: 270
VPM: 91%

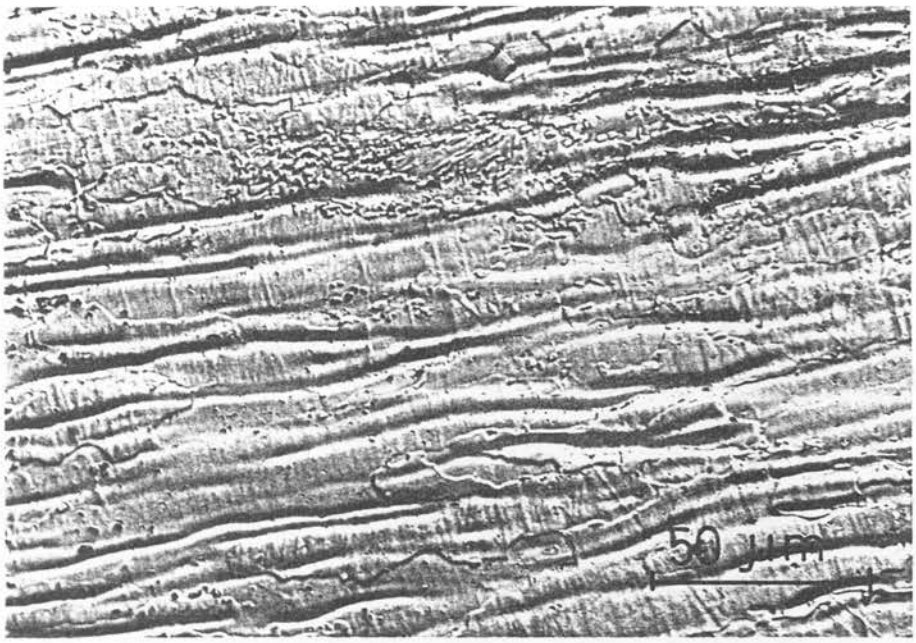

Photo 5.10
As-received + quench from 730°C
HV_{30}: 158

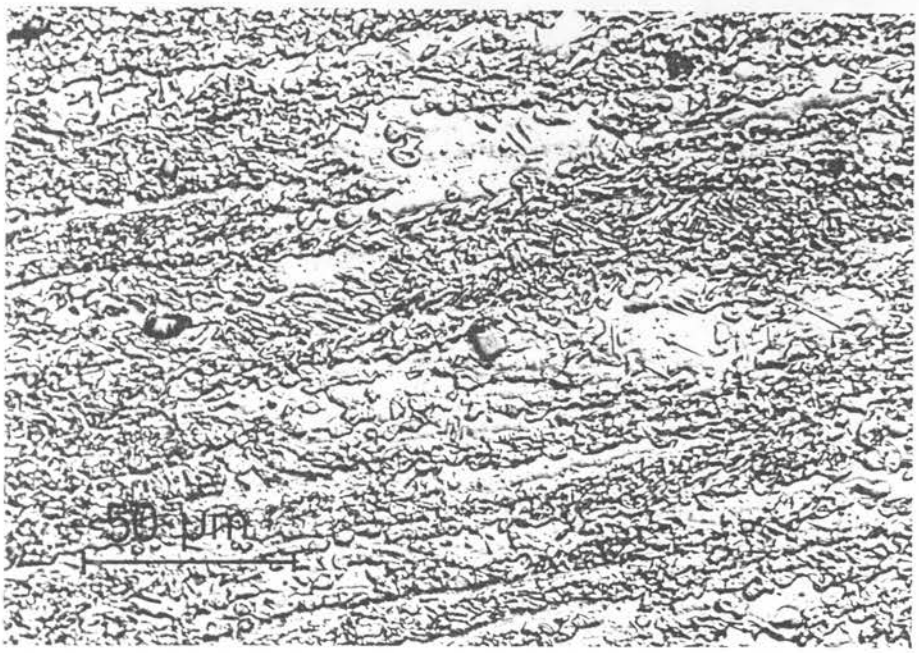

Photo 5.11
As-received + quench from 778°C
HV_{30}: 231

Fig. 5.5: Microstructures of 3CR12Ni indicating the temperature at which austenite begins to nucleate. Thermal history: as-received and soaked at indicated temperature for 1 hour.

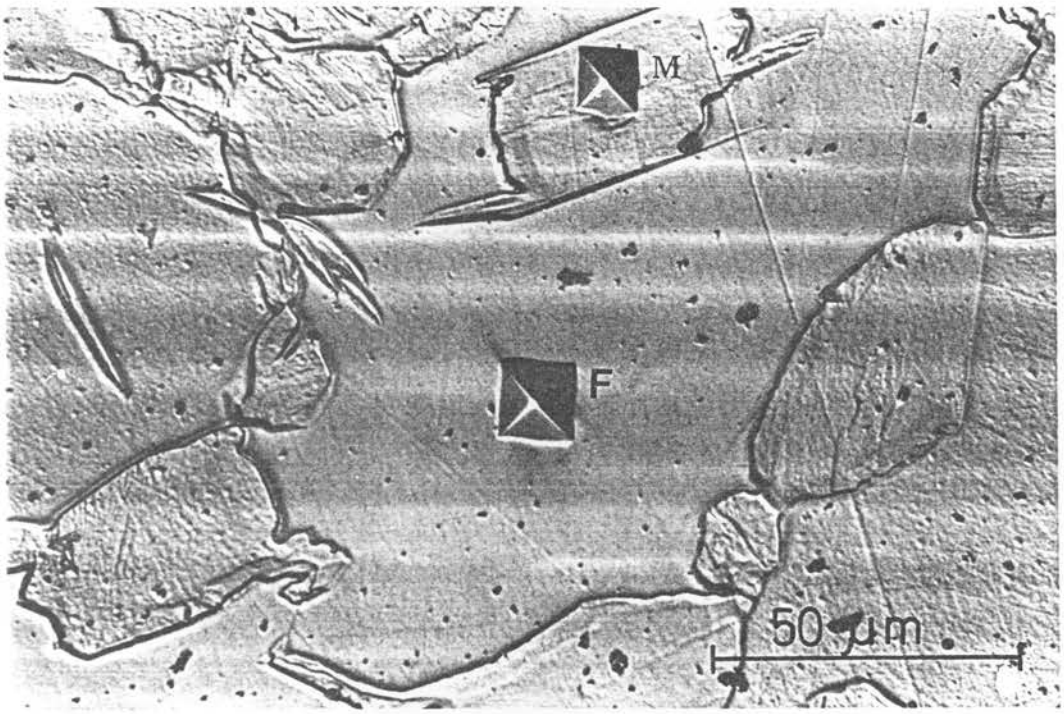

Photo 5.12 3CR12(2) quenched from 1150°C after soaking for 1 hour. The grain size has increased almost four fold compared to that found at 800°C. F and M are micro-hardness indentations giving a micro-hardness (15 pond) of 98 for ferrite and 171 for martensite.

5.2 THE EFFECT OF TEST TEMPERATURE AND STRAIN RATE ON THE MECHANICAL PROPERTIES OF 3CR12 ALLOYS

5.2.1 Young's Modulus

The elastic constant (E) for 3CR12 and 3CR12Ni in the as-received condition were recorded at 25°C and are given in Table 5.4.

MATERIAL	E VALUE (GPa)
3CR12	198.0
3CR12Ni	196.5

TABLE 5.4 YOUNG'S MODULUS FOR 3CR12 AND 3CR12Ni

As discussed in section 4.7, the resolution of the test rig was insufficient to determine values for the Young's Modulus accurately. However, with increasing test temperature, the slopes of the stress-strain curves within the elastic region were noted to attenuate and values for E were calculated by correcting the slopes by a factor related to the values obtained at room temperture value. The relationship is given in figure 5.6

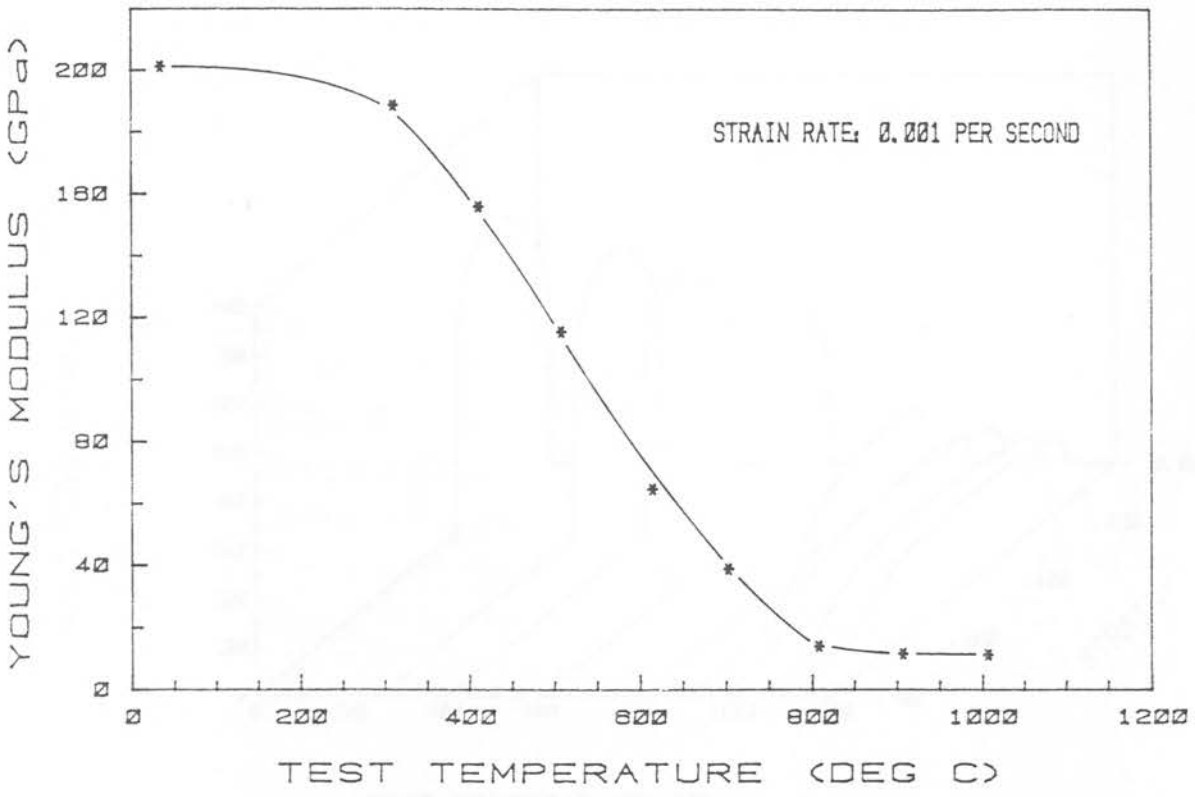

FIGURE 5.6: VARIATION OF THE YOUNG'S MODULUS WITH TEST TEMPERATURE FOR 3CR12 (1)

5.2.2 Tensile properties

Temperature intervals for tests conducted at the strain rate of 10^{-1} per second were selected at relatively close intervals in order to obtain a detailed profile of results. This then enabled a selective choice of temperature intervals for the slower strain rates and which correspondingly necessitated fewer tests at 10^{-4} per second.

The mechanical properties vary considerably in the temperature range from 25°C to 1150°C and Figure 5.7 gives a graphical indication of the differences encountered in the stress-strain flow curves for 3CR12 at various test temperatures within this range. The series of graphs (Figures 5.10 to 5.25) and tables (5.5 to 5.8) display the mechanical properties and the deformation energies (area under the stress-strain curve) for both 3CR12 and 3CR12Ni at strain rates of 10^{-1} and 10^{-4} per second.

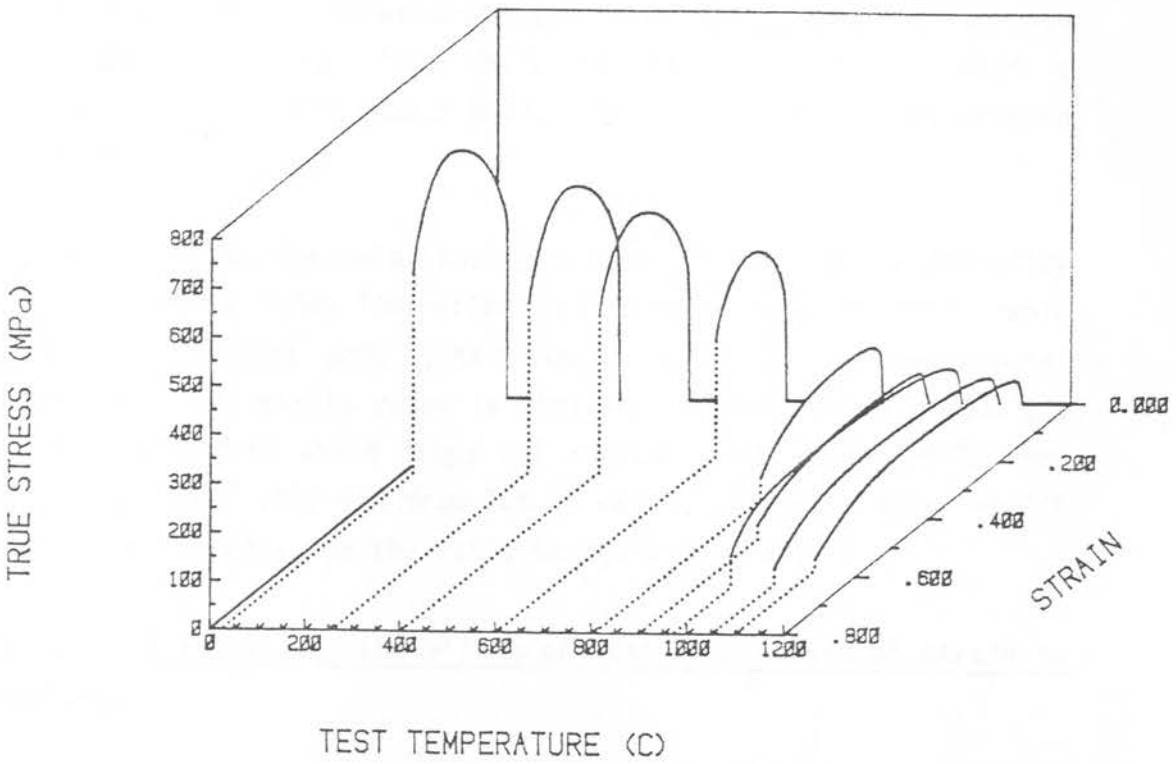

Fig. 5.7: Stress-strain relationships for 3CR12 in the test temperature range of 25°C to 1150 °C at a strain rate of 0.1 per second.

(i) 3CR12

Figures 5.8 and 5.10: UTS and yield stress as a function of temperature.

The ultimate tensile strength (UTS) and 0.2% proof stress (PS) decrease with increasing temperature to a minimum at around 900°C. At a strain rate of 10^{-4} per second there is a sharp drop off between ~600°C and ~800°C. The faster strain rate of 10^{-1} per second, however, causes a more gradual attenuation, but compared to the 10^{-4} case gives a very pronounced maximum in both UTS and PS at 950°C. The UTS of 3CR12 at 850°C (98 MPa) is similar to that at 1100°C (99 MPa) when pulled apart at 10^{-1} per second. At 10^{-4} per second, although fewer tests were done in this range, the behaviour

tends to be similar, demonstrating a retention of strength through the temperature range from 850°C to 1000°C (~38 MPa) with a moderate peak at 950°C (50.2 MPa). By 1150°C the UTS has dropped to 18 MPa.

Figure 5.12 gives the relationship between YP and UTS for the alloy at both strain rates.The effect of strain rate on this ratio becomes significant only after ~700°C, although the behavioural pattern for both strain rates is similar. In the region of ~800°C a maximum is reached which drops off radically at around 930°C from 98% to 70% (10^{-4} s^{-1}) and from 70% to 45% (10^{-1} s^{-1}). Above ~950°C there is a tendency for the ratio to again increase.

Figures 5.9 and 5.11: The effect of test temperature on strain to fracture.

The failure strain vs temperature relationship becomes noticeably strain rate sensitive only after ~900°C, and the curves for both strain rates demonstrate local minima at around 600°C (20-22%) with local maxima at around 1000°C. At 10^{-4} per second this peak is 132% and for 10^{-1} per second it is 99%.

Figures 5.13 to 5.16: The effect of test temperature on deformation energy.

The energy required to deform a material per unit volume is given as the area under the true stress-true strain curve. Three specific areas are indicated: the area up to the strains corresponding to 0.2% proof stress, to the UTS and to failure. Although these calculated values can only be assumed to be correct for strain up to the point of neck initiation (after which the true stress-true strain calculations become invalid), the areas under the curves to failure are nevertheless presented, as they give a relative, if not absolute, indication of the deformation energies as a function of test temperature. Strictly, for comparison purposes, the strain to necking (Considére point of instability)

should be used in place of the strain to UTS, but as there is good correlation between the two values this was considered unnecessary. The deformation energies to UTS and fracture follow the same pattern as for the yield and UTS values, demonstrating minima at around 900°C. Generally, the lower the strain rate the less the deformation energy required. This, however, is not true for the energy to the temporary strain (elastic and plastic) value at which the 0.2% proof stress occurs. This value remains strain rate and temperature insensitive throughout the test temperature range.

Test Temp °C	Engineering Strain	UTS (MPa)	At Strain	0.2% Proof (MPa)	At Strain	UTS/Proof Stress (%)	Instability Stress(MPa)	At Strain	WORK (kJ) DONE TO DEFORM TO:		
									Yield ($x10^3$)	UTS ($x10^5$)	Failure ($x10^5$)
25	0.302	600.3	0.166	357.8	0.003	59	588	0.133	0.68	0.87	1.4
100	0.294	580.5	0.165	361.2	0.004	62	566	0.128	0.96	0.84	1.3
259	0.286	520.9	0.154	302.8	0.006	58	512	0.126	1.00	0.69	1.1
343	0.265	485.4	0.142	296.2	0.0043	61	476	0.117	0.88	0.60	1.0
403	0.284	470.7	0.161	260.6	0.0053	55	458	0.124	0.75	0.65	1.0
500	0.251	431.4	0.136	231.8	0.0055	54	427	0.119	0.62	0.50	0.84
603	0.222	361.3	0.110	213.0	0.0062	59	357	0.088	0.69	0.34	0.63
709	0.270	268.3	0.116	175.4	0.0048	65	263	0.082	0.53	0.28	0.56
805	0.410	142.5	0.121	98.9	0.0065	70	139	0.068	0.32	0.16	0.41
852	0.566	97.6	0.146	66.1	0.008	68	94	0.064	0.30	0.13	0.37
900	0.614	90.1	0.196	67.1	0.0175	74	86	0.090	0.55	0.16	0.36
937	0.800	140.2	0.388	69.2	0.0143	49	-	-	0.38	0.47	0.72
970	0.900	142.6	0.385	70.5	0.0165	50	130	0.195	0.44	0.47	0.80
998	0.991	135.0	0.361	60.5	0.0102	44	124	0.184	0.22	0.42	0.79
1050	0.862	115.0	0.357	62.2	0.0234	54	106	0.199	0.70	0.35	0.60
1098	0.795	98.7	0.300	50.8	0.0145	52	93	0.197	0.30	0.25	0.46

TABLE 5.5: MECHANICAL PROPERTIES FOR 3CR12 (STRAIN RATE: 10^{-1} PER SECOND).

Test Temp °C	Engineering Strain	UTS (MPa)	At Strain	0.2% Proof (MPa)	At Strain	UTS/Proof Stress (%)	Instability Stress(MPa)	At Strain	WORK (kJ) DONE TO DEFORM TO:		
									Yield ($x10^3$)	UTS ($x10^5$)	Failure ($x10^5$)
25	0.276	557.2	0.154	338.9	0.040	61	545.7	0.126	1.0	0.75	1.2
196	0.296	523.8	0.151	307.8	0.0046	59	517.8	0.124	0.98	0.69	1.1
392	1 0.263	491.0	0.143	274.5	0.0036	56	485.5	0.126	0.73	0.61	0.96
603	0.202	420.9	0.129	244.0	0.0033	58	414.0	0.107	0.61	0.48	0.74
709	0.207	295.2	0.151	185.9	0.0043	64	287.9	0.115	0.56	0.40	0.50
783	0.307	109.2	0.092	84.4	0.0050	77	106.1	0.070	0.30	0.092	0.24
850	0.453	38.8	0.043	38.3	0.0064	98	38.5	0.010	0.16	0.016	0.11
900	0.524	38.2	0.089	33.3	0.0058	87	37.1	0.042	0.12	0.032	0.12
950	1.310	50.2	0.190	36.5	0.0042	73	40.7	0.095	0.11	0.089	0.29
1000	1.322	39.0	0.242	27.7	0.0070	71	37.4	0.108	0.12	0.087	0.26
1150	0.877	18.2	0.173	14.3	0.0040	79	17.3	0.071	0.042	0.029	0.099

TABLE 5.6: MECHANICAL PROPERTIES OF 3CR12 (STRAIN RATE 10^{-4} PER SECOND)

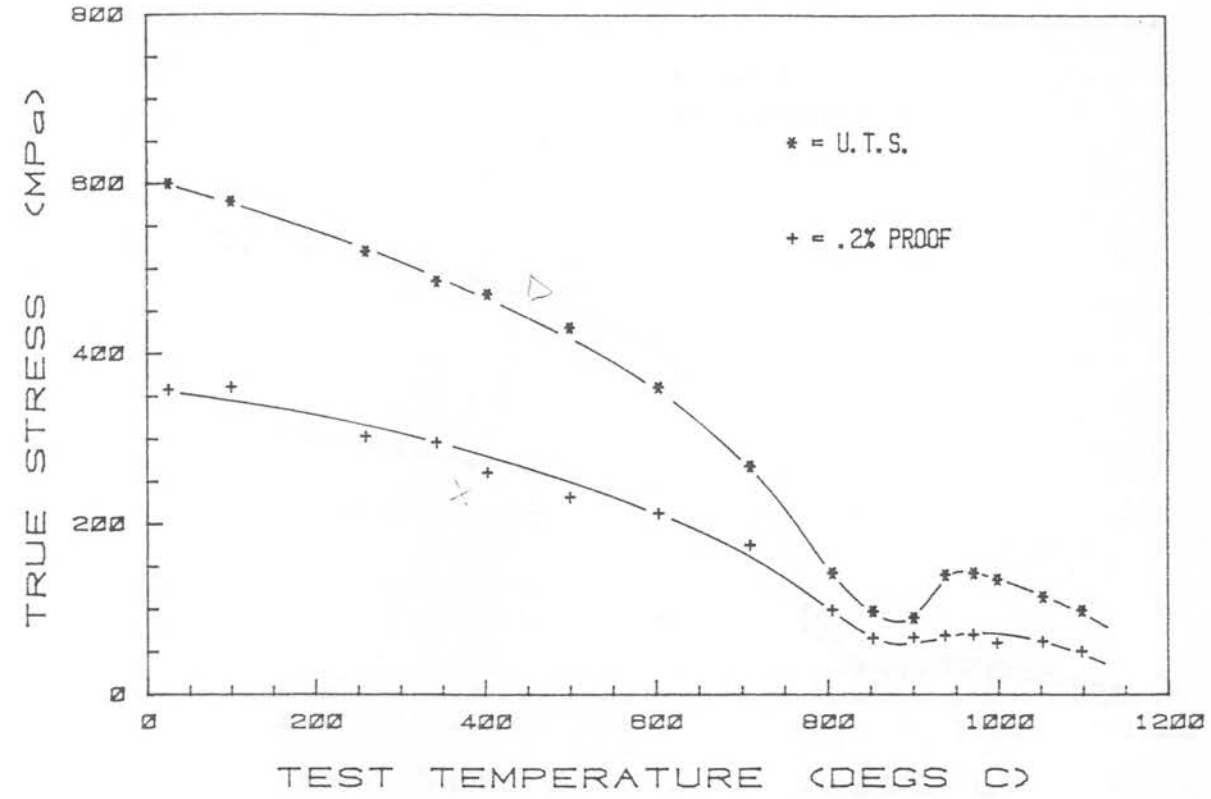

FIGURE 5.8: TENSILE PROPERTIES Vs. TEMPERATURE FOR 3CR12
(STRAIN RATE: 0.1 PER SECOND)

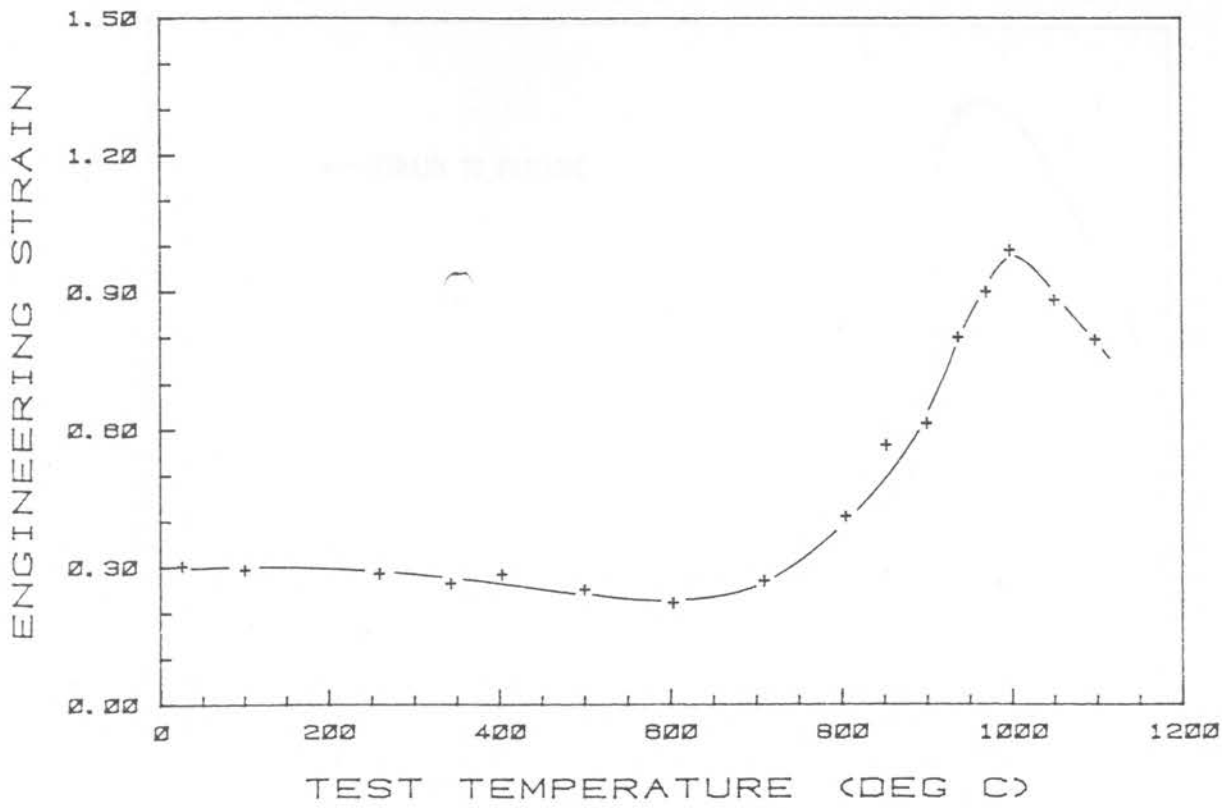

FIGURE 5.9: FAILURE STRAIN Vs. TEMPERATURE FOR 3CR12
(STRAIN RATE: 0.1 PER SECOND)

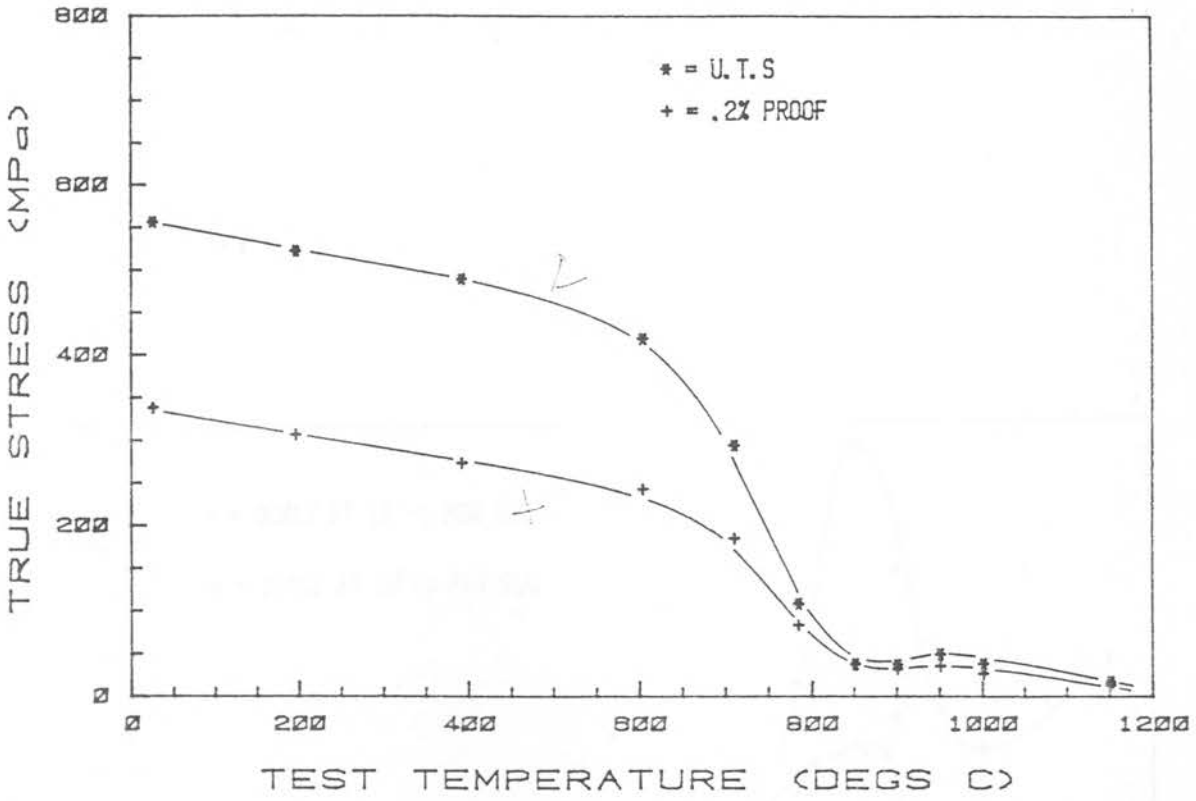

FIGURE 5.10: TENSILE PROPERTIES Vs. TEMPERATURE FOR 3CR12
(STRAIN RATE: 0.0001 PER SECOND)

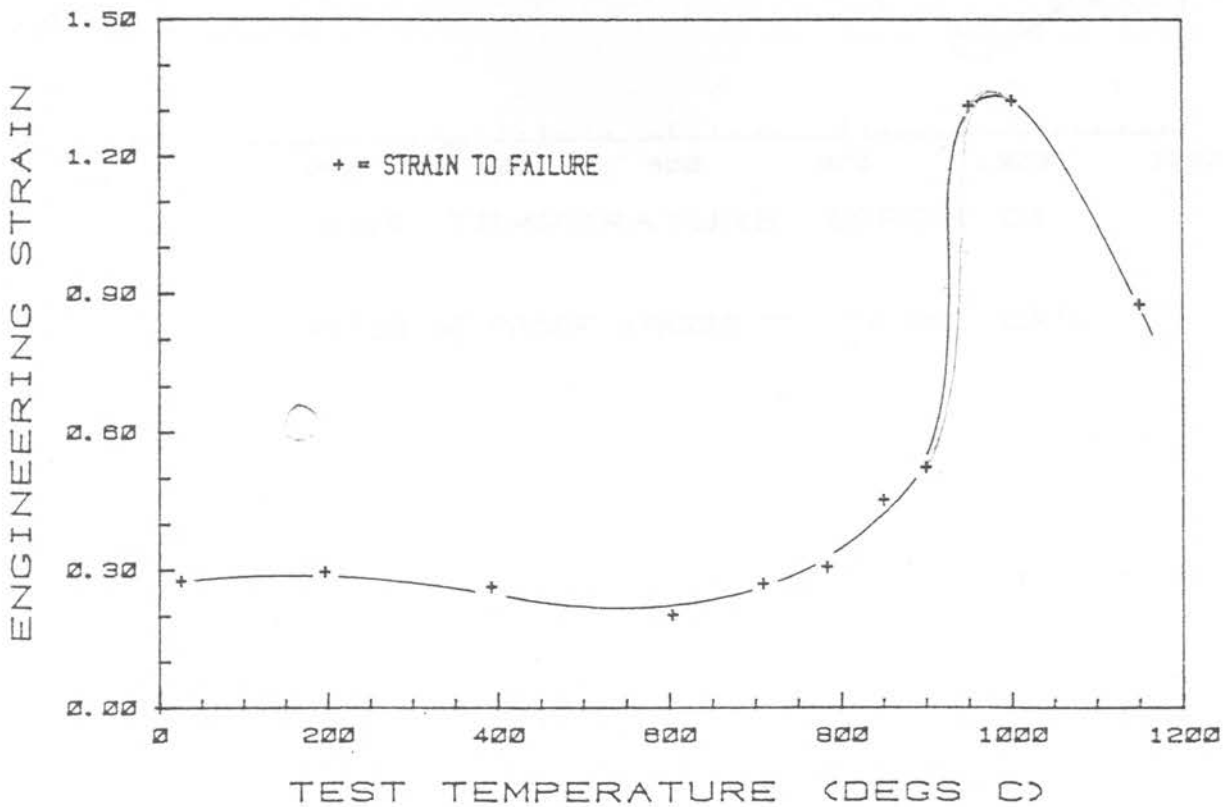

FIGURE 5.11: FAILURE STRAIN VS. TEMPERATURE FOR 3CR12
(STRAIN RATE: 0.0001 PER SECOND)

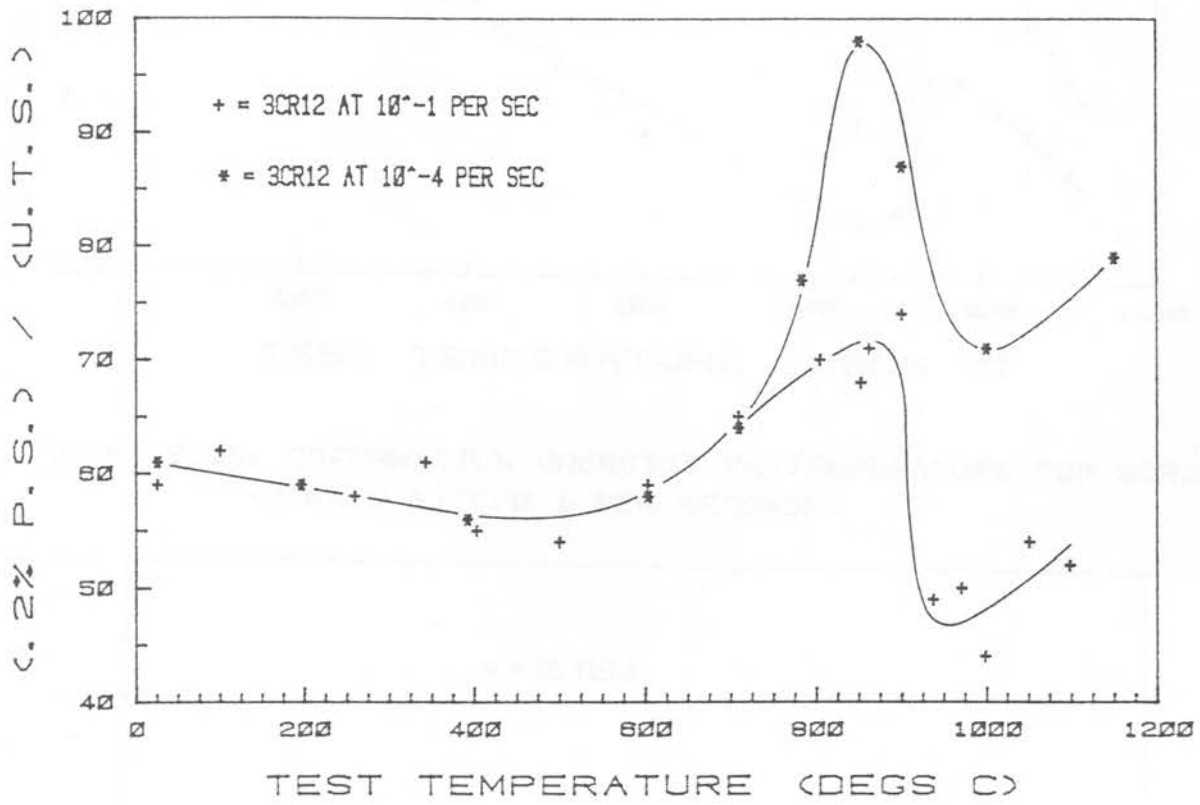

FIGURE 5.12: RATIO OF PROOF STRESS TO UTS FOR 3CR12

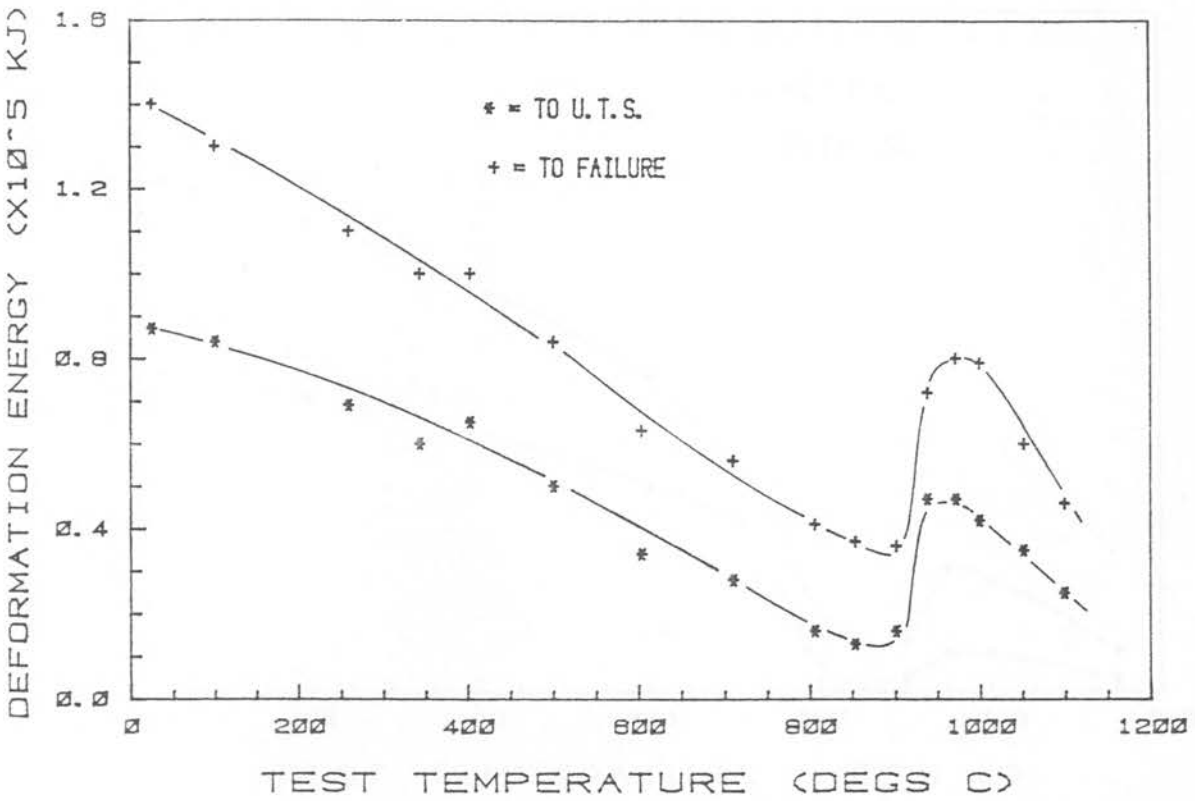

FIGURE 5.13: DEFORMATION ENERGIES VS. TEMPERATURE FOR 3CR12 (STRAIN RATE: 0.1 PER SECOND)

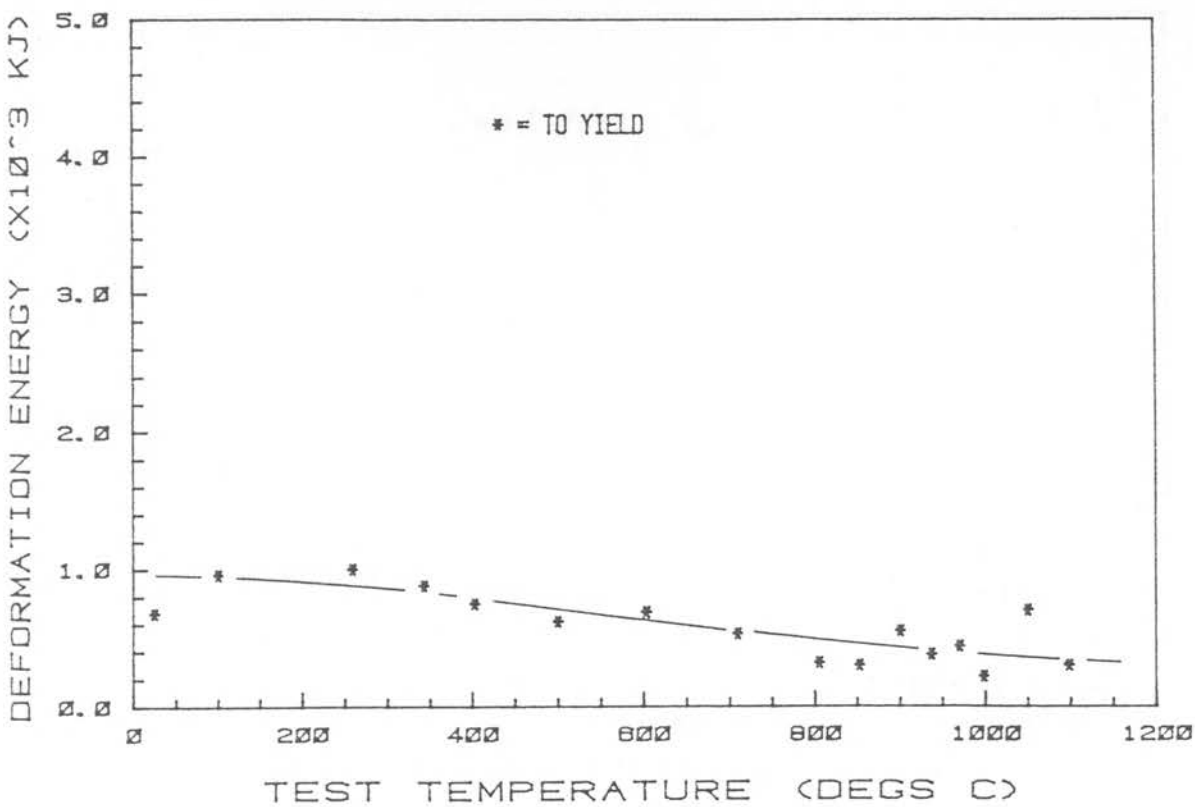

FIGURE 5.14: DEFORMATION ENERGY VS. TEMPERATURE FOR 3CR12 (STRAIN RATE: 0.1 PER SECOND)

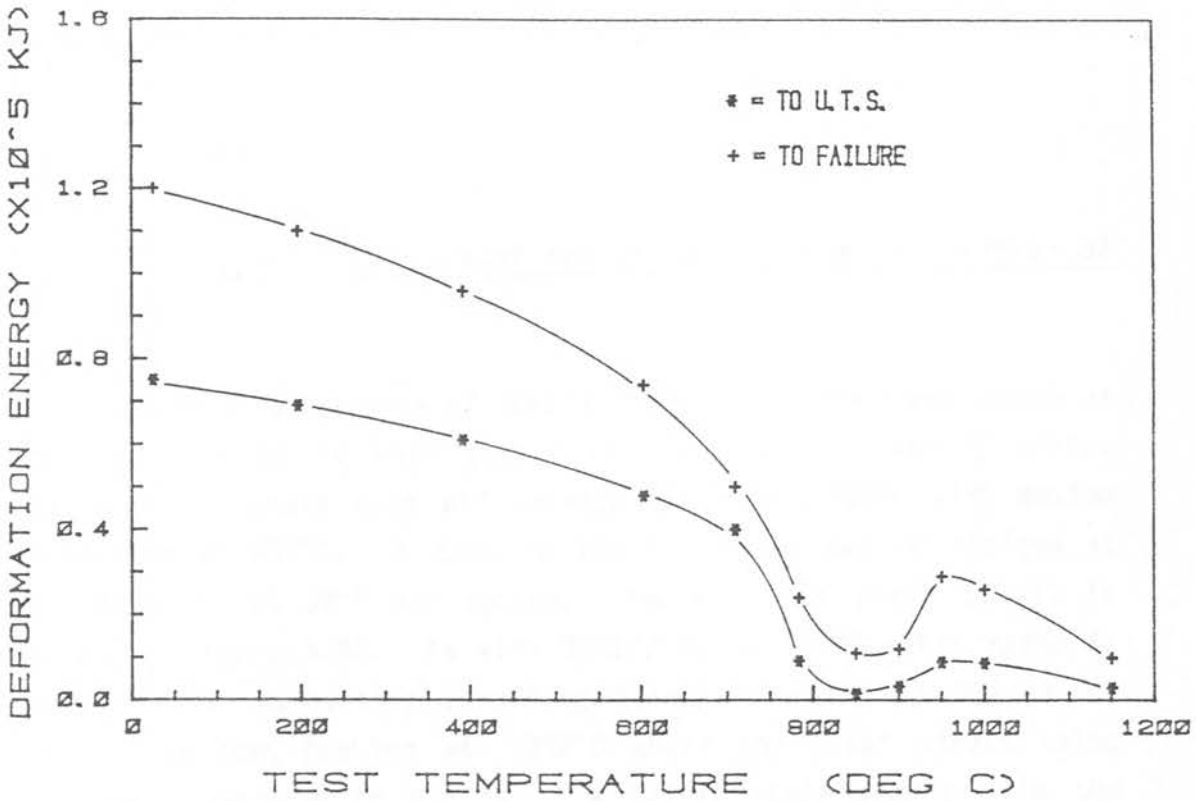

FIGURE 5.15: DEFORMATION ENERGIES VS. TEMPERATURE FOR 3CR12 (STRAIN RATE: 0.0001 PER SECOND)

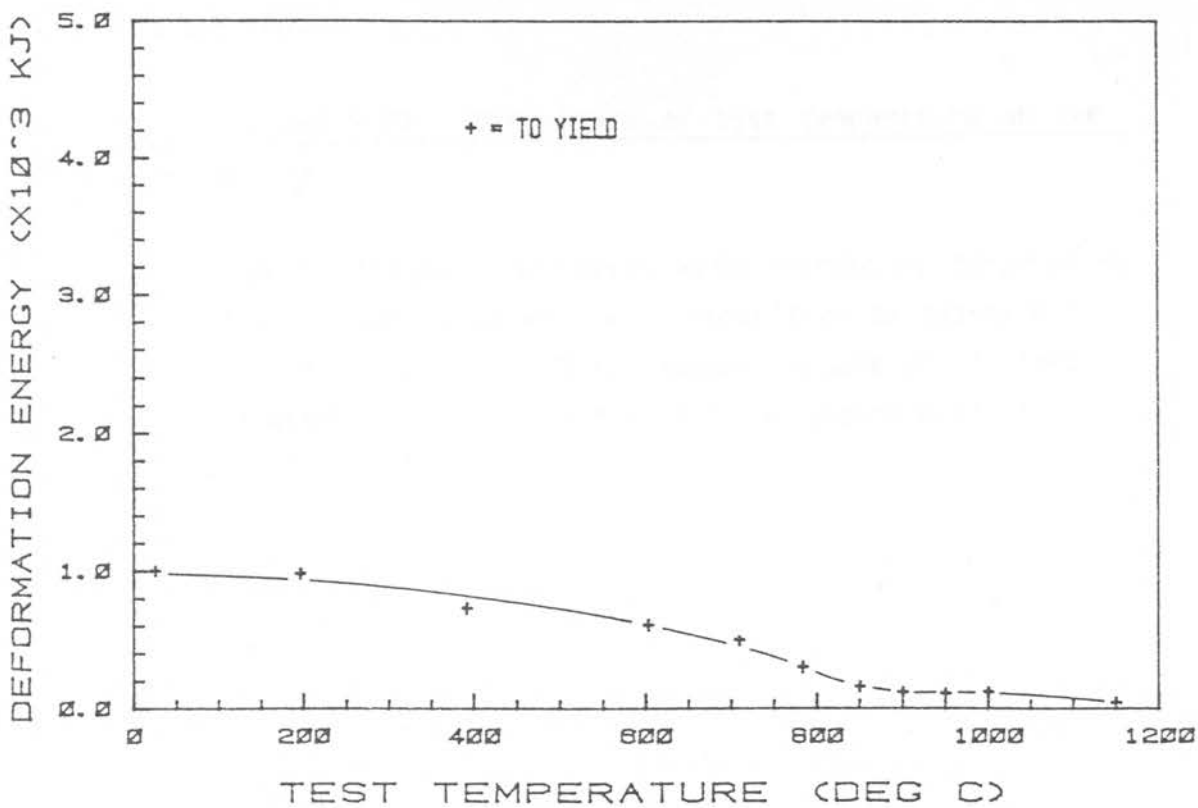

FIGURE 5.16: DEFORMATION ENERGY VS. TEMPERATURE FOR 3CR12 (STRAIN RATE: 0.0001 PER SECOND)

(ii) 3CR12NI

Figures 5.17 and 5.19: Proof and yield stress as a function of temperature.

The mechanical properties of 3CR12Ni follow much the same trends as those for 3CR12 at both strain rates. The UTS and YS values experience a sharp drop off between 725°C and 780°C with maxima appearing at 930°C. A drop in the UTS value can be noticed at around 400°C at 10^{-1} per second. The ratio of yield to UTS is given in figure 5.21. As with 3CR12, below 700°C this ratio is strain rate insensitive remaining fairly constant at 90% up to 600°C and then peaking at 730°C where the proof stress value becomes comparable to the UTS. A fairly steep drop off in the ratio is then experienced, which attenuates with increasing temperature and with decrease in strain rate. At 1100°C the respective values for the strain rates of 10^{-1} and 10^{-4} per second are -40% and -60%.

Figures 5.18 and 5.20: The effect of test temperature on the strain to failure.

The elongation to fracture decreases with increasing temperature until 725°C (19%) and is strain rate insensitive to approximately 850°C. For a strain rate of 10^{-4} per second, a peak is attained at ~900°C (140%) which drops back to the 10^{-1} per second maximum value of ~80% at 1150°C.

Figures 5.22 to 5.23: The effect of test temperature on deformation energy.

As with 3CR12, the deformation energies to failure follow the same trends as do the PS and UTS, showing a mimimum at ~790°C and a maximum at 930°C. A minimum in deformation energy to the UTS is also exhibited at ~790°C, but this is far less pronounced. Sensitivity to strain rate becomes apparent after ~750°C. At temperatures higher than this a faster strain rate leads to a higher energy value. In contrast to 3CR12, 3CR12Ni requires

proportionally far more energy to be deformed from UTS to failure. Energy to deform to the temporary strain value at which the 0.2% proof stress occurs is not significantly strain rate sensitive and contrary to 3CR12, displays a temperature dependence similar to that for the energy to failure values.

Test Temp °C	Engineering Strain	UTS (MPa)	At Strain	0.2% Proof (MPa)	At Strain	UTS/Proof Stress (%)	Instability Stress(MPa)	At Strain	WORK (kJ) DONE TO DEFORM TO:		
									Yield ($x10^3$)	UTS ($x10^5$)	Failure ($x10^5$)
25	0.190	991.0	0.027	906.0	0.0058	91	988.0	0.021	3.4	0.24	-
200	0.167	960.4	0.023	852.9	0.0040	89	956.9	0.018	2.4	0.20	1.2
390	0.142	880.0	0.017	811.0	0.0045	92	878.4	0.015	2.6	0.13	0.94
600	0.153	858.0	0.025	778.3	0.0079	91	853.9	0.020	3.5	0.18	0.95
696	0.158	683.0	0.010	672.0	0.0040	98	693.7	0.069	2.0	0.06	0.72
717	0.152	599.7	0.007	595.0	0.0048	99	599.2	0.006	1.5	0.028	0.58
725	0.159	569.5	0.010	563.5	0.0077	99	569.3	0.009	2.7	0.04	0.56
782	0.368	133.9	0.058	117.0	0.0335	87	133.3	0.055	1.8	0.05	0.30
846	0.574	130.9	0.199	86.1	0.0137	66	125.4	0.091	0.59	0.24	0.51
898	0.377	153.9	0.147	105.6	0.0085	69	150.3	0.095	0.48	0.20	0.41
930	0.713	167.0	0.323	94.4	0.0094	57	152.9	0.139	0.50	0.48	0.79
947	0.665	162.7	0.291	90.6	0.0197	56	1253.3	0.169	0.79	0.40	0.69
1000	0.637	147.0	0.292	75.5	0.0219	51	139.0	0.189	0.80	0.36	0.58
1046	0.742	126.8	0.324	62.5	0.0279	49	119.4	0.216	0.83	0.33	0.55
1096	0.756	106.5	0.317	51.0	0.0232	48	100.7	0.218	0.54	0.27	0.47
1150	0.835	86.4	0.302	39.2	0.0190	45	80.8	0.212	0.34	0.21	0.40
1154	0.756	85.1	0.291	42.1	0.0201	49	81.6	0.213	0.38	0.20	0.36

TABLE 5.7: MECHANICAL PROPERTIES FOR 3CR12NI (STRAIN RATE: 10^{-1} PER SECOND)

Test Temp °C	Engineering Strain	UTS (MPa)	At Strain	0.2% Proof (MPa)	At Strain	UTS/Proof Stress (%)	Instability Stress(MPa)	At Strain	WORK (kJ) DONE TO DEFORM TO:		
									Yield ($x10^3$)	UTS ($x10^5$)	Failure ($x10^5$)
25	0.157	1000.4	0.029	900.5	0.0082	90	1000.6	0.024	4.4	0.25	1.3
200	0.142	964.7	0.022	860.8	0.0056	89	962.9	0.019	3.1	0.19	1.1
397	0.123	969.5	0.027	866.7	0.0056	89	964.7	0.018	3.1	0.23	1.0
603	0.119	874.0	0.022	800.5	0.0068	92	872.5	0.019	3.4	0.17	0.88
730	0.272	163.3	0.026	149.3	0.003	91	163	0.019	0.34	-	-
800	0.326	92.1	0.055	74.9	0.0053	82	91.0	0.036	0.26	0.47	0.20
900	1.398	64.2	0.134	48.5	0.0103	76	62.3	0.069	0.30	0.08	0.39
1000	1.200	27.7	0.193	21.5	0.0070	77	26.6	0.083	0.089	0.05	0.18
1150	0.794	23.9	0.292	14.3	0.0091	60	21.9	0.114	0.064	0.06	0.12

TABLE 5.8: MECHANICAL PROPERTIES OF 3CR12NI (STRAIN RATE 10^{-4} PER SECOND)

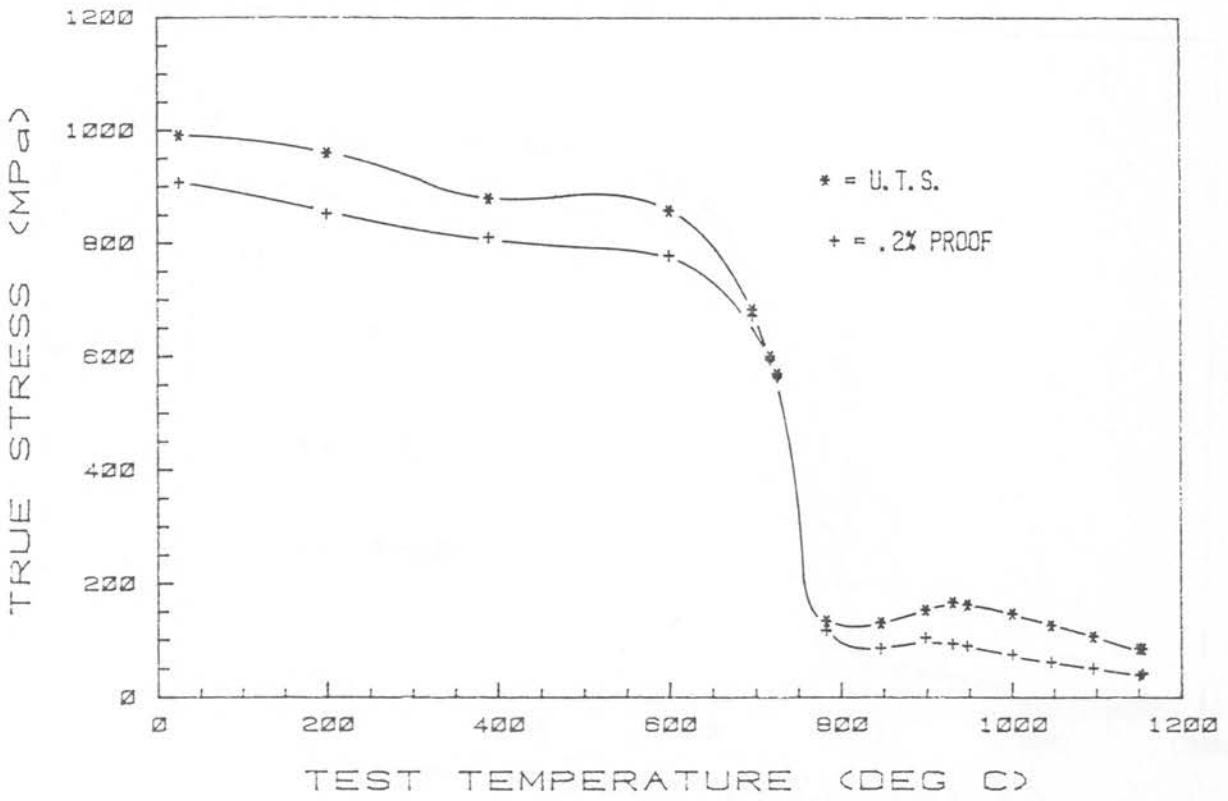

FIGURE 5.17: TENSILE PROPERTIES VS. TEMPERATURE FOR 3CR12NI (STRAIN RATE: 0.1 PER SECOND)

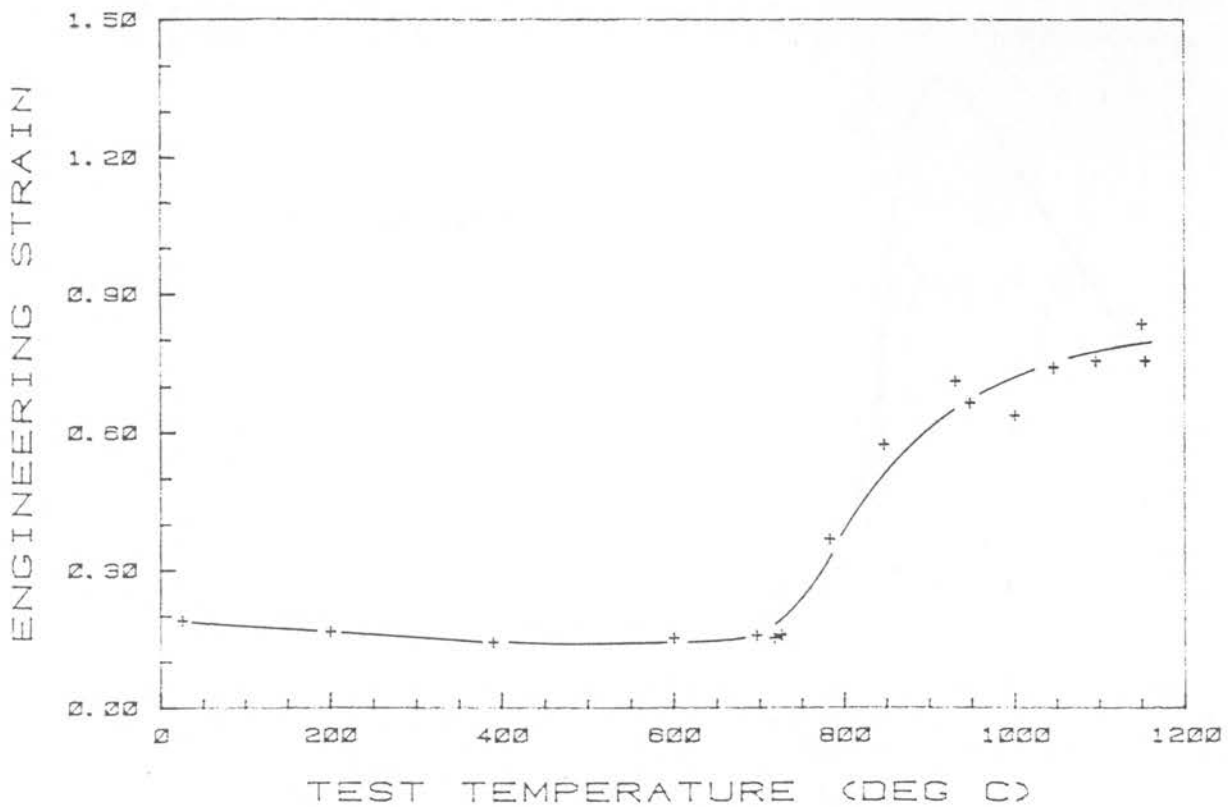

FIGURE 5.18: FAILURE STRAIN VS. TEMPERATURE FOR 3CR12NI (STRAIN RATE: 0.1 PER SECOND)

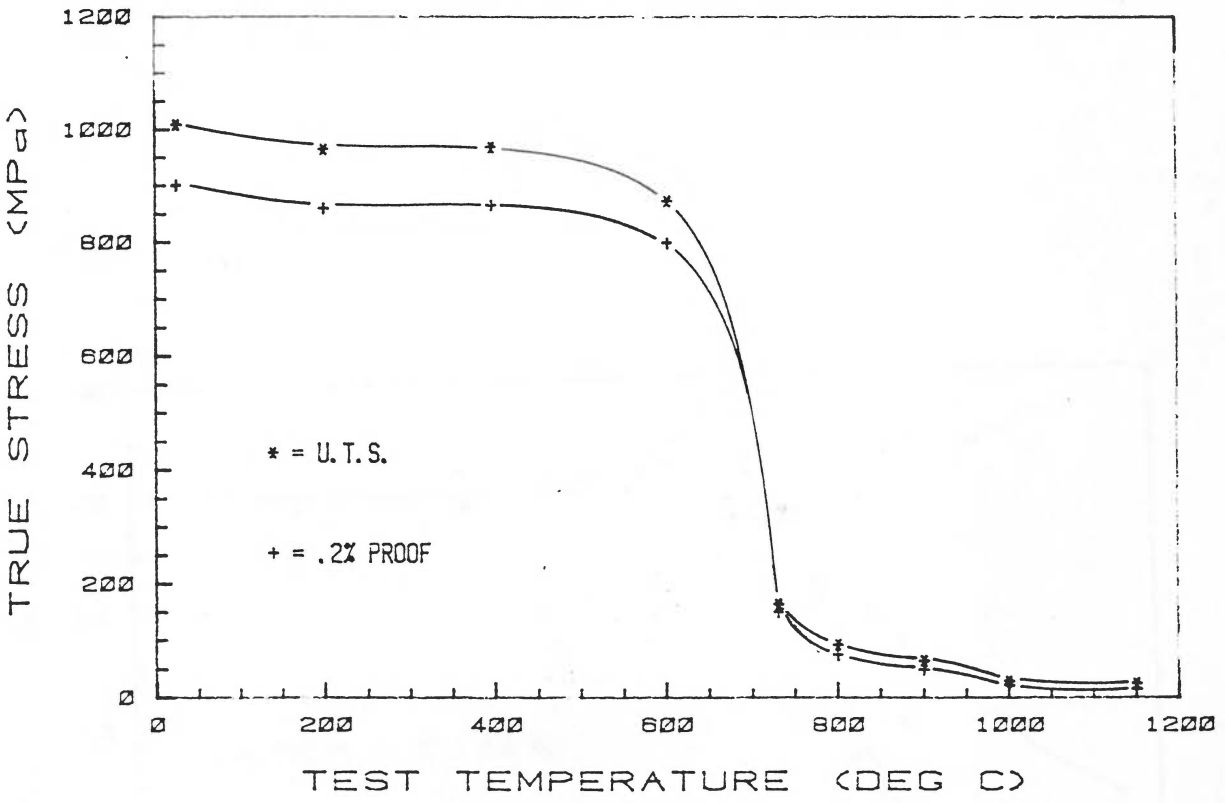

FIGURE 5.19: TENSILE PROPERTIES VS. TEMPERATURE FOR 3CR12NI (STRAIN RATE: 0.0001 PER SECOND)

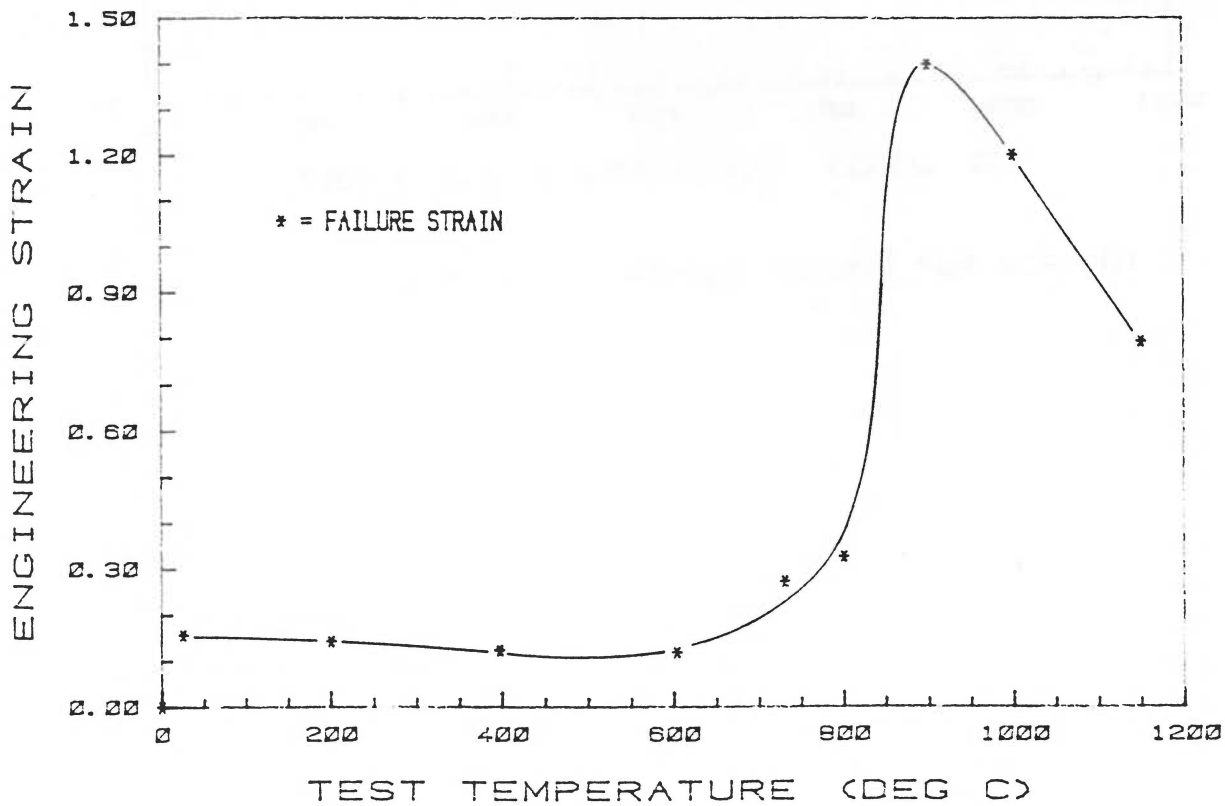

FIGURE 5.20: FAILURE STRAIN VS. TEMPERATURE FOR 3CR12NI (STRAIN RATE: 0.0001 PER SECOND)

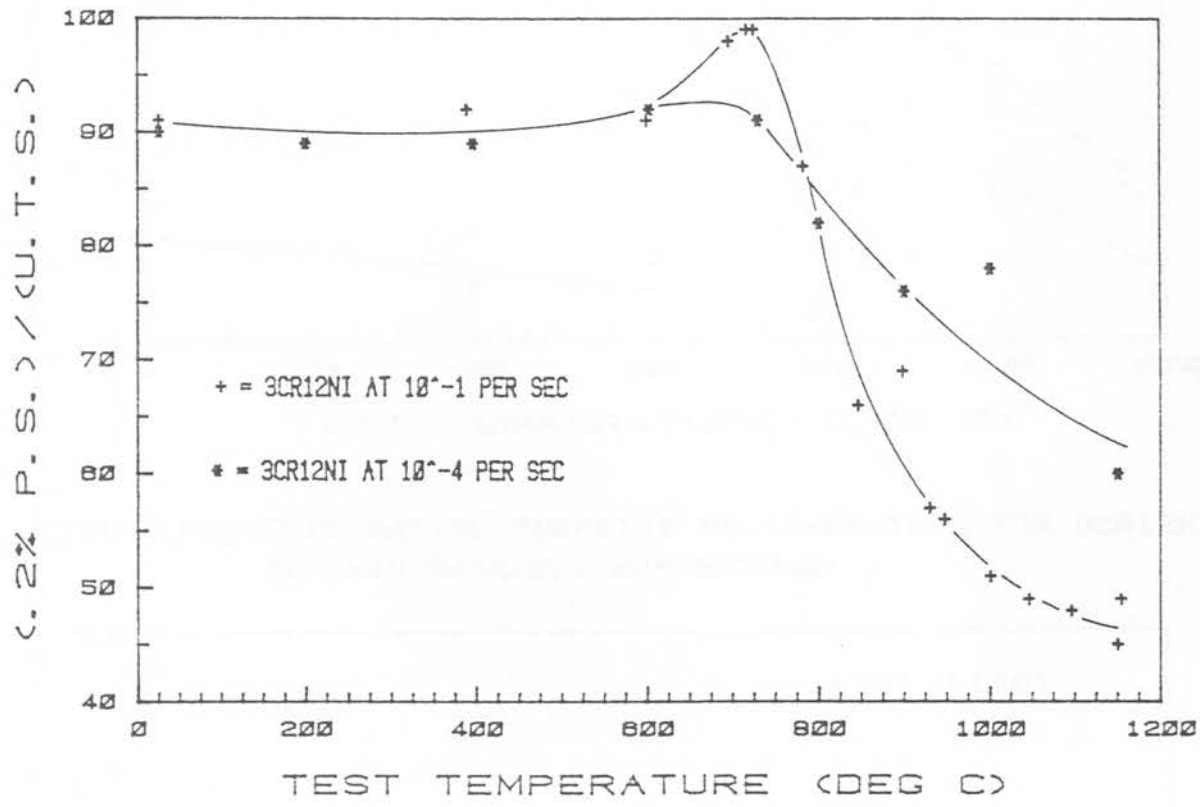

FIGURE 5.21: RATIO OF PROOF STRESS TO UTS FOR 3CR12NI

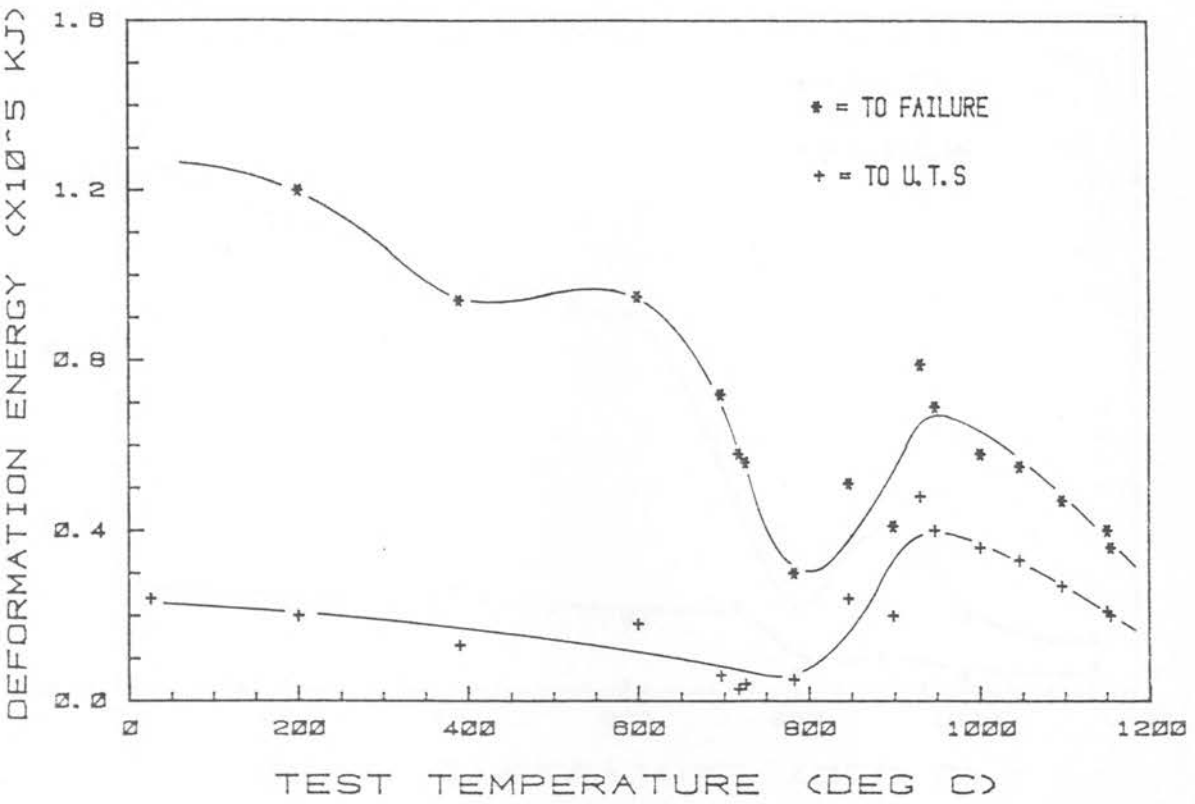

FIGURE:5.22: DEFORMATION ENERGIES VS. TEMPEATURE FOR 3CR12NI (STRAIN RATE: 0.1 PER SECOND)

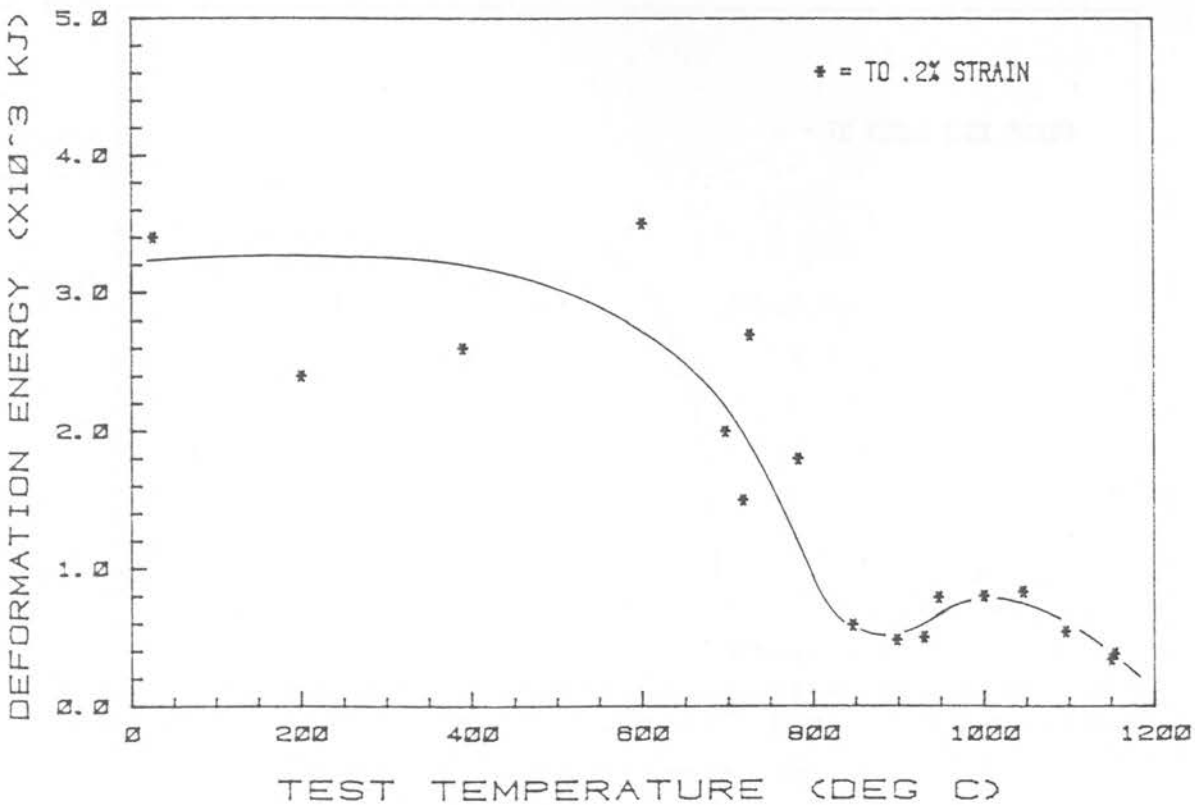

FIGURE 5.23: DEFORMATION ENERGY VS. TEMPERATURE FOR 3CR12NI (STRAIN RATE: 0.1 PER SECOND)

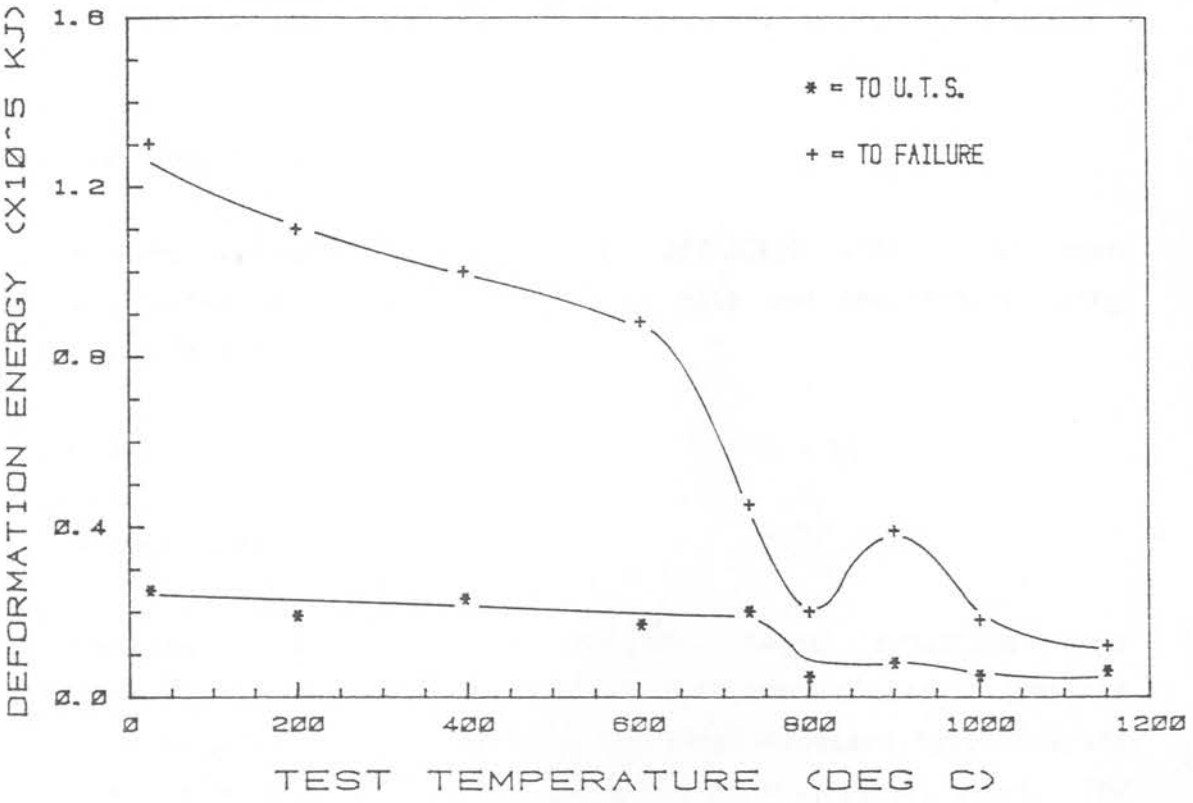

FIGURE 5.24: DEFORMATION ENERGIES VS. TEMPERATURE FOR 3CR12NI
(STRAIN RATE: 0.0001 PER SECOND)

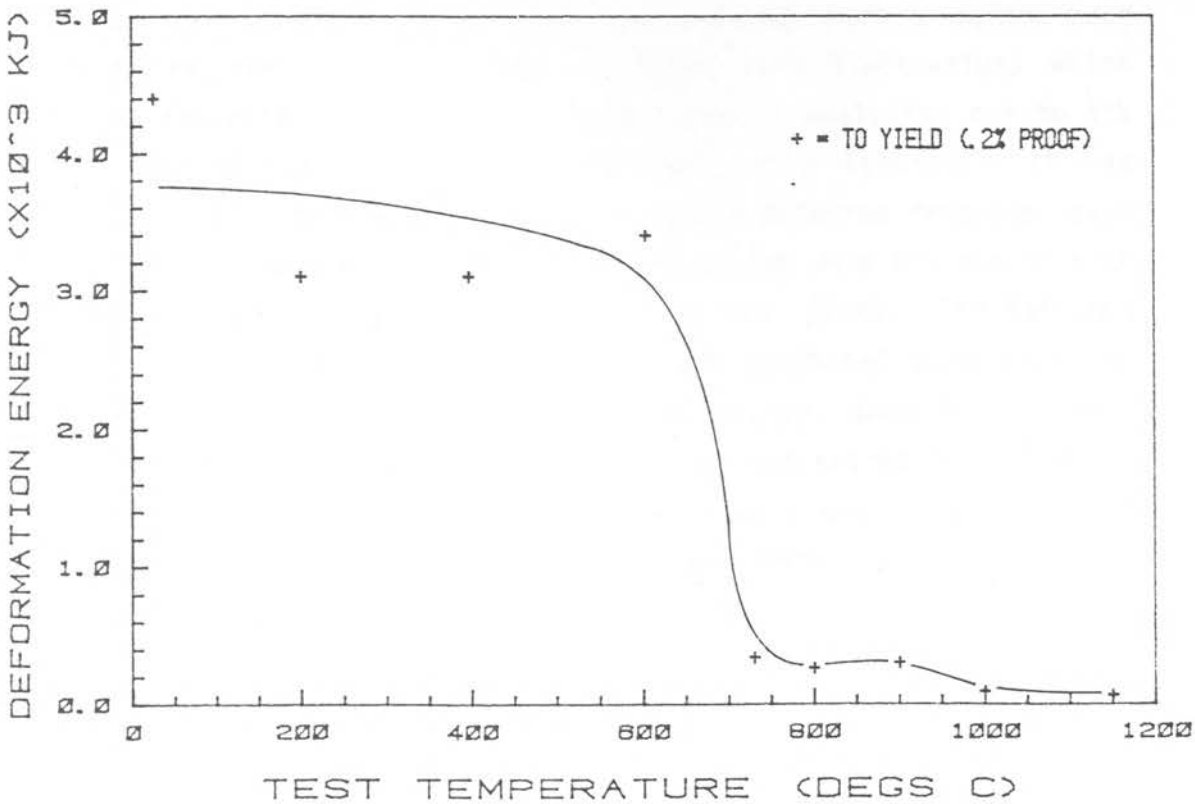

FIGURE 5.25: DEFORMATION ENERGY VS. TEMPERATURE FOR 3CR12NI
(STRAIN RATE: 0.0001 PER SECOND)

5.2.3 Work hardening

The work hardening characteristics of 3CR12 alloys have been investigated as a function of strain rate and temperature using three relationships:

Holloman : $\sigma = K \epsilon^{n}$

Ludwik : $\sigma = \sigma_o + K' \epsilon^{n'}$

Modified Swift : $\epsilon = \epsilon_o + C \sigma^{n''}$

Both the Ludwik and the Modified Swift equations were differentiated and the work hardening parameters n' and n" obtained for various delineated regions by the Jaoul-Crussard type analysis (plots of $\ln(d\sigma/d\epsilon)$ vs $\ln\epsilon$ and $\ln(d\sigma/d\epsilon)$ vs $\ln\sigma$ respectively). The Holloman n parameter was obtained directly from the slope of the $\ln\sigma$ versus $\ln\epsilon$ plot. It was found, however, that deformation stages did not always yield a linear region in such diagrams for any one particular analysis, but an attempt was made to define near linear regions in such cases. Short term fluctuations which become inherent in the Jaoul-Crussard type of analysis, due to its high sensitivity to strain fluctuations, were ignored. It was noted, though, that where transition points occurred from one stage to another, these were normally consistent for data plotted on both the $\ln(d\sigma/d\epsilon)$ vs $\ln\epsilon$ and $\ln(d\sigma/d\epsilon)$ vs $\ln\sigma$ plots. The Hollomon analysis, being more insensitive, seldom exhibited more than one deformation regime. At certain temperatures, some tests showed excellent correlation with linear regions determined by all three analyses, whereas at other temperatures, only one or sometimes no analysis would yield a linear deformation regime.

5.2.3.1 3CR12

(1) Hollomon analysis: Tables 5.9 - 5.10 and Figures 5.26 - 5.29 refer.

Generally, the Hollomon analysis yielded straight lines between the yield and instability strains and n values could be calculated with good correlation coefficients. In the temperature range from 25°C to 200°C at 10^{-4} per second, two n values could be delineated over the range between yield and instability strains. At 850°C, for both strain rates, the $\ln \sigma$ vs $\ln \epsilon$ relationship exhibited non-linear behaviour and the n values became essentially undefineable. (n = 0.004 with a correlation coefficient of 0.69 at 10^{-4} per second).

Considering Figures 5.26 and 5.28 it can be noted that the work hardening values increase slightly with increasing test temperature (from 0.173 at 25°C to 0.193 at 500°C for the 10^{-1} per second strain rate) until around 500°C, after which the n values drop off to an undefineable value at ~850°C, as mentioned above. No significant strain rate sensitivity in the n values to this temperature can be noted. From 900°C to 1150°C, however, the faster strain rate causes a more significant increase in the n value with increased temperature. Peaks are exhibited at around 1050°C (0.236 for 10^{-1} per second) and at 1000°C (0.105 for 10^{-4} per second) before dropping off slightly at the extreme limits of the temperature ranges. It can be noted that the Considére point of instability follows closely the behaviour of the Hollomon parameters, especially at elevated temperatures.

The strength factor K (Figures 5.27 & 5.29) follows essentially the same kind of pattern as does the UTS for this material and responds similarly, too, in its strain rate sensitivity.

TEST TEMPERATURE °C	n VALUE	LINEAR CORRELATION COEFFICIENT	STRENGTH FACTOR K
25	0.173	0.997	834
100	0.178	1.000	825
259	0.194	0.999	778
343	0.176	0.999	701
403	0.190	0.998	683
500	0.193	0.996	627
603	0.174	0.998	550
709	0.134	0.995	374
805	0.115	0.989	190
852	0.080	0.977	117
900	0.102	0.996	110
970	0.206	0.998	183
998	0.219	0.998	180
1050	0.236	0.998	158
1098	0.214	1.000	132

TABLE 5.9: THE HOLLOMAN WORK HARDENING PARAMETERS n AND K FOR 3CR12 (STRAIN RATE: 10^{-1} PER SECOND).

TEST TEMPERATURE °C	n VALUE	LINEAR CORRELATION COEFFICIENT	STRENGTH FACTOR K
25	0.102	0.998	593
	0.172	0.999	783
196	0.113	0.997	563
	0.194	0.999	783
392	0.207	0.998	755
603	0.163	0.996	596
709	0.136	0.998	387
783	0.099	0.995	140
850	0.004	0.690	39
	undefineable	-	-
900	0.046	0.994	42
950	0.091	0.998	60
1000	0.105	0.995	47
1150	0.067	0.989	20

TABLE 5.10: THE HOLLOMON WORK HARDENING PARAMETERS n AND K FOR 3CR12.
(STRAIN RATE: 10^{-4} PER SECOND).

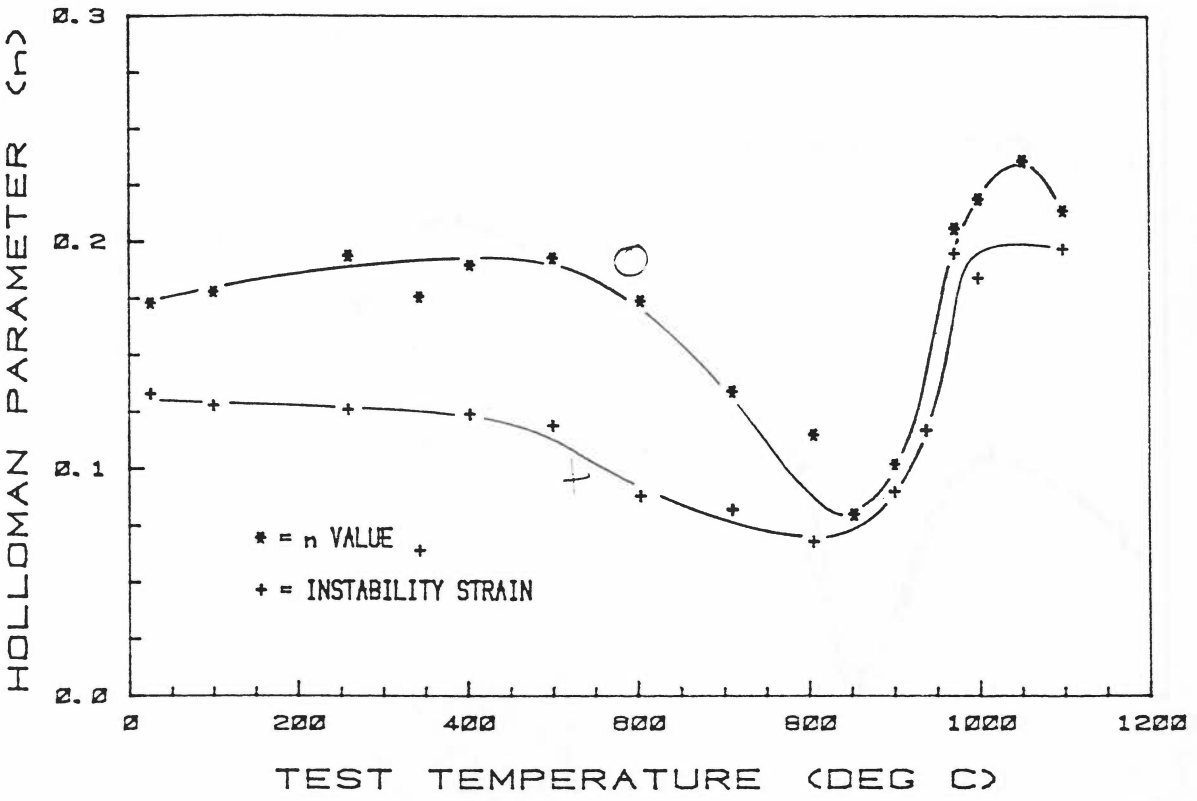

FIGURE 5.26: HOLLOMAN n PARAMETER VS. TEMPERATURE FOR 3CR12
(STRAIN RATE: Ø.1 PER SECOND)

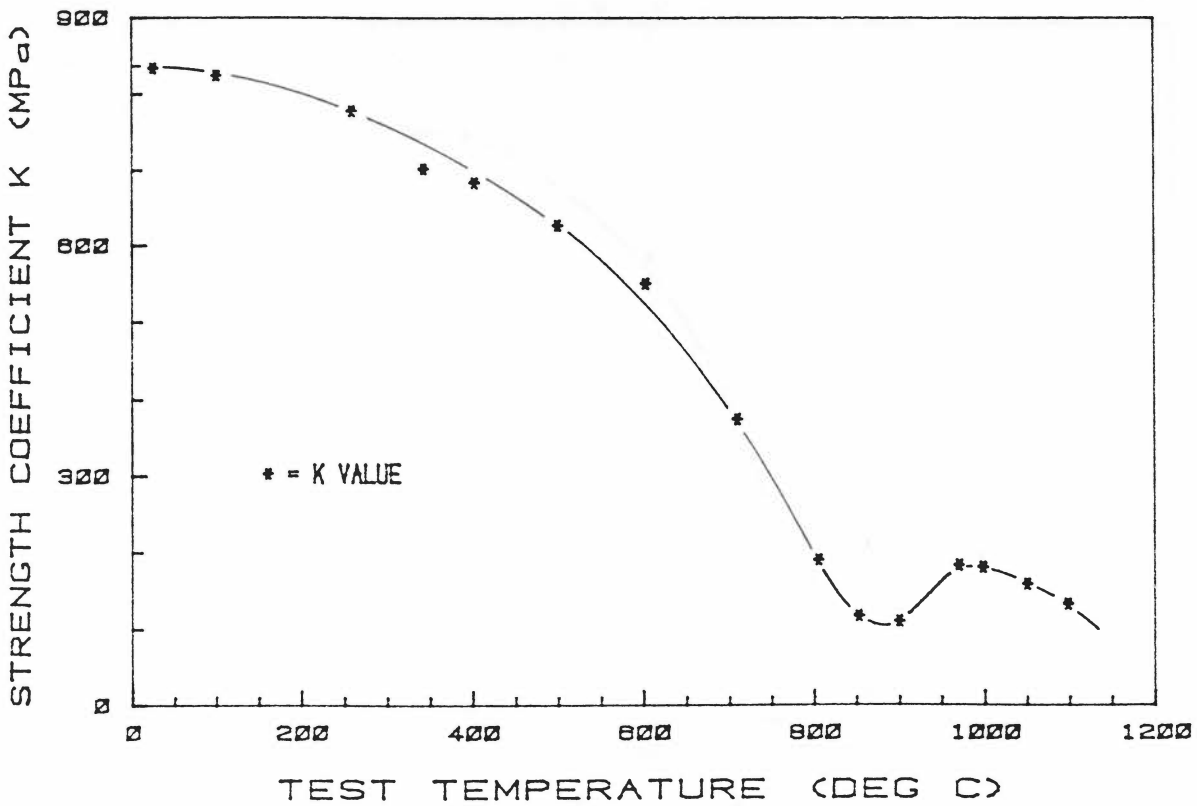

FIGURE 5.27: STRENGTH COEFFICIENT K VS. TEMPERATURE FOR 3CR12
(STRAIN RATE: Ø.1 PER SECOND)

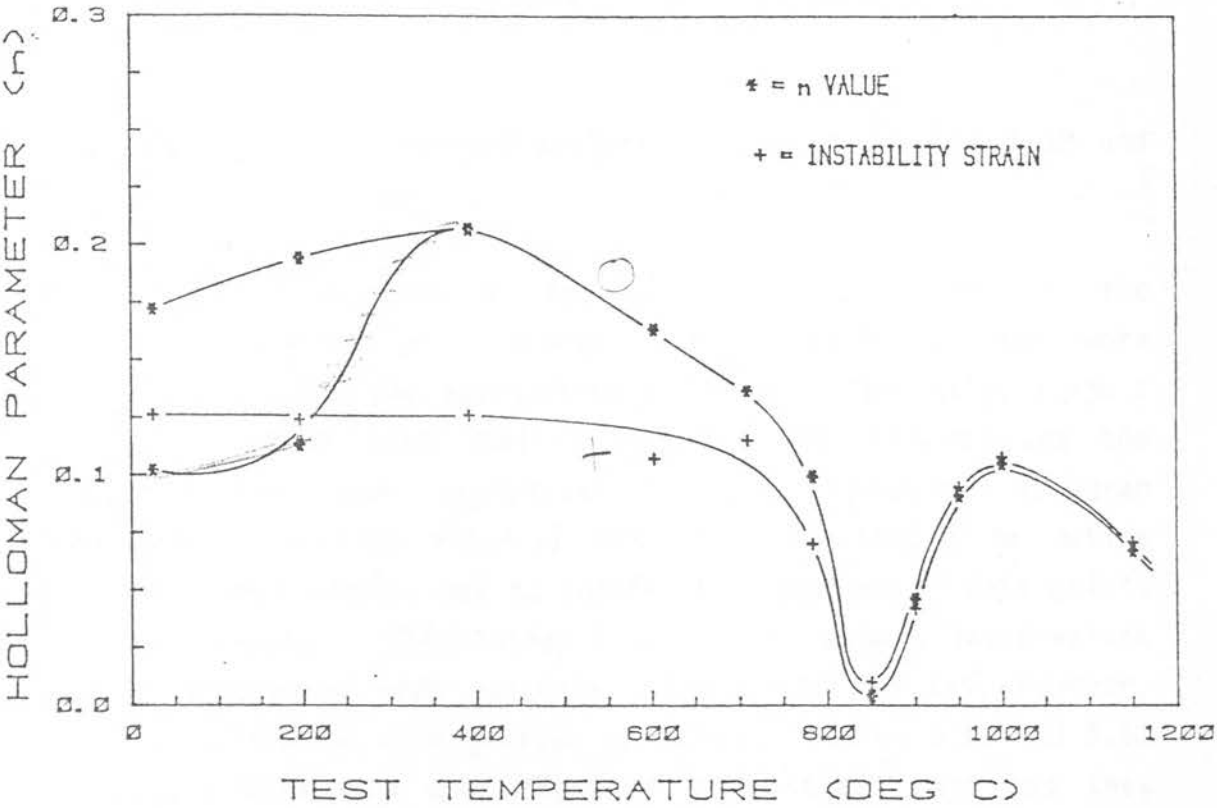

FIGURE 5.28: HOLLOMAN PARAMETER VS. TEMPERATURE FOR 3CR12
(STRAIN RATE: Ø.ØØØ1 PER SECOND)

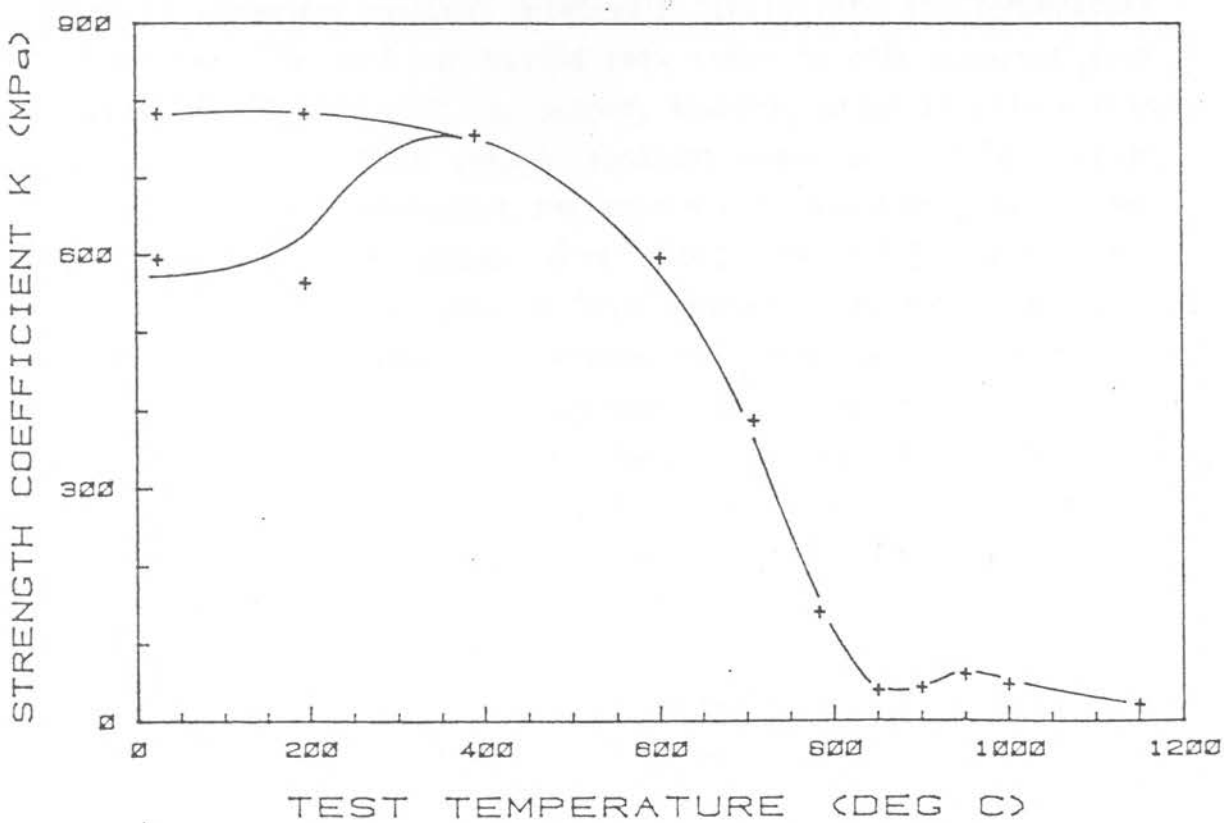

FIGURE 5.29: STRENGTH COEFFICIENT K VS. TEMPERATURE FOR 3CR12
(STRAIN RATE: Ø.ØØØ1 PER SECOND)

(ii) Ludwik (Jaoul-Crussard analysis): Tables 5.11 to 5.12 and Figure 5.30 refer:

Stages designated from I to III were delineated in the Jaoul-Crussard plots of $\ln d\sigma/d\epsilon$ vs $\ln\epsilon$ and their slopes were calculated to yield the appropriate n' values. Typically, stage I is encountered at very small plastic strains ($\sim$0.01) and the resolution of the analytical computer program (program "Workharden"; section 4.5.2.1) was at times unable to define accurately this regime, due to insufficient numbers of data points at these strains. Where stage I values are quoted, these values are not considered very accurate. Stages II and III, however, could be delineated with greater certainty. Tables 5.11 and 5.12 and Figure 5.30 show the effect of both strain rate and test temperature on the n' parameter for $3CR12_{(2)}$. Similar to the Hollomon n parameter, the n' parameter is not well defined at ~850°C, especially at the strain rate of 10^{-4} per second.
Stage II behaviour remains relatively strain rate and temperature insensitive. At 10^{-1} per second this stage is only apparent from 25°C to 500°C. At 10^{-4} per second, however, Stage II exists from 25°C to 800°C and then becomes apparent again at ~1150°C. Stage III behaviour is temperature and strain rate dependent, except for in the temperature range from ~900°C to ~1150°C where the significance of strain rate is less apparent. In this stage, the work hardening parameter n' behaves in a similar fashion to the Hollomon n parameter in that they both demonstrate two maxima and a minimum in approximately the same temperature ranges. At the 10^{-4} per second strain rate, however, the first peak appears at a much lower temperature (~200°C as opposed to ~400°C for the 10^{-1} per second case).

Notice can be made of the values of the n' and K' which become negative at most temperatures. This indicates that these parameters do not always have a simple significance. As differences in the change of work hardening behaviour with temperature is most strongly influenced by the exponential n' in the Ludwik equation, the σ_o constant values were not considered to be important and are thus not presented.

TEMPERATURE °C	n' VALUE	K'	REGIME	STRAIN RANGE	CORRELATION COEFFICIENT
25	-0.484	-12	1	0.0107 - 0.0146	0.968
	0.459	781	2	0.0162 - 0.0712	0.974
	-0.215	-268	3	0.0729 - 0.1183	0.993
100	0.609	990	2	0.0168 - 0.0375	0.995
	0.160	872	3	0.0391 - 0.0901	0.995
343	0.544	886	2	0.0106 - 0.0229	0.965
	0.219	671	3	0.0246 - 0.0594	0.997
403	0.404	690	2	0.0114 - 0.0533	0.996
	-0.055	-1300	3	0.0550 - 0.0970	0.986
500	0.508	897	2	0.0114 - 0.0228	0.794
	0.156	832	3	0.0243 - 0.0687	0.992
603	-0.091	-502	3	0.0243 - 0.0710	0.996
709	-0.239	-56	3	0.0096 - 0.0866	0.986
805	-0.337	-14	3	0.0122 - 0.0621	0.992
852	undefineable	-	-	-	-
900	-0.3218	-11	3	0.0312 - 0.0886	0.999
937	-0.0355	-59	3	0.0223 - 0.1649	0.997
970	0.0090	2819	3	0.0280 - 0.1771	0.998
998	0.0447	566	3	0.0175 - 0.1698	0.999
1050	0.0337	675	3	0.0410 - 0.1493	0.998
1098	0.1617	156	3	0.0316 - 0.1788	0.996

TABLE 5.11: LUDWIK PARAMETERS n' AND K' FOR 3CR12 (STRAIN RATE 10^{-1} PER SECOND).

TEMPERATURE °C	n' VALUE	K'	REGIME	STRAIN RANGE	CORRELATION COEFFICIENT
25	-0.560	-3.5	1	0.0034 - 0.0067	0.998
	0.483	770	2	0.0100 - 0.0526	0.982
	0.020	4600	3	0.0538 - 0.1011	0.997
196	-1.062	-0.11	1	0.0041 - 0.0057	0.998
	0.589	1000	2	0.0065 - 0.0371	0.992
	0.118	1100	3	0.0380 - 0.0941	0.963
392	-1.111	-0.03	1	0.0044 - 0.0073	0.987
	0.478	140	2	0.0148 - 0.0212	0.989
	-0.250	-19	3	0.0297 - 0.0630	0.988
603	0.301	560	2	0.0041 - 0.061	0.979
	-0.723	-14	3	0.0613 - 0.1019	0.987
709	0.210	330	2	0.0065 - 0.0590	0.998
	-1.000	-6.6	3	0.0781 - 0.114	0.995
783	-1.111	-0.02	1	0.0044 - 0.0086	0.987
852	undefineable	-	-	-	-
900	-1.065		3	0.0246 - 0.0315	0.998
950	-0.049	-6.8	3	0.0038 - 0.0834	0.981
1000	-1.162	-0.02	1	0.0038 - 0.0104	0.979
	0.160	38	3	0.0176 - 0.1054	0.988
1150	-2.005	-0.02	1	0.0038 - 0.0048	1.00
	0.742	3.1	2	0.0132 - 0.0225	0.906
	0.013	110	3	0.0234 - 0.0637	0.933

TABLE 5.12: LUDWIK PARAMETERS n' AND K' FOR 3CR12(2) (STRAIN RATE 10^{-4} PER SECOND).

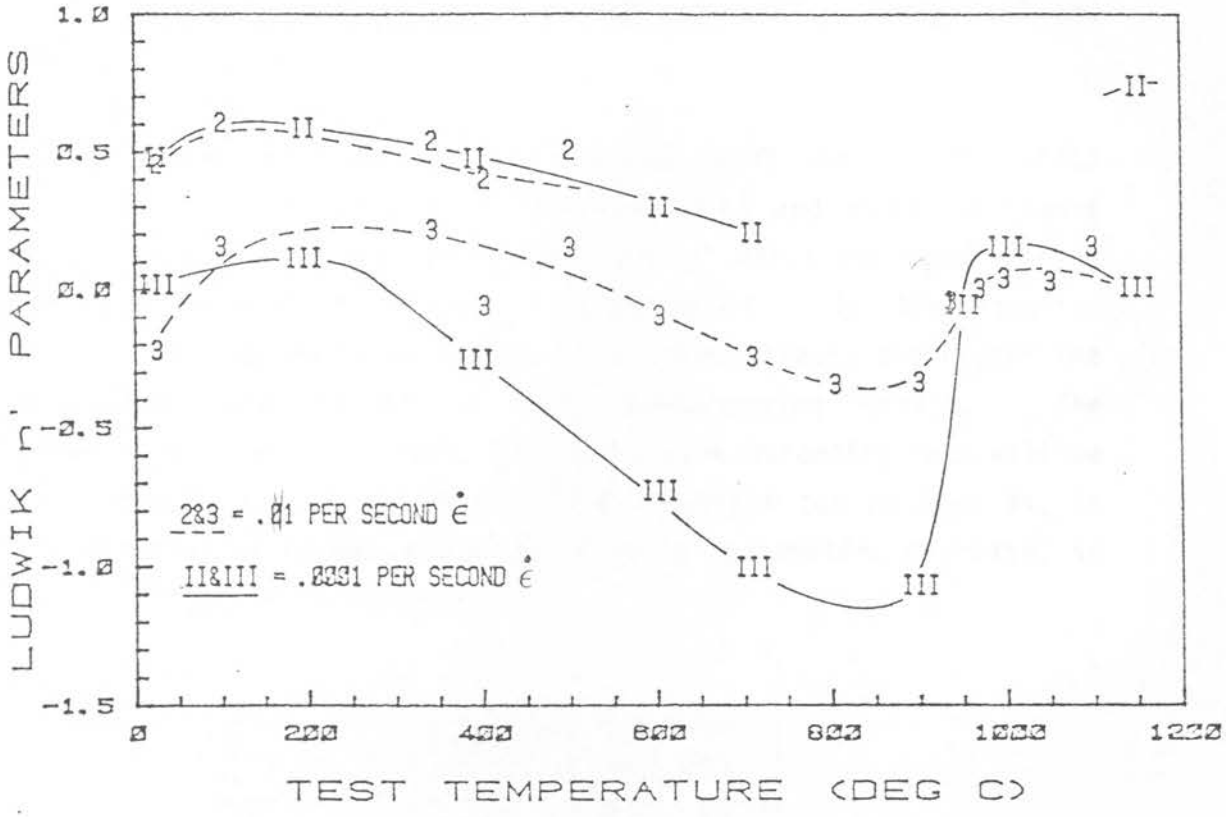

FIGURE 5.30: LUDWIK n' PARAMETERS AS A FUNCTION OF TEST TEMPERATURE FOR SCR12

(iii) Modified Swift (Jaoul-Crussard analysis): Table 5.13 and Figure 5.31 refer.

The n" values obtained from the Modified Swift analysis for 3CR12 at 10^{-1} per second are given in Table 5.13 and shown in Figure 5.31. By virtue of its definition, the n" value increases when a decrease in work hardening is experienced. In the equation $\epsilon = \epsilon_0 + c\sigma^{n"}$, it can be seen that for a given stress, the higher the n" value, the larger is the corresponding strain. The interpretation of this means that a low work hardening rate will be reflected in a high n" value. This behaviour can be seen as, in the temperature ranges where the n and n' parameters decrease, so the n" parameter increases.

TEST TEMPERATURE °C	n" VALUE	REGIME	STRESS RANGE MPa
25	3.1	2	334 - 508
	6.6	3	508 - 571
100	3.3	2	408 - 460
	5.7	3	460 - 533
259	4.2	2	361 - 448
	7.7	3	448 - 502
343	4.3	2	300 - 389
	6.5	3	389 - 444
403	4.0	2	291 - 391
	7.0	3	391 - 450
500	4.5	2	310 - 376
	8.7	3	376 - 426
603	5.2	2	253 - 314
	8.0	3	314 - 351
709	undefineable		
805	16.15	3	128 - 138
852	15.5	3	89 - 98
900	13.7	3	77 - 86
937	5.8	3	91 - 127
970	5.5	3	83 - 129
998	5.4	3	72 - 123
1050	5.8	3	58 - 93
1098	5.0	3	58 - 92

TABLE 5.13: MODIFIED SWIFT PARAMETERS n" FOR 3CR12.
(STRAIN RATE 10^{-1} PER SECOND).

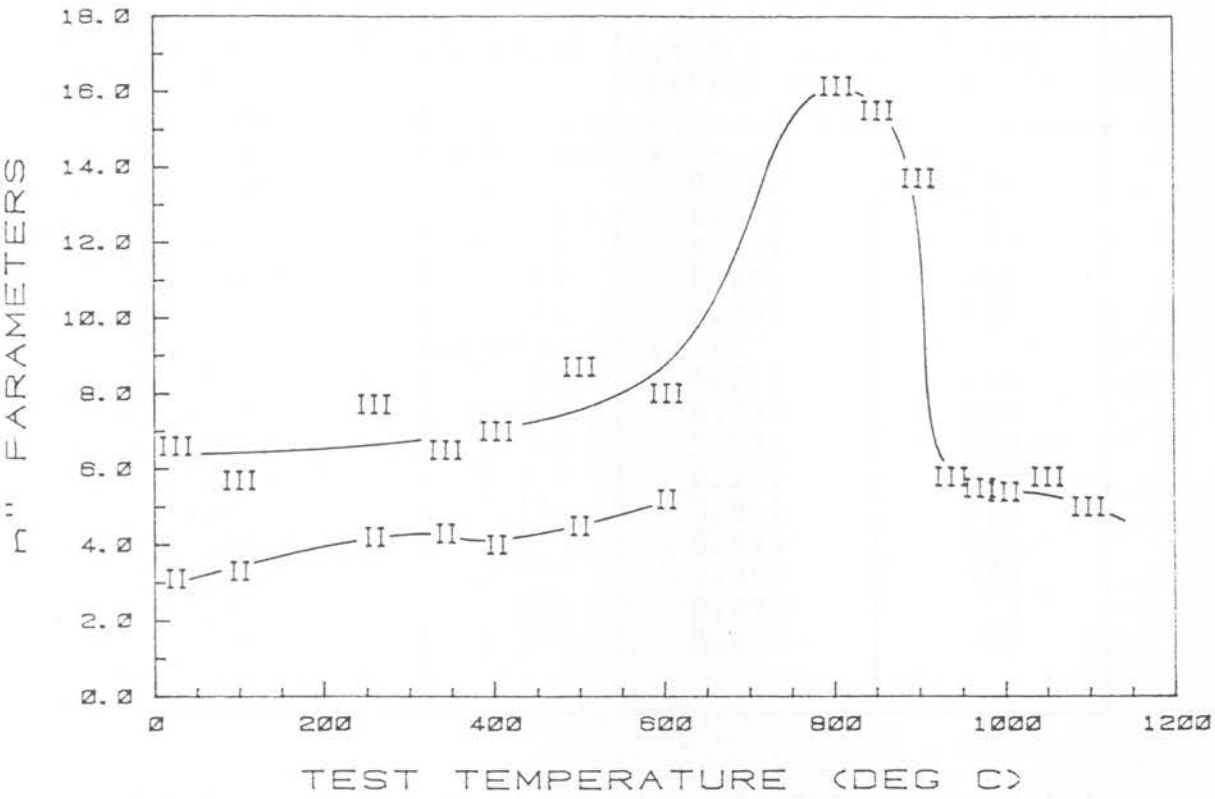

FIGURE 5.31: MODIFIED SWIFT "n" PARAMETERS VS. TEST TEMPERATURE FOR 3CR12 (STRAIN RATE: 0.1 PER SECOND)

5.3.2.2 3CR12Ni

Hollomon analysis: Tables 5.14 & 5.15 and Figures 5.32 to 5.33 refer.

The Hollomon work hardening behaviour for 3CR12Ni at 10^{-1} per second follows very much the same trend as for 3CR12. Analysis of the data at 10^{-4} per second, however, did not yield consistant results and there were many instances where no linear regions could be demarcated. It is interesting to note that the minima in the work hardening parameters noted in 3CR12 also occur in 3CR12Ni; but the temperature is lower and is between 650°C and 800°C.

TEST TEMPERATURE °C	n VALUE	LINEAR CORRELATION COEFFICIENT	STRENGTH FACTOR K
25	undefineable	-	-
200	0.134	0.990	1779
390	0.116	0.992	1515
600	0.079	0.985	1173
696	0.069	0.993	984
717	0.069	0.966	858
725	undefineable	-	-
846	0.096	0.997	158
898	0.121	0.999	200
930	0.160	0.999	210
947	0.214	0.995	226
1000	0.249	0.994	213
1046	0.277	0.995	185
1096	0.275	0.997	155
1150	0.256	0.995	119
1154	0.264	0.999	124

TABLE 5.14: THE HOLLOMAN WORK HARDENING PARAMETERS n AND K FOR 3CR12NI (STRAIN RATE OF 10^{-1} PER SECOND).

TEST TEMPERATURE °C	n VALUE	LINEAR CORRELATION COEFFICIENT	STRENGTH FACTOR K
25	undefineable	-	-
200	undefineable	-	-
397	undefineable	-	-
603	undefineable	-	-
783	undefineable	-	-
800	0.065	0.984	113
900	0.086	0.994	79
1000	0.080	0.998	33
1150	undefineable	-	-

TABLE 5.15: THE HOLLOMON WORK HARDENING PARAMETERS n AND K FOR 3CR12NI. (STRAIN RATE 10^{-4} PER SECOND).

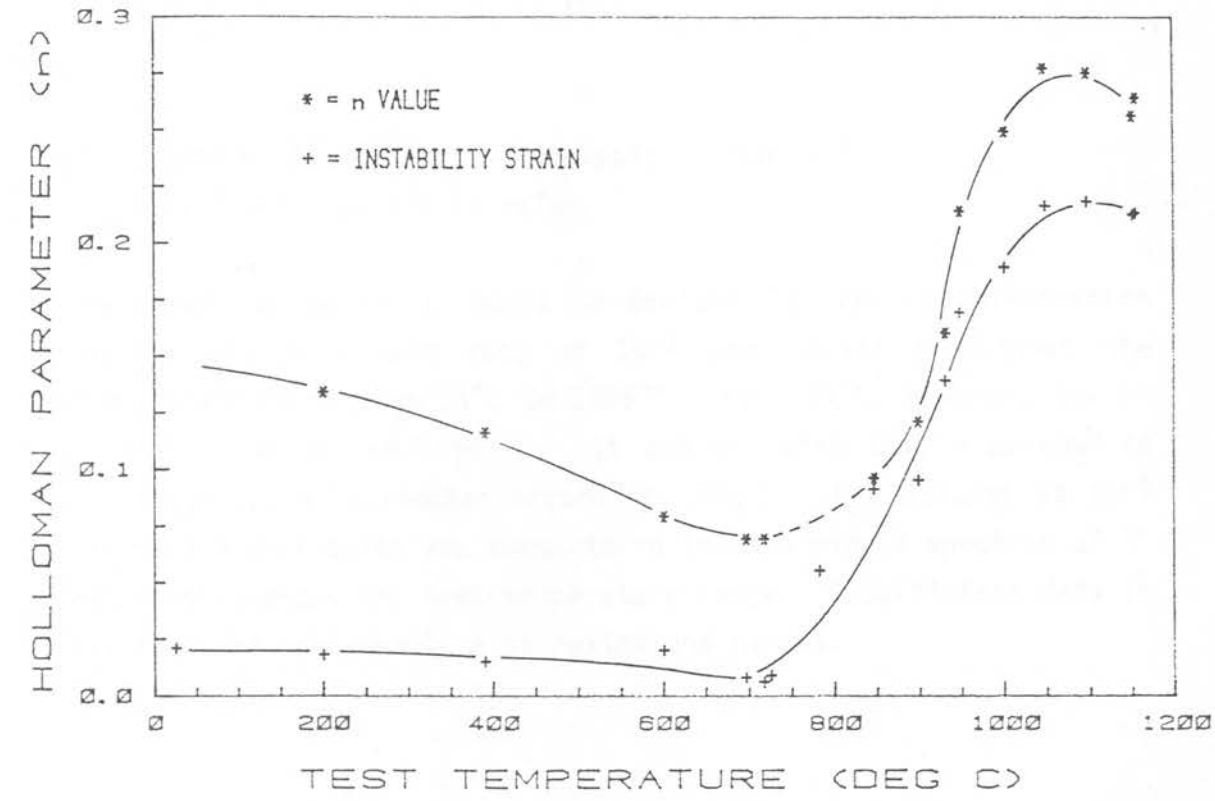

FIGURE 5.32: HOLLOMAN PARAMETER VS TEMPERATURE FOR 3CR12NI
(STRAIN RATE: Ø.1 PER SECOND)

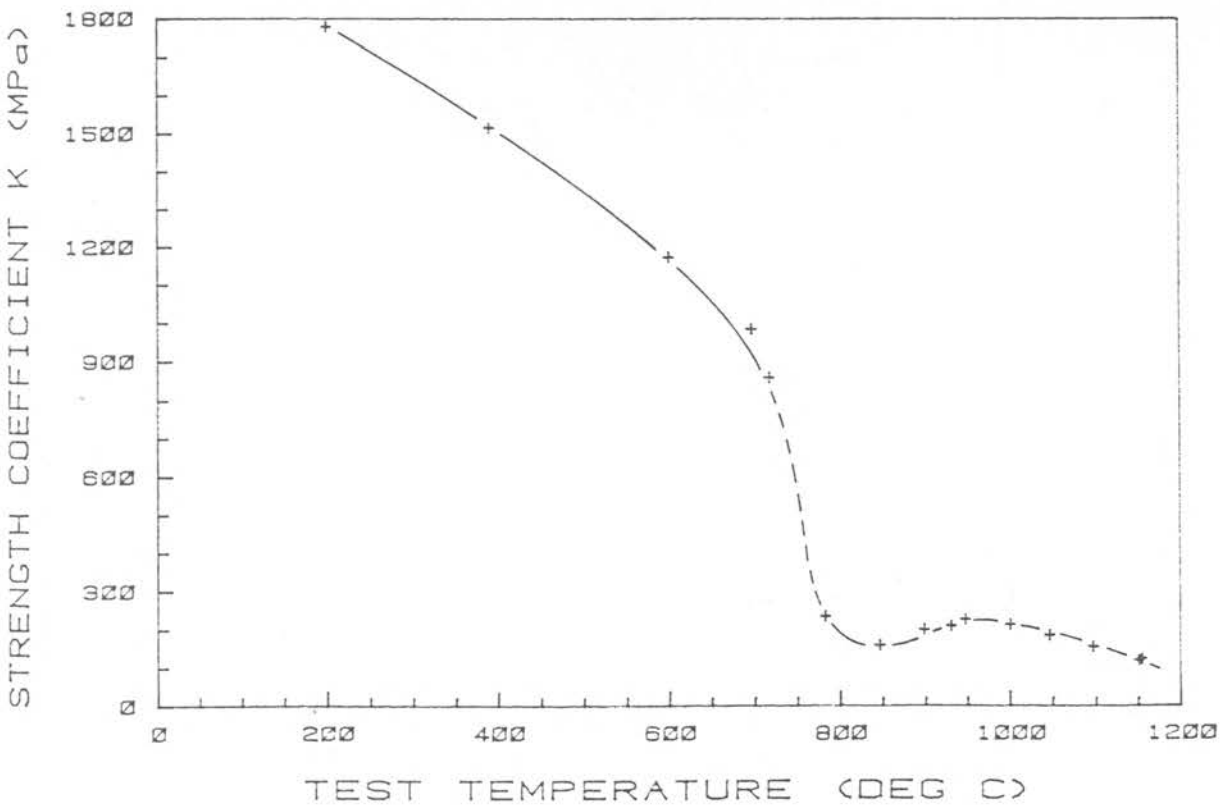

FIGURE 5.33: STRENGTH COEFFICIENT K VS. TEST TEMPERATURE FOR 3CR12NI
(STRAIN RATE: Ø.1 PER SECOND)

(ii) Ludwik (Jaoul-Crussard analysis): Tables 5.16 to 5.17 and Figure 5.34 refer.

The Ludwik parameter n' could be defined for various deformation regimes at the strain rate of 10^{-1} per second throughout the temperature range from 25°C to 1096°C. At 1154°C, however, the n' parameter was not defineable. It can be noted that a minimum in the stage III n' parameter occurs at ~700°C. For 3CR12Ni at 10^{-4} per second difficulty was encountered in obtaining a spectrum of n' values throughout the test temperature range. Insufficient data is available to confidently plot maxima and minima.

TEMPERATURE °C	n' VALUE	K'	REGIME	STRAIN RANGE	CORRELATION COEFFICIENT
25°C	-0.114	-630	2	0.0054 - 0.0063	0.904
	-1.555	0.033	3	0.0079 - 0.0210	0.994
200	-.786	2.2	3	0.0032 - 0.0106	0.995
390	-0.920	-72	3	0.0035 - 0.0116	0.992
600	-1.120	0	2	0.0113 - 0.0157	0.995
	-4.783	0 0	3	0.0182 - 0.0225	0.976
696	-1.404	-0.002	2	0.0033 - 0.0055	0.955
	-6.262	0 0	3	0.0059 - 0.0073	0.982
782	-0.797	-4.8	2	0.0311 - 0.0386	0.973
	-4.976	0 0	3	0.0397 - 0.0530	0.992
846	-1.430	-0.003	1	0.0156 - 0.0299	0.998
	-0.507	-6	3	0.0303 - 0.0842	0.996
898	-1.160	-0.16	1	0.0079 - 0.0171	0.984
	0.034	700	3	0.0264 - 0.1363	0.985
947	-1.473	-0.1	1	0.0177 - 0.0243	0.996
	-0.136	-1500	3	0.0278 - 0.1647	0.994
1000	-1.034	-0.77	1	0.0195 - 0.0263	1.00
	-0.105	-220	3	0.0298 - 0.1884	0.998
1046	-0.0367	-690	3	0.0451 - 0.2162	0.998
1096	0.1051	+270		0.0567 - 0.1932	0.999
1154	undefineable -		-	-	-

TABLE 5.16 : THE LUDWIK WORK HARDENING PARAMETERS FOR 3CR12NI AT 10^{-1} PER SECOND.

TEMPERATURE °C	n' VALUE	K'	REGIME	STRAIN RANGE	CORRELATION COEFFICIENT
25	-1.989	-0.009	3	0.0088 - 0.0242	0.998
200	undefineable -		-	-	-
397	-1.071	-0.56	2	0.006 - 0.0134	0.999
	-5.056	0	3	0.0142 - 0.0164	1.000
600	-1.446	-0.07	2	0.0067 - 0.0151	0.997
	-3.508	0	3	0.0160 - 0.179	0.997
800	-0.798	-0.36	3	0.0036 - 0.0303	0.992
900	-1.176	-0.08	1	0.0096 - 0.0259	0.999
	-0.476	-2.5	3	0.0277 - 0.0659	0.988
1000	-0.458	-0.62	1	0.0082 - 0.176	0.999
	0.166	2.2	3	0.0181 - 0.0772	0.983
1150	-2.658	0	1	0.0061 - 0.0095	1.000
	0.248	2.8	2	0.0194 - 0.0466	0.989
	-0.978	-0.32	3	0.0660 - 0.1119	0.985

TABLE 5.17: THE LUDWIK WORK HARDENING PARAMETERS FOR 3CR12NI AT 10^{-4} PER SECOND.

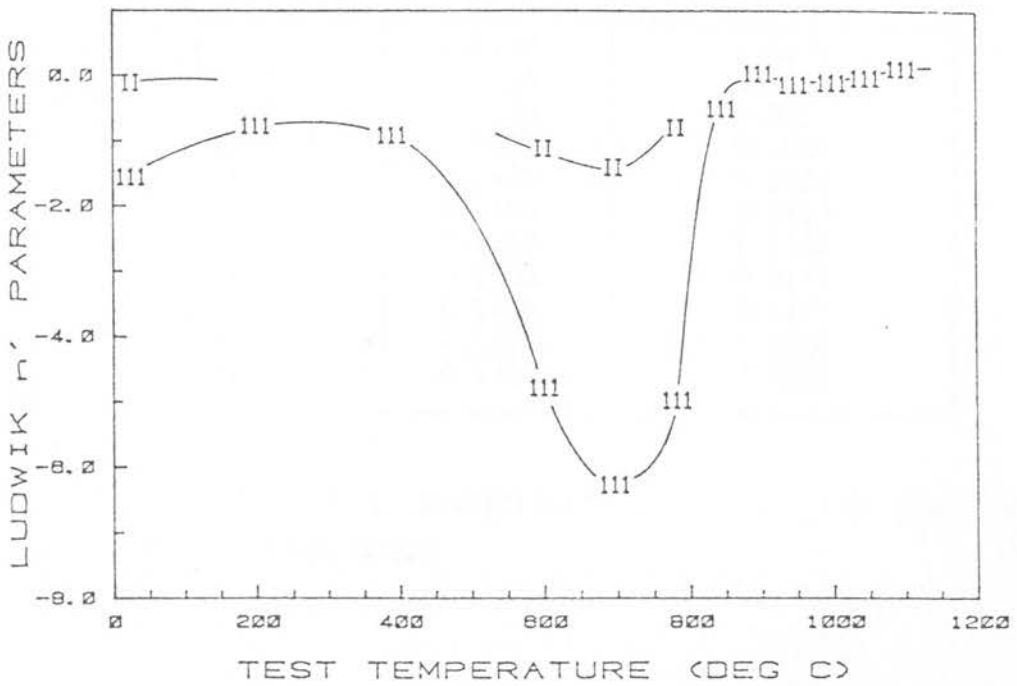

FIGURE 5.34: LUDWIK n' PARAMETERS AS A FUNCTION OF TEST TEMPERATURE FOR 3CR12NI (STRAIN RATE: 0.1 PER SECOND)

5.2.4 Strain rate sensitivity index

The strain rate sensitivity index m for $3CR12_{(2)}$ observed in the temperature range from 25°C to 1150°C is shown in Table 5.18 and depicted graphically in Figure 5.35 as a function of temperature. The influence of change of strain rate at low temperatures does not much alter the stress-strain relationships found at room temperature (m = 0.0104 at 25°C). At 400°C a slight lowering of the observed m value is noted (m = 0.0063). However, between 680°C and 800°C the strain rate sensitivity increases very rapidly to a value of 0.1160. The rate of increase attenuates from 800°C and at 1150°C, m has an average value of 0.171.

The m value for 3CR12Ni at 900°C was determined to be 0.1325. This is simillar to the value for 3CR12 at the same temperature.

TEST TEMPERATURE (°C)	m VALUE	STANDARD DEVIATION
25	0.0104	0.0026
188	0.0104	0.0013
400	0.0063	0.0011
680	0.0164	0.0009
770	0.0672	0.0080
800	0.1160	0.0160
893	0.1310	0.0100
894	0.1330	0.0170
1000	0.1380	0.0170
1082	0.1480	0.0120
1152	0.1710	0.0230

TABLE 5.18 STRAIN RATE SENSITIVITY VALUES (m) FOR 3CR12 AS A FUNCTION OF TEST TEMPERATURE.

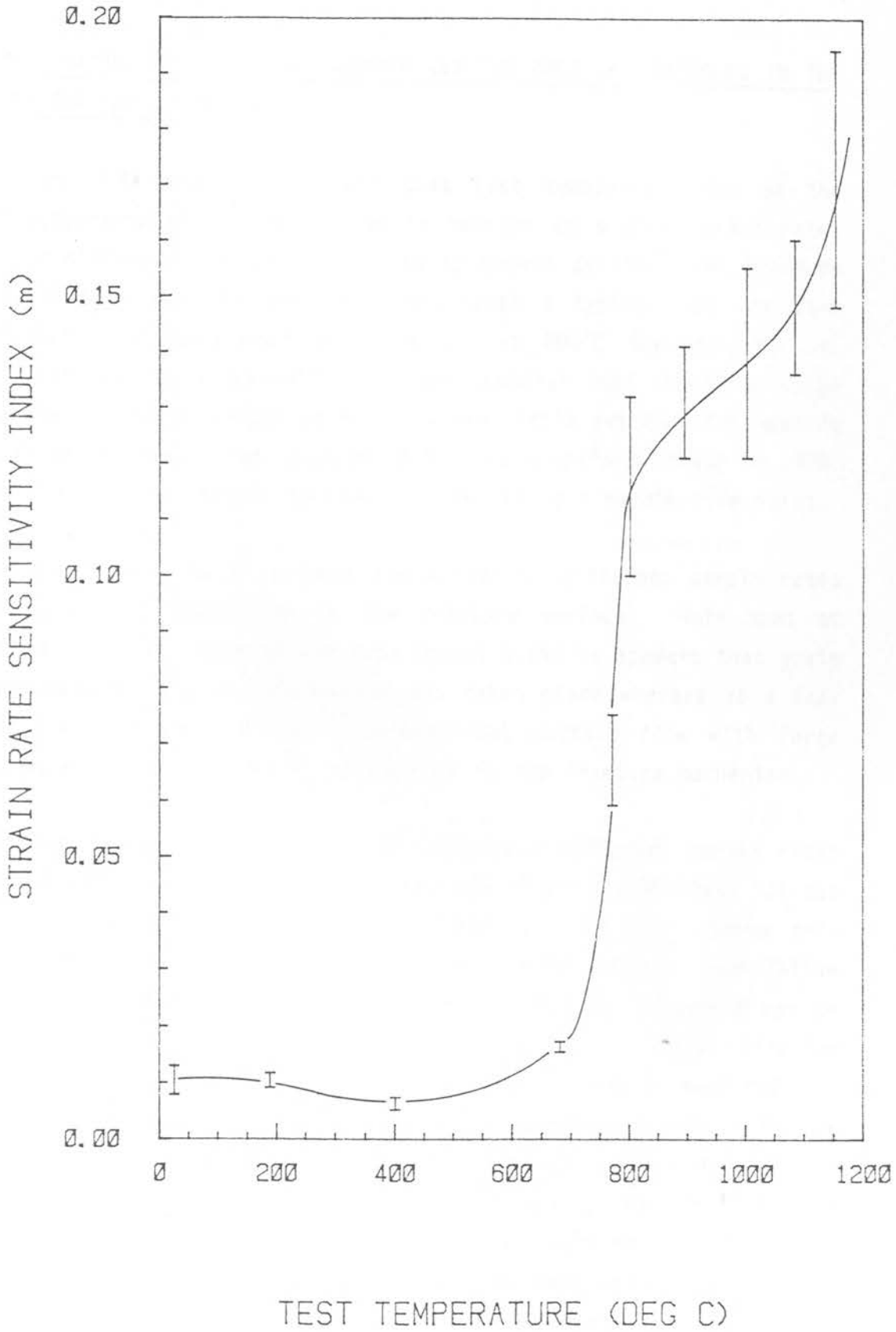

FIGURE 5.35: STRAIN RATE SENSITIVITY VALUES (m) FOR 3CR12 AS A FUNCTION OF TEST TEMPERATURE

5.3 TEMPERATURE RELATED FRACTOGRAPHY AND THE ROLE OF PARTICLES IN THE DEFORMATION MECHANISM

Figure 5.36 shows the effect that test temperature has on the fractography of 3CR12Ni pulled in tension at a slow strain rate. Four different fracture types can be noted: at 196°C the fracture is ductile and the surface demonstrates a typical cup and cone relief with associated shear lips; at 800°C the specimen has necked down to a "chisel" type form; special note should be taken of the fracture surface at 900°C, where little evidence for necking can be observed. The specimen exhibited a uniform strain to 140%. At 1000°C, the tensile specimen has necked to a needle-like point.

Photos 5.13 to 5.16 contrast the effect of different strain rates at similar temperatures on the fracture surface. Note that at 1150°C and at a slow strain rate (photo 5.16) it appears that grain boundary sliding and decohesion has taken place whereas at a fast strain rate the failure is conventional ductile flow with large dimple formation playing a major role in the fracture mechanism.

Photos 5.17 to 5.36 compare the effects of different strain rates and different test temperatures for both 3CR12 and 3CR12Ni. It can be noticed that the fracture surfaces at the high strain rate throughout the test temperature range exhibit dimple type failue and at the low strain rate this type of failure mechanism can be clearly noted up to 800°C (photo 5.26). Cubic titanium carbo-nitride particles can be seen at the bottom of most dimples, but photo's 5.26 and 5.31 give the best examples of this. At the position marked x in photo 5.30, evidence of surface rumpling of the dimple walls can be seen. These wavy linear features are reminiscent of the intense deformation markings on the free surfaces of tensile specimens which have been well strained into the plastic region, the implication being that the dimple walls were free surfaces during a portion of the tensile deformation of the matrix and that large amounts of plastic deformation occurred after void initiation. Coalescence of voids is quite commonly

noted: the arrow in photo 5.21 shows three small voids that have coalesced with a larger void. In contrast to the micro-void initiation of the fracture observed under most conditions, specimens tested at a low strain rate in the temperature range 900°C to 1160°C show evidence for rupture associated with grain boundary decohesion.

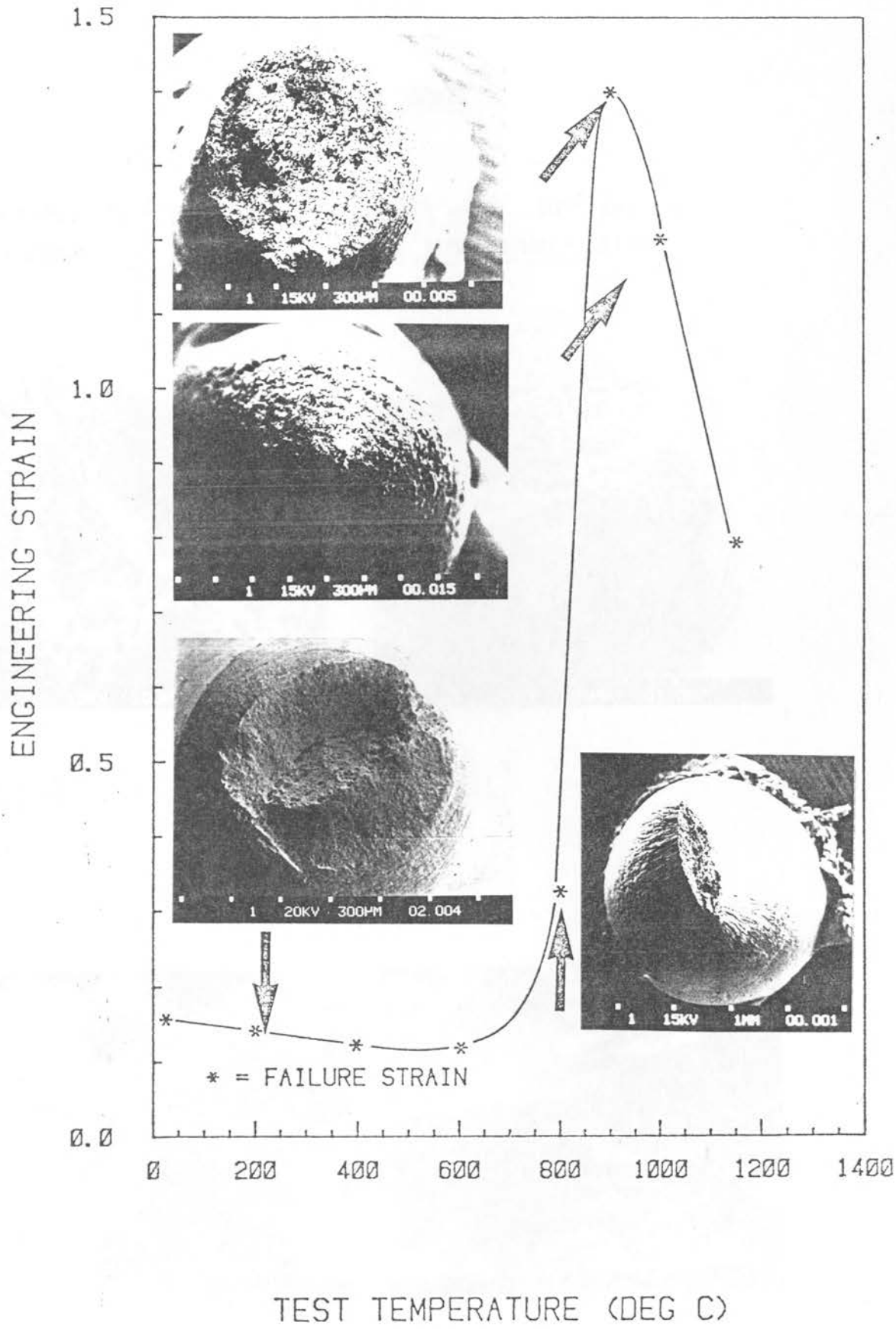

FIGURE 5.36: THE EFFECT OF TEST TEMPERATURE ON THE FRACTOGRAPHY OF 3CR12NI (STRAIN RATE: .0001 PER SECOND)

MATERIAL : 3CR12

STRAIN RATE: 10^{-1} per sec.
TEST TEMPERATURE: 1098°C

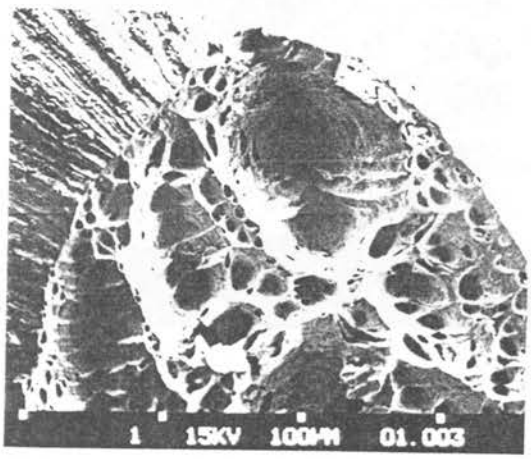

Photo 5.13

STRAIN RATE: 10^{-4} per sec.
TEST TEMPERATURE: 1150°C

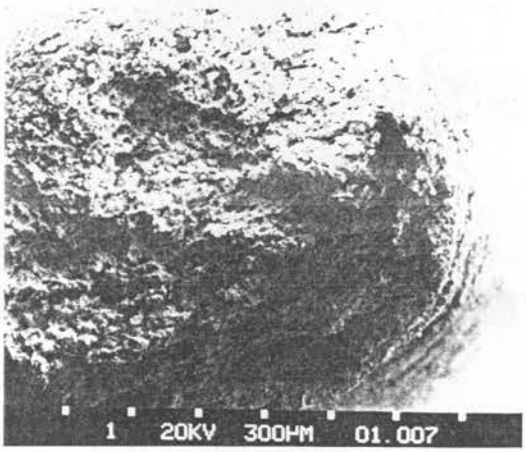

Photo 5.14

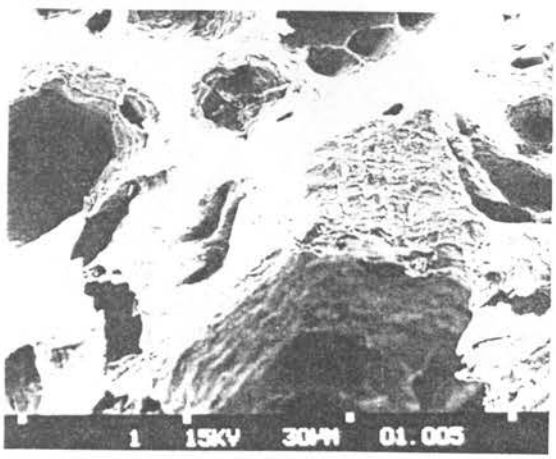

Photo 5.15

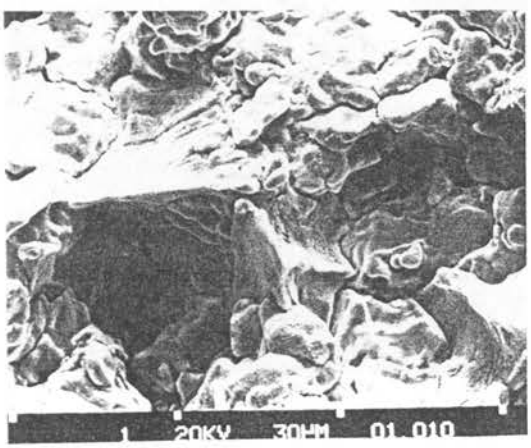

Photo 5.16

STRAIN RATE: 10^{-1} per sec.

STRAIN RATE: 10^{-4} per sec.

MATERIAL : 3CR12

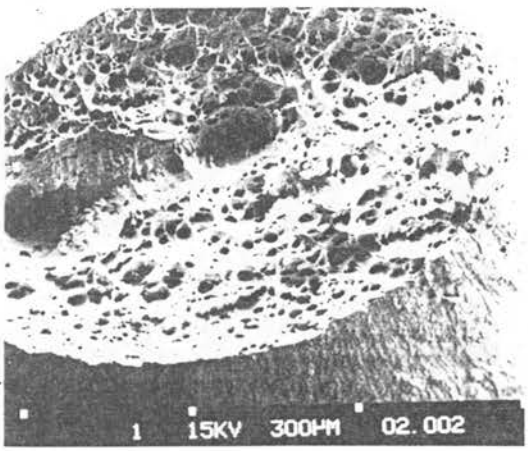

Photo 5.17

Test temperature: 998°C

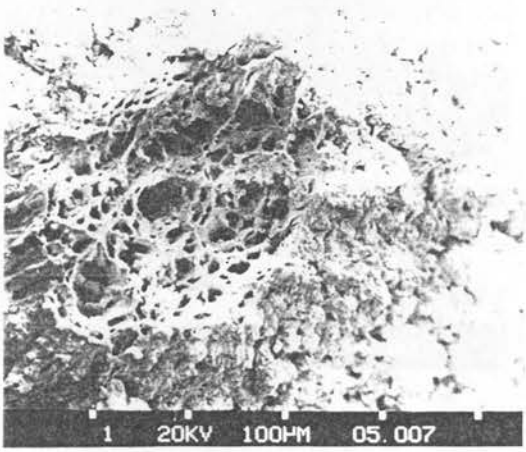

Photo 5.18

Test temperature: 1000°C

MATERIAL : 3CR12NI

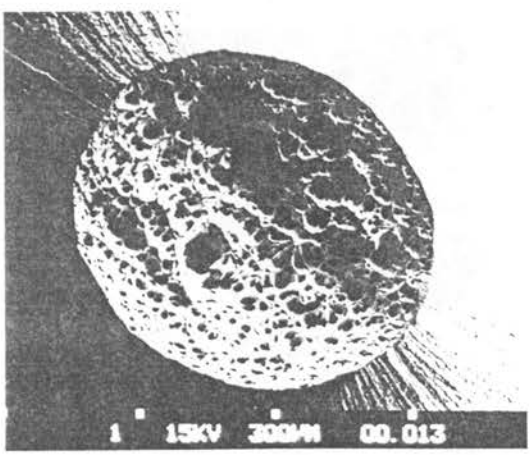

Photo 5.19

Test temperature: 1000°C

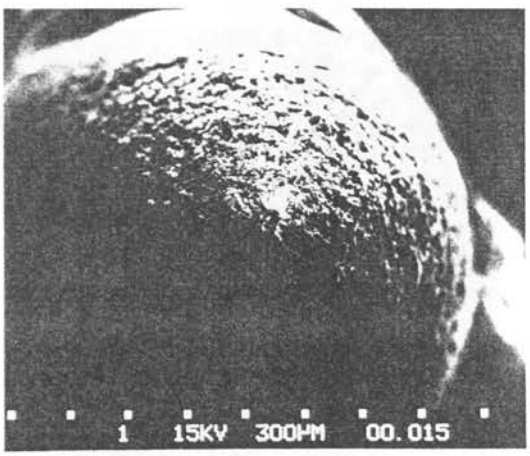

Photo 5.20

Test temperature: 1000°C

STRAIN RATE: 10^{-1} per sec.

STRAIN RATE: 10^{-4} per sec.

MATERIAL: 3CR12

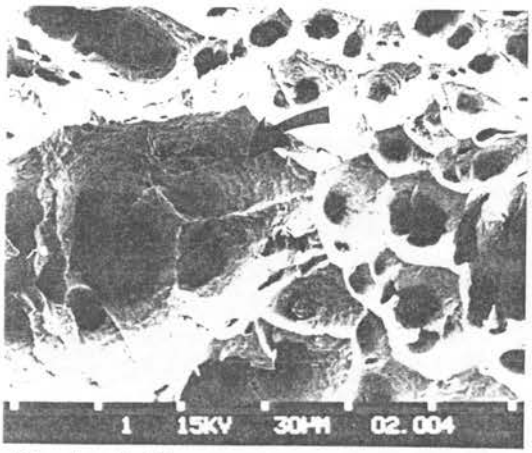

Photo 5.21

Test temperature: 998°C

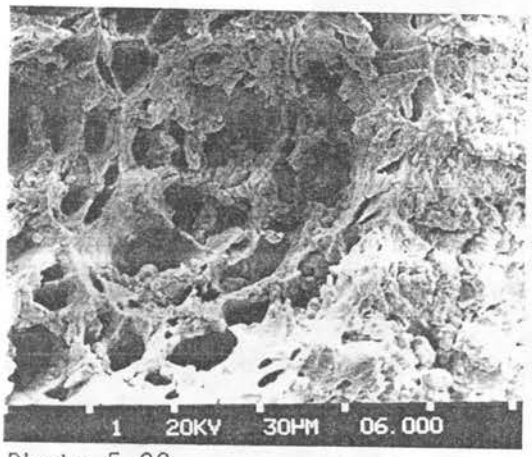

Photo 5.22

Test temperature: 1000°C

MATERIAL: 3CR12NI

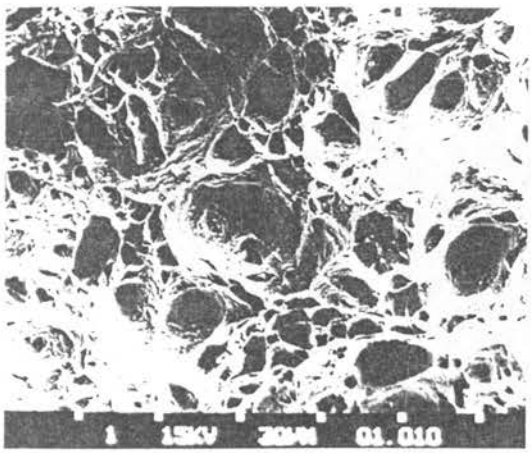

Photo 5.23

Test temperature: 898°C

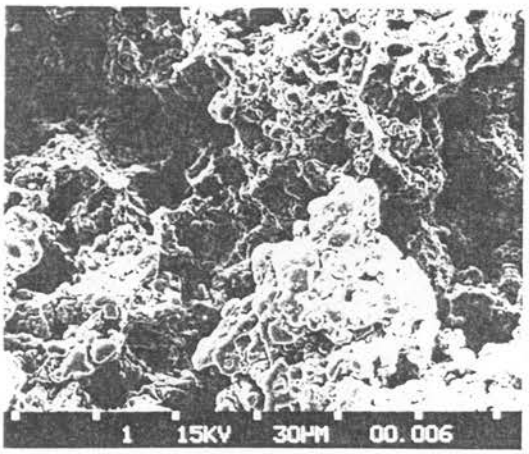

Photo 5.24

Test temperature: 900°C

MATERIAL : 3CR12NI

STRAIN RATE: 10^{-4} per sec.

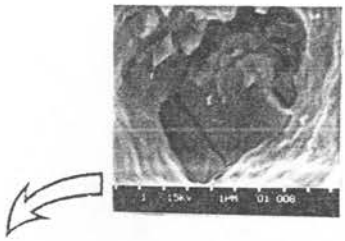

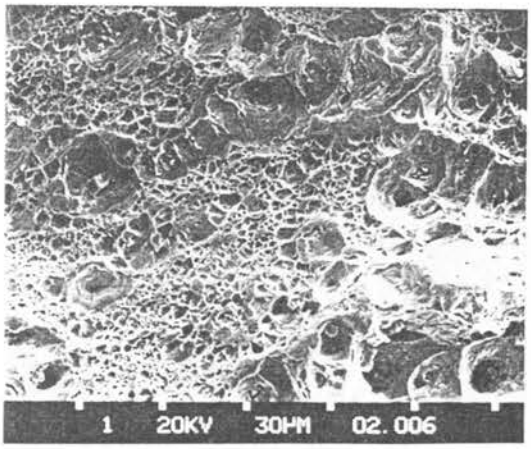

Photo 5.25

Test temperature: 196°C

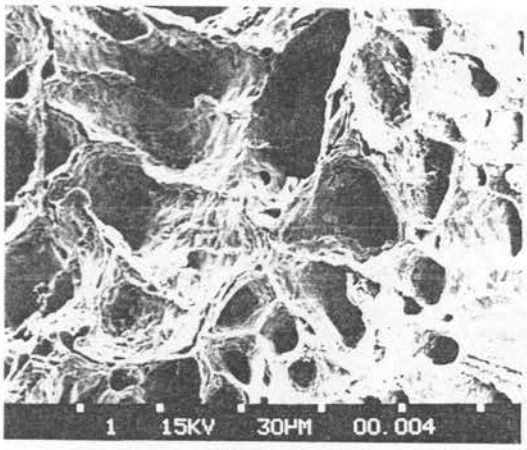

Photo 5.26

Test temperature: 800°C

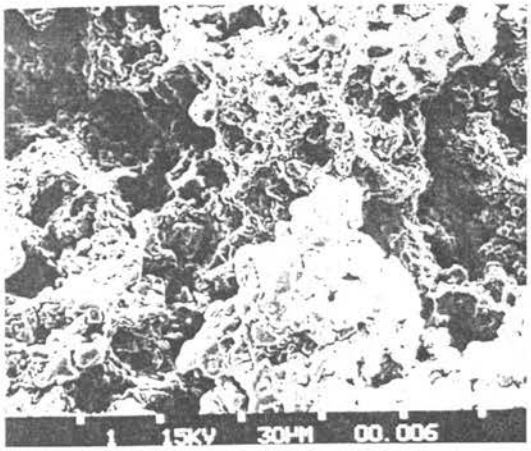

Photo 5.27

Test temperature: 900°C

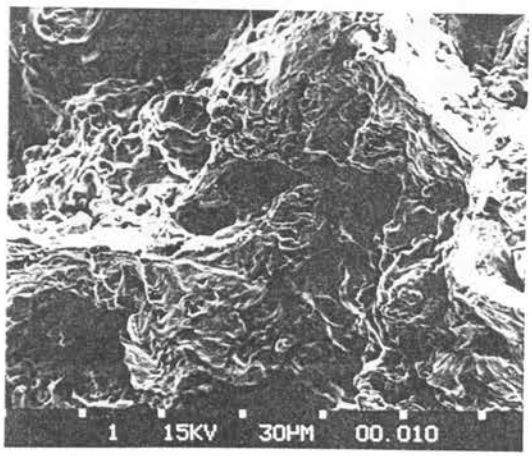

Photo 5.28

Test temperature: 1155°C

MATERIAL : 3CR12

STRAIN RATE: 10^{-1} per sec.

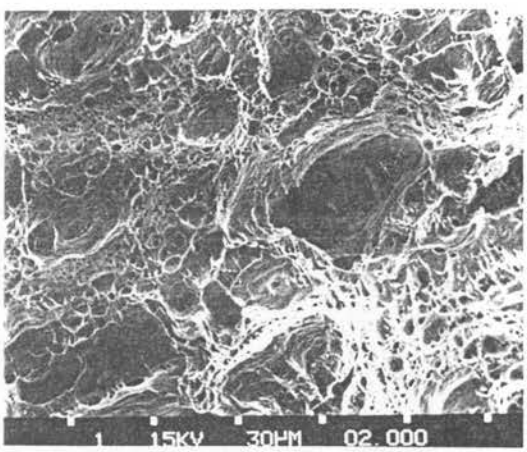

Photo 5.29
Test temperature: 603°C

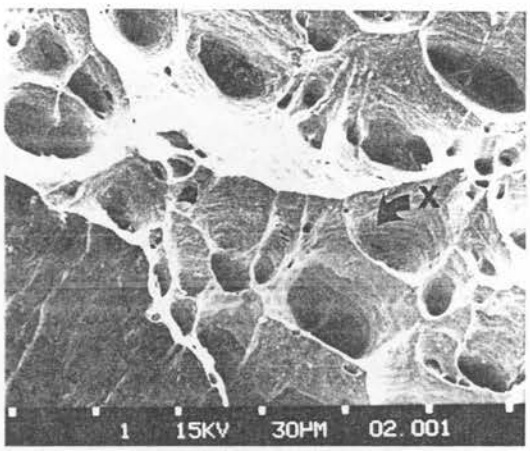

Photo 5.30
Test temperature: 852°C

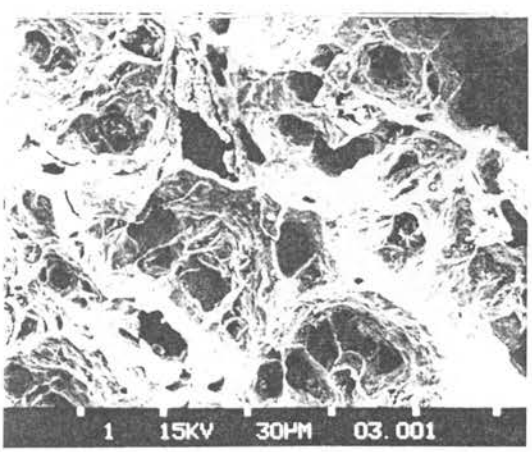

Photo 5.31
Test temperature: 937°C

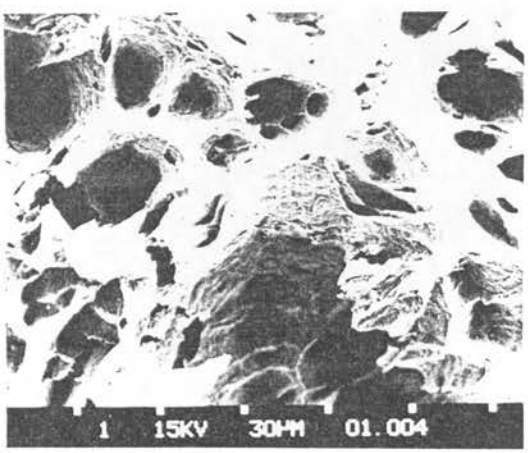

Photo 5.32
Test temperature: 1098°C

STRAIN RATE: 10^{-1} per sec.
TEST TEMPERATURE: 25°C

MATERIAL : 3CR12

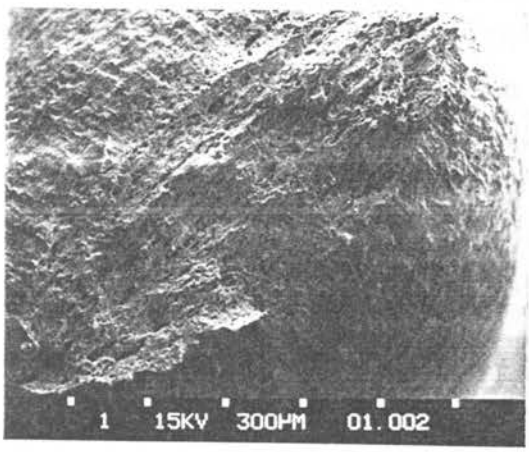

Photo 5.33

MATERIAL : 3CR12NI

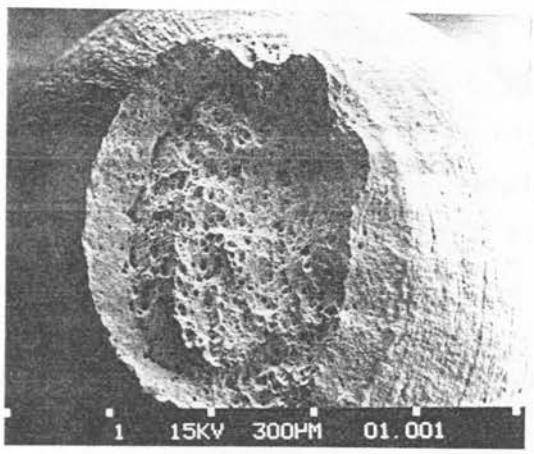

Photo 5.34

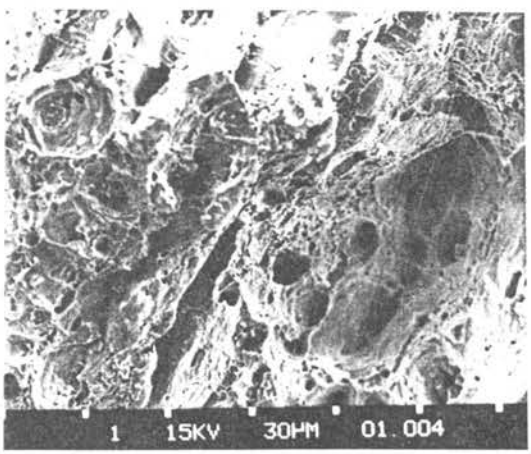

Photo 5.35

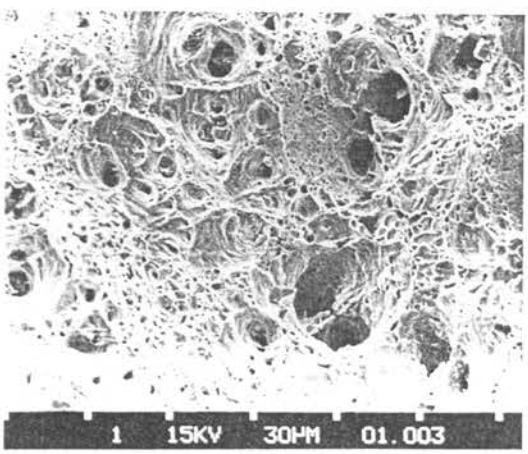

Photo 5.36

5.3.1 Titanium carbo-nitrides

Titanium carbo-nitrides have been observed to play a significant role in the deformation of 3CR12 alloys under most conditions of strain rate and temperature. Photo 5.37 demonstrates how these particles seem to band together in the microstructure, particularly along ferrite stringers. It was noticed, too, that the carbides associated together in rows, are, on average, larger than those with a more random distribution. The fracture surface of a tensile specimen, pulled apart in slow tension at room temperature (photo 5.38), shows a laminated trench relief and in photo 5.39 this relief is magnified to reveal clusters of titanium carbo-nitrides associated with the trenches. Figure 5.37 shows the results of EDAX analyses of a titanium particle. It can be seen that both sulphur and silicon are associated with the inclusion.

Notice the large separation observed between the pieces of the shattered titanium carbo-nitride in photo A of Figure 5.37. The surrounding matrix represents a strain similar to the macroscopic strain at fracture (30%) of the tensile specimen itself. This indicates that the void nucleation takes place at small plastic strains. Photo D suggests that void formation has been initiated by decohesion of the sulphide/titanium particle interface.

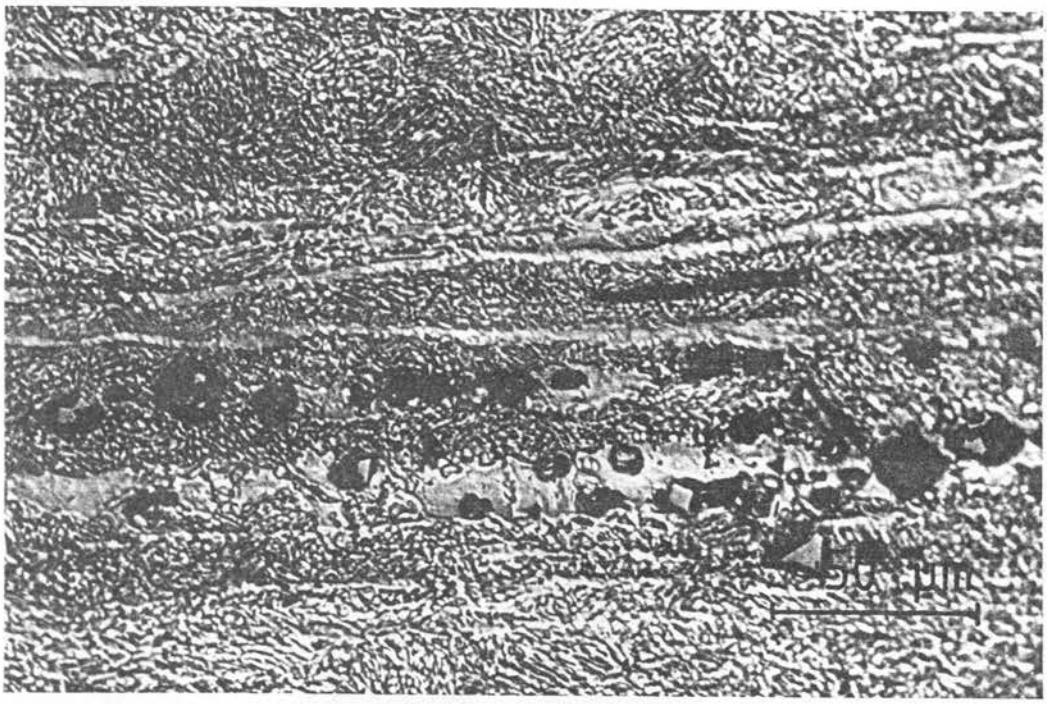

Photo 5.37 Microstructure of a 3CR12 specimen pulled apart in slow tension showing delta ferrite stringers. Ti(C,N) inclusions are seen to be associated with the ferrite.

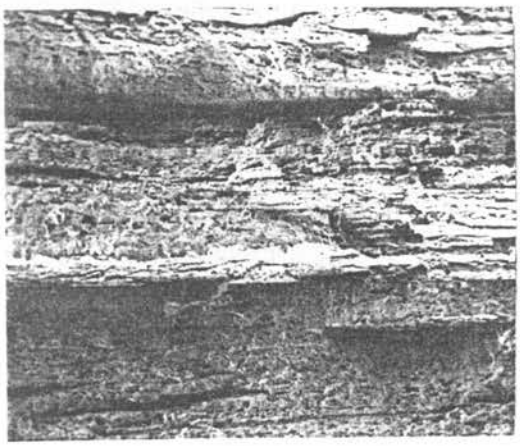

Photo 5.38 Fracture surface showing
(magnification 15x)

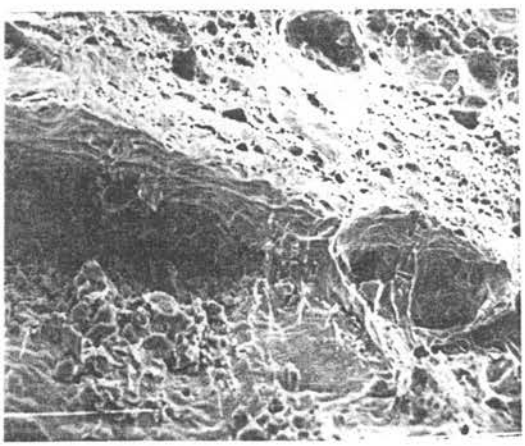

Photo 5.39 Clusters of Ti(C,N) particles.
(magnification 1000x)

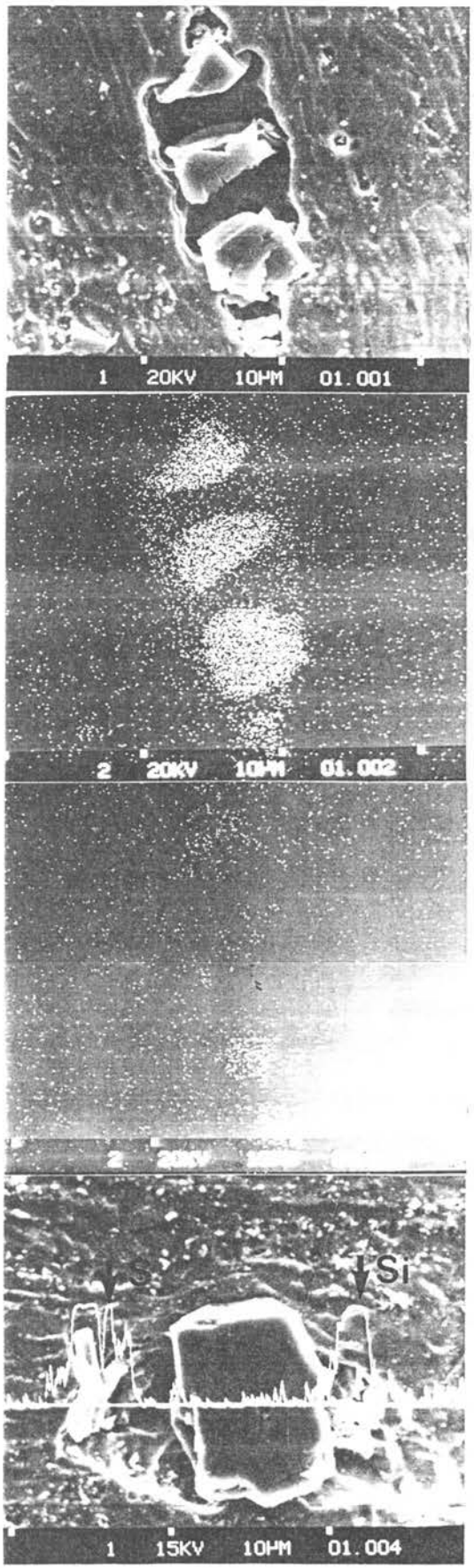

A:

A titanium carbo-nitride split in tension

B:

Titanium map of A

C:
Sulphur map of A

D:

Line scan through a titanium carbo-nitride particle showing presence of both sulphur and silicon

Figure 5.37: EDAX analysis of inclusions

CHAPTER SIX

DISCUSSION OF RESULTS

6.1 THE MICROSTRUCTURAL RESPONSE OF 3CR12 ALLOYS TO HEAT TREATMENT

The major reasons for a metallographical investigation of the 3CR12 alloys used in this dissertation were firstly to quantify the effect of increased nickel content and secondly to gain an understanding of both the steels' microstructural condition and behaviour during high temperature tensile testing. As mentioned in Section 4.1, for purposes of this discussion $3CR12_{(1)}$ and $3CR12_{(2)}$ may be considered to behave in a similar fashion both microstructurally and mechanically and therefore their subscripts will no longer be retained.

It was realised that metallographical information relevant to the static annealing response of both 3CR12 alloys could not be used to accurately predict the exact microstructure of a tensile specimen in a dynamically deforming situation, where processes such as dynamic recovery and dynamic recrystallisation would alter the grain type and structure. At slow strain rates (i.e. at 10^{-4} per second) where an elevated temperature tensile test could last for three hours, the time element becomes very important, allowing more time for factors such as grain growth and transformation reactions to occur.

Although both 3CR12 and 3CR12Ni can be referred to as dual-phase steels, this is only true if, on cooling, the steel passes through the duplex $\alpha + \gamma$ region. With reference to the iron-nickel phase diagram for 3CR12 alloys (figure 2.2) it can be seen that both 3CR12 and 3CR12Ni should be dual-phase from approximately 800°C to 950°C and that above the Ae_3, both alloys become fully austenitic before re-entering the dual-phase region at approximately 1200°C.

Experimentally, however, the lower nickel alloy does not become fully austenitic in the predicted range, as shown in photo 5.4, where on quenching after a one hour anneal at 1000°C, the resultant microstructure of 3CR12 is still dual-phase. In contrast, photo 5.5 shows that 3CR12Ni quenched from 1000°C after a similar time is fully martensitic, indicating that an austenitic regime does exist for this alloy at 1000°C as predicted. It has been mentioned previously that minor changes in the composition of 3CR12 alloys can lead to significant differences in their behaviour and the fact that the austenite structure predicted by figure 2.2 does not arise in 3CR12 could be due to the slightly different composition that this steel has, excluding nickel, compared to those which were used for the determination of the phase diagram.

Although 3CR12 and 3CR12Ni have different compositions, in photos 5.4 and 5.5 it can be seen that the dual-phase microstructure of 3CR12, refined by the nucleation of austenite, has a smaller grain size compared with that of the fully martensitic 3CR12Ni after a similar heat treatment. This can have an important bearing on the formability of the steel, as the work hardening of a material is improved with a decrease in grain size.

As a consequence of their high hardenability, which is substantiated by martensite formation even during a furnace cool, 3CR12 alloys do not retain austenite at room temperature and all the austenite present at elevated temperatures is spontaneously transformed to martensite before this temperature is reached. This fact has been confirmed by transmission electron microscopy carried out by Schaffer (1983) on the $3CR12_{(2)}$ and 3CR12Ni alloy used in this thesis. The very low carbon content of these alloys (~0.03) dictates the nature of the martensite which transforms from austenite. It is essentially a very low carbon lath martensite and can alternatively be described as a heavily dislocated ferrite. For this reason 3CR12Ni in a fully hardened condition, as in photo 5.5, has a hardness of only 302 VPN.

Figures 5.1 and 5.2 show the change in microstructure and bulkhardness of as-received 3CR12 and 3CR12Ni which have been soaked at various temperatures for one hour, followed by an oil quench. It can be seen that both alloys experience a gradual increase in their bulk hardness with increase in annealing temperature (up to 600°C for 3CR12Ni and 400°C for 3CR12). This increase can be attributed to the carbide precipitation which occurs in the mentioned temperature range as a result of the tempering of the lath martensite present in both alloys. The carbides produce a precipitation hardening effect by pinning the dislocations and thus restricting their movement. A further increase in annealing temperature provides sufficient thermal energy to induce substantial martensitic decomposition. Considering figure 5.1 it can be seen that in 3CR12 the martensite decomposes rapidly after 600°C and by 700°C the microstructure consists of a course grained ferrite plus large carbide particles, accounting for the low hardness values observed in this region. The dual-phase regime is then entered at around 800°C and with the nucleation of austenite, a grain refining influence on the microstructure is achieved. The quenched hardness increases since the precipitated carbides, which are insoluble in ferrite, redissolve in the nucleating austenite regions and, on cooling, martensite is formed. As the annealing temperature is increased to ~1050°C, the solubility of carbon in the austenite progressively increases, as does the amount of new austenite and therefore the hardness on quenching, too. The fact that the dual-phase microstructure is still retained in 3CR12 at these temperatures indicates that this alloy may lie in the nose of the $\alpha + \gamma$ region depicted in figure 2.2. Compared to the duplex microstructure which exists at 850°C, however, the islands of austenite become significantly enlarged by around 1000°C and this increase in grain size could explain the gradual attenuation in the rate of increase in hardness which occurs between the two annealing temperatures of 850°C and 1050°C. The 3CR12Ni alloy in figure 5.2 behaves somewhat differently compared to the lower nickel containing 3CR12 after its drop-off in hardness at ~400°C; as this alloy has a larger martensite content, its relative martensite decomposition to ferrite and carbides is slower for the one hour

soak time and as the dual-phase regime is reached at around 730°C (photos 5.10 &5.11), new austenite nucleates amongst existing martensite. The amount of austenite increases up to ~900°C, above which the transformation to austenite becomes complete. This results in a fully martensitic structure when quenched. Small islands of delta ferrite, however, do remain within the martensitic structure of 3CR12Ni and will only form at temperatures of above 1200°C. The fact that the 3CR12Ni alloy enters the dual-phase region at a lower temperature to that of 3CR12 can be explained by its higher nickel content. Nickel is an austenitising agent and as such increases the stability of austenite at lower temperatures.

A similar argument to that used for the variation of hardness can be used to describe the changes experienced in the yield and tensile strengths of 3CR12 measured at room temperature after anneals at various temperatures (Figure 5.3). The starting structure was dual-phase and similar to that in photo 5.4. The decrease in ductility experienced at around 400°C can be attributed to temper embrittlement of the martensite which normally occurs between 250°C and 500°C and which is caused by the growth of Fe_3C and alloy carbide particles. These particles act to pin the motion of dislocations. With an increase in soaking temperature to 600°C, additional ferrite is produced by the breakdown of martensite, the carbides over-age and the system becomes correspondingly more ductile. A fine grained, dual-phase and very ductile microstructure regenerates at around 800°C, but this becomes gradually less ductile as the grain size and volume percent martensite increases. This decrease in ductility is a well documented fact for dual-phase steels and is in agreement with authors such as Tomato and Kuraki (1976), Davies (1978), Rigsby et al (1979) and Rashid (1981).

Both the hardness and strength of 3CR12 annealed at 1000°C are higher after a further hour at 1000°C, as can be seen at the extreme temperature limits in figures 5.1 to 5.3. This difference can be explained by virtue of the different cooling rates imposed on the steels after their various heat treatments. In all cases

the 1000°C prior anneal was followed by a furnace cool which had an auto-tempering effect on the transformed martensite. As discussed, martensite forms readily at fairly high temperatures for 3CR12 alloys (the M_S was determined by Protopappas to be approximately 450°C). The subsequent experimental reheating to 1000°C was followed by an oil quench which would leave an internally strained martensitic grain structure with a correspondingly higher strength, hardness and lower ductility.

Referring to figure 5.4 it can be seen that for $3CR12_{(2)}$, two distinct regimes exist for the relationship between bulk hardness and volume percent martensite (VPM). These are from 0 to 75 VPM and from 75 to 90 VPM. This delineation may be explained by the increase of carbon solubility in austenite with increasing annealing temperature, together with the grain refining influence that the nucleation of austenite has within the dual-phase region; this in turn controls the differences in ferrite grain size and dislocation densities encountered within this temperature range.

As 3CR12 alloys have a very low carbon concentration the martensite which transforms in these steels correspondingly has a low carbon content. It could then be expected that, because of this limited amount of carbon, any increase in the amount of austenite encountered at elevated temperatures would cause a lowering of the overall concentration of dissolved carbon within the austenite, resulting in an associated lowering of the carbon content of the martensite which would transform from this phase on cooling. This would lead to a softer martensite. Contrary to this logic, however, figure 5.4 indicates that the micro-hardness at room temperature of martensite increases with increasing volume percent martensite. This can only be explained by the fact that the solubility of carbon in austenite at elevated temperatures increases with increasing temperature and that at lower temperatures not all the available carbon is being dissolved. For the given experimental conditions then, it can be seen that below ~840°C, there is little change in this solubility, but above this temperature, the amount of carbon which can dissolve in austenite

is significantly increased. An increase in the carbon content of the austenite then causes a corresponding increase in the hardness of the transformed martensite.

Another cause for the delineated increase in hardness with increasing volume percent martensite can be attributed to the effect of ferrite grain size and the increase in dislocation activity associated with the presence of martensite grains. In general, grain boundaries are obstacles to the passage of slip planes through a material. It has been suggestd by Davies (1979) that the strength of a dual-phase structure with a low volume fraction of martensite is dependent on the ferrite grain size and volume fraction of the martensite and is independent of the composition and strength of martensite. He claims that above 50% martensite the tensile strength (and therefore the hardness) is independent of grain size. For the 3CR12 alloy at low VPM values, only isolated islands of martensite are evident within a matrix of largely unrefined ferrite (photo 5.7: 3CR12 quenched from 800°C yielding 8% martensite). Any grain refining effect that the nucleation of austenite has on this matrix is limited and is confined only to areas within the microstructure associated with the transformation. A large percentage of the ferrite grains thus remain unrefined and relatively large encompassing, at room temperature, isolated islands of martensite. The areas of dislocation activity associated with these isolated regions are, however, generally too far apart to significantly interact with each other to have any overall hardening effect. With increasing VPM (photo 5.8: 3CR12 quenched from 843°C yielding 78% martensite) the presence of martensite becomes more universal within the grain structure and as such the grain refining effect becomes common to the entire microstructure. In addition, at higher VPM levels the areas of dislocation activity surrounding martensite grains also begin to interact. A steady increase in hardness can thus be attributed to both the decrease in ferrite grain size together with an increase in the dislocation activity. With an increase in annealing temperature above 843°C, the grain refining process becomes less significant and the hardness increase becomes

attributable to the presence of the martensite alone.

From this study of the microstructural responce of 3CR12 alloys to heat treatment, it can be seen that a wide variation in room temperature properties can be exhibited which are microstructure related. During elevated temperature testing therefore, the mechanical properties and deformation characteristics of these alloys must also be related to the microstructure which exists at the particular test temperature concerned. However, as mentioned before, the microstructure obtained at a specific temperature under static conditions cannot be a true reflection of the condition of the steel whilst undergoing dynamic deformation for extended periods at a similar temperature. The room temperature microstructures can thus serve only to give a guideline as to the materials' thermal response under elevated temperature testing conditions.

6.2 THE EFFECT OF TEST TEMPERATURE AND STRAIN RATE ON THE MECHANICAL PROPERTIES OF 3CR12 ALLOYS

It has been demonstrated in section 5.1 that the microstructures of 3CR12 and 3CR12Ni are very sensitive to both soaking temperature and the soaking time, especially at high temperatures where grain growth occurs. When considering the mechanical properties of these two steels as a function of temperature one must therefore take into account the effect temperature has on the flow stresses, together with the microstructure which the materials are experiencing at that particular temperature. Temperature has a striking effect on the stress-strain curves for 3CR12 alloys, as shown in figure 5.7, where at any one temperature the crystal lattice structure may consist of varying combinations of body centered cubic ferrite, body centered tetragonal martensite and face centered cubic austenite. The plastic deformation of these structures on a micro-scale will depend on their relative stacking fault energies, different active slip systems and concentrations of interstitial atoms, such as carbon and nitrogen, which can affect

the passage of dislocations. These factors combine to control elements such as the rate of work hardening and strain rate sensitivity of the material, which in turn are influenced by processes such as dynamic strain ageing, recovery and recrystallisation. Dynamic strain ageing acts to increase the rate of accumulation of dislocations during deformation while dynamic recovery and recrystalisation tend to both alter the distribution of dislocations and eliminate them. Changes in grain size and the relative volume fractions of phases due to phase transformations at elevated temperatures can also act to influence the deformation characteristics of the 3CR12 alloys.

6.2.1 Young's Moduli

The Young's moduli (E) measured at room temperature for 3CR12 and 3CR12Ni in the as-received condition were 198 and 196.5 GPa respectively. These values can be compared to those of published values for mild steel (Smithels,1976) in the annealed state (210.0 GPa) and in the hardened condition (201.5 GPa). The fact that 3CR12Ni, which is essentially martensitic in the as-received condition, has a lower elastic modulus than 3CR12 (which has a low volume percent martensite in the as-received condition) is consistant with the pattern exhibited for mild steel. Martensite, with its distorted body centered tetragonal crystal structure has, on average, more widely spaced iron atoms (this spacing is dependent upon carbon content) compared to body centered cubic ferrite. As the elastic modulus of a material is essentially related to the interactive forces between atoms within the crystal lattice, this greater atom separation enables more strain energy to be absorbed, which in turn allows a higher elastic response for a given load. This concept can best be described by considering figure 6.1.

The behaviour of two atoms (Fe atoms in this case) are shown in figure 6.1, which gives the potential energy due to the attractive (curve A), repulsive (curve B) and total (curve C) forces acting between the nuclei as they are brought together from infinity.

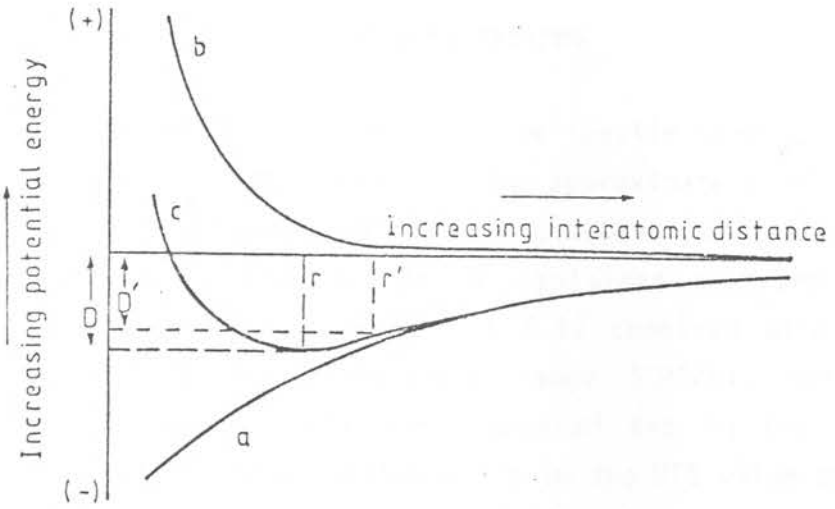

Fig. 6.1 The potential energy between atoms.

The potential energy well is deepest at the equillibrium spacing r and its depth D there is equal to the work required to disassociate the atoms completely. If the distance between the nuclei is increased to r', as the iron nuclei are when forced into the body centred tetragonal shape by interstitial carbon atoms whilst transforming to martensite, the distance D' and therefore the work necessary to separate the iron atoms is decreased, decreasing the Young's modulus accordingly.

Figure 5.6 indicates the effect of test temperature on the elastic response for 3CR12. The values were calculated from the slopes of the elastic regions from each test and corrected by a constant room temperature factor. The loading slopes obtained from elevated temperature tests could not, in general, be compared to the true modulus, because of the anelastic strain produced during the loading interval prior to macroscopic flow. This strain arises from the operation of thermally activated dynamic recovery that is rate controlled in the temperature range, and therefore increases with a higher temperature and lower rate of loading. However, when comparing the general effect of temperature on the elastic response for 3CR12, the values obtained can be seen to follow the same trend as Routbourt et al (1971) found for iron-silicon in the same temperature range (figure 2.4).

6.2.2 Strength at high temperatures

The fact that 3CR12Ni retains its tensile strength at a relatively constant strength level up to approximately 600°C compared to 3CR12, which demonstrates a progressive decline in strength with increased temperature can be explained by virtue of different microstrucures (figures 5.8 & 5.10 compared with figures 5.17 & 5.18). In this temperature range 3CR12Ni, being martensitic, becomes progressively more tempered and in the region of 400°C (figure 5.17) demonstrates a dip in the UTS value characteristic of temper embrittlement. At 600°C the sharp drop off in both tensile strength and proof stress corresponds to the temperature at which there has been a significant increase in the rate of transformation of the remaining martensite to a ferritic microstructure containing carbides (figure 5.2) which has a much lower mechanical strength. In contrast, 3CR12, with its high ferritic content in the as-received condition, demonstrates a more gradual attenuation in strength with increase in tempering temperature, because it experiences a much lower proportional change from martensite to ferrite plus carbides.

The recovery in strength experienced by both alloys at around 950°C can be explained by the presence of austenite at this temperature. Austenite has a low stacking fault energy and therefore demonstrates a higher work hardening capacity and better high temperature properties compared to the ferrite, which is also found at this temperature, but in small amounts. At the higher strain rate, the increase in strength is more pronounced because less time is available for recrystallisation, recovery and other creep processes, such as grain boundary sliding (photo 5.16), to take place. Above 950°C, however, the increase in grain size plays an increasingly more important role in controlling the mechanical properties of 3CR12 alloys (photo 5.12) and the strength, already deminished by thermal activation, is decreased considerably.

A relevant point when considering the economics for the hot-forming of the 3CR12 alloys is that they both experience a dip in their

strength and deformation energy values at around 900°C (Figs. 5.13 & 5.15 and Figs. 5.22 & 5.23). Strict temperature control, however, would have to be maintained if any advantage was to be derived from this fact, as an increase of only 50°C above the minimum value (900°C in the case of for 3CR12) can cause an increase, at high strain rates, of some 200% in the energy required to achieve the ultimate tensile strength of the material. A lowering of the temperature below 900°C would have a similar effect.

Both 3CR12 and 3CR12Ni exhibit continuous yielding characteristics throughout the test temperature range. It has been pointed out by Rigsby and Van der Arend (1979) that at room temperature the continuous yielding at low strengths in dual-phase steels is promoted by yielding in the ferrite which is initiated by a high mobile dislocation density in regions adjacent to the martensite. This mobile dislocation density is created during cooling from the annealing temperature range by differential contraction effects between austenite and ferrite and by the austenite-to-martensite phase transformation. This mechanism will be valid in dual-phase 3CR12 alloys for increasing temperatures until the martensite can no longer act as a dislocation source (up to ~650°C). Above this temperature it is presumed that there is enough thermal energy to prevent dislocation locking by interstitial atoms and thereby maintain the continuous yielding behaviour.

In view of the fact that both 3CR12 and 3CR12Ni exhibit useful strengths up to ~650°C (~400 MPa and ~600 MPa respectively) consideration of their 0.2% proof stress/UTS ratio can be important if these materials are to be used for structural applications (figures 5.12 & 5.21). In this temperature range the ratio for 3CR12 (~60%) is preferable to that for 3CR12Ni (~90%), as with a lower relative yield strength to its ultimate tensile strength, early plastic yielding can provide a warning for imminent catastrophic failure.

6.2.3 Work hardening

Although the physical delineation of the work hardening regimes was something of a personal judgement, the variation in strain intervals corresponding to the interstage transition points are within reasonable agreement with the stage behaviour cited in the literature, and this gives weight to the validity of the numerical assignment of the stages I, II and III observed in the 3CR12 alloys.

The work hardening parameters n, n' and n" obtained for these steels cannot be compared quantitatively with each other by virtue of their different definitions (equations 1,2 & 4). However, the n and n' values should vary in a similar fashion to each other for any particular test series, and that differences do arise can be attributed to the different methods employed to obtain these values. The Jaoul-Crussard type analysis yields both the n' and n" values which can be essentially described as second derivative terms and therefore are indicative of the rate of change of the slope of the tangents to the slope of the stress-strain curve with respect to either increasing stress (n") or increasing strain (n'). As such, these values are very sensitive to minor fluctuations in the flow curve. The fact that this type of analysis could yield different delineated work hardening regimes each with specific work hardening parameters for any specific test, whereas the Hollomon analysis could usually only yield one, provides the main reason why the n and n' values cannot be compared directly. It is felt that because of its relative insensitivity, the Hollomon parameter is less representative of the variation in work hardening for the 3CR12 alloys with temperature. As mentioned in section 5.2.3.1 (iii) the value of n" is a measure of the expected increase in strain for a given stress and for this reason any fluctuation in the n" value is concomitant with an opposite fluctuation in both the n and n' values for the same region of the flow curve.

The negative values obtained for n' and n" parameters are not

unusual and other investigators such as Monteiro and Reed-Hill (1973) and Ramos et al (1979), who have used the Jaoul-Crussard type analysis, also observed this. These negative values indicate that the parameters obtained by the Jaoul-Crussard method do not have a simple significance and Monteiro and Reed-Hill (1971) suggest that negative parameters correspond to deformation under conditions such as work softening where dynamic recovery is strong. For the purposes of this work it was felt that the variation in the work hardening trends for the 3CR12 alloys can be adequately outlined by the exponential n' and n" values. Therefore, as there was no intention to carry out a purely quantitative investigation in this area, the parameters K', C, ϵ_o , and σ_o in equations (2) and (4) have not been considered.

As the work hardening behaviour for both 3CR12 and 3CR12Ni tends to follow similar trends throughout the test temperature range it is preferable to discuss these trends in terms of 3CR12 only and where necessary attention will be drawn to the 3CR12Ni alloy. The initial increase in work hardening with increase in temperature from 25°C, demonstrated in figures 5.26 & 5.28, has been observed in materials such as alpha-iron (Bergström and Aronsson, 1970) and titanium (Garde, Santhanam and Reed-Hill, 1972). The general consensus is that this increase is due to a dynamic strain ageing effect although no attempt was made to find any sub-structural evidence for this in this work. However, the dynamic strain ageing phenomenon is strongly related to strain rate. An increase in strain rate can be expected to delay a particular dynamic ageing effect by decreasing the time allowed for the migration of foreign atoms, such as iron and alloy carbides, to dislocations. Here, existing with less elastic strain, they have an immobilizing or pinning effect on the dislocation movement with a resultant increase in strength. An indication that strain ageing occurs in 3CR12 alloys can be seen by comparing the ultimate tensile strengths for 3CR12 at 10^{-1} and 10^{-4} per second (figure 6.2) where, contrary to expectation, in the temperature range from 225°C to ~750°C, it can be seen that the slower strain test series exhibit a higher strength.

As the test temperature is increased from room temperature under straining conditions, two opposing processes are active in controlling the work hardening of a material. Dislocation interaction between other dislocations and solute particles tend to cause dislocation tangles which impede their motion through the lattice and thereby increase the work hardening process. This is normally categorised as Stage II work hardening. Directly opposing the above process are the recovery and recrystallising processes which manifest their effect during type III work hardening. Figure 5.30 shows the stage behaviour of the n' parameter observed for 3CR12 at both high and low strain rates as a function of temperature. As mentioned before, stage I, which is the earliest stage in work hardening and which occurs in the micro-strain region of less than 0.01 strain, was not delineated with certainty and the relevance of this stage is therefore not discussed here. The

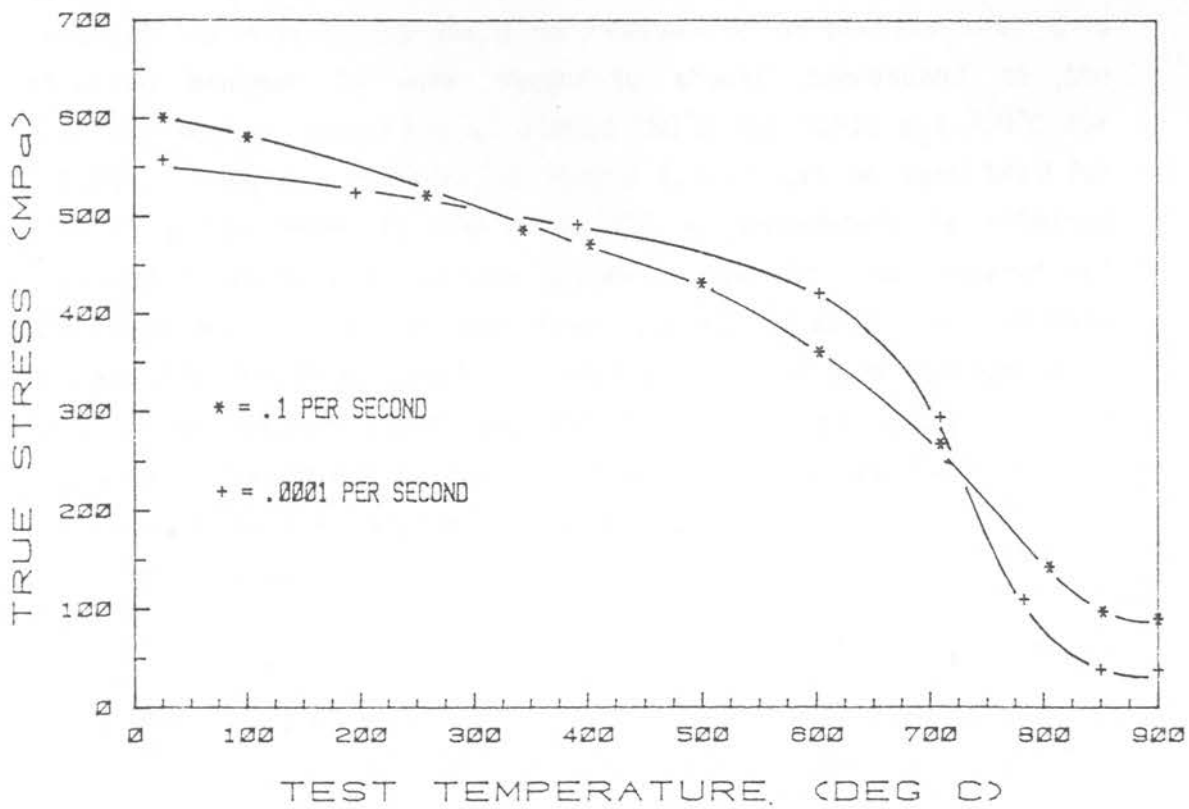

Fig. 6.2 The effect of strain rate on the strain on 3CR12 showing evidence for dynamic strain ageing.

average rate of work hardening during stage II is not strain rate sensitive and is in agreement with Monteiro et al (1981) who made a similar observation for an austenitic stainless steel at elevated temperatures. However, stage III can be seen to differ markedly with strain rate between 200°C and 950°C, where the lower value is associated with the slower strain rate. The fact that stage III is normally associated with dynamic annealing processes explains the above observation, as with the slower strain rate more time is available for such processes to occur.

A general attenuation of stage III work hardening to an undefineable minimum between 800°C and 900°C (corresponding to a more sharply defined maximum for the n" parameter in figure 5.31 at 850°C) and also exhibited by the Hollomon n parameters (figures 5.26 & 5.28) was observed. Because of the high stacking fault energy of ferrite and because of the relatively large grain structure of the 3CR12 alloys in the ferritic condition (figures 5.1 & 5.2), it would be reasonable to predict that this observed minimum in work hardening should correspond to the ferritic region, occurring at around 780°C for 3CR12 and 730°C for 3CR12Ni. However, considering figure 6.3 it can be seen that for 3CR12 the low level in the stage III n' parameters is retained until 900°C where a 91% volume austenite (VPM at room temperature) was observed after a one hour static anneal. A proposed explanation for this anomaly is that under straining conditions in the region between 800°C and 900°C, 3CR12 experiences a rapid increase in the dynamic recrystallisation of ferrite together with an increase in the rate of nucleation of austenite grains induced by a straining matrix.

Between 800°C and 900°C, 3CR12 is within the dual-phase region where both ferrite and austenite co-exist. After a one hour soak at this temperature, the volume percent austenite ranges from 8% at 800°C to 86% at 900°C (Table 5.2). When straining occurs, ferrite, with its high stacking fault energy, will tend to develop a dislocation cell structure and hence have a greater propensity for

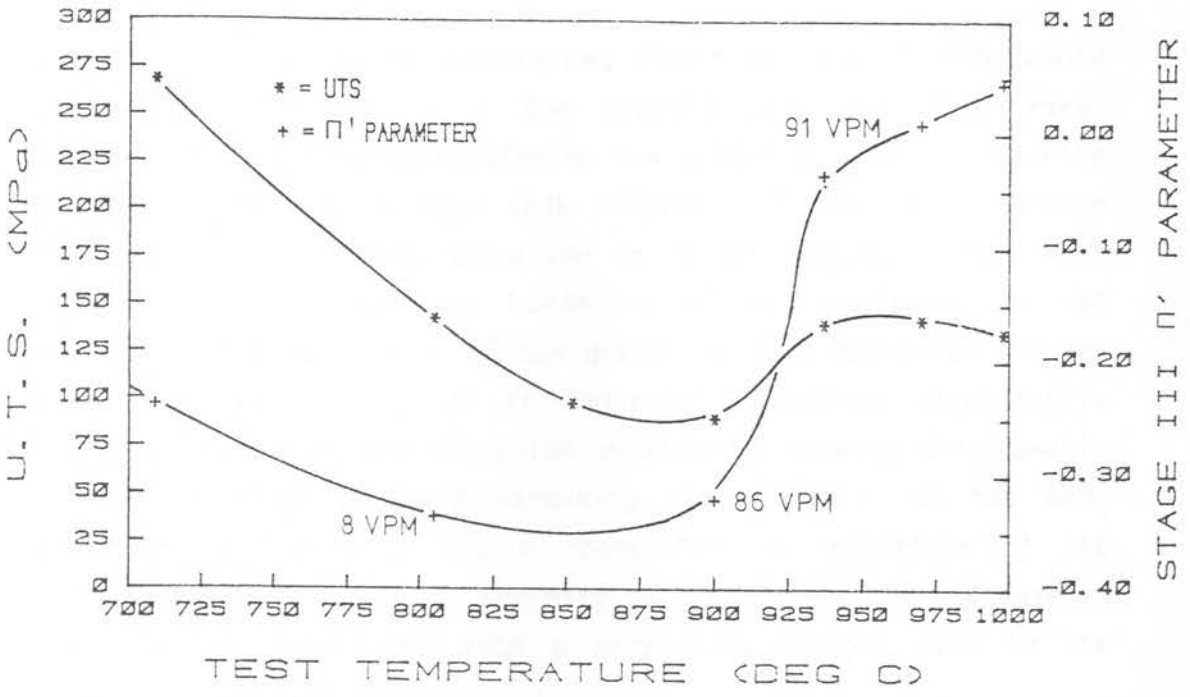

Fig. 6.3: The relationship between the Ludwick n' parameter and the UTS for 3CR12 pulled in tension at 10^{-1} per second.

dynamic recovery and recrystallisation than the austenite present, which, having a lower stacking fault energy, is able to accommodate the build-up of internal stress. The deforming ferrite grains, with their dislocation cell structure, will preferably tend to eliminate internal strain by dynamically recrystallising into new strain-free grains. Thus, under test conditions where the microstructure consists of a high volume fraction of ferrite, the work hardening rate can be retained at a very low value, as observed.

Straining of the tensile specimens was only initiated after a one hour soak period, but it can be seen in figure 2.3 that at 860°C the nucleation of austenite in 3CR12 is only complete after some 5 hours at this temperature. It may be assumed that deformation during the tensile tests, at least below 860°C, took place on a transforming dual-phase microstructure not yet in equilibrium. The straining of the matrix could thus have the effect of inducing the premature nucleation and growth of new strain-free austenite

grains. In their initial unstrained condition, these grains could then also contribute to a low overall work hardening rate. However, at 900°C the nucleation of new austenite from old ferrite is complete after a one hour soak (figure 2.3) and strain induced nucleation of this phase therefore no longer occurs. Thus, with increased strain, the work hardening of the austenite is not retarded by the nucleation of new grains by this mechanism and the work hardening capacity of the material increases accordingly. Figure 6.3 describes the situation graphically showing the dramatic increase in stage III work hardening after 900°C. As has been mentioned, a low stage III n' parameter is indicative of the operation of work softening processes and therefore the increase at 900°C can be associated with a very much reduced rate in the dynamic annealing process.

At temperatures above 950°C, stage III behaviour becomes strain rate insensitive (figure 5.30) indicating that in this region there is sufficient thermal activation for the dynamic annealing processes to proceed to completion in very short time intervals.

6.2.4 Strain rate sensitivity

The physical significance of the strain rate sensitivity index m in developing high tensile elongations has been explained in section 2.2.3 of Chapter 2. The strain rate sensitivity is described as relating to the capability of a material to resist plastic instability with a higher value of m corresponding to a greater resistance to necking. This can be seen by comparing the elongations to fracture for 3CR12 (Figures 5.9 & 5.11) with the m values obtained for this material (Figure 5.35). It can be seen that the failure strains for the 3CR12Ni alloys (Figures 5.18 & 5.20) follow a similar trend to that for 3CR12, and the m value obtained for 3CR12Ni at 900°C is similar to that of 3CR12 at this temperature

The elongation to fracture for 3CR12 alloys becomes sensitive to test temperature only after 650°C - 700°C depending on the strain rate and nickel concentration. Below this temperature there is a

tendency for the elongations (and the m value for 3CR12) to actually decrease with temperature. As mentoned previously, this phenomenon can be attributed to the precipitation of carbides which pin the dislocations and thus cause a harder and more brittle structure. Up to 500°C the only carbides to form are those of iron (temper embrittlement). Above this temperature, however, the formation of titanium and chromium alloy carbides introduce a secondary hardening effect and form within the range of 500°C to 600°C. The stable fine grained dual-phase austenite and ferrite structure intrinsic to the 3CR12 alloys at temperatures above 750°C - 800°C contributes to the increased elongations and m values. The maximum in elongation for the 3CR12Ni alloy was obtained at 900°C (140%) and for 3CR12 at 1000°C (130%), both at the strain rate of 10^{-4} per second. It is tempting to attribute these large elongations to a superplastic type flow mechanism, especially in the case of 3CR12Ni, where the 140% elongation was associated with minimum necking in the specimen (figure 5.36) and as evidence for grain boundary sliding was noted (photo 5.24). Photo 5.22 shows that in the case of 3CR12, although grain boundary sliding has taken place to some extent, void nucleation, coalesence and growth within the specimen has been the ultimate failure mechanism. Consideration of the m values for both alloys at these temperatures (~0.14 in both cases) shows that these values are nowhere near the value of 0.5 normally associated with superplastic deformation.

It should be noted that the strain rate in a constant cross-head velocity test is not constant during a tensile test, especially at higher temperatures where larger strains are encountered causing the strain rate to progressively decrease as the specimen elongates. For this reason the m values for the 3CR12 alloys may be higher than recorded, especially at elevated temperatures where larger strain intervals were considered. The precise effect, however, is complicated, because grain growth and strain both affect the value of m.

Values for the Hollomon work hardening parameter n for 3CR12

(Tables 5.9 & 5.10) and corresponding m values for the strain rate sensitivity were substituted into equations (6) and (7), relisted below, using the stress values obtained at the two strain rates (10^{-1} and 10^{-4} per second) and at three constant strains. This allowed the constants C_2 and k to be calculated. Table 6.1 shows typical values obtained and the percentage error in the values of C_2 and k can be examined for consistancy.

$$\sigma_{\epsilon,T} = C_2\dot{\epsilon}^m \qquad (6)$$

$$\sigma_{\epsilon,T} = k\dot{\epsilon}^m\epsilon^n \qquad (7)$$

At 25°C it can be seen that by applying equations (6) and (7) to 3CR12, consistant values for C_2 as well as for k are obtained.

STRAIN RATE (PER SECOND)				m	STRAIN	STRAIN RATE (PER SECOND)						PERCENTAGE DIFFERENCE BETWEEN PARAMETERS	
10^{-1}		10^{-4}				10^{-1}			10^{-4}				
TEMP °C	n	TEMP °C	n			STRESS MPa	C_2	k	STRESS	C_2	k	C_2	k
25	0.173	25	0.172	0.010	0.03	453.4	464.0	851.1	428.1	469.4	857.9	1.15	0.79
					0.05	495.9	507.5	852.1	466.9	511.9	857.0	0.86	0.57
					0.13	586.9	600.6	854.8	548.6	601.5	854.4	0.20	0.05
600	0.174	603	0.163	0.010	0.03	296.0	303.9	559.3	336.7	372.6	659.9	18.43	15.24
					0.05	327.6	336.0	565.8	366.3	405.4	660.6	17.11	14.27
					0.09	358.0	367.2	558.3	406.9	450.3	666.8	18.45	16.27
852	0	850	0	0.125	0.03	88.9	118.4	-	38.5	121.8	-	2.79	-
					0.05	92.7	123.7	-	38.4	121.4	-	1.86	-
					0.07	94.7	126.3	-	38.3	121.0	-	4.20	-
900	0.102	900	0.046	0.132	0.03	76.2	103.3	147.7	36.6	123.3	144.9	16.22	1.89
					0.05	81.3	110.1	149.5	37.3	125.7	144.3	12.41	3.48
					0.09	86.5	117.2	149.8	38.2	129.0	144.1	9.14	3.80

TABLE 6.1: Calculated strain rate sensitivity constants C_2 and k for 3CR12 at various temperatures. By comparing the percentage error of C_2 and k obtained at both 10^{-1} and 10^{-4} per second, the validity of equations (5) and (6) can be checked.

However, due to dynamic strain ageing, at 600°C the stress at any given strain for the faster strain rate is lower than for the slower strain rate. Calculated constants C_2 and k thus do not compare favourably and equations (6) and (7) become invalid for 3CR12 under the test conditions used. At 850°C the n values were found to be extremely low, if not undefineable and therefore no k value was determined. This value, however, would be very similar to the C_2 value and is consistent for both strain rates. The validity of incorporating the work hardening parameter into equation (7) can be seen by the result obtained for deformation at 900°C where the relationship between strain rate, strain and stress is described well by equation (7), but not at all by equation (6). The inhibition of grain growth in the dual-phase region may also be partly responsible for the high temperature validity of equation (7). At higher temperatures, however, both equations (6) and (7) were found to be inconsistant.

6.3 THE EFFECT OF TITANIUM CARBO-NITRIDES ON THE PLASTIC DEFORMATION OF 3CR12 ALLOYS

It has been observed that cavitation occurs during the tensile deformation of both the 3CR12 alloys and that cavity growth and coalescence is an important factor in the failure mechanism for these steels. It can be see that cracking between the matrix and titanium carbo-nitride particles occur at early strains (Fig. 5.37, photo A) as the void growth about the cracked inclusion, grown in the direction of greatest localised deformation, represents a strain similar to the macro-strain achieved by the specimen itself. Actual fracture of the tensile specimen then progresses by the coalescence of adjacent voids, as can be seen by the highly dimpled character of most fracture surfaces. Concentrations of titanium carbo-nitrides will lead to localised high densities of voids during deformation and these will tend to coalesce more rapidly than a random distribution, resulting in much lower elongations to fracture. Surface finish in these alloys may be

seriously impaired and pitting corrosion induced by small cavities which can result from the extraction of exposed carbo-nitrides during polishing processes.

An interesting fact which has been noted (photo 5.37) is the tendency for the titanium carbo-nitrides to band together in rows. This elongated clustering effect has a marked and detrimental influence on the fracture of the steel by inducing the occurrence of delamination during tensile deformation (photo 5.33 & 5.38). It was noticed that these banded precipitates were usually far larger than the precipitates found at random in the matrix. A similar observation has been made by Matsuda and Okumura (1979) who found that, under welding conditions, titanium nitride particles in low carbon alloy steels tended to form rows on reprecipitation. In 3CR12 alloys, the titanium carbo-nitride rows tend to be associated with ferrite stringers and a possible explanation for this phenomenon is offered. During manufacture of the steel prior to casting, it can be presumed that above ~1250°C all the titanium is in solution and only below this temperature do the titanium carbo-nitrides begin to precipitate. In general, microscopic non-uniformities in the distribution of solute elements can be considered to exist in any specimen and this can be represented

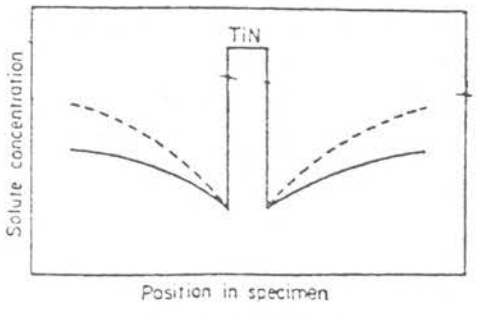

Fig. 6.4 : Theoretical non-uniformities in titanium concentration.

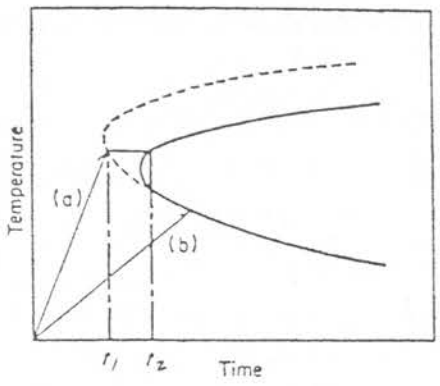

Fig. 6.5 : Schematic representation of the C-curve for carbide precipitation

grahically by figure 6.4, where the dotted lines represent areas of higher titanium concentration. Figure 6.5 is a schematic representation of the C-curve associated with the titanium carbo-nitride precipitation. The C-curve shape is determined by the degree of nucleation at the temperatures higher than the temperature of the nose and, at temperatures lower than the nose, by the limiting factors of the diffusion rates of those elements which are to precipitate.

In an area where the titanium concentration is unusually high (in the case of 3CR12 alloys this would be in the delta-ferrite regions as preferential partitioning of titanium to this phase can be expected to occur when austenite begins to precipitate), the nose of the C-curve is shifted to the shorter time side (curve a), because of the increased possibility of a nucleation event taking place. In the case of curve (b) then, precipitation begins at time t_1 in the locality of high solute concentration, but at this time no precipitation is yet possible in other low concentration places (curve a), as precipitation is held up until time t_2. Between times t_1 and t_2, however, the already precipitated titanium carbo-nitride particles can continue to grow by drawing solute atoms from surrounding areas according to Ficks first law. When time t_2 is finally reached, titanium carbo-nitride particles start precipitating at other sites and the amount of solute migrating to the previously precipitated particle becomes less.

At temperatures of around 1250°C, both 3CR12 alloys have a dual-phase microstructure and, as titanium is a ferritising agent, it is reasonable to assume that ferrite grains would tend to be associated with high concentrations of titanium. Under such conditions and given the precipitation mechanism outlined above, fairly large titanium carbo-nitride carbide particles would tend to precipitate and grow in the ferrite grains. During the hot-rolling process these grains are elongated and the resultant microstructure can thus be seen to co-exist of larger than average particles associated with ferrite stringers and smaller particles within the matrix having a more random distribution. During cooling from the

melt and during subsequent heat treatments, the larger particles will tend to grow by an Oswald ripening type process at the expense of the smaller precipitates. Subsequent heat treatments could, however, tend to recrystallise the ferrite stringers, but the row morphology of the titanium carbo-nitrides would remain, unless reheating to temperatures greater than 1250°C for an appreciable length of time takes place.

Examination of a number of voids associated with titanium carbo-nitrides (Fig. 5.37) suggests that voids are initiated by decohesion along the sulphide/titanium carbo-nitride interface. Cracking of the titanium carbo-nitride particles themselves was observed rather less often than decohesion and is evidently restricted to inclusions possessing a strong cohesive bond between themselves and the matrix.

This section of the work thus indicates that the most important microstructural features governing the plastic fracture of 3CR12 alloys are the void nucleating titanium carbo-nitride particles. It is felt that the toughness of these alloys may be most readily improved by decreasing the number and size of these inclusions. By refining the size of the carbides and dispersing them more generally through the matrix, void initiation could be delayed with a resultant improvement of toughness. As observed in AISI 4340 steel (Cox and Low, 1974) where a tendency existed for manganese sulphide particles to nucleate on deoxidation products present in the melt, it might be possible to suitably seed or otherwise increase the nucleation of the titanium particles in 3CR12 alloys for a given concentration level, thus producing a finer dispersion of these inclusions in the final product.

CONCLUSIONS

The main objective of this investigation was to gain an understanding of the elevated temperature mechanical properties of the 3CR12 alloys with particular reference to their deformation behaviour. The following work was completed:

(1) An elevated temperature tensile testing rig was designed and successfully commissioned which could operate at a maximum of 1160°C under vacuum. A computerised system linked to the testing rig was incorporated to enable data capture and processing.

(2) It was verified that an understanding of the microstructural response of 3CR12 alloys to heat treatment is important if the mechanical properties are to be optimised for any particular use. The fine grained dual-phase microstructure consisting of ferrite and low carbon lath martensite at room temperature can confer good formability characteristics on these steels, but the ductility is decreased with increasing volume percent martensite. At elevated temperatures the degree of martensite decomposition and the relative amounts of both ferrite and austenite were found to influence the high temperature mechanical properties.

(3) Hot-rolled 3CR12 alloys exhibit a good retention of strength up to 600°C (400 and 600 MPa respectively) before displaying a sharp decrease in their tensile properties due to the formation of a fully ferritic microstructure. Contrary to 3CR12Ni, 3CR12 demonstrates a low yield strength to ultimate tensile strength ratio up to 700°C.

(4) Both 3CR12 and 3CR12Ni experience minima in deformation energies at around 900°C. This could be an important fact in terms of hot-forming operations. These minima are also associated with low work hardening rates and low tensile strengths.

(5) Analysis of the deformation behaviour of these alloys showed that work hardening at most temperatures could not be represented in terms of a single work hardening parameter, but that various

stages in work hardening could be delineated, each with individual parameters. These stages, designated from I to III, are representative of specific work hardening modes. It is shown that the work hardening in the dual-phase temperature regime attenuates to a very low value and this fact can be attributed to dynamic recrystallisation of straining ferrite and the deformation induced nucleation of strain-free austenite.

(6) The strain rate sensitivity for 3CR12 was shown to rise sharply within the dual-phase temperature region, reaching a maximum of 0.17 at 1152°C. Evidence to suggest the existance of superplasticity in 3CR12Ni alloy during slow tensile deformation was found at 900°C, where a low necking tendency and grain boundary sliding and separation was observed. The observed m value (~0.14) for this temperature, however, is too low for true superplastic behaviour.

(7) The stress at a constant strain and temperature for 3CR12 was found to obey the relationship below for certain temperatures:

$$\sigma_{\epsilon,T} = k\dot{\epsilon}^{m}\epsilon^{n}$$

At room temperature and in the dual-phase temperature range where competitive grain growth maintains a fine grain size, experimental results showed good consistancy. At 600°C, however, increased dynamic strain ageing at slow strain rates is responsible for the breakdown in this relationship.

(8) The presence of large cuboid titanium carbo-nitride particles within the steel have been found to be responsible for void initiation during tensile deformation. Associated with these particles are inclusions of sulphur and silicon which tend to decrease the cohesive strength between the deforming matrix and the titanium carbo-nitride particles. The elongation to fracture and therefore the toughness of the 3CR12 alloys are detrimentally influenced due to the coalescence and growth of these voids. The development of second generation alloys based on 3CR12 will need to deel with this problem by compromising formability and ductility with weldability.

REFERENCES

Argon, A.S., Im, J. and Safoglu, R. (1975): "Cavity formation from inclusions in ductile fracture", Met. Trans., 6A, pp 825-837.

Ball, A. and Hoffman, J.P. (1981): "Microstructure and properties of a steel containing 12% Cr", Metals Technology, 8, 9, pp 329-338.

Ball, A. and Hutchison, M.M. (1969): "Superplasticity in the Aluminium Zink Eutectoid", J. Metal Science, 3, pp 1-7.

Ashby, M.F. (1966): Philos. Mag., 1966, 14, 1157 cited in Ballinger, N.K. and Gladman, T. (1981): "Work hardening of dual-phase steels", Metal Science, pp 95-108.

Baker, T.J. and Charles, J.A. (1972): J. Iron and Steel Inst., Vol. 210, pp 680-90.

Bergström, Y. and Aronsson, B. (1970): "Effects of change in temperature and strain rate on the 'double-n' behaviour of Alpha-iron", Met. Trans. 1, pp 1029-1030.

Burke, M.A. and Nix, W.D. (1975): "Plastic instabilities in tension creep", Acta Met., 23, p 793.

Cox, T.B. and Low, J.R. (1974): "An investigation into the plastic fracture of AISI 4340 and 18 Nickel-200 grade maraging steels", Metallurgical Transactions, 5, p 1457.

Cribb, W.R. and Rigsby, J.M. (1979): "Work hardening behaviour and its relationship to the microstructure and mechanical properties of dual-phase steels", "Structure and properties of dual-phase steels", Proc. AIME Symposium, New Orleans, J.W. Morris Jr. and R. Kot, eds. pp 91-117.

Davies, R.G. (1978): "The deformation behaviour of a vanadium-strengthened dual-phase steel", Met. Trans., 9A, p 41.

Davies, R.G. (1979): "Influence of martensite composition and content on the properties of dual-phase steels", Met. Trans., 9A, pp 671-679.

Demeri, M.Y. (1981): "The formability of a dual-phase steel", Met. Trans., 12A, pp 1187-1196.

Department of Materials Science and Metallurgical Engineering, (1981): "Research on 3CR12 for Southern Cross Steel - 1981", University of Pretoria.

Follstaedt, D.M. (1980): "Microstructure of TiC precipitates in Ti-implanted alpha-Fe", J. Appl. Phys., 51, 2, pp 1001-1010.

Freeman, S. and Honeycombe, R.W.K. (1977): "Strengthening of titanium steels by carbide precipitation", Metal Science, pp 59-64.

Garde, A.M., Santhanam, A.T. and Reed-Hill, R.E. (1972): "The significance of dynamic strain ageing in titanium", Acta Met. 20, pp 215-220.

Ghosh, A.K. (1977): "Tensile instability and necking in materials with strain hardening and strain rate hardening", Acta. Met., 25, pp 1413-1424.

Hamilton, C.H. and Ghosh, A.K. (1980): "Determination of strain rate sensitivity index in superplastic Ti-6Al-4V", Met. Trans., 11A, pp 1494-1496.

Hart, E.W. (1967): Acta Met., 15, p 351.

Hedworth, J. and Stowell, M.J. (1971): J. Mater.Sci., 6, pp 1661-69.

Hedworth, J. and Stowell, M.J. (1971): "The measurement of strain rate sensitivity in superplastic alloys", J. Mat. Sci., 6, p 1061.

Hilliard, J.E. (1968): "Measurement of volume in volume", "Quantitative Microscopy", R.T. De Hoff and F.N. Rhones, eds., McGraw-Hill, New York.
Hilliard, J.E. and Cahn, J.W. (1961): "An evaluation of procedures in quantitative metallography for volume fraction analysis", Trans. Met. Soc. AIME, 221, pp 344-352.

Honeycombe, R.W.K. (1968): "The Plastic Deformation of Metals", p 135. London: Edward Arnold.

Honeycombe, R.W.K. (1976): "Transformation from austenite in alloy steels", Met. Trans., 7A, pp 915-936.

Honeycombe, R.W.K. (1981): "Steels, microstructure and properties", 1st ed., p 228. London: Edward Arnold.

Humphries, C.W. and Ridley, N. (1974): "Cavitation in alloy steels during superplastic deformation", J. Mat. Sci. 9, p 1429.

Immarigeon, J.P.A. and Jones, J.J. (1974): "The deformation of Armco iron and silicon steel in the vicinity of the Curie temperature", Acta Met., 22, pp 1235-1347.

Jonas, J.J. (1969): "Back stress in high temperature deformation", Acta. Met., 17, pp 397-405.

Jonas, J.J., Holt, R.A. and Coleman, C.E. (1976): "Plastic instability in tension and compression", Acta. Met., 24, pp 911-918.

Klevebring, B., Borgren, E. and Mahrs, R. (1975): "Determination of the critical inclusion size with respect to void formation during hot working", Met. Trans., 6A, pp 319-327.

Koo, J.Y. and Thomas, G. (1977): Met. Trans. 8A, pp 525-528.

Lagneborg, R. (1972): Met. Rev., 17, p 130.

Luton, M.J. and Jonas, J.J. (1970): "A model for high temperture deformation based on dislocation dynamics, rate theory and periodic internal stress", Acta. Met., 18, pp 511-517.

Luton, M.J. and Sellars, C.M. (1969): "Dynamic recrystallisation in nickel and nickel-iron alloys during high temperature deformation", Acta Met., 17, pp 1033-1043.

McClintock, F.A. (1971): "Fracture", H. Liebowitz, ed., Vol. 3, p 106, Academic Press, New York.

McGammon, E. (1971): "The making, shaping and treating of steel", (1971); ninth edition, ed. McGammon, E., Pennsylvania: Herbick and Held.

McGregor Tegart, W.J. (1966): "Elements of mechanical metallurgy", ed. Morris E. Fine, Johannes Weertman and Julia Uteertman, p 37, London: Collier-Macmillan Limited.

Marder, A.R. (1982): "Deformation characteristics of dual-phase steels", Met. Trans., 13A, pp 85-92.

Matlock, D.K., Kraus, G., Ramos, L.F. and Huppi, G.S. (1979): "A correlation of variables with the deformation behaviour of dual-phase steels", "Structure and properties of dual-phase steels", Proc. AIME Symposium, New Orleans, J.W. Morris Jr. and R.Knot, eds., pp 62-90.

Matsuda, S. and Okumura, N. (1978): "Effect of distribution of TiN precipitate particles on the austenite grain size of low carbon low alloy steels", Transactions ISIJ, 18, pp 198-205.

Matsuoka, T. and Yamamori, K. (1975): "Metallurgical aspects in cold rolled high strength steel sheets", Met. Trans., 6A, p 1613.

Mileiko, S.T. (1979): J. Mat Sci., 4, p 974.

Monteiro, S.N. and Reed-Hill, R.E. (1971): "On the Double-n Behaviour of Iron", Met. Trans., 2, pp 2947-2948.

Monteiro, S.N. and Reed-Hill, R.E. (1973): "An empirical analysis of titanium stress-strain curves", Met. Trans., 4, pp 1011-1015.

Monteiro, S.N., Le May, I. and de Almeida, L.H. (1981): "Effects of strain rate and dynamic strain ageing on work hardening of an austenitic stainless steel", Scripta Met., 15, pp 581-584.

Morrison, W.B. (1968): Trans. ASM., 61, p 423.

Noël, R.E.J. (1981): "The abrasive-corrosive wear behaviour of metals", M.Sc. Thesis, University of Cape Town.

Peckner, D. and Bernstein, I.M. (1977): "Handbook of stainless steels", 4, p 49, McGraw-Hill, New York.

Protopappas, E., (1983): M.Sc. Thesis, University of Cape Town.

Rai, G. and Grant, N.J. (1975): "On the measurements of superplasticity in an Al-Cu Alloy", Met. Trans., 6A, pp 385-90.

Ramos, L.F., Matlock, D.K. and Kraus, G. (1979): "On the deformation behaviour of dual-phase steels", Met. Trans., 10A, pp 259-261.

Rashid, M.S. (1977): SAE Preprint 770211. Cited by Rigsby, M.J. and van der Arend, P.J. (1979): "Structure-property relationships in dual-phase HSLA steels", "Formable HSLA and dual-phase steels", Proc. TMS-AIME Symposium, Chicago, Illinois. A.T.

Rashid, M.S. (1981): "Dual phase steels", Ann. Rev. Mater. Sci., 11, pp 245-266.

Rice, J.R. and Tracey, D.M. (1969): J. Mech. Solids, Vol. 17, p 171, New York: McGraw Hill.

Rigsby, J.M. and Van der Arend, P.J. (1979): "Laboratory studies of microstructures and structure-property relationships in dual-phase HSLA steels", "Formable HSLA and dual-phase steels", Proc. TMS-AIME Symposium, Chicago, Illinois, A.T. Davenport, ed., pp 56-84.

Rigsby, J.M., Abraham, J.K., Davenport, A.T., Franklin, J.E. and Pickens, J.W. (1979): "Structure processing and structure-property relationships in commercially processed dual-phase steels", "Structure and properties of dual-phase steels", Proc. AIME Symposium, New Orleans, J.W. Morris Jr. and R. Kot, eds. pp 305-329.

Rizk, A. and Bourell, D.L. (1982): "Dislocation density contribution to strength of dual-phase steels", Scripta Met., 16, pp 1321-1324.

Rossard, C. (1966): Rev. Met., 63, p 225.

Routbourt, J.L., Reid, C.N., Fischer, E.S., and Dever, D.J. (1971): "High temperature elastic constants and the phase stability of silicon-iron", Acta. Met., 19, pp 1307-1316.

Rozovsky, E., Hahn, W.C. and Avitzur, B. (1973): "The behaviour of particles during plastic deformation of metals", Met. Trans., Vol. 4, pp 927-30.

Schaffer, G.B. (1983): "A constitutional study of a dual-phase steel containing 12% Chromium", M.Sc. Thesis, University of Cape Town.

Sherby, O.D., Caligiuri, R.D., Kayali, E.S. and White, R.A. (1981): "Fundametals of superplasticity and its application", "Advances in metal processing", Proc. Twenty-fifth Sagamore Army Materials Research Conference, Lake George, New York, pp 133-172, New York: Plenum Press.

Smallman, R.E. (1983): "Microstructure and deformation aspects of some speciality steels and hard metals", "Speciality steels and hard materials", Proc. International Conference on Recent Developments in Speciality Steels and Hard Materials, Pretoria, Comins, N.R. and Clark, J.B., eds. pp 141-152.

Smith, C.I., Norgate, B. and Ridley, N. (1976): "Superplastic deformation and cavitation in a microduplex stainless steel", Metal Science, 5, pp 182-188.

Smithels, C.J. ed. (1976): "Metals Reference Book", Fifth ed. p 975.

Sondenberg, R. (1980): "Research on 3CR12 - University of Pretoria", Internal report, Middleburg Steel and Alloys (Pty) Ltd.

Southern Cross Laboratories (1981): "3CR12 Development work - 1981", Internal report, Middleburg Steel and Alloys (Pty) Ltd.

Szewczyk, A.F. and Gurland, J. (1982): "A study of the deformation and fracture of a dual-phase steel", Met. Trans., 13A, pp 1821-1826.

Tomota, Y. and Kuroki, K. (1976): "Tensile deformation of two-ductile-phase alloys: Flow curves of alpha-gamma Fe-Cr-Ni alloys", Materials Science and Engineering, 24, pp 85-94.

APPENDIX I

COMPUTER PROGRAMS

1.1 ACQUISITION AND DATA PROCESSING

Figure 1.1 illustrates the software sequence utilised to acquire, process and analyse the output signal from the ESH to produce graphical stress-strain curve from the tensile tests. A brief description of each program is given overleaf accompanied by the BASIC coding.

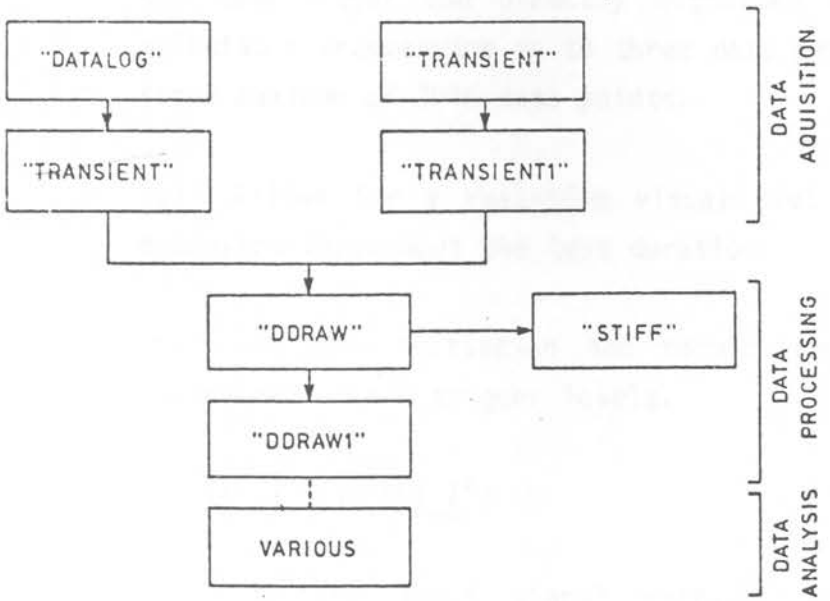

Fig. 1.1 Program sequence

1.1 PROGRAM "DATA LOG":

(a) Initializes the system to incorporate the data logger as the data acquisition unit.

(b) Allows for experimental details such as specimen dimensions and full scale settings to be inputted.

1.2 PROGRAM "TRANSIENT":

(a) Initializes the system to incorporate the transient recorder as the data acquisition unit.

(b) Allows for experimental details to be inputted.

1.3 PROGRAM "DATALOG 1":

(a) Enables the input signal voltages to be acquired by the data logger and directly outputted to the HP85 at selectable frequencies up to three data points per second, for a maximum of 2048 data points.

(b) Allows for a real-time visual plot of load versus extension throughout the test duration.

(c) Controls initiation and termination of a test by programmable load trigger levels.

1.4 PROGRAM "TRANSIENT 1":

(a) Enables input signal voltages acquired by the transient recorder to be outputted to the HP85 by a fast handshake in the form of a character string, after completion of the test.

1.5 PROGRAM "DDRAW":

(a) Stores raw test data (in volts) on disc.

(b) Converts test data into load elongation values.

(c) Provides an averaging facility which can smooth out superimposed noise influences from the load cell. This is achieved by selecting a data sample group of x data points and then averaging all values from data point 1 to data point x. A new group of points from data point 2 to x + 1 is then automatically selected and averaged, the process continuing until all data points is processed.

(d) Allows for a hard copy of experimental detail and data points on request.

1.6 PROGRAM "STIFF":

(a) This program provides the option to correct and store extension data for load chain compliance effects. As the compliance effect was not a linear function with load (especially at low loads), it was not feasible to simply apply a proportional correction factor to test extension data, but necessary to select a corresponding compliance correction value for every test data point at its own particular load.

(b) The program is capable of acquireing and storeing load-elongation stiffness data, used for compliance correction, at any selected strain rate. This data is obtained by loading up an "inextensible" bar in the test rig in the normal manner, to a load equivalent to the maximum test load used. The deformation incurred in this load range is then a measure of the compliance or "stretch" experienced by the load chain during normal testing.

1.7 PROGRAM "DDRAW 1":

(a) Converts load-elongation data into:

(i) true stress-true strain values and
(ii) engineering stress-engineering strain values by using the conventional equations for the conversions:

$$\sigma = \sigma_e(1 + \epsilon_e)$$

$$\epsilon = \ln(1 + \epsilon_e)$$

where σ is true stress, σ_e is engineering stress, ϵ is true strain and ϵ_e is engineering strain.

(b) Measurement of the following values is automatic:

(i) UTS and corresponding its strain
(ii) 0,2% proof stress and the corresponding strain
(iii) Maximum engineering strain to failure
(iv) Areas under the curve to:
a) yield point
b) UTS
c) fracture.

The area analysis was done by a numerical integration process.

(c) Plots the stress-strain diagram for the test and labels the data listed in (b).

Various further programs were used to process the basic stress-strain data thus aquired, with the aim of investigating parameters such as work hardening exponants and strain rate sensitivity values. These however, are not listed.

BASIC CODING

```
******** PROGRAN DATALOG ********


  REM *****DATALOG ******
10 OPTION BASE 1
20 COM SHORT X(2048,2),T$[10],N,P$[1],S$[1],M$[20],P3,P4,06,T3$[20],G5

25 COM A1$[15],A2$[10],A3$[18],A4$[10],A5$[10],A6$[10],A7$[10],A8$[80]
 A9$[10],B1$[10],B2$[20]
50 CLEAR
40 PRINT "********* E S H TEST ********"
60 PRINT @ PRINT @ PRINT
60 DISP "RECORD NEW  EXPERIMENTAL DETAIL" @ DISP "                (Y/N)"
70 INPUT P$
80 IF P$="N" THEN 470
90 DISP @ DISP
100 DISP "TEST #"
110 INPUT A1$
120 PRINT "TEST#";TAB(20);A1$
130 DISP "DATE"
140 INPUT A2$
150 PRINT "DATE";TAB(20);A2$
160 DISP "MATERIAL TYPE'
170 INPUT A3$
180 PRINT "MATERIAL TYPE';TAB(20);A3$
190 DISP "GAUGE LENGTH (mm)"
200 INPUT A4$
210 PRINT "GAUGE LENGTH";TAB(20);A4$;" mm"
220 DISP "DIAMETER (mm)"
230 INPUT A5$
240 PRINT "DIAMETER (mm)";TAB(20);A5$;" mm"
310 DISP "ESH FS LOAD (KN)"
320 INPUT A9$
330 PRINT "ESH FS LOAD (KN)";TAB(20);A9$;" KN"
340 DISP "ESH FS STROKE (mm)"
350 INPUT B1$
360 PRINT "ESH  STROKE (mm)";TAB(20);B1$;" mm"
370 DISP "RAMP RATE (V/S)"
380 INPUT B2$
390 PRINT "RAMP RATE";TAB(20);B2$;" V/S"
410 DISP "HISTORY'
415 DISP "-------------3------2-----1"
420 INPUT A8$
421 DISP "TEST TEMPERATURE (*C)"
422 INPUT A6$
423 PRINT "TEST TEMP (*C)";TAB(20);A6$;" *C"
424 DISP "VACUUM (TORR)"
425 INPUT A7$
426 PRINT "VACUUM";TAB(20);A7$;" torr"
430 PRINT "HISTORY              ";TAB(20);A8$
440 ASSIGN# 1 TO "JUNK"
450 PRINT# 1 ; A1$,A2$,A3$,A4$,A5$,A6$,A7$,A8$,A9$,B1$,B2$
460 ASSIGN# 1 TO *
470 CHAIN "DATALOG1"
```

******* PROGRAM TRANSIENT *******

```
1 REM ****TRANSIENT ******
10 COM Q1$[4500],A,F$[1],F,F1
20 CLEAR
30 PRINT "********* E S H TEST ********"
40 PRINT @ PRINT @ PRINT
50 DISP "RECORD NEW  EXPERIMENTAL DETAIL" @ DISP "                (Y/N
60 INPUT P$
70 IF P$="N" THEN GOTO 570
80 DISP @ DISP
90 DISP "TEST #"
100 INPUT A1$
110 PRINT "TEST#";TAB(20);A1$
120 DISP "DATE"
130 INPUT A2$
140 PRINT "DATE";TAB(20);A2$
150 DISP "MATERIAL TYPE"
160 INPUT A3$
170 PRINT "MATERIAL TYPE";TAB(20);A3$
180 DISP "GAUGE LENGTH (mm)"
190 INPUT A4$
200 PRINT "GAUGE LENGTH";TAB(20);A4$;" mm"
210 DISP "DIAMETER (mm)"
220 INPUT A5$
222 PRINT "DIAMETER (mm)";TAB(20);A5$;" mm"
225 DISP "TEST TEMPERATURE (*C)"
226 INPUT A6$
227 PRINT "TEST TEMP (*C)";TAB(20);A6$;" *C"
240 DISP "VACUUM (TORR)"
250 INPUT A7$
260 PRINT "VACUUM";TAB(20);A7$;" torr"
270 DISP "ESH FS LOAD (KN)"
280 INPUT A9$
290 PRINT "ESH FS LOAD (KN)";TAB(20);A7$;" KN"
300 DISP "ESH FS STROKE (mm)"
310 INPUT B1$
320 PRINT "ESH  STROKE (mm)";TAB(20);B1$;" mm"
330 DISP "RAMP RATE (V/S)"
340 INPUT B2$
350 PRINT "RAMP RATE";TAB(20);B2$;" V/S"
360 DISP "TR FS LOAD (V)"
370 INPUT B3$
380 PRINT "TR FS LOAD";TAB(20);B3$;" V"
390 DISP "TR FS STROKE (V)"
400 INPUT B4$
410 PRINT "TR FS STROKE";TAB(20);B4$;" V"
420 DISP "SAMPLING RATE (S)"
430 INPUT B5$
440 PRINT "SAMPLING RATE";TAB(20);B5$;" mS"
445 B5$="%"&B5$
450 DIM A$[80]
```

```
660 DISP "HISTORY"
670 DISP "---------------3------2-----1"
675 INPUT A8$
680 PRINT "HISTORY          ";TAB(20);A8$
690 ASSIGN# 1 TO "JUNK"
600 PRINT# 1 ; A1$,A2$,A3$,A4$,A5$,A6$,A7$,A8$,A9$,B1$,B2$,B3$,B4$,B5$

610 ASSIGN# 1 TO *
670 CHAIN "TRANSIENT1"
```

******** PROGRAM DATALOG 1 ********

```
10 REM *** DATALOG1 ***
20 G5,T2=0
30 N8=0 @ CLEAR
40 REM MODIFIED TO ACCEPT COMPRESSION DATA
50 DISP "INPUT TRIGGER LEVEL (V)"
60 INPUT V
70 OPTION BASE 1
80 COM SHORT X(2048,2),T$[10],N,P$[1],S$[1],M$[20],P3,P4,O6,T3$[20],G6

90 COM A1$[15],A2$[10],A3$[18],A4$[10],A5$[10],A6$[10],A7$[10],A8$[80]
,A9$[10],B1$[10],B2$[20]
100 CLEAR
110 DISP "      ******** KEY **********"
120 DISP @ DISP @ DISP "      INPUT FREQUENCY"
130 DISP @ DISP @ DISP USING 140 ; "TRIGGERS WHEN LOAD=";V;" V"
140 IMAGE 20A, 2D.3D,2A
150 ON KEY# 1,"RUN" GOTO 260
160 ON KEY# 2,".25" GOTO 720
170 ON KEY# 3,".5" GOTO 740
180 ON KEY# 4,"1 " GOTO 760
190 ON KEY# 5,"2 " GOTO 780
200 ON KEY# 6,"5 " GOTO 800
210 ON KEY# 7,"10" GOTO 820
220 ON KEY# 8,"STOP" GOTO 840
230 KEY LABEL @ COPY
240 GOSUB 880
250 BEEP 50,50 @ BEEP 100,50 @ GOTO 250
260 CLEAR @ T=0
270 SETGU @ MOVE 10,90 @ LORG 1
280 LABEL "****   TESTING   *****"
290 SETUU
300 N=3
310 CLEAR 709
320 OUTPUT 709 ;"ARTEOAF1;A L12VR3VT1SV1S01"
330 OUTPUT 709 ;"AS"
340 ENTER 709 ; C
350 OUTPUT 709 ;"AS"
360 ENTER 709 ; D
370 OUTPUT 709 ;"AS"
380 ENTER 709 ; C1
390 OUTPUT 709 ;"AS"
400 ENTER 709 ; D1
410 IF C1>V THEN GOTO 420 ELSE GOTO 330
420 OUTPUT 709 ;"TE2"
430 WAIT T2
440 OUTPUT 709 ;"AS"
450 ENTER 709 ; X(N,1)
460 OUTPUT 709 ;"AS"
470 ENTER 709 ; X(N,2)
480 IF G5=4 THEN GOTO 570
490 IF X(N,1)<V AND N>100 THEN 570
```

```
500 N8=N8+1
510 PENUP
520 IF N8=100 THEN PRINT USING "4D,3X,3D.3D,6X,3D.3D" ; N,X(N,1),X(N,2
)
530 PLOT X(N,2),X(N,1)
540 N=N+1
550 IF N8=100 THEN N8=0
560 GOTO 430
570 OUTPUT 709 ;"TE"
580 ENTER 709 ; T$@ BEEP @ BEEP
590 X(1,1)=C @ X(1,2)=D
600 X(2,1)=C1 @ X(2,2)=D1
610 IF C<V THEN GOTO 620 ELSE GOTO 630
620 X(1,1)=X(2,1) @ X(1,2)=X(2,2)
630 T=VAL(T$)
640 OUTPUT 709 ;"TEOAR"
650 CLEAR @ COPY
660 PRINT USING 680 ; "DURATION OF TEST ";T;"S"
670 PRINT USING 690 ; "DATA POINTS ";N
680 IMAGE 18A,2X,4D,1X,1A
690 IMAGE 12A,3X,4D
700 GRAPH @ COPY
710 CHAIN "DDRAW"
720 GOSUB 860
730 T2=0 @ GOTO 430
740 GOSUB 860
750 T2=500 @ GOTO 430
760 GOSUB 860
770 T2=1000 @ GOTO 430
780 GOSUB 860
790 T2=2000 @ GOTO 430
800 GOSUB 860
810 T2=5000 @ GOTO 430
820 GOSUB 860
830 T2=10000 @ GOTO 430
840 GOSUB 860
850 G5=4 @ GOTO 430
860 OUTPUT 709 ;"AR   AF11A L12VR3VT1SV1S01"
870 RETURN
880 CLEAR @ GCLEAR
890 DISP "INPUT STROKE LEVEL "
900 INPUT X
910 PLOTTER IS 1
920 LOCATE 20,100,20,80
930 FRAME
940 X3=X+10
950 IF X3>10 THEN X3=10
960 SCALE X,X3,0,10
970 FXD 1,1
980 LAXES 1,1,X,0,1,1
990 RETURN
```

******** PROGRAM TRANSIENT1 ********

```
10 REM **** TRANSIENT1 ***
20 09=10 @ 09$,08$=""
30 DIM A8$[80]
40 COM Q1$[4500],A,P$[1],F,F1
50 DIM Q2$[4104]
60 IOBUFFER Q1$
70 IOBUFFER Q2$
80 ON INTR 7 GOSUB 1320
90 ON KEY# 1,"INIT   " GOSUB 250
100 ON KEY# 5,"RE-RUN" GOTO 1780
110 ON KEY# 4,"TRACE IP      " GOTO 1760
120 ON KEY# 8,"BASE IP        " GOTO 1730
130 ON KEY# 2,"ARM" GOSUB 810
140 ON KEY# 3,"TRIGGER" GOSUB 850
150 ON KEY# 7,"Q1$TOX" GOTO 1650
160 ON KEY# 6,"STORE" GOTO 1340
170 CLEAR @ KEY LABEL
180 BEEP 100,60 @ DISP "INITIALISE BEFORE CONTINUING" @ DISP @ DISP
190 IF 09<>1 AND 09$="" THEN DISP "BASELINE LIMITS NOT YET OBTAINED "
200 IF 09=0 THEN DISP "TRACE OBTAINED"
210 IF 09=1 THEN DISP "BASE LINE OBTAINED          "
220 IF 08$="0" AND 09$="0" THEN DISP "BASE LINE AND TRACE OBTAINED
    "
230 GOTO 230
240 GOTO 170
250 CLEAR
260 GCLEAR
270 GOSUB 320
280 GOSUB 90
290 CLEAR @ DISP "PROGRAM END"
300 RETURN
310 END
320 REM   INITIALISATION
330 C=0 @ INTEGER A(255),D
340 DIM L$[20]
350 N=8
360 RETURN
370 CLEAR @ GCLEAR
380 ALPHA
390 DISP "DO YOU WANT TO FILE DATA Y/N";
400 INPUT V$
410 IF V$="N" THEN 670
420 DISP "FILE NAME";
430 INPUT M$
440 PRINT "FILE NAME.....";M$
450 DISP "CREATE Y/N";
460 INPUT N$
470 IF N$="Y" THEN CREATE M$,2,17000
480 IF C=2 THEN Q1$=Q2$
490 ASSIGN# 1 TO M$
```

```
500 PRINT# 1 ; Q1$
510 ASSIGN# 1 TO *
520 RETURN
530 REM  DATA TRANSFER INTO HP85
540 SEND 7 ; UNL UNT @ CLEAR 700+N @ WAIT 1000
550 CLEAR
560 REM
570 C=2
580 IF C<1 THEN 560
590 IF C>2 THEN 560
600 SEND 7 ; MLA @ RESUME 7
610 CLEAR
620 DISP "IF NO BEEP THEN RESET"
630 S=SPOLL(700+N)
640 IF C=1 THEN CONTROL Q1$,0 ; 1,0@ TRANSFER 700+N TO Q1$ FHS ; COUNT
 2048
650 ENABLE INTR 7;8
660 ALPHA
670 IF C=2 THEN CONTROL Q2$,0 ; 1,0@ TRANSFER 700+N TO Q2$ FHS ; COUNT
 4096
680 BEEP 100,250
690 ENTER 700+N USING "#,B" ; X
700 SEND 7 ; UNL UNT @ CLEAR 700+N
710 CLEAR @ DISP "CHANNEL(S) TRANSFERRED TO Q";C;"$"
720 WAIT 1500
730 IF D9=0 THEN 800
740 P,P1,N=0
750 FOR I=1 TO 2048 STEP 50 @ B=NUM(Q2$[I+2048]) @ B1=NUM(Q2$[I])
760 P=P+B @ P1=P1+B1 @ N=N+1
770 NEXT I
780 P=P/N @ P1=P1/N
790 GOTO 800
800 GOTO 170
810 REM  ARM/TRIGGER RECORDER
820 SEND 7 ; UNL UNT @ CLEAR 700+N
830 SEND 7 ; MTA LISTEN N CMD 8,63
840 RETURN
850 REM   RESET T/RECORDER
860 SEND 7 ; UNL UNT
870 CLEAR 700+N
880 RETURN
890 REM   SERIAL POLL & INSTRUMENT STATUS
900 S=SPOLL(700+N)
910 CLEAR
920 DISP "SERIAL POLL & CONTINUOUS DISPLAY OF INSTRUMENT STATUS"
930 DISP ""
940 DISP "RECORD BIT(1) :       ";BIT(S,0)
950 DISP "PLOT BIT(2)   :       ";BIT(S,1)
960 DISP "DIG O/P BIT(3):       ";BIT(S,2)
970 DISP "NRT BIT(4)    :       ";BIT(S,3)
980 DISP "DISPLAY BIT(5):       ";BIT(S,4)
990 DISP "RQS BIT(7)    :       ";BIT(S,6)
1000 DISP "" @ DISP "PRESS RETURN TO UPDATE,R TO EXIT"
1010 INPUT N$
1020 IF N$="R" THEN RETURN
```

```
1030 GOTO 900
1040 REM  GRAPHIC PLOT OF WAVEFORM
1050 IF C=1 THEN CONTROL @1$,0 ; 1,2048
1060 IF C=2 THEN CONTROL @2$,0 ; 1,4096
1070 GCLEAR
1080 SCALE 0,2047,0,255
1090 XAXIS 0,255,0,2047
1100 YAXIS 0,32,0,255
1110 IF C=2 THEN 1180
1120 MOVE 500,220 @ LABEL "DL902,2K POINTS"
1130 MOVE 0,NUM(@1$[1,1])
1140 FOR J=1 TO 2048 STEP 20
1150 DRAW J,NUM(@1$[J,J])
1160 NEXT J
1170 GOTO 1300
1180 MOVE 350,220 @ LABEL "DL 902,2K POINTS(CH.1)"
1190 MOVE 0,NUM(@2$[1,1])
1200 FOR J=1 TO 2048 STEP 20
1210 DRAW J,NUM(@2$[J,J])
1220 NEXT J
1230 INPUT N$
1240 GCLEAR @ MOVE 350,220 @ LABEL "DL 902,2K POINTS(CH.2)"
1250 XAXIS 0,255,0,2047 @ YAXIS 0,32,0,255
1260 MOVE 0,NUM(@2$[2049,2049])
1270 FOR J=1 TO 2048 STEP 20
1280 DRAW J,NUM(@2$[2048+J,2048+J])
1290 NEXT J
1300 INPUT N$
1310 RETURN
1320 STATUS 7,1 ; A
1330 ENABLE INTR 7;8 @ RETURN
1340 Y$=""
1350 IF C=2 THEN @1$=@2$ @ L1=2
1360 REM
1370 N=2048
1380 IF Y$="*" THEN GOTO 1430
1390 ASSIGN# 1 TO "JUNK"
1400 READ# 1 ; A1$,A2$,A3$,A4$,A5$,A6$,A7$,A8$,A9$,B1$,B2$,B3$,B4$,B5$

1410 ASSIGN# 1 TO *
1420 T$=B5$
1430 CLEAR @ DISP "LOAD DATA DISC" @ BEEP 50,50 @ PAUSE
1440 CAT @ DISP "FILE NAME" @ INPUT M$
1450 PRINT "FILE NAME:",M$
1460 DISP "CREATE? (Y/N)" @ INPUT W$@ IF W$="Y" THEN CREATE M$,2,N*8+1
000
1470 DISP "IS THIS A STIFFNESS CURVE?(Y/N)" @ INPUT R8$@ CLEAR
1480 IF R8$="Y" THEN N=250 ! STIFFNESS
1490 DISP "     ************************          " @ DISP "     * WAI
T FOR SIX MINUTES * "
1500 DISP "     ************************          " @ BEEP 400,100
1510 IF R8$="Y" THEN GOTO 1790 ! STIFFNESS
1520 ASSIGN# 2 TO M$
1530 PRINT# 2 ; A1$,A2$,A3$,A4$,A5$,A6$,A7$,A8$,A9$,B1$,B2$,N,T$
1540 IF R8$="Y" THEN GOTO 1790
```

```
1550 FOR I=1 TO 2048
1560 B=NUM(Q1$[I+2048])
1570 B1=NUM(Q1$[I])-P1
1580 B=B/256*VAL(B4$)*2
1590 B1=B1/256*VAL(B3$)*2
1600 PRINT# 2 ; B1,B
1610 NEXT I
1620 ASSIGN# 2 TO *
1630 BEEP @ CLEAR @ DISP USING "5A,1A,5A,1A,6A" ; "LOAD",CHR$(34),"DDR
AW",CHR$(34)," @ RUN"
1640 END
1650 CLEAR @ DISP "LOAD DATA DISC"
1660 BEEP @ PAUSE
1670 CAT @ DISP "FILE NAME?" @ INPUT M$
1680 PRINT "FILE NAME TO BE CHANGED:",M$
1690 ASSIGN# 5 TO M$
1700 READ# 5 ; Q1$,A1$,A2$,A3$,A4$,A5$,A6$,A7$,A8$,A9$,B1$,B2$,B3$,B4$
,B5$,P,P1
1710 ASSIGN# 5 TO *
1720 Y$="*" @ GOTO 1360
1730 O8$="O" @ O9=1 ! BASE LINE
1740 GOTO 530
1750 A1=A1+1
1760 O9=0 @ O9$="O" ! TRACE
1770 GOTO 530
1780 CHAIN "TRANSIENT"
1790 REM *** STIFFNESS DATA  ****
1800 GOSUB 2030 ! COUNT DATA
1810 ASSIGN# 2 TO M$
1820 PRINT# 2 ; A1$,A2$,A3$,A4$,A5$,A6$,A7$,A8$,A9$,B1$,B2$,N,T$
1830 A1,W1,W,A7=0
1840 FOR I=A TO 2048
1850 A1=A1+1
1860 B=NUM(Q1$[I+2048])
1870 B1=NUM(Q1$[I])-P1
1880 B=B/256*VAL(B4$)*2
1890 B1=B1/256*VAL(B3$)*2
1900 W1=W1+B1 @ W=W+B
1910 IF A1=A9 THEN GOTO 1920 ELSE GOTO 1950
1920 B1=W1/A9 @ B=W/A9 @ W,W1,A1=0
1930 A7=A7+1
1940 PRINT# 2 ; B1,B
1950 NEXT I
1960 ASSIGN# 2 TO *
1970 BEEP @ CLEAR @ DISP USING "5A,1A,5A,1A,6A" ; "LOAD",CHR$(34),"DDR
AW",CHR$(34)," @ RUN"
1980 PRINT "N ",N
1990 PRINT "A9",A9
2000 PRINT "A1",A1
2010 PRINT "A7",A7
2020 END
2030 REM *** COUNT DATA ****
2040 A=0
2050 FOR I=1 TO 2048
```

```
2060 B1=NUM(Q1$[I])-P1
2070 B1=B1/256*VAL(B3$)*2
2080 IF B1<.5/VAL(B1$) THEN GOTO 2100 ELSE A=I
2090 A9=IP((2048-A)/190) @ N=IP((2048-A)/A9) @ GOTO 2110
2100 NEXT I
2110 RETURN
```

```
******** PROGRAM DDRAW ********


10 REM  DDRAW
20 A$="" @ N$="" @ R3=-2
30 OPTION BASE 1@ PLOTTER IS 1
40 COM SHORT X(2048,2),T$[10],N,P$[1],S$[1],M$[20],P3,P4,O6,T3$[20],G5

50 COM A1$[15],A2$[10],A3$[18],A4$[10],A5$[10],A6$[10],A7$[10],A8$[80]
,A9$[10],B1$[10],B2$[20]
60 CLEAR @ GCLEAR
70 DISP "IS DATA ON FILE? (Y/N)" @ INPUT Y$
80 IF Y$="Y" THEN GOSUB 250
90 ASSIGN# 1 TO "JUNK"
100 READ# 1 ; A1$,A2$,A3$,A4$,A5$,A6$,A7$,A8$,A9$,B1$,B2$
110 ASSIGN# 1 TO *
120 DISP "STORE DATA? (Y/N)" @ INPUT F$@ IF F$="Y" THEN GOTO 140
130 M$=" ESH TEST" @ CHAIN "DDRAW1"
140 DISP "LOAD DATA DISC AND CONT" @ PAUSE
150 DISP "FILE NAME?" @ INPUT M$
160 PRINT "FILE NAME:";M$
170 O=N*2*8+2000
180 CLEAR
190 CAT @ DISP "CREATE? (Y/N)" @ INPUT W$@ IF W$="Y" THEN CREATE M$,1,
O
200 ASSIGN# 2 TO M$
210 PRINT# 2 ; A1$,A2$,A3$,A4$,A5$,A6$,A7$,A8$,A9$,B1$,B2$,N,T$
220 FOR I=1 TO N @ PRINT# 2 ; X(I,1),X(I,2) @ NEXT I
230 ASSIGN# 2 TO *
240 GOTO 10
250 DISP "LOAD DATA DISC AND CONT" @ BEEP 70,50 @ PAUSE
260 CAT @ DISP "FILE NAME" @ INPUT M$
270 GOSUB 900
280 ASSIGN# 1 TO M$
290 READ# 1 ; A1$,A2$,A3$,A4$,A5$,A6$,A7$,A8$,A9$,B1$,B2$,N,T$
300 IF N>2048 THEN N=2048
310 DISP USING "5D,18A" ; N," RAW DATA POINTS"
320 IF M$[1,1]="*" THEN GOTO 330 ELSE GOTO 360
330 DISP "READING DATA FILE"
340 FOR I=1 TO N @ READ# 1 ; X(I,1),X(I,2)@ NEXT I
350 GOTO 510
360 DISP "ENTER DATA STEP" @ INPUT G5
370 DISP "ENTER SIZE GROUP TO BE AVERAGED"
380 INPUT K3@ DISP "READING DATA FILE"
390 O,O1,O2,O3=0
400 FOR I=1 TO N
410 O2=O2+1
420 READ# 1 ; X(I,1),X(I,2)
430 O1=O1+X(I,1) @ O=O+X(I,2)
```

```
440 IF O2=65 THEN GOTO 450 ELSE GOTO 480
450 O3=O3+1
460 X(O3,1)=O1/O2 @ X(O3,2)=O/O2
470 O,O1,O2=0
480 NEXT I
490 IF N>600 THEN N=O3
500 IF N<=600 THEN N=O3
510 ASSIGN# 1 TO *
520 IF M$[1,1]="*" THEN GOTO 570
530 GOSUB 1540
540 GOTO 570
550 DISP "DO YOU WANT A RAW DATA  PLOT?" @ INPUT X7$@ IF X7$="N" THEN
GOTO 570
560 GOSUB 1350
570 IF T$[1,1]="*" THEN T3$="T" ELSE T3$="D"
580 IF T3$="T" THEN GOTO 590 ELSE GOTO 630
590 IF M$[1,1]<>"*" THEN T3=VAL(T$[2,LEN(T$)])*G5
600 IF M$[1,1]<>"*" THEN T$="*"&VAL$(T3)
610 GOTO 950
620 N=N-2
630 FOR I=1 TO N
640 IF I=1 THEN Y=X(I,2)
650 B=X(I,2)-Y
660 X(I,2)=B*VAL(B1$)/10
670 X(I,1)=X(I,1)*VAL(A9$)/10
680 NEXT I
690 !
700 IF T$[1,1]="*" THEN 710 ELSE 1100
710 GOSUB 1690
720 GOSUB 740
730 GOTO 1180
740 CLEAR @ DISP "PRINT EXP DETAIL?" @ INPUT X1$
750 IF X1$="N" THEN GOTO 730
760 PRINT " E S H TEST " @ PRINT @ PRINT
770 PRINT "TEST#";TAB(20);A1$
780 PRINT "DATE";TAB(20);A2$
790 PRINT "MATERIAL TYPE";TAB(20);A3$
800 PRINT "GAUGE LENGTH ";TAB(20);A4$;" mm"
810 PRINT "DIAMETER ";TAB(20);A5$;" mm"
820 PRINT "TEST TEMP";TAB(20);A6$
830 PRINT "VACUUM        ";TAB(20);A7$;" Torr"
840 PRINT "ESH FS LOAD";TAB(20);A9$;" KN"
850 PRINT "ESH FS STROKE";TAB(20);B1$;" mm"
860 IF M$[1,1]="*" THEN GOTO 880
870 PRINT "RAMP RATE";TAB(20);B2$;" V/S"
880 PRINT "HISTORY";TAB(20);;A8$ @ PRINT @ PRINT
890 RETURN
900 CLEAR @ DISP "*********************************"
910 DISP "*     CALCULATING !!              *"
920 DISP "*  PLEASE BE PATIENT              *"
930 DISP "*********************************"
940 RETURN
950 REM ** DATA FIELD IN Q1$ **
960 I4=0 @ GOSUB 900
```

```
970 V8=.5/VAL(A9$) ! VOLTAGE FOR 5KG
980 FOR I=1 TO N
990 IF X(I,1)<=V8 THEN GOTO 1080
1000 IF X(I,1)<=V8*1.2 AND I4>90 THEN GOTO 1090
1010 I4=I4+1
1020 IF I4=1 THEN Y=X(I,2)
1030 B=X(I,2)-Y
1040 X(I,2)=B*VAL(B1$)/10
1050 X(I,1)=X(I,1)*VAL(A9$)/10
1060 X(I4,1)=X(I,1)
1070 X(I4,2)=X(I,2)
1080 NEXT I
1090 N=I4
1100 N=N-50 ! FRACT POINT
1110 M=ABS(X(N-1,1)) @ DISP M
1120 FOR I=N TO N+49
1130 M1=ABS(X(I+1,1)) @ DISP M1
1140 IF M>=1.04*M1 THEN GOTO 1160
1150 M=M1 @ NEXT I
1160 IF M$[1,1]<>"*" THEN N=I-4 ELSE N=I
1170 GOTO 710
1180 REM  STIFFNESS
1190 IF M$[1,1]<>"*" THEN GOTO 1260
1200 ! G5=NUM(B2$) @ CHAIN "DDRAW1"
1210 DISP "LOAD PROGRAM DISC & CONT" @ PAUSE
1220 DISP "DELTA STRAIN RATE?" @ INPUT S$
1230 IF S$="N" THEN GOTO 1250
1240 CHAIN "DELTA STRAIN"
1250 CHAIN "DDRAW1"
1260 DISP "CORRECT FOR STIFFNESS?(Y/N)" @ INPUT S$
1270 IF S$="Y" THEN GOTO 1330
1280 DISP "LOAD PROGRAM DISC&CONT" @ PAUSE
1290 DISP "DELTA STRAIN RATE?" @ INPUT S$
1300 IF S$="N" THEN GOTO 1320
1310 CHAIN "DELTA STRAIN"
1320 CHAIN "DDRAW1"
1330 BEEP 50,100 @ DISP "LOAD STIFFNESS  PROGRAM DISC" @ PAUSE
1340 CHAIN "STIFF"
1350 ! LINEAR
1360 H,V=1.E21 @ H1,V1=-1.E21
1370 FOR I=1 TO N
1380 H=MIN(X(I,2),H)
1390 V=MIN(X(I,1),V)
1400 V1=MAX(X(I,1),V1)
1410 H1=MAX(X(I,2),H1)
1420 NEXT I
1430 GCLEAR @ CLEAR @ PLOTTER IS 1
1440 LOCATE 30,100,30,90
1450 FRAME @ SETUU @ SCALE 0,10,0,10 @ FXD 0,0
1460 LGRID -1,1,0,0,10,1 @ LORG 1
1470 FOR I=1 TO N
1480 T=(X(I,2)-H)*10/(H1-H)
1490 T1=(X(I,1)-V)*10/(V1-V)
1500 MOVE T,T1 @ LABEL "."
1510 NEXT I
```

```
1520 BEEP 100,50 @ PAUSE
1530 RETURN
1540 DISP "ENTERING AVERAGING ROUTINE"
1550 K2,K4,K5,K6,I=0
1560 IF K2+K3-1>=N THEN GOTO 1680
1570 K2=K2+1
1580 I=I+1
1590 K4=K4+1
1600 K5=K5+X(K4,1) @ K6=K6+X(K4,2)
1610 IF I=K3 THEN GOTO 1620 ELSE GOTO 1580
1620 I=0 @ K4=K2
1630 K5=K5/K3 @ K6=K6/K3
1640 X(K2,1)=K5 @ X(K2,2)=K6
1650 K5,K6=0
1660 GOTO 1560
1670 N=K2-K3
1680 RETURN
1690 FOR I=N-20 TO N
1700 IF X(I,1)>X(I-1,1) THEN 1710 ELSE 1730
1710 X(I,1)=X(I-1,1)
1720 X(I,2)=X(I-1,2)
1730 NEXT I
1740 RETURN
```

******** PROGRAM STIFF ********

```
10 REM ***** STIFF *****
15 CLEAR
20 OPTION BASE 1
30 DIM W8$[80]
40 SHORT J4(200,2)
50 COM SHORT X(2048,2),T$[10],N,P$[1],S$[1],M$[20],P3,P4,D6,T3$[20],G5

60 COM A1$[15],A2$[10],A3$[18],A4$[10],A5$[10],A6$[10],A7$[10],A8$[80]
,A9$[10],B1$[10],B2$[20]
70 M2$="" @ M2$="*" @ M$=M2$&M$
80 BEEP 50,50 @ DISP "LOAD STIFFNESS DATA AND CONT" @ PAUSE
90 CAT @ DISP "FILE NAME" @ INPUT M1$
100 ASSIGN# 1 TO M1$
110 READ# 1 ; W1$,W2$,W3$,W4$,W5$,W6$,W7$,W8$,W9$,V1$,V2$,N1,T1$
120 IF N1>200 THEN N1=200 ! J4 ONLY TAKES 200 DATA POINTS
130 CLEAR @ GOSUB 1090
140 S,A=0
150 V8=.5/VAL(V1$) ! VOLTAGE FOR 5KG
160 FOR I=1 TO N1 @ READ# 1 ; J4(I,1),J4(I,2)
170 IF M1$[1,1]="*" THEN GOTO 190
180 IF J4(I,1)<=V8 THEN GOTO 270
190 A=A+1
200 IF A=1 THEN Y=J4(I,2)
210 B=J4(I,2)-Y
220 J4(A,2)=B*VAL(V1$)/10
230 J4(A,1)=J4(I,1)*VAL(W9$)/10
240 IF A<4 THEN GOTO 270
250 S=MAX(J4(A-1,1),J4(A,1))
260 IF J4(A-3,1)=J4(A-2,1) AND S=J4(A,1) THEN GOTO 280 ELSE GOTO 270
270 NEXT I
275 IF M1$[1,1]="*" THEN GOSUB 8000
280 IF M1$[1,1]="*" THEN GOTO 300
290 N1=A-1
295 GOSUB 6000
300 ASSIGN# 1 TO *
310 IF M1$[1,1]="*" THEN GOTO 340
320 GOSUB 1320
330 GOSUB 1650
340 DISP "STIFFNESS POINTS",N1
345 GOTO 490
350 DISP "PRINT EXPERIMENTAL DETAIL?(Y/N)" @ INPUT X1$
360 IF X1$="N" THEN GOTO 490
370 PRINT "********* E S H TEST *********" @ PRINT @ PRINT @ PRINT "STI
FFNESS INFORMATION" @ PRINT
380 PRINT "TEST#";TAB(20);W1$
390 PRINT "DATE";TAB(20);W2$
400 PRINT "MATERIAL TYPE";TAB(20);W3$
410 PRINT "GAUGE LENGTH ";TAB(20);W4$;" mm"
420 PRINT "DIAMETER ";TAB(20);W5$;" mm"
430 PRINT "TEST TEMP";TAB(20);A4$
440 PRINT "VACUUM       ";TAB(20);W7$;" Torr"
```

```
450 PRINT "ESH FS LOAD";TAB(20);W9$;" KN"
460 PRINT "ESH FS STROKE";TAB(20);V1$;" mm"
470 PRINT "RAMP RATE";TAB(20);V2$;" V/S"
480 PRINT "HISTORY";TAB(20);;W8$ @ PRINT @ PRINT
490 REM
500 REM
510 Z=1
520 P=1
530 I=1
540 IF J4(P,1)>=X(I,1) THEN GOTO 570
550 P=P+1
560 GOTO 540
570 P1=P
580 GOTO 710
590 I=I+Z
600 IF J4(P1,1)>=X(I,1) THEN GOTO 620
610 GOTO 670
620 IF P1=1 THEN GOTO 580
630 P1=P1-1
640 IF P1=1 THEN GOTO 580
650 IF J4(P1,1)<=X(I,1) THEN GOTO 670
660 GOTO 630
670 P1=P1+1 @ IF P1=N1-1 THEN GOTO 680 ELSE GOTO 690
680 DISP "LOAD EXCEEDS MAX STIFFNESS LOAD" @ GOTO 860
690 IF J4(P1,1)>=X(I,1) THEN GOTO 580
700 GOTO 670
710 REM  *** M4 ***
720 IF P1=1 THEN GOTO 770
730 R8=P1-1
740 M3=ABS(J4(P1,1)-X(I,1))*ABS(J4(P1,2)-J4(R8,2))/ABS(J4(P1,1)-J4(R8,
1))
750 M4=J4(P1,2)-M3+X(I,1)*Q1
760 GOTO 790
770 M3=ABS(J4(P1,1)-X(I,1))*ABS(J4(P1,2))/J4(P1,1)
780 M4=J4(P1,2)-M3+X(I,1)*Q1
790 X(I,2)=X(I,2)-M4
800 DISP I,P1
810 IF I=N THEN 830
820 GOTO 590
830 S$="*" @ DISP "STORE CORRCTED DATA? (Y/N)" @ INPUT F$@ IF F$="Y" T
HEN GOSUB 1150
840 ! BEEP 100,50 @ DISP "LOAD PROGRAM DISC AND CONT" @ PAUSE
850 CHAIN "DDRAW"
860 REM *** AVERAGE SLOPE   ***
870 L1,L2,L3,L4,L5,E9=0
880 FOR P=N1/1.5 TO N1
890 B=J4(P,2)
900 B1=J4(P,1)
910 IF E9=1 THEN R5=P
920 Y7=B1 @ X7=B
930 L1=L1+X7*Y7
940 L2=L2+X7
950 L3=L3+Y7
960 L4=L4+X7^2
970 L5=L5+Y7^2
980 E9=E9+1
990 NEXT P
```

```
1000 REM ** Y=G9+K1*X  ***
1010 K1=(L1-L2*L3/E9)/(L4-L2^2/E9)
1020 G9=L3/E9-K1*L2/E9
1030 O6=-G9/K1
1040 IF I=N THEN GOTO 830
1050 M4=(X(I,1)-G9)/K1+X(I,1)*01
1060 X(I,2)=X(I,2)-M4
1070 DISP I
1080 I=I+1 @ GOTO 1040
1090 CLEAR @ DISP "*********************************"
1100 DISP "*     CALCULATING !!              *"
1110 DISP "*  PLEASE BE PATIENT              *"
1120 DISP "*********************************"
1130 RETURN
1140 N=I-1 @ GOTO 830
1150 REM ** STORE DATA **
1160 DISP "LOAD DATA DISC AND CONT" @ BEEP 60,40 @ PAUSE
1170 PRINT "FILE NAME:";M$
1180 O=N*2*6+2000
1190 CLEAR
1200 CAT @ DISP "CREATE? (Y/N)" @ INPUT W$@ IF W$="Y" THEN CREATE M$,1
,O
1210 GOSUB 1090
1220 ASSIGN# 2 TO M$
1230 PRINT# 2 ; A1$,A2$,A3$,A4$,A5$,A6$,A7$,A8$,A9$,B1$,B2$,N,T$
1240 FOR I=1 TO N
1250 B1=X(I,1) @ B=X(I,2)
1260 B1=B1*10/VAL(A9$)
1270 B=B*10/VAL(B1$)
1280 PRINT# 2 ; B1,B
1290 NEXT I
1300 ASSIGN# 2 TO *
1310 RETURN
1320 ! LINEAR
1330 H,V=1.E21 @ H1,V1=-1.E21
1340 FOR I=1 TO N1
1350 H=MIN(J4(I,2),H)
1360 V=MIN(J4(I,1),V)
1370 V1=MAX(J4(I,1),V1)
1380 H1=MAX(J4(I,2),H1)
1390 NEXT I
1400 GCLEAR @ CLEAR @ PLOTTER IS 1
1410 MOVE 1,95
1420 LABEL "UN-CORRECTED STIFF ",M1$
1430 LOCATE 30,100,30,90
1440 FRAME @ SETUU @ SCALE 0,10,0,10 @ FXD 0,0
1450 LGRID -1,1,0,0,10,1 @ LORG 1
1460 FOR I=1 TO N1
1470 T=(J4(I,2)-H)*10/(H1-H)
1480 T1=(J4(I,1)-V)*10/(V1-V)
1490 MOVE T,T1 @ LABEL "."
1500 NEXT I
1510 LORG 5 @ SETGU @ MOVE 65,10 @ LABEL "LINEAR MIN,MAX "
1520 MOVE 30,2 @ INPUT R,R1
1530 SETUU
1540 R=R*(V1-V)/10+V
```

```
1550 R1=R1*(V1-V)/10+V
1560 FOR I=1 TO N1
1570 IF J4(I,1)>=R THEN GOTO 1590
1580 NEXT I
1590 R3=I
1600 FOR I=1 TO N1
1610 IF J4(I,1)>=R1 THEN GOTO 1630
1620 NEXT I
1630 R4=I-1
1640 RETURN
1650 REM  X-AXIS INTERCEPT
1660 L1,L2,L3,L4,L5,E9=0
1670 FOR I=1 TO N1
1680 B=J4(I,2)
1690 B1=J4(I,1)
1700 IF I<=R3 THEN GOTO 1800
1710 IF I>=R4 THEN GOTO 1810
1720 IF E9=1 THEN R3=I
1730 Y7=B1 @ X7=B
1740 L1=L1+X7*Y7
1750 L2=L2+X7
1760 L3=L3+Y7
1770 L4=L4+X7^2
1780 L5=L5+Y7^2
1790 E9=E9+1
1800 NEXT I
1810 REM Y=G9+K1*X
1820 K1=(L1-L2*L3/E9)/(L4-L2^2/E9)
1830 G9=L3/E9-K1*L2/E9
1840 O6=-G9/K1
1850 O3=0
1860 FOR I=1 TO N1 ! RIDS NEG STRAIN
1870 O=J4(I,2)-O6
1880 IF O<0 THEN GOTO 1910
1890 O3=O3+1
1900 J4(O3,2)=O
1910 NEXT I
1920 N1=O3
1930 GOSUB 1950
1940 RETURN
1950 REM ** STORE DATA **
1960 DISP "LOAD DATA DISC AND CONT" @ BEEP 60,40 @ PAUSE
1970 CLEAR @ DISP "ENTER SIZE TO BE AVERAGED IF YOU WANT TO SMOOTH DAT
A FURTHER" @ INPUT O4
1980 M2$="" @ M2$="*"&M1$
1990 PRINT "FILE NAME:";M2$
2000 O=N1*2*8+2000
2010 CLEAR
2020 CAT @ DISP "CREATE? (Y/N)" @ INPUT W$@ IF W$="Y" THEN CREATE M2$
1,O
2030 GOSUB 1070
2040 O,O1,O2,O3=0
2050 FOR I=1 TO N1
2060 O2=O2+1
2070 B1=J4(I,1) @ B=J4(I,2)
2080 B1=B1*10/VAL(W9$)
```

```
2090 B=B*10/VAL(V1$)
2100 O=O+B @ O1=O1+B1
2110 IF O2=04 THEN GOTO 2120 ELSE GOTO 2150
2120 O3=O3+1
2130 J4(O3,2)=O/O2 @ J4(O3,1)=O1/O2
2140 O,O1,O2=0
2150 NEXT I
2160 N1=O3
2170 ASSIGN# 2 TO M2$
2180 PRINT# 2 ; W1$,W2$,W3$,W4$,W5$,W6$,W7$,W8$,W9$,V1$,V2$,N1,T1$
2190 FOR I=1 TO N1
2200 PRINT# 2 ; J4(I,1),J4(I,2)
2210 NEXT I
2220 ASSIGN# 2 TO *
2230 M1$=M2$ @ CLEAR @ DISP "STIFFNESS DATA STORED" @ END
2240 K3=5
6000 ! AVERAGE DATA
6002 ! K3=8
6003 K3=3
6005 K2,K4,K5,K6,I=0
6010 IF K2+K3-1=N1 THEN GOTO 7000
6020 K2=K2+1
6030 I=I+1
6040 K4=K4+1
6050 K5=K5+J4(K4,1) @ K6=K6+J4(K4,2)
6060 IF I=K3 THEN GOTO 6070 ELSE GOTO 6030
6070 I=0 @ K4=K2
6080 K5=K5/K3 @ K6=K6/K3
6090 J4(K2,1)=K5 @ J4(K2,2)=K6
6095 DISP K2
6096 K5,K6=0
6100 GOTO 6010
6110 N1=K2
7000 RETURN
8000 REM CORRECTION FACTOR
8010 ! ENTER LOAD*(1/(CORR ,WITH OUT @1,SLOPE)-1/THEOR.SLOPE)
8015 ! 13 FOR 10^-1 STRAIN RATE
8016 ! 34 FOR 10^-4
8020 ! THEOR KN=E*A/G.L
8030 O=200*10^9*(VAL(A3$)/2)^2*PI/VAL(A4$)
8040 @1=1/44-1/O
8050 RETURN
```

******** PROGRAM DDRAW 1 ********

```
10 REM *** DDRAW1 ***
20 RAD
30 DIM P2$[25]
40 A$="" @ N$="" @ R3=-2
50 OPTION BASE 1@ PLOTTER IS 1
60 COM SHORT X(2048,2),T$[10],N,P$[1],S$[1],M$[20],P3,P4,06,T3$[20],G5

70 COM A1$[15],A2$[10],A3$[18],A4$[10],A5$[10],A6$[10],A7$[10],A8$[80]
,A9$[10],B1$[10],B2$[20]
80 C$="LOAD"
90 DIM P3$[45]
100 ON KEY# 1,"DDRAW " GOTO 3440
110 ON KEY# 2,"LOAD" GOTO 2600
120 ON KEY# 5,"TRUE" GOTO 2620
130 ON KEY# 8,"N" GOTO 2900
140 ON KEY# 3,"RE-PLOT" GOSUB 890
150 ON KEY# 4,"RE-ARM" GOSUB 1610
160 CLEAR @ GCLEAR
170 IF C$="LOAD" AND A$<>"" THEN DISP "X CONTAINS LOAD DATA"
180 IF C$="TRUE" THEN DISP "X CONTAINS TRUE DATA"
190 IF C$="ENG" THEN DISP "X CONTAINS ENG  DATA"
200 KEY LABEL
210 GOTO 210
220 CLEAR
230 GOSUB 2240
240 A=(VAL(A5$)/2*10^-3)^2*PI
250 IF C$="LOAD" THEN GOTO 370
260 IF C$="TRUE" THEN GOTO 270 ELSE GOTO 320
270 FOR I=1 TO N
280 Z=FND1(X(I,2))
290 X(I,1)=FNB1(X(I,1))
300 X(I,2)=Z
310 NEXT I
320 IF C$="ENG" THEN GOTO 330 ELSE GOTO 370
330 FOR I=1 TO N
340 X(I,2)=FNC1(X(I,2))
350 X(I,1)=FNA1(X(I,1))
360 NEXT I
370 IF A$="1" THEN GOTO 380 ELSE GOTO 440
380 C$="LOAD"
390 P1$="ELONGATION IN mm" @ P2$="LOAD IN KN"
400 P3$="" @ P3$="EXTENSION CURVE FOR "&M$
410 P5$="MAX LOAD (KN)" @ P8$=" mm"
420 P6$="MAX STROKE (mm)"
430 P7$=".2% PROOF (KN) "
440 IF A$="2" THEN GOTO 450 ELSE GOTO 570 '
450 FOR I=1 TO N
460 Z=FND(X(I,2))
470 X(I,1)=FNB(X(I,1))
480 X(I,2)=Z
490 NEXT I
500 C$="TRUE"
```

```
510 P2$="TRUE STRESS IN MPa"
520 P1$="TRUE STRAIN"
530 P3$="" @ P3$="FLOW CURVE FOR "&M$
540 P5$="MAX STRESS(MPa)" @ P8$=" STRAIN"
550 P6$="MAX STRAIN"
560 P7$=".2% PROOF (MPa)"
570 IF A$="3" THEN GOTO 580 ELSE GOTO 700
580 FOR I=1 TO N
590 X(I,1)=FNA(X(I,1))
600 X(I,2)=FNC(X(I,2))
610 NEXT I
620 C$="ENG"
630 P1$="ENGINEERING STRAIN"
640 P2$="ENGINEERING STRESS in MPa"
650 P3$="" @ P3$="STRESS STRAIN CURVE FOR "&M$
660 P5$="MAX STRESS(MPa)"
670 P6$="MAX STRAIN"
680 P7$=".2% PROOF(MPa)"
690 P8$=" STRAIN"
700 GOTO 710
710 GOSUB 2240
720 REM  ABSOLUTE VALS
730 FOR I=1 TO N
740 B=X(I,2) @ B1=X(I,1)
750 IF I=1 THEN C1=B
760 IF I=1 THEN C3=B1
770 IF I=1 THEN C=B
780 IF I=1 THEN C2=B1
790 IF B>C THEN C=B
800 IF B1<=C2 THEN GOTO 820
810 C2=B1 @ P4=I
820 IF I>N/2 THEN 840
830 IF B<C1 AND B>0 THEN C1=B
840 IF B1<C3 THEN C3=B1
850 NEXT I
860 R5=1 @ O6=0
870 GOSUB 1970 ! CALC O6
880 CLEAR
890 BEEP 1000,50 @ BEEP 50,80 @ CLEAR
900 DISP "ENTER VERTICAL MAX,MIN VALUES"
910 DISP @ DISP USING 940 ; "MAX...",C2
920 DISP USING 940 ; "MIN...",C3
930 INPUT C4,C5
940 IMAGE 10A,3D.5D
950 DISP " VERT TIC STEP," @ DISP "No DIGITS AFTER DECIMAL POINT" @ IN
PUT C9,S9
960 DISP "ENTER HORI MAX,MIN VALUES"
970 DISP @ DISP USING 940 ; "MAX...",C
980 DISP USING 940 ; "MIN...",C1
990 INPUT C6,C7
1000 DISP "ENTER HORI TIC STEP," @ DISP "No DIGITS AFTER DECIMAL POINT
" @ INPUT C8,S8
1010 ! DISP "ENTER NO POINTS TO BE AVERAGED" @ INPUT F5
1020 F5=1
1030 ! DISP "GRAPH ON CRT OR AT PLOTTER"
```

```
1040 ! DISP "ENTER 1 OR 2 " @ INPUT Z5
1050 Z5=2
1060 GCLEAR
1070 IF Z5=1 THEN PLOTTER IS 1 ELSE PLOTTER IS 705
1080 ! DISP " PRINT VALUES? " @ INPUT H$
1090 H$="N"
1100 ! DISP "POINT OR LINE (P/L)" @ INPUT G$
1110 G$="L"
1120 DISP "PAPER?????" @ PAUSE
1130 D1=C4-C5 @ D2=C6-C7
1140 CSIZE 3,.6,0
1150 LOCATE 25,135,15,85 @ FRAME
1160 FXD 88,89
1170 SCALE C7,C6,C5,C4
1180 S,N2,N3,R,R1,I1=0
1190 GOSUB 2290 ! PROOF
1200 GOSUB 3010 !  AREA
1210 FOR I=R5 TO N
1220 N2=N2+1
1230 B=X(I,2)-C6
1240 B1=X(I,1)
1250 R=B+R @ R1=B1+R1
1260 IF N2<>F5 THEN GOTO 1410
1270 R=R/F5 @ R1=R1/F5
1280 IMAGE 4D.4D,4X,4D.4D,
1290 IF H$="N" THEN 1320
1300 IF I=R5 THEN PRINT "LOAD      STROKE" @ PRINT
1310 PRINT USING 1280 ; R1,R
1320 IF R>=C7 AND R<=C6 THEN GOTO 1330 ELSE GOTO 1340
1330 IF R1>=C5 AND R1<=C4 THEN GOTO 1350 ELSE 1340
1340 IF R>C6 OR R1>C4 THEN GOTO 1420 ELSE GOTO 1400
1350 I1=I1+1
1360 IF G$="L" THEN GOTO 1390
1370 MOVE R,R1 @ PLOT R,R1,-1
1380 GOTO 1400
1390 IF I1=1 THEN MOVE 0,0 ELSE DRAW R,R1 @ GOTO 1400
1400 N2,R,R1=0
1410 NEXT I
1420 !
1430 IF T3$="0" THEN T3=VAL(T$) ELSE T3=VAL(T$[2,LEN(T$)])*I1/1000*F
1440 IF C$="LOAD" THEN B6=C/VAL(A4$)/T3
1450 IF C$="TRUE" THEN B6=(2.71828182^C-1)/T3
1460 IF C$="ENG" THEN B6=C/T3
1470 PRINT @ PRINT @ PRINT USING 1480 ; "STRAIN RATE(PER S)";B6
1480 IMAGE 18A,1X,1D.3DE
1490 LAXES -C8/5,C9/5,C7,C5,5,5
1500 CSIZE 3,.5,PI/8 @ LORG 5
1510 LDIR 0 @ SETGU
1520 MOVE 80,5 @ LABEL P1$
1530 LDIR PI/2 @ MOVE 13,50 @ LABEL P2$
1540 MOVE 80,89
1550 LDIR 0 @ CSIZE 5,1,0 @ LABEL P3$
1560 CLEAR
1570 BEEP 50,50 @ DISP "LABEL EXP DETAIL (Y/N) " @ INPUT P4$
```

```
1580 IF P4$="Y" THEN GOSUB 1630 ELSE GOTO 1590
1590 SETGU @ MOVE 130,100 @ SETUU
1600 GOTO 100
1610 DISP " PROGRAM DISC" @ PAUSE
1620 CHAIN "DATALOG"
1630 LDIR 0 @ CSIZE 2.2,.8,0 @ DISP "LOCATE PEN" @ DIGITIZE X4,Y4
1640 MOVE X4,Y4 @ LORG 1
1650 IMAGE 19A,17
1660 IMAGE 19A,FA,5A
1670 IMAGE 19A,1D.1DE
1680 LABEL "TEST#                ",A1$
1690 LABEL "DATE                 ",A2$
1700 LABEL "MATERIAL TYPE        ",A3$
1710 LABEL "GAUGE LENGTH         ",A4$;" mm"
1720 LABEL "DIAMETER             ",A5$;" mm"
1730 LABEL "TEST TEMP            ",A6$
1740 LABEL "VACUUM               ",A7$;" Torr"
1750 LABEL USING 1670 ; "STRAIN PER SEC ",B6
1760 LABEL USING "19A,3D.1D,3A,2D.3D,8A" ; P5$,C2," AT",X(P4,2)-06,P8$

1770 LABEL USING "19A,3D.1D,3A,2D.4D,8A" ; P7$,X(P3,1)," AT",X(P3,2)-0
6,P8$
1780 IF C$="TRUE" THEN LABEL USING "19A,3D.3D" ; "ENG.STRAIN",2.718282
^C-1
1790 LABEL USING "19A,3D.3D    " ; P6$,C
1800 IF C$="TRUE" THEN LABEL USING 1810 ; "WORK TO YIELD(KJ)",04*1000
1810 IMAGE 19A,1D.1DE
1820 IF C$="TRUE" THEN LABEL USING 1810 ; "WORK TO UTS  (KJ)",05*1000
1830 IF C$="TRUE" THEN LABEL USING 1810 ; "TOTAL WORK   (KJ)",03*1000
1840 G1$=" " @ LABEL
1850 FOR I=1 TO 80 @ IF LEN(A8$)=80 THEN 1870 ELSE A8$=A8$&G1$
1860 NEXT I
1870 LABEL USING "19A,25A" ; "HISTORY",A8$[1,25]
1880 LABEL USING "19X,25A" ; A8$[26,50]
1890 LABEL USING "19X,25A" ; A8$[51,75]
1900 CSIZE 3,.6,PI/7
1910 CLEAR @ DISP "PRINT COMMENT?" @ DISP "ENTER COMMENT OR END LINE"
@ BEEP 100,20
1920 DIM L$[80]
1930 INPUT L$
1940 IF L$="" THEN GOTO 1950 ELSE LABEL L$
1950 CSIZE 3,.6,0
1960 RETURN
1970 REM  X-AXIS INTERCEPT
1980 IF R3=-2 THEN GOTO 2230
1990 IF R3>0 THEN DISP "CALIBRATE SLOPE?" @ INPUT K5$
2000 IF K5$="Y" THEN GOSUB 3130
2010 IF R3=-1 THEN GOSUB 3130 ! LINEAR
2020 L1,L2,L3,L4,L5,E9=0
2030 FOR I=1 TO N
2040 B=X(I,2)
2050 B1=X(I,1)
2060 IF I<=R3 THEN GOTO 2160
2070 IF I>=R4 THEN GOTO 2170
2080 IF E9=1 THEN R5=I
```

```
2090 Y7=B1 @ X7=B
2100 L1=L1+X7*Y7
2110 L2=L2+X7
2120 L3=L3+Y7
2130 L4=L4+X7^2
2140 L5=L5+Y7^2
2150 E9=E9+1
2160 NEXT I
2170 REM Y=G9+K1*X
2180 K1=(L1-L2*L3/E9)/(L4-L2^2/E9)
2190 G9=L3/E9-K1*L2/E9
2200 O6=-G9/K1
2210 C=C-O6
2220 RETURN
2230 R3=-1 @ GOTO 2010
2240 CLEAR @ DISP "**********************************"
2250 DISP "*     CALCULATING !!              *"
2260 DISP "*  PLEASE BE PATIENT              *"
2270 DISP "**********************************"
2280 RETURN
2290 REM PROOF
2300 IF C$="LOAD" THEN P1=.2/100*VAL(A4$) ELSE P1=.2/100
2310 Y2=-K1*P1 ! Y INTERCEPT
2320 FOR I=N TO R5 STEP -1
2330 IF (X(I,1)-Y2)/K1-(X(I,2)-O6)<0 THEN GOTO 2340 ELSE GOTO 2350
2340 NEXT I
2350 DIM S(6),T(5),U(5),I(5)
2360 P3=I+1
2370 FOR I=P3 TO 1 STEP -1
2380 IF X(I,2)<X(P3,2) AND X(I,1)<X(P3,1) THEN 2400
2390 NEXT I
2400 S(6)=I
2410 S(1)=X(S(6),2)-O6 @ S(2)=X(P3,2)-O6
2420 T(1)=X(S(6),1) @ T(2)=X(P3,1)
2430 U(2)=ATN(ABS(T(1)-T(2))/ABS(S(1)-S(2)))
2440 S(3)=(T(1)-Y2)/K1
2450 I(4)=S(3)-S(1)
2460 I(1)=I(4)*SIN(U(2))/SIN(90-U(2))
2470 U(3)=90-K1
2480 U(5)=U(2)+90
2490 U(4)=90-U(2)
2500 I(5)=SIN(U(3))*I(1)/SIN(U(4))
2510 I(2)=I(5)*SIN(U(2))
2520 I(3)=I(5)*SIN(U(4))
2530 S(4)=S(1)+I(4)+I(3)
2540 T(4)=T(1)+I(1)+I(2)
2550 X(P3,1)=T(4)
2560 X(P3,2)=S(4)+O6
2570 PRINT USING "15A,3D.3D,2X,3D.3D" ; ",2%PROOF :",X(P3,1),X(P3,2)-O
6
2580 LDIR 0 @ LORG 2 @ MOVE X(P3,2)-O6,X(P3,1) @ LABEL "-"
2590 RETURN
2600 A$="1" ! LOAD WANTED
2610 GOTO 230
```

```
2620 A$="2" ! TRUE WANTED
2630 GOTO 230
2640 A$="3" ! ENG WANTED
2650 GOTO 230
2660 REM FNA:LOAD TO ENG
2670 DEF FNA(B1)
2680 B1=B1/A*10^-3 @ FNA=B1 @ FN END
2690 REM FNB:LOAD TO TRUE
2700 DEF FNB(B1)
2710 B1=B1/A*10^-3*(1+X(I,2)/VAL(A4$)) @ FNB=B1 @ FN END
2720 REM FNC:ELON TO ENG
2730 DEF FNC(B)
2740 B=B/VAL(A4$) @ FNC=B @ FN END
2750 REM ELON TO TRUE
2760 DEF FND(B)
2770 B=LOG(1+B/VAL(A4$)) @ FND=B @ FN END
2780 REM TRUE TO ELONG
2790 DEF FND1(B)
2800 B=(2.718281828^B-1)*VAL(A4$) @ FND1=B @ FN END
2810 REM TRUE TO LOAD
2820 DEF FNB1(B1)
2830 B1=B1*10^3/(1+Z/VAL(A4$))*A @ FNB1=B1 @ FN END
2840 REM ENG TO ELONG
2850 DEF FNC1(B)
2860 B=B*VAL(A4$) @ FNC1=B @ FN END
2870 REM ENG TO LOAD
2880 DEF FNA1(B1)
2890 B1=B1*A*10^3 @ FNA1=B1 @ FN END
2900 REM
2910 IF C$="TRUE" THEN GOTO 2920 ELSE GOTO 2990
2920 CLEAR @ DISP "LOAD PROG DISC AND CONT" @ PAUSE
2930 ASSIGN# 2 TO "JUNK"
2940 P5=5
2950 N1=P4-P3+10 @ PRINT# 2 ; A1$,M$,N1
2960 FOR I=P3-P5 TO P4+5 @ PRINT# 2 ; X(I,1),X(I,2)-C6 @ NEXT I
2970 ASSIGN# 2 TO *
2980 CLEAR @ DISP USING "4A,1A,1A,1A,5A" ; "LOAD",CHR$(34),"N",CHR$(34
),"@ RUN" @ PAUSE
2990 BEEP 1000,100 @ BEEP 10,50
3000 GOTO 160
3010 REM AREA
3020 IF C$="LOAD" OR C$="ENG" THEN GOTO 3120
3030 03=0
3040 CLEAR @ DISP "CALCULATING AREA"
3050 FOR I=R5+1 TO N
3060 01=(X(I,1)+X(I-1,1))/2
3070 02=X(I,2)-X(I-1,2)
3080 03=01*02+03
3090 IF I=P3 THEN 04=03 ! YIELD
3100 IF I=P4 THEN 05=03 ! UTS
3110 NEXT I
3120 RETURN
3130 ! LINEAR
3140 H,V=1.E21 @ H1,V1=-1.E21
```

```
3150 FOR I=1 TO N
3160 H=MIN(X(I,2),H)
3170 V=MIN(X(I,1),V)
3180 V1=MAX(X(I,1),V1)
3190 H1=MAX(X(I,2),H1)
3200 NEXT I
3210 GCLEAR @ CLEAR @ PLOTTER IS 1
3220 LOCATE 30,100,30,90
3230 FRAME @ SETUU @ SCALE 0,10,0,10 @ FXD 0,0
3240 LGRID -1,1,0,0,10,1 @ LORG 1
3250 FOR I=1 TO N
3260 T=(X(I,2)-H)*10/(H1-H)
3270 T1=(X(I,1)-V)*10/(V1-V)
3280 MOVE T,T1 @ LABEL "."
3290 NEXT I
3300 LORG 5 @ SETGU @ MOVE 65,10 @ LABEL "LINEAR MIN,MAX "
3310 MOVE 30,2 @ INPUT R,R1
3320 SETUU
3330 R=R*(V1-V)/10+V
3340 R1=R1*(V1-V)/10+V
3350 FOR I=1 TO N
3360 IF X(I,1)>=R THEN GOTO 3380
3370 NEXT I
3380 R3=I
3390 FOR I=1 TO N
3400 IF X(I,1)>=R1 THEN GOTO 3420
3410 NEXT I
3420 R4=I-1
3430 RETURN
3440 CHAIN "DDRAW"
```